Final Report

Fabrication and investigation of luminescence properties of recycled window glasses as gamma-radiation dosimeter

Cherdsak Bootjomchai

May 2015

Contract No. MRG5680114

Final Report

Fabrication and investigation of luminescence properties of recycled window glasses as gamma-radiation dosimeter

Cherdsak Bootjomchai (Researcher) **Ubon Ratchathani University**

Raewat Laopaiboon (Mentor) **Ubon Ratchathani University**

This project granted by the Thailand Research Fund

Abstract

Project Code: MRG5680114

Project Title: Fabrication and investigation of luminescence properties of recycled window glasses as gamma-radiation dosimeter

Investigator: Cherdsak Bootjomchai

E-mail Address: cherdsak_per@hotmail.co.th
cherdsak2303@gmail.com

Project Period: 2 years (3 June 2013 to 3 June 2015)

Abstract:

The luminescence and structural properties of recycled window glasses (RWG) doped with different some transition metal oxides (TMOs) and some rare earth oxides (ROs) were carried out. All glasses were prepared and irradiated under the same conditions. The luminescence properties were investigated in terms of the TL response, TL glow curve, linearity, lower detection limits (D_{LDL}), reproducibility and fading. The structural properties were studied in terms of elastic moduli, micro-hardness, FTIR and expand to optical properties such as UV-visible absorption coefficient. These properties of the glass samples will be examined to be applying these glasses as the gamma-radiation dosimeter.

Keywords: Luminescence; elastic moduli; gamma-radiation; rare earth; glasses

Fabrication and investigation of luminescence properties of recycled window glasses as gamma-radiation dosimeter

1. Abstract

The luminescence and structural properties of recycled window glasses (RWG) doped with different some transition metal oxides (TMOs) and some rare earth oxides (ROs) were carried out. All glasses were prepared and irradiated under the same conditions. The luminescence properties were investigated in terms of the TL response, TL glow curve, linearity, lower detection limits (D_{LDL}), reproducibility and fading. The structural properties were studied in terms of elastic moduli, micro-hardness, FTIR and expand to optical properties such as UV-visible absorption coefficient. These properties of the glass samples will be examined to be applying these glasses as the gamma-radiation dosimeter.

Keywords: Luminescence; elastic moduli; gamma-radiation; rare earth; glasses

2. Executive summary

2.1 Introduction

Today, nuclear energy and its applications have become interesting in many fields such as nuclear power plant, industry, food technology, medicine, sciencetific and etc. Moreover, the global citizen have electricity demand is unlimited. Many countries are building the nuclear power plants for response this requirement. Although nuclear power has many advantages but it also has very dangerous as well. For example, The Fukushima Daiichi nuclear disaster which is the largest nuclear disaster since the Chernobyl disaster of 1986. However, nuclear power is indispensable for electric generator, industrial and medical. Therefore, the radiation detections and radiation protection is highly necessary.

Radiation dosimetry with solid luminescent materials is a well-established technique of monitoring ionizing radiation. Successful applications of thermoluminescence (TL) dosimetry are a result of search for materials that can be used as detectors of ionizing radiation and analysis of their properties [1].

Inorganic crystals such as LiF: Mg, Ti and LiF: Mg, Cu, P have been traditionally used for gamma and X-ray TL dosimetry applications. Various TL materials are in use today as dosimeters; however, as far as optically stimulated luminescence (OSL) is concerned, Al_2O_3: C is virtually the only synthetic material currently used in medical, environmental and personal dosimetry [2]. OSL has certain advantages over TL, such as higher precision, flexibility and ease of use, as well as the possibility of performing real-time measurements and future dose reassessments, if desired. Extensive research is underway to introduce new dosimetric systems into traditional in-phantom measurements, mailed dosimetric services for radiotherapy beam calibrations and two-dimensional TL dosimetry. Promising solutions are also being developed for online in-vivo dosimetry using OSL systems [3].

TL and OSL glass dosimeters are of particular interest because of their optical transparency, which results in an overall improvement of the efficiency of phosphor. Various authors have recently proposed the use of glass samples as ionizing radiation detectors in different fields [4-6]; above all, there is an increasing interest on glasses which can be in contact or very close to exposed persons and be used as emergency dosimeters. Glass has valuable properties such as easy handling, chemical inertness and rigidity. Recently, we found that many authors have been studies the standard window glass as an accidental dosimeter. Due to the standard window glass is widely available in every house and laboratory, which makes it very attractive as dosimetric when occurred radiation accident [7].

In basic principles, thermoluminescence is the thermally stimulated emission of light from an insulator or a semiconductor following the previous absorption of energy from ionizing radiation. The thermoluminescence process can be understood in terms of the band structure model of insulators. In a pure insulator there are two relevant energy bands: (i) an almost completely filled valence band and (ii) an almost empty conduction band. The two energy bands are separated by a forbidden gap, which means that between these two bands there are no electronic energy levels. Transitions of electrons between the valence band and the conduction band are allowed and they produce free electrons in the conduction band and free holes in the valence band. The energy difference between the two bands is denoted by the band-gap energy (E_g). Imperfections in the crystal, associated with impurities and/or lattice defects may create new localized energy levels in the forbidden band gap. The positions of the energy levels depend on the nature of the imperfections/defects and the host lattice. Some of these defects are capable to trap an electron or a hole. Therefore the centers are referred to as electron or hole traps and after trapping an electron or hole the new defects are called trapped electron or trapped hole centers, respectively. The trapping sites may be the metal cations that

constitute the glass structure, ions of admixtures to the main composition and/or the structural defects due to impurities in the glass. Thus this process leads to the formation of (i) silicon electron centers, (ii) non-bridging oxygen hole centers and (iii) silicon oxygen hole centers. It can be seen that the defects and/or impurities in the lattice structure cause to the occurring of TL properties of glass materials. The sensitivity of TL glass dosimetry is a consequence of radiative recombination between the electrons and an antibonding or non-bridging oxygen hole centers.

The properties of glasses are closely related to inter-atomic forces and potentials in lattice structure. Thus, any change in lattice due to doping and/or irradiation can be directly noted. The elastic properties, Poisson's ratio, Debye temperature and microhardness are of important material properties to investigation of glass and have been interpreted in terms of the structure or transformation of cross-linkages in the glass network [8]. To study the structure of oxide glasses, the coordination number of the net work former and the change of oxygen bonds of the frame work induced by the cation modifiers need to be investigated. This information can be obtained from FTIR spectroscopy. The majority of structural investigations on the glasses before and after irradiation have been using the ultrasonic studies [9-10]. The ultrasonic technique is a versatile tool for investigating the change in microstructure, the deformation process and mechanical properties of materials.

Recycling glass is one of the many ways we can help reduce pollution and waste. Everyday we throw away tones of rubbish and glass is a significant part of it. Instead of letting landfills pile up with glass objects that are a threat to safety and the environment, we can use it again. The aim of this work is focused on the study of the luminescence properties of glass samples and study the structural properties of the recycled window glasses (RWG) before and after gamma-irradiated by using the ultrasonic technique. In order to explore the validity of this method, the FTIR spectroscopy was used both before and after gamma-irradiation.

2.2 Literature reviews

V. Kortov [1] has been studies and applications of thermoluminescence (TL) dosimetric materials are reviewed. It is shown that the properties of commercial TL dosimeters satisfy a set of stringent requirements. The search and development of storage materials with required TL properties is based on approaches that involve the evaluation of the luminescence light yield. The specific features required for the dosimetry of high- energy particles and fast and

thermal neutrons are considered. The use of TL with deep traps in high-temperature dosimetry is discussed. Results of pioneering studies of TL in nanosized materials are briefly presented.

Various TL materials (e.g. lithium fluoride, calcium fluoride, calcium sulfate, lithium borate, quartz) are in use today as dosimeters in medical, personnel, archeological, and environmental applications. As far as OSL is concerned, to studies increasingly about the OSL since 2006, Yoshimura and Yukihara [2] studies on the optically stimulated luminescence (OSL) for new dosimetric materials**.** They found that, some materials, as barium aluminoborate glasses, although showing intense OSL signals, present a high fading at room temperature. In that situation the OSL signal is related to low temperature TL peaks that also fade at room temperature. None of the investigated materials was specially prepared to be used as an OSL dosimeter, which means that work can be done, mainly in the impurity nature and content, in order to improve OSL signals and to overcome some of the shortcomings that were noticed.

Olko [3] has been studies on advantages and disadvantages of luminescence dosimetry. He stated that the OSL has certain advantages over TL, such as higher precision, flexibility and ease of use, as well as the possibility of performing real-time measurements and future dose reassessments.

Many authors have been reported, TL and OSL glass dosimeters are of particular interest because of their optical transparency, which results in an overall improvement of the efficiency of phosphor [4-6].

Kharita et al., [7] studied the standard window glass as potential accidental radiation dosimeters. However, the results demonstrate that the standard window glass can be used as high-dose accidental dosimeters for doses ranging between 8 and 200 Gy.

Many researchers have been mentioned the effects of radiation on the structural properties of the glasses. Sharma et al., [8] studies the structural properties of the bismuth borate glasses under the influence of gamma-irradiation through ultrasonic. The obtained result indicates that BB3 glass (0.35 mole fraction of Bi_2O_3) is most affected by irradiation.

Laopaiboon et al., [9] have been studies the elastic properties of gamma-radiated barium lead borosilicate glass by using ultrasonic technique. He stated that changes in the structure of the glass ($BO_3 \rightarrow BO_4$) due to the effect of radiation and resulting to the more compactness structure.

Bootjomchai et al., [10] have been reported that the structural investigation of borosilicate recycled-barium-bismuth glass system under the influence of gamma-irradiation by using ultrasonic and FTIR. The obtained results indicated the change in the structure of the glasses due to the composition effect as well as the irradiation effect.

From reviews above mentioned, many authors attempt created defects in the lattice structure for improve the TL properties of materials. This will be a guideline for author to develop the recycled window glasses as the radiation dosimeter.

3. Objective

1) To prepare the glass samples from recycled window glass as radiation dosimeter.
2) To study the luminescence properties of the gamma-ray irradiated glass samples.
3) To investigate the side effect of gamma-irradiation on the structure of glass samples.

4. Research methodology

4.1 Glass preparations

4.1.1 Window glass (RWG)

The window glass samples were used for the TL analysis before and after exposure to an X-ray exposure machine. All of the samples were taken from the same window glass plate. The window glass was common window glass sold in Ubon Ratchathani, Thailand. The chemical composition analyses of the window glass were carried out by using the WDXRF method. The window glass was cleaned and cut into small pieces of dimensions $5 \times 5 \times 2\ \mathrm{mm}^3$ for the TL and XRD measurements. X-ray diffraction studies were carried out to confirm the amorphous structure of the window glass. A Philips X'Pert PANalytical diffractrometer was used during the investigations. The radiation used was $\mathrm{CuK}\alpha$ and the pattern was recorded at a scanning rate of 4 °/min and an angular range (2θ) of 5-80°.

4.1.2 Preparation and determination of the final composition of based glass

Binary $(100-x)\mathrm{RWG}-(x)\mathrm{Na_2O}$ glass with different concentrations of Na_2O, where *x* is 5, 10, 15 and 20 mol%, was prepared using the melt-quenched technique. The sodium oxide (Na_2O) used was of analytical reagent grade. The RWG was common window glass sold in Ubon Ratchathani, Thailand. Preparation of the recycling glass from window glass (RWG) involved a thorough cleaning and it was then ground to a powder. The quantities of Na_2O and RWG powder were weighed, using an electronic balance with accuracy of the order of 0.0001 g. They were calculated and mixed to give 50 g samples. The starting materials were mixed carefully in ceramic crucibles. To ensure homogeneity, the mixtures were melted at 1250 °C in an electrical furnace, constructed at the Glass Technology Excellent Center (GTEC),

Department of Physics, Faculty of Science, Ubon Ratchathani University. The melted glasses were poured into stainless steel moulds and immediately annealed at 500 °C for two hours before natural cooling to room temperature. The glass samples were cut into small pieces with dimensions $5\times5\times2\ \mathrm{mm}^3$ for TL measurements at 14 mGy. The sensitivity of the TL signal was normalized with respect to the weights of each condition of glass sample as shown in Figure 1. Results showed that the $(90)\mathrm{RWG}-(10)\mathrm{Na_2O}$ glass system had the highest sensitivity, therefore this condition was selected as the base glass ($\mathrm{G}-0$).

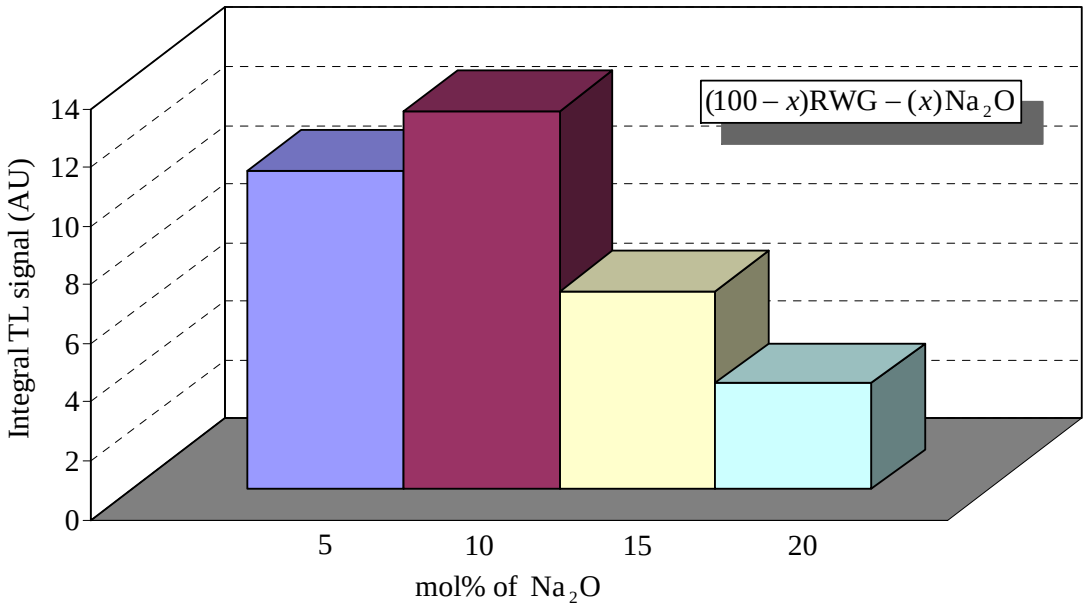

Figure 1 Integral TL signal of $(100-x)\mathrm{RWG}-(x)\mathrm{Na_2O}$ glass system irradiated with X-ray photon energy of 100 keV at dose of 14 mGy. The sensitivity of TL signal was normalized with respect to the respective weights of the samples.

4.1.3 Preparation of glass samples were added with dopants

For this study $(90)\mathrm{RWG}-(10)\mathrm{Na_2O}-(x)\mathrm{R_mO_n}$ glass systems (where *x* is 0.001, 0.010, 0.100 and 1.000 mol%) were prepared. The $\mathrm{R_mO_n}$ is the oxide of Dy_2O_3, CeO_2, Nd_2O_3 and MnO_2. For each glass, the thermal history; melting temperature, melting time, annealing temperature, annealing time and all preparation conditions were kept as similar as possible. The oxides used were of analytical reagent grade.

4.1.4 Other glass systems were prepared for structural investigations

For more comprehensive about the effect of dopants on structural properties the other glass systems such as borosilicate, silicate and alkali-borosilicate have been prepared.

4.2 Thermoluminescence

All samples were annealed at 400 °C for 1 h and then 100 °C for 2 h (dual step technique). The X-ray machine (KELEX) was used (X-ray tube model MD1100). The X-ray tube has an inherent filtration by oil-insulated with vacuum system and added filtration by lead-shielded housing for reduce a low photon energy. The samples were then irradiated with X-ray photon energy (in air kerma) at 100 keV and 30 mA with a dose range of 0 to14 mGy (with absorbed dose rate at 0.29 $\mathrm{mGy \cdot s^{-1}}$) to determine the thermoluminescence responses and glow curves. The doses were measured by using pocket dosimeter (Aloka, Model: PDM-253). The irradiated glass samples were carried out TL signal immediately. TL light emitted from the glass samples were detected using a thermoluminescence detector (TLD) reader (Harshaw/Bicron Model 3500 Manual Reader). The glow curves were recorded from room temperature up to a maximum of 300 °C at a heating rate of 10 °C/s. The region of interest facility available in the TLD reader was used to evaluate the responses of different glow peaks resulting from the Computerised Glow Curve Deconvolution (CGCD) procedure. The CGCD data was carried out by take notes from the MS-DOS files to Excel program. Each datum point was obtained from an average of five detections. For investigation of trap depth parameters, general expressions for evaluating activation energy and trap depth were derived by Chen [11]. His method is useful for a broad range of energies ranging between 0.1 eV and 2.0 eV, and for values of the pre-exponential factors between $10^{5}\ \mathrm{s^{-1}}$ and $10^{23}\ \mathrm{s^{-1}}$. Chen's method does not make use of any iterative procedures and does not require knowledge of the kinetic order, which is found by using the symmetry factor ($\mu = \frac{T_2 - T_M}{T_2 - T_1}$) from the peak shape. The equations can be summarised up as Eq. (1):

$$E_\alpha = c_\alpha\left(\frac{KT_M^2}{\alpha}\right) - b_\alpha(2KT_M) \qquad (1)$$

where K is the Boltzmann constant, T_M is the glow peak temperature, α is τ or δ ($\tau = T_M - T_1$ and $\delta = T_2 - T_M$), T_1 (rising end) and T_2 (falling end) are the temperatures at the half widths of the glow peak. The values of c_α and b_α are summarised in Eqs. (2) - (3).

$$c_\tau = 1.510 + 3.0(\mu - 0.42) \quad \text{and} \quad b_\tau = 1.58 + 4.2(\mu - 0.42) \qquad (2)$$

$$c_\delta = 0.976 + 7.3(\mu - 0.42) \quad \text{and} \quad b_\delta = 0 \qquad (3)$$

Frequency factor (S) is a constant characteristic of the electron trap, called the preexponential frequency factor or attempt-to-escape frequency. This parameter is proportional to the frequency of the collisions of the electron with the lattice phonons. The frequency factor can be calculated using the following equation (4):

$$\frac{\beta E}{KT_M^2} = (S)\exp\left(-\frac{E}{KT_M}\right)\left[1 + (b-1)\left(\frac{2KT_M}{E}\right)\right] \qquad (4)$$

where β is the heating rate.

4.3 UV-Vis spectroscopic measurements

Absorption spectra of all the samples were recorded using the bulk form of the samples. All spectra were measured at the Chemistry Department, Ubon Ratchathani University. The spectrophotometer (Perkin Elmer Instrument, Lambda 25) results were recorded at a range of 300-900 nm with a resolution of 0.1 nm.

4.4 Density and molar volume measurements

The density (ρ) of each sample was measured using Archimedes' principle with n-hexane as the immersion liquid. The experiments were repeated three times to obtain an accurate value of the density. The molar volume (V_a) was calculated for each glass sample from the expression; $V_a = \frac{M}{\rho}$, where M is the molecular weight of the glass, calculated according to the relation (5) [12].

$$M = \sum_i x_i M_i \qquad (5)$$

where x_i is the mole fraction of the component oxide i and M_i is its molecular weight. The glass packing density can be calculated from the following equations (6)-(7) [13]

$$\mathrm{V_t} = \frac{\rho}{\mathrm{M}} \sum_i x_i \mathrm{V}_i \qquad (6)$$

where V_i is given by,

$$\mathrm{V}_i = \frac{4\pi \mathrm{N_A}}{3}\left(x\mathrm{r_M^3} + y\mathrm{r_O^3}\right) \qquad (7)$$

where $\mathrm{N_A}$ is Avogadro's number, and where $\mathrm{r_M}$ and $\mathrm{r_O}$ are the ionic radii of the cation and anion of the oxide $\mathrm{M}_x\mathrm{O}_y$, respectively. The errors in molar volume and packing density were acquired from experiments repeated three times of densities.

4.5 Effective atomic number calculations

The effective atomic number (Z_{eff}) for all types of materials, compounds and mixtures, can be written in terms of the fraction abundance as Equation (8) [14]

$$\mathrm{Z_{eff}} = \frac{\sum_i \mathrm{f}_i \mathrm{A}_i \left(\mu/\rho\right)_i}{\sum_j \mathrm{f}_j \frac{\mathrm{A}_j}{\mathrm{z}_j}\left(\mu/\rho\right)_j} \qquad (8)$$

where $\mathrm{f}_i = \frac{\mathrm{n}_i}{\sum_j \mathrm{n}_j}$ is the fractional abundance of constituent element *i*, n_i is the total number of atoms and $\sum_j \mathrm{n}_j$ is the total number of atoms present in the molecular formula, A_i and z_i are the atomic weight and atomic number, respectively. $(\mu/\rho)_i$ is the mass attenuation coefficient obtained from the WinXCom program [15].

4.6 Ion concentration

The variation of ion concentration (N) can be calculated using the following equation [16]:

$$N = \frac{(\text{mol\% of dopant})(\rho)(N_A)}{M} \quad (\text{ions} \cdot \text{cm}^{-3}) \qquad (9)$$

where N_A is Avogadro's number. After determination of the ion concentration, three other related physical properties can be calculated using the standard relations [16-17]:

Polaron radius: $r_P = \frac{1}{2}\left(\frac{\pi}{6N}\right)^{1/3} \quad (\text{Å})$ (10)

Interatomic distance: $r_i = \left(\frac{1}{N}\right)^{1/3} \quad (\text{Å})$ (11)

Field strength: $F = \left(\frac{Z}{r_P^2}\right) \quad (\text{cm}^{-2})$ (12)

where Z is the valence number of the dopants.

4.7 Gamma irradiation

The glass samples were irradiated by an exposure machine (THREATRON 780C) using a Co-60 gamma-ray source at a dose rate of $1.16\ \text{Gy} \cdot \text{min}^{-1}$ and field size of $30 \times 30\ \text{cm}^2$, at a distance of 30 cm from the gamma-ray source, and at room temperature. The samples were irradiated for sufficiently long enough to achieve to overall dose of requirements.

4.8 Ultrasonic measurements

An ultrasonic flaw detector, SONATEST Sitescan 230, was used to measure ultrasonic velocity. The ultrasonic waves were generated from a ceramic transducer (Probe model: SLG4-10 for longitudinal velocity and SA04-45 for shear velocity) with a resonant frequency of 4 MHz, and acting as transmitter-receiver at the same time. The ultrasonic wave velocity (V) can be calculated by following equation (13) [18]

$$v = \frac{2d}{\Delta t} \quad (cm \cdot s^{-1}) \qquad (13)$$

where d is the samples thickness (cm) and Δt is the time interval (s). The measurements were repeated three times to check the reproducibility of the data.

4.9 FTIR measurements

FTIR spectra of powdered glass samples were recorded at room temperature using KBr disc technique. The spectra in the wave number range of $400 - 4000\ cm^{-1}$ with a resolution of $4\ cm^{-1}$ were obtained using Perkin-Elmer spectrometer.

4.10 Determination of elastic moduli

Elastic moduli include longitudinal (L), shear (G), bulk (K), and Young's (E) modulus as well as Debye temperature (θ_D), softening temperature (T_s), micro-hardness (H) and Poisson's ratio (σ) of glass samples have been determined from the measured the ultrasonic velocities and densities using the standard relations (14)-(21) [19]:

Longitudinal modulus: $L = \rho v_L^2$ (14)

Shear modulus: $G = \rho v_S^2$ (15)

Bulk modulus: $K = L - \frac{4}{3}G$ (16)

Young's modulus: $E = (1+\sigma)2G$ (17)

Poisson's ratio: $\sigma = \frac{L - 2G}{2(L - G)}$ (18)

Micro-hardness: $H = \frac{(1-2\sigma)E}{6(1+\sigma)}$ (19)

Debye temperature: $\theta_D = \left(\frac{h}{k_B}\right)\left(\frac{3zN_A}{4\pi V_a}\right)^{1/3} v_m$ (20)

Softening temperature: $T_s = \frac{v_S M}{C^2 z}$ (21)

where h is Planck's constant, k_B is Boltzmann's constant, N_A is Avogadro's number, z is the number of atoms in the chemical formula, C is the constant of proportionality (equals

$507.4\ \mathrm{m \cdot s^{-1} \cdot K^{1/2}}$) and v_m is the mean ultrasonic velocity defined by the relationship (22) [20].

$$v_m = \left[\frac{3v_L^3 v_S^3}{v_L^3 + v_S^3} \right]^{1/3} \tag{22}$$

The uncertainties in elastic moduli, Poisson's ratio, micro-hardness, Debye temperature and softening temperature were acquired from experiments repeated three times of the densities and the ultrasonic velocities.

4.11 Theoretical models

A bond compression model is a helpful introduce for structures containing only on type of bond. For a three dimensional multicomponent oxide glass, the bond compression bulk modulus is given by equation (23) [21]

$$K_{bc} = \frac{n_b \overline{F}}{9} r^2 \tag{23}$$

where r is the bond length between anion and cation and n_b is the number of network bonds per unit volume of the glass given by equation (24) [21]

$$n_b = \frac{N_A}{V_a} \sum_i (x n_f)_i \tag{24}$$

where x is the mole fraction of the component oxide i. $\overline{F}$ is the average of stretching force constant and can be calculated from following equation (25) [22]

$$\overline{F} = \frac{\sum (x n_f F)_i}{\sum (x n_f)_i} \tag{25}$$

where n_f is the coordination number of the cation and F is the stretching force constant of the oxide. The average atomic ring size (l) of a structure consisting of a three-dimensional network according to the ring deformation model is shown in the form of equation (26) [23]

$$l = \left[0.0106 \frac{\overline{\mathrm{F}}}{\mathrm{K}_{\mathrm{exp}}} \right]^{0.26} \quad (26)$$

The calculation of Poisson's ratio for the multicomponent oxide glasses according to the bond compression model is given by equation (27) [21]

$$\sigma_{\mathrm{cal}} = 0.28(\overline{\mathrm{n}}_{\mathrm{c}})^{-0.25} \quad (27)$$

where $\overline{\mathrm{n}}_{\mathrm{c}}$ is the average cross-link density of the glass network and is given by equation (28) [21]

$$\overline{\mathrm{n}}_{\mathrm{c}} = \frac{1}{\eta} \sum_{i} (\mathrm{n}_{\mathrm{c}})_i (\mathrm{N}_{\mathrm{c}})_i \quad (28)$$

where n_{c} is the number of cross-links per cation (number of bridging bonds per cation minus two) in oxide i. N_{c} is the number of cations per glass formula unit and $\eta = \sum (\mathrm{N}_{\mathrm{c}})_i$ is the total number of cations per glass formula unit. The theoretical bulk modulus ($\mathrm{K}_{\mathrm{cal}}$) can be calculated from equation (29) [22]

$$\mathrm{K}_{\mathrm{cal}} = 1.062 \times 10^{-29}\, \overline{\mathrm{F}} l^{-4.0022} \quad (29)$$

The other theoretical elastic moduli can be obtained from the bulk modulus and Poisson's ratio for each glass system as equations (30)-(32) [22]

$$\mathrm{G}_{\mathrm{cal}} = (1.5)\mathrm{K}_{\mathrm{cal}} \left[\frac{1 - 2\sigma_{\mathrm{cal}}}{1 + \sigma_{\mathrm{cal}}} \right] \quad (30)$$

$$\mathrm{L}_{\mathrm{cal}} = \mathrm{K}_{\mathrm{cal}} + (1.33)\mathrm{G}_{\mathrm{cal}} \quad (31)$$

$$\mathrm{E}_{\mathrm{cal}} = 2(1 + \sigma_{\mathrm{cal}})\mathrm{G}_{\mathrm{cal}} \quad (32)$$

The number of vibrating atoms per unit volume (N/V) will be expressed as follows (33) [24]

$$\frac{\mathrm{N}}{\mathrm{V}} = \frac{\mathrm{N}_{\mathrm{A}}}{\mathrm{V}_{\mathrm{a}}} \sum_{i} x(\mathrm{n} + \mathrm{m})_i \quad (33)$$

where $(n+m)$ is the sum of the atoms present in the $i-th$ oxide of the chemical formula.

5. Results and discussions

5.1 Results of RWG testing

Table 1 shows the condition of quantitative measurement of the chemical composition of recycled window glass (RWG) by using the WDXRF method. The major components of window glass are SiO_2, Na_2O, CaO, MgO, Al_2O_3, Fe_2O_3, TiO_2 and K_2O respectively. The absence of crystallization peaks in the XRD data showed that the window glass was amorphous (Figure 2). The thermoluminescence samples irradiated with 100 keV photon energy at doses of 2.01, 4.07, 6.00, 8.03, 10.06 and 14.05 mGy were measured and are shown in Figure 3. From observations, the glow curves centered at about 235 °C and the relative light intensity of TL signals increased with increasing irradiation dose. The investigation of the dependence of the TL signal on irradiation dose was carried out on window glass samples exposed to photons for doses between 0-14.05 mGy. The average integrated TL signals of each dose were recorded and the relative standard deviations were calculated.

Table 1 Condition of quantitative measurement of chemical composition of recycled window glasses (RWG) by using WDXRF method.

Chemical	line	Crystal	Detector	Collimator (μm)	kV	mA	Concentration (%)
Na_2O	K_α	PX1	Flow	4000	24	125	15.1700
MgO	K_α	PX1	Flow	4000	24	125	3.4030
SiO_2	K_α	PE002	Flow	300	24	125	73.3900
Al_2O_3	K_α	PE002	Flow	300	24	125	0.5866
CaO	K_α	LiF200	Flow	300	24	125	7.3390
Fe_2O_3	K_α	LiF200	Duplex	300	50	60	0.0635
TiO_2	K_α	LiF200	Flow	300	125	125	0.0263
K_2O	K_α	LiF200	Flow	300	125	125	0.0238

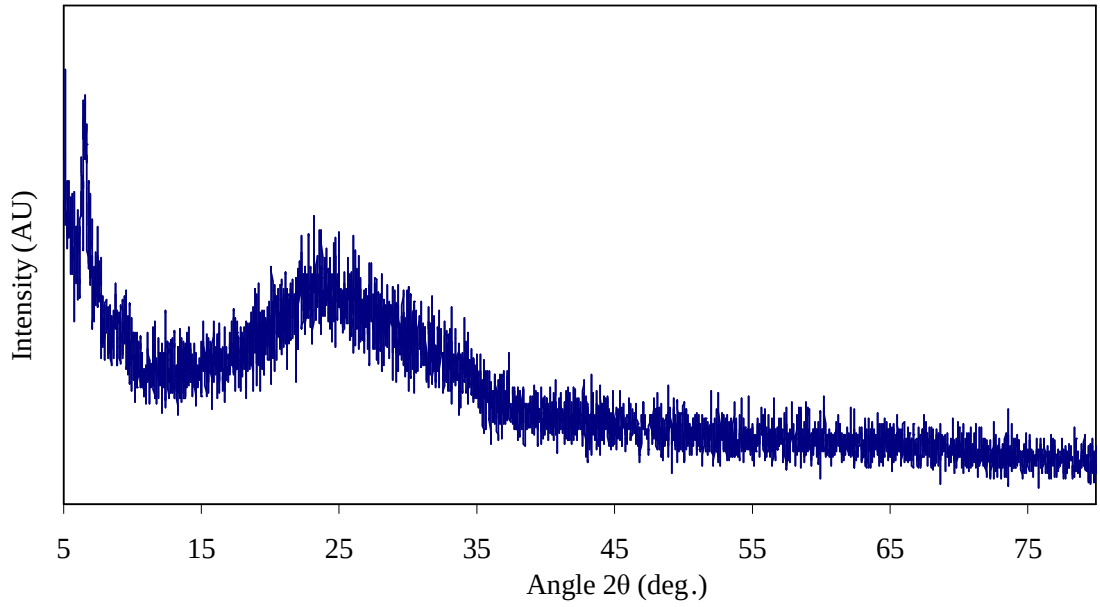

Figure 2. XRD pattern of window glasses (RWG)

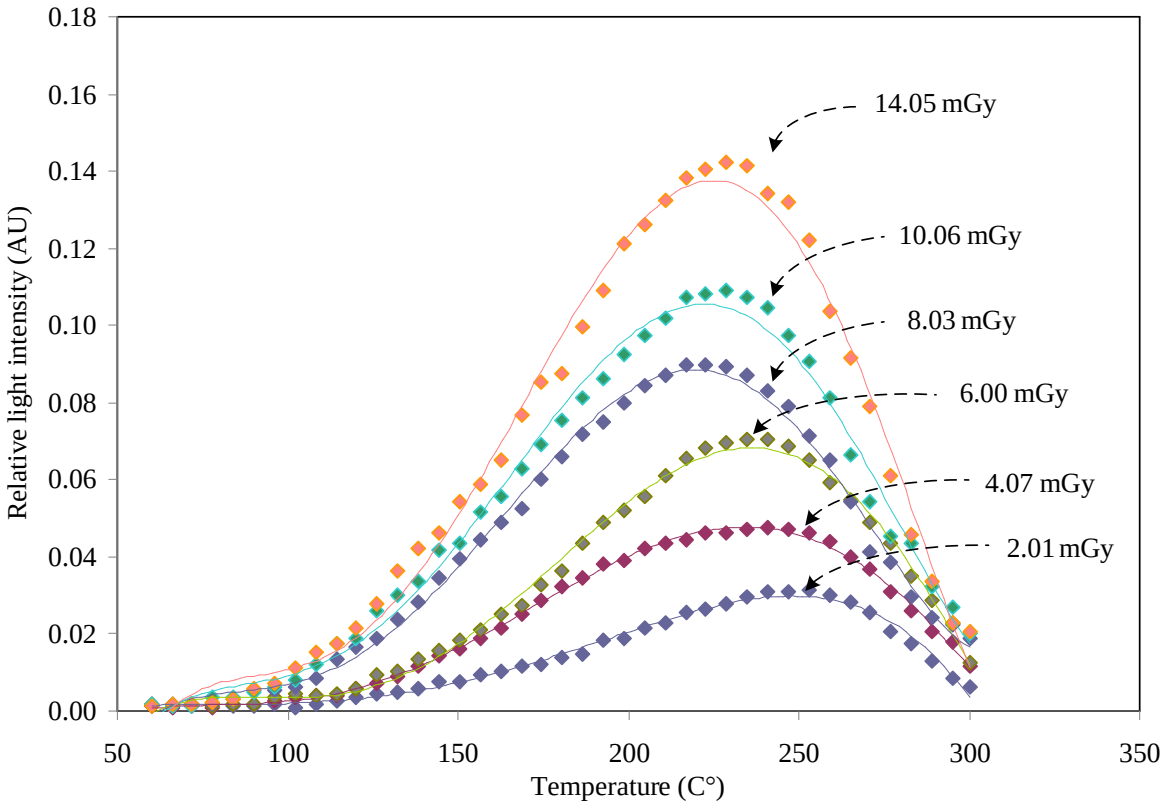

Figure 3. Glow curve of window glass (RWG) irradiated with different doses

Figure 4 shows the experimental trend obtained and the corresponding calibration line of best fit resulting from the processing of the experimental points. The correlation coefficient (R^2) was calculated to confirm the linearity of the dose response in the investigated dose range. The minimum detectable dose (MMD) value of window glass samples was determined as a dose of 3 times the corresponding value of the standard deviations of 10 un-irradiated samples. The estimated value of MMD obtained was about 0.15 mGy. Hence thermoluminescence intensities of the window glass were shown as likely to be used for low radiation doses.

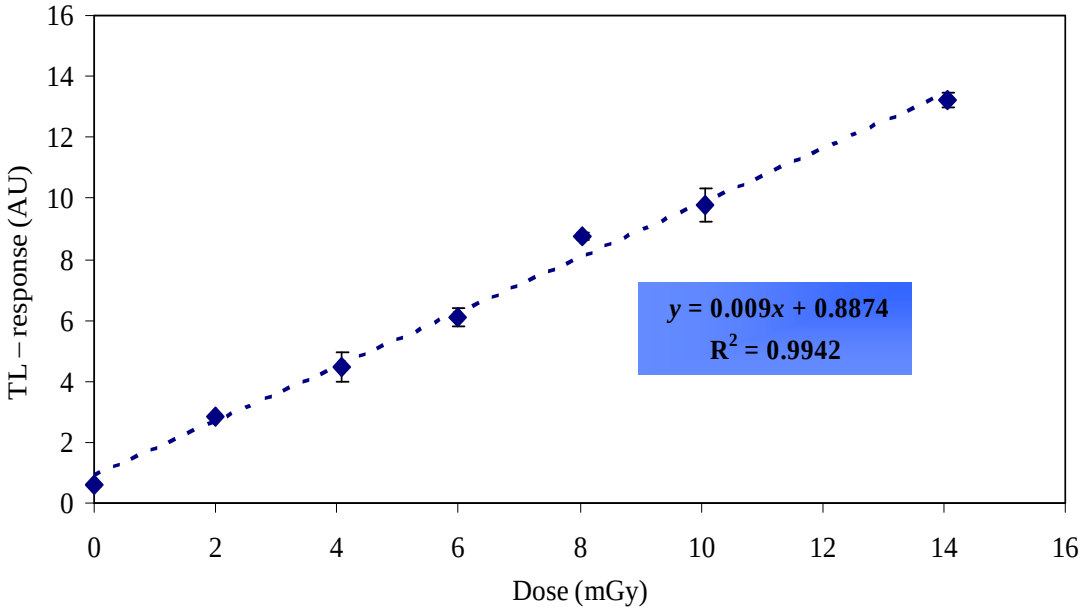

Figure 4. Linear relationship between TL-response and irradiation dose of RWG

From the Figure 5, the Figure 5 shows the reproducibility of the window glass (annealing $\rightarrow$ irradiation $\rightarrow$ readout). Data from Figure 5 reveal that the calibration lines for the first and the second irradiation are matching at low doses. For more information, the 10 samples were annealed by using a dual step process, and then irradiated with 10.08 mGy, and the TL signal was read out. This procedure was carried out for five cycles. The experimental values obtained are reported in Table 2 and the average values are shown in Figure 6. The results indicated that after the reproducibility procedure the sensitivity increased as shown in Figure 5. This was due to the improvement of the electron trap by heat treatment [25].

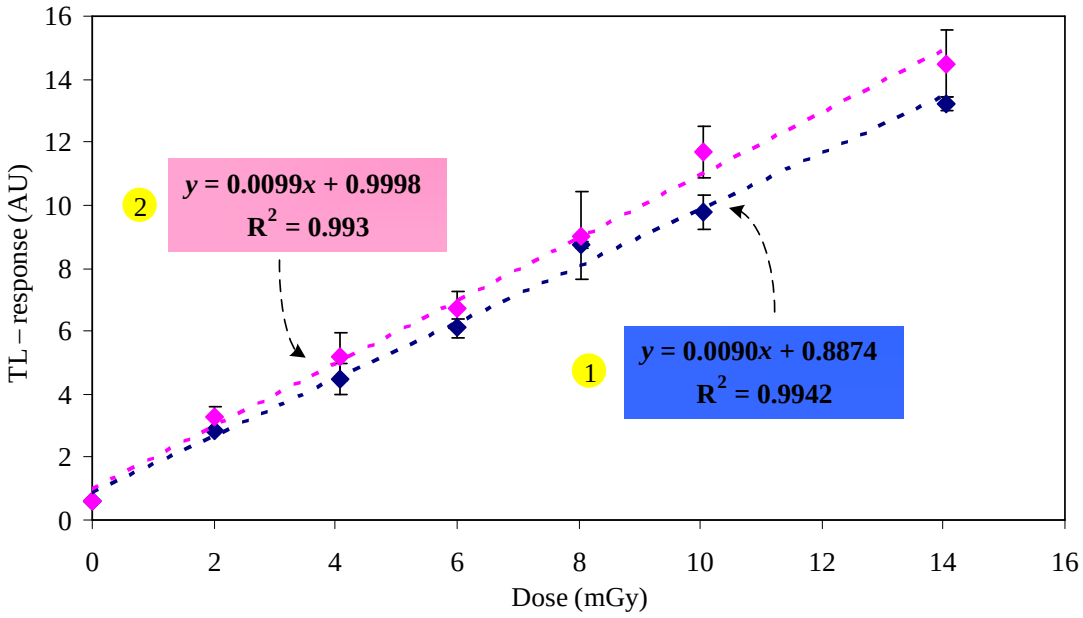

Figure 5. Reproducibility of window glasses with blue line (1) is first irradiation and pink line (2) is second irradiation

Table 2 Data for reproducibility of TLD measurement of recycled window glasses (RWG)

Chip No.	1st reading	2nd reading	3rd reading	4th reading	5th reading
1	12.550	12.010	12.780	12.320	12.220
2	11.850	12.720	12.580	12.310	12.340
3	9.656	10.150	10.530	9.231	10.100
4	12.390	11.940	12.110	12.320	12.430
5	13.930	12.430	13.210	12.780	13.560
6	11.580	10.750	11.570	11.120	11.780
7	11.440	10.600	11.330	10.450	11.250
8	11.060	10.880	11.420	10.970	10.190
9	7.435	7.971	8.190	7.952	8.342
10	8.585	8.933	9.112	8.631	9.210

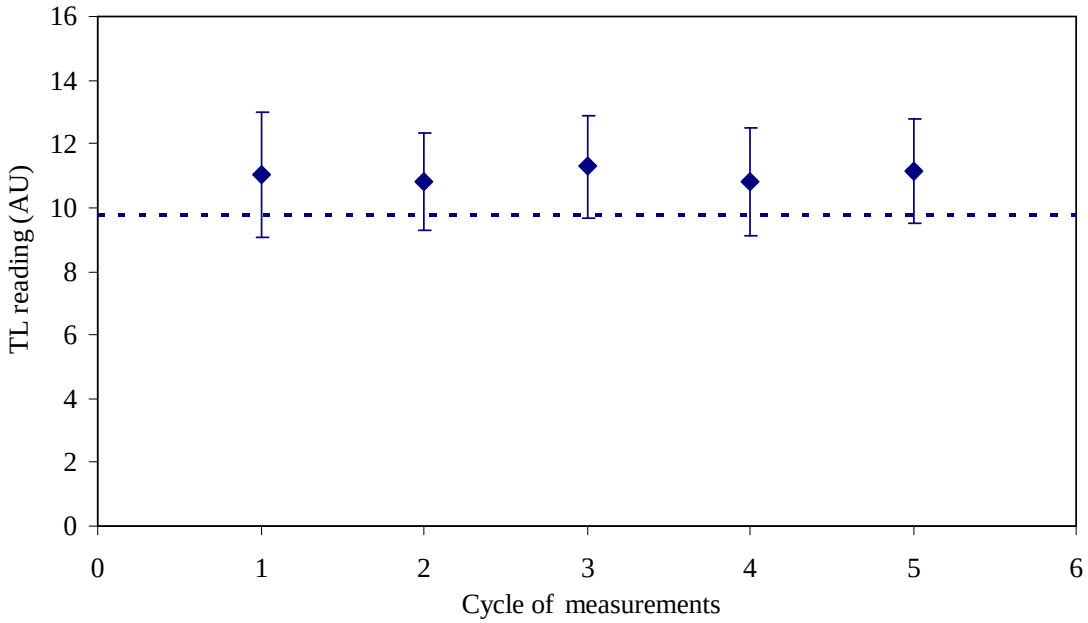

Figure 6. Reproducibility of window glass samples (RWG) with 10.08 mGy for five cycles (dash line is initial read out). Error bars correspond to one standard deviation

The statistical analysis to represent the reproducibility used the coefficients of variation analysis method. Covariance (CV) is a measure of how much two random variables change together. The following coefficients of variation can be defined [25] as:

The system variability index (SVI) or $\%\overline{CV} = \frac{SD}{\overline{X}} \times 100$; this is the mean value of percent standard deviations of each TL detector. This quantity gives a measure of the reproducibility of the whole system. The variation of SVI is 3.6% (Table 3).

The reader variability index (RVI) or $\%CV = \frac{SD}{mean} \times 100$; this is the percent standard deviations of the mean values of each cycle of readings. This quantity gives a measure of the long-term reader reproducibility. The variation of RVI is 1.8% (Table 4).

The detector variability index (DVI); this quantity gives a measure of the reproducibility of the TL detectors (samples), and is defined as:

$$DVI = \sqrt{(SVI)^2 - (RVI)^2} = 3.1\%$$

Table 3 Calculation of system variability index (SVI). The average values of the five reading calculated from Table 2.

Chip No.	Average values of the five reading: $\overline{X}$	Standard deviation: SD	Covariance: $CV = SD/\overline{X}$
1	12.376	0.298	0.024
2	12.360	0.332	0.027
3	9.933	0.500	0.050
4	12.238	0.207	0.017
5	13.182	0.598	0.045
6	11.360	0.418	0.037
7	11.014	0.455	0.041
8	10.904	0.449	0.041
9	7.978	0.344	0.043
10	8.894	0.280	0.031
$\overline{CV}$			0.036
$SVI = \overline{CV} \times 100$			3.6%

Table 4 Calculation of reader variability index (RVI). The values of each reading are average of TL signal of all Chip No. in Table 2.

1st reading	2nd reading	3rd reading	4th reading	5th reading	mean	SD	$RVI = \frac{SD}{mean} \times 100$
11.048	10.838	11.283	10.808	11.142	11.024	0.202	1.8%

The DVI values indicated the high reproducibility of samples. However, the reproducibility of window glass samples required improvement when compared with the initial read out (Figure 6). The author suggests that electron trapping should be improved by adding the modifier for constant trapping in the structure of the glass. This point is worthy of further investigation in the near future.

The most important problems in TL technique applied to different fields of dosimetry, such as personal, environmental and clinical dosimetry, are related to the loss of the stored TL signal after irradiation, generally called thermal fading (trapped charge effects), and to its evaluation [26]. Figure 7 shows the average integrated TL intensity after a storage period of

1440 hours at a dose of 14.05 mGy. This figure demonstrates a large decrease in the TL signal in the initial range (about 65% decreased at 0-200 hours). These results suggest that the high loss of TL signal is due to un-stabilization of trapped charge effects. However, the TL signals become constant after a storage period of 200 hours.

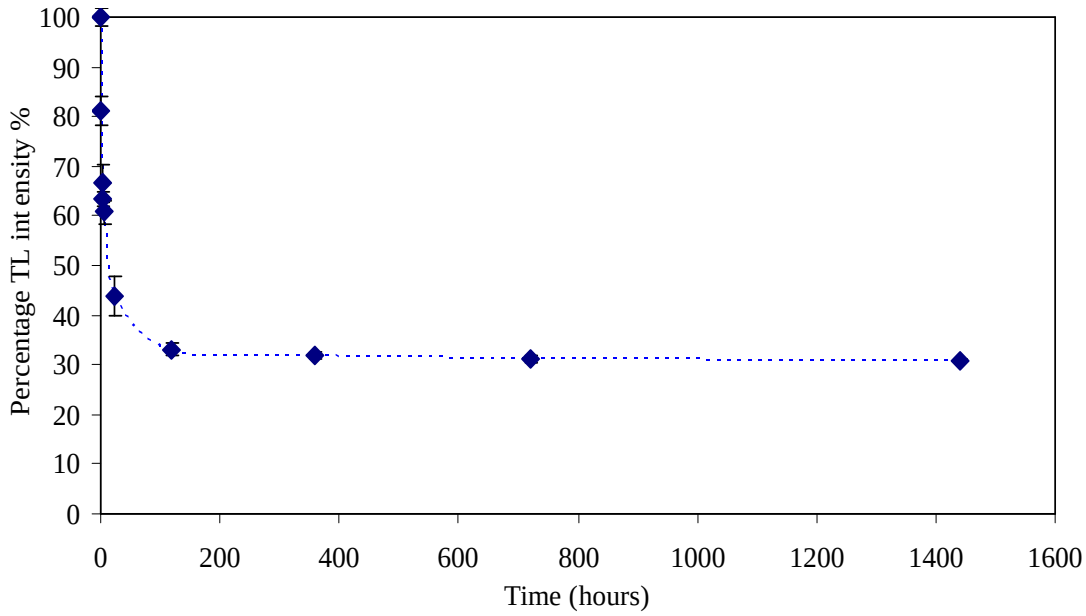

Figure 7. Fading of irradiated window glass at room temperature

Figure 8 shows the average integrated TL intensity after the irradiation of window glass at 6.00 mGy with different radiation energies (25, 50, 75, 100 and 110 keV, respectively) which predict the energy dependent behavior of the window glass. The energy dependence for window glass may be highly related with the value of effective atomic number (Z_{eff}) [5]. Figure 9 shows the effective atomic numbers of window glass. It has been observed that the effective atomic numbers decrease with incident photon energy up to 15 keV. Then, effective atomic numbers suddenly increase with incident photon energy up to 150 keV. After that, effective atomic numbers become relatively constant with incident photon energy in the range 200-7000 keV. Effective atomic numbers slightly decrease with photon energy in the range 8-50 MeV. Then, effective atomic numbers become independent of the incident photon energy in the range 60-100000 MeV. The investigated energy range from 25 to 110 keV shows a linear increase of effective atomic number. This can be explained on the basis of dominance of the photoelectric process. For the photoelectric interaction near the K-edge of the elements with the high Z numbers [27] (Table 1), the effect of impurity of the window glass on the photoelectric effect is

higher than the Compton effect in the studied energy range. Moreover, the effective atomic numbers obtained in this study show that it is very close to human biological tissues (Z_{eff} = 6.7—8.4 at studied energy).

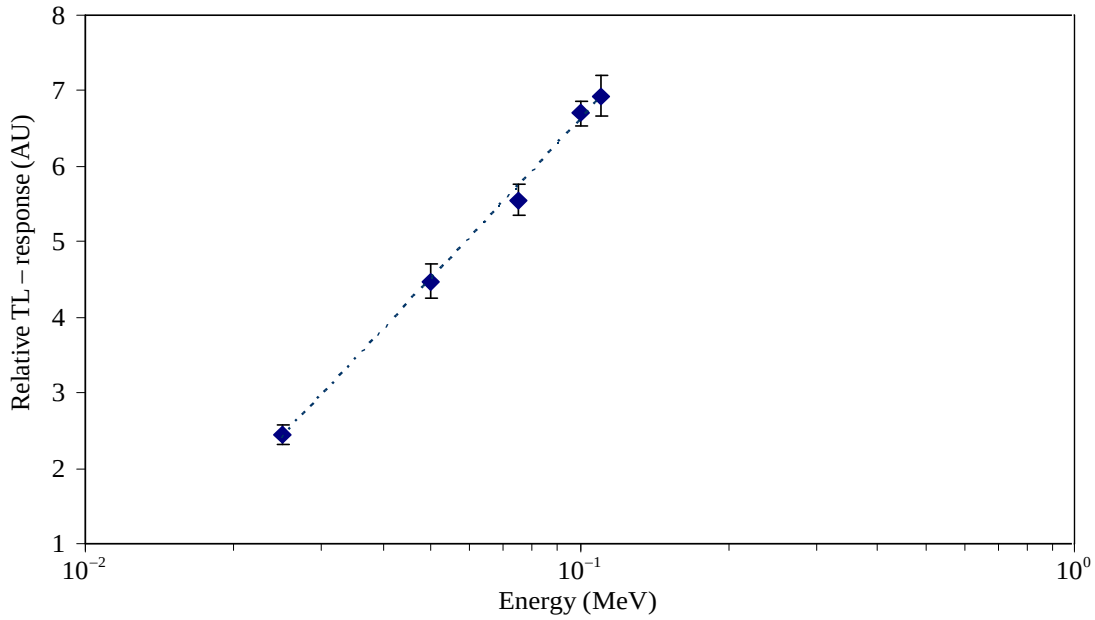

Figure 8. The photon energy dependence of window glasses

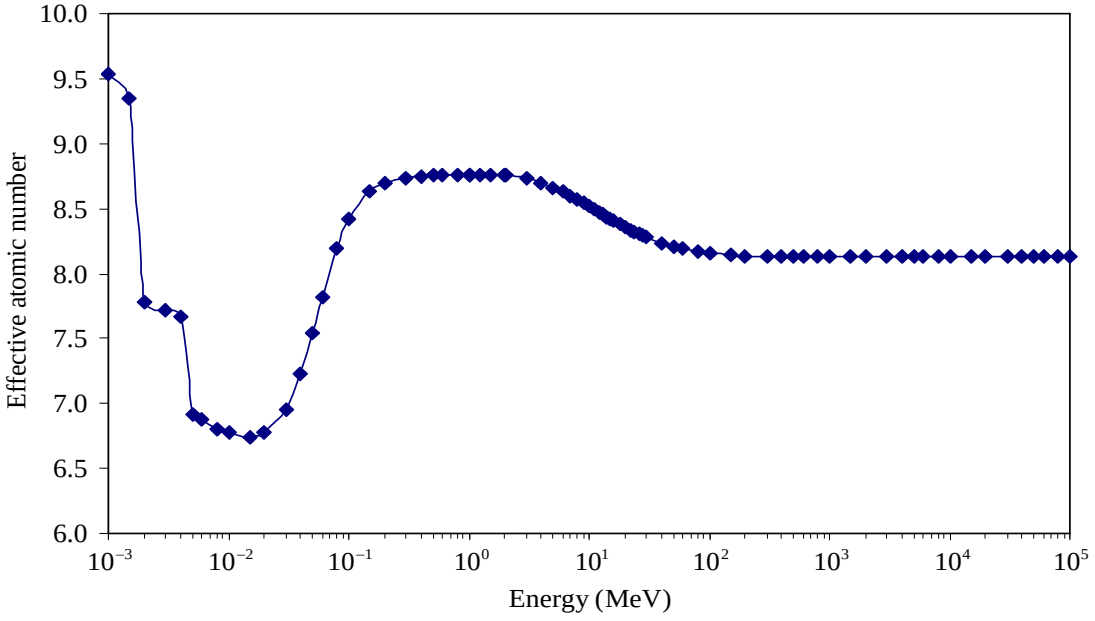

Figure 9. The effective atomic number of window glasses with difference photon energy

To confirm these results, the mass energy absorption coefficients were calculated by comparison between window glass and soft tissue. The mass attenuation coefficients of window glass were obtained from the WinXCom program. The mass energy absorption coefficients of soft tissue were obtained from ICRU-44 [28]. The results are shown in Figure 10, with good agreement of trend lines of mass energy absorption coefficients between samples and soft tissue. In order to verify that the window glass is tissue equivalent, the ratio of Z_{eff} for window glass and the Z_{eff} for soft tissue was considered. Alajerami et al. [29] reported that the human tissue Z_{eff} is 7.42. Therefore, the effective atomic number of window glass was compared with the Z_{eff} of human tissue [29]. The ratio $\left(R = \frac{Z_{eff} \text{ of sample}}{Z_{eff} \text{ of human tissue}} \right)$ is in the range of 0.9—1.1 (at studied energy) which is close to 1. The result was sufficient to state that the window glass is tissue equivalent.

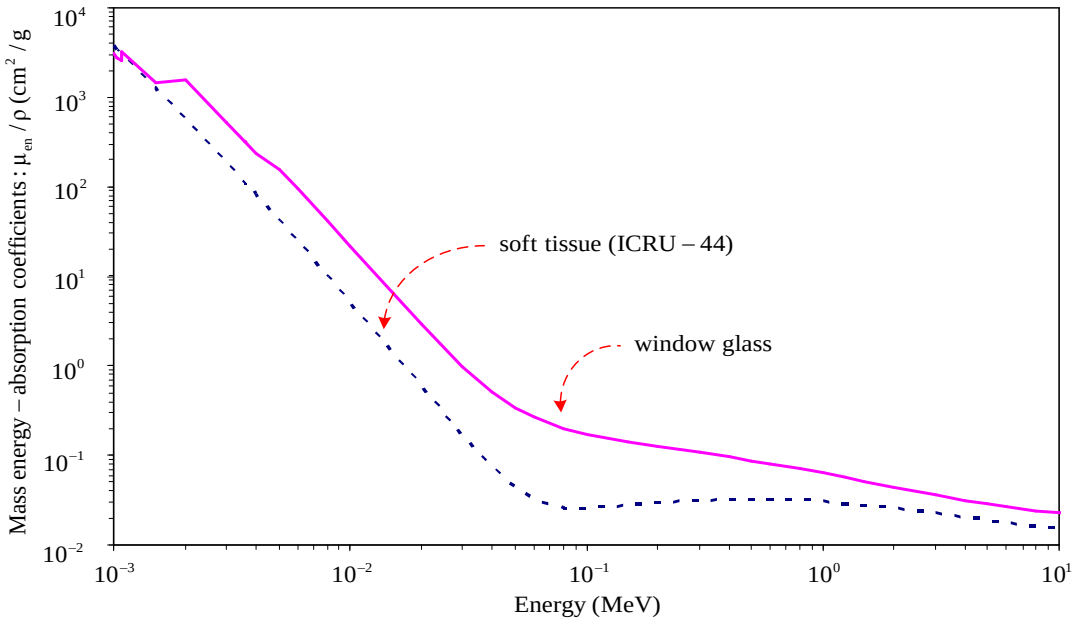

Figure 10. Comparison mass energy-absorption coefficients between window glass and soft tissue (ICRU-44)

The results obtained show that the window glass (RWG) sold in Ubon Ratchathani province, Thailand, is potentially a good candidate for retrospective dosimetry or personal dosimetry due to its common materials, easy sample preparation, linearity of TL response and because its effective atomic number is close to that of human biological tissues. However, the results also show differences in reproducibility and a high fading of the TL signal of window

glass. Therefore, the improvements of TL properties of window glass as starting materials would provide an interesting study.

5.2 Thermoluminescence properties of glass samples

The Binary $(100-x)\mathrm{RWG}-(x)\mathrm{Na_2O}$ glass with different concentrations of Na_2O was prepared. The results showed that the $(90)\mathrm{RWG}-(10)\mathrm{Na_2O}$ glass system had the highest sensitivity (Figure 1), therefore this condition was selected as the base glass ($\mathrm{G}-0$). Then, the $(90)\mathrm{RWG}-(10)\mathrm{Na_2O}-(x)\mathrm{R_mO_n}$ glass systems were prepared as mentioned in section 4.1.3. The chemical composition of the glass samples are shown in Table 5.

Table 5 Details of the chemical composition of the glass samples.

Glass sample	Compositions (mol%)				
	RWG	Na_2O	CeO_2	Nd_2O_3	MnO_2
$\mathrm{S-Ce1}$	90	10	0.001	-	-
$\mathrm{S-Ce2}$	90	10	0.010	-	-
$\mathrm{S-Ce3}$	90	10	0.100	-	-
$\mathrm{S-Ce4}$	90	10	1.000	-	-
$\mathrm{S-Nd1}$	90	10	-	0.001	-
$\mathrm{S-Nd2}$	90	10	-	0.010	-
$\mathrm{S-Nd3}$	90	10	-	0.100	-
$\mathrm{S-Nd4}$	90	10	-	1.000	-
$\mathrm{S-Mn1}$	90	10	-	-	0.001
$\mathrm{S-Mn2}$	90	10	-	-	0.010
$\mathrm{S-Mn3}$	90	10	-	-	0.100
$\mathrm{S-Mn4}$	90	10	-	-	1.000

The main glow curves of the various concentrations of CeO_2, Nd_2O_3 and MnO_2 doped soda lime glasses exposed with 100 keV of photon energy at a dose of 14 mGy are presented in Figures 11 to 13. They show a single main glow curve for CeO_2 and Nd_2O_3 doped glass samples, with all samples exhibiting a TL peak at 180 °C and 195 °C. The MnO_2 doped glass samples show similar main glow curves for all concentrations, centred with peaks 1 and 2 at 185 °C and 266 °C respectively. The dopants caused significant changes in the TL signal. The results indicated that electron trap created by the dopants. However, the more concentration of

dopant leads to the break down of the host structure and resulting to decrease of the TL signal. The highest TL intensity reflected by either the total integrated area under the glow peaks, or that recorded in the reading system, was at 0.010 mol% for CeO_2 $(S-Ce2)$, 0.100 mol% for Nd_2O_3 $(S-Nd3)$ and 0.010 mol% for MnO_2 $(S-Mn2)$ as shown in Figure 11 (a), 12 (a) and 13 (a) respectively. The important role played by the dopant ions in TL emission is in the trap filling process that may arise through the direct transfer of electrons from the excited state of dopants to trap centres [30-32]. Linearity is a very important property of any thermoluminescence dosimetric application and defines a linear relationship between the TL signal and the irradiated dose. The linearity range depends on the particular thermoluminescence material. The preferred response of TL emission is linear at low irradiation dose values, becoming supralinear and finally saturated at high values [33]. In this study, an investigation of the dependence of the TL signal on irradiation dose was performed on glass samples exposed to photons for doses between 0 and 14 mGy. The average integrated TL signal of each dose was recorded and the relative standard deviation calculated as shown in Figures 11 (b) to 13 (b). The Figures show the experimental trend obtained and the corresponding calibration line of best fit, resulting from processing the experimental points. The correlation coefficients (R^2) were calculated to confirm the linearity of the response in the investigated dose range. The results indicated that glass samples doped with CeO_2 at 0.010 mol% $(S-Ce2)$, Nd_2O_3 at 0.100 mol% $(S-Nd3)$ and MnO_2 at 0.010 mol% $(S-Mn2)$ gave the best linearity, as shown in Figures 11 (b) to 13 (b). From these results (Figures 11 to 13), a lower detection limit values of $S-Ce2$, $S-Nd3$ and $S-Mn2$ glass samples were determined as three times the corresponding values of the standard deviations of ten non-irradiated of each samples. The D_{LDL} can be calculated by following relation [34]:

$$D_{LDL} = (3\sigma_{BKG})\Phi_C \qquad (34)$$

where σ_{BKG} is the standard deviation of the zero-dose reading. The calibration factor $\left(\Phi_C = \frac{D_C}{\overline{M}}\right)$ for the TL reader is given by the ratio of the calibration dose (D_C) divided by the average value of the net TL reading $(\overline{M})$. The estimated values of D_{LDL} obtained were 1.21 mGy, 1.82 mGy and 2.59 mGy for the $S-Ce2$, $S-Nd3$ and $S-Mn2$ glass samples respectively.

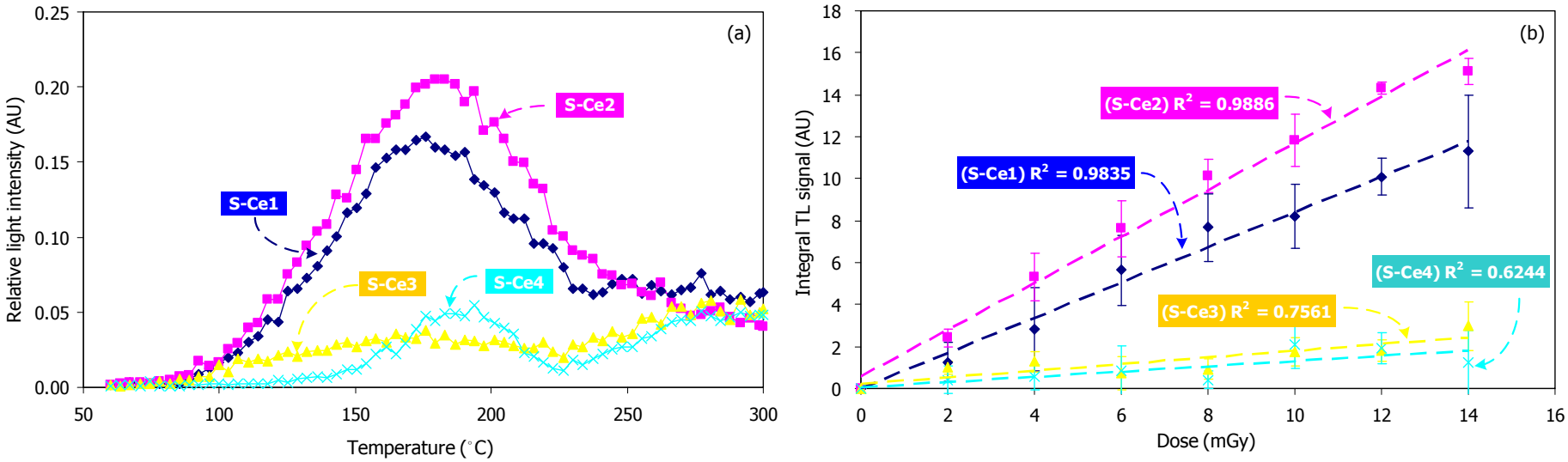

Figure 11 (a) Glow curve of the glass samples (doped with CeO_2) irradiated with X-ray photon energy of 100 keV at dose of 14 mGy, **(b)** linear relationship between TL response and irradiation dose of glass samples (doped with CeO_2).

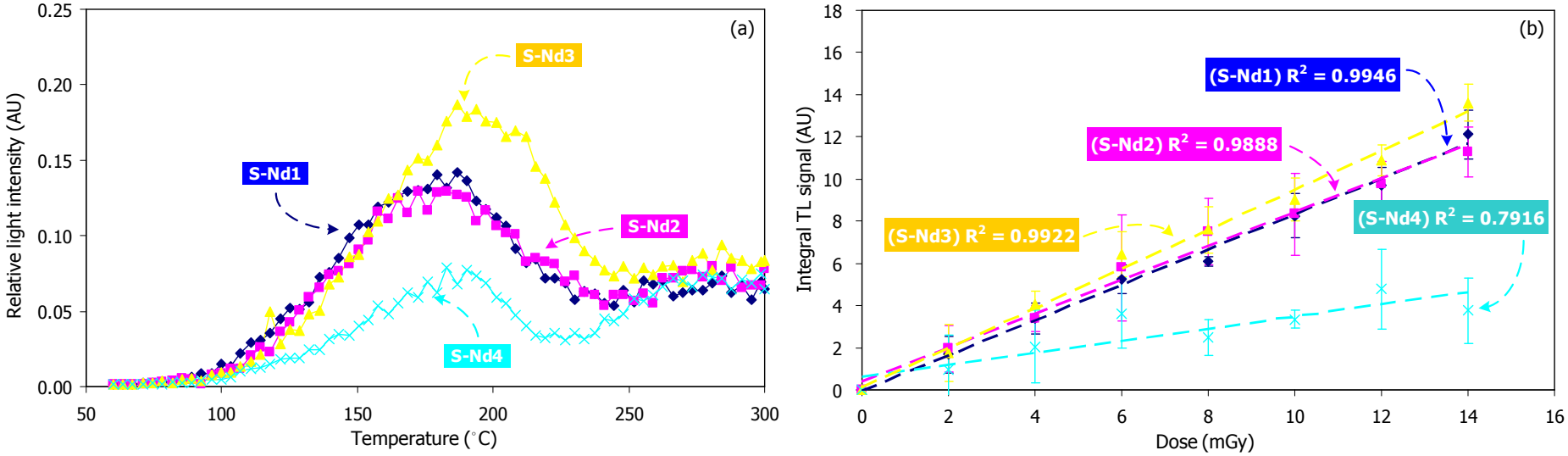

Figure 12 (a) Glow curve of the glass samples (doped with Nd_2O_3) irradiated with X-ray photon energy of 100 keV at dose of 14 mGy, **(b)** linear relationship between TL response and irradiation dose of glass samples (doped with Nd_2O_3).

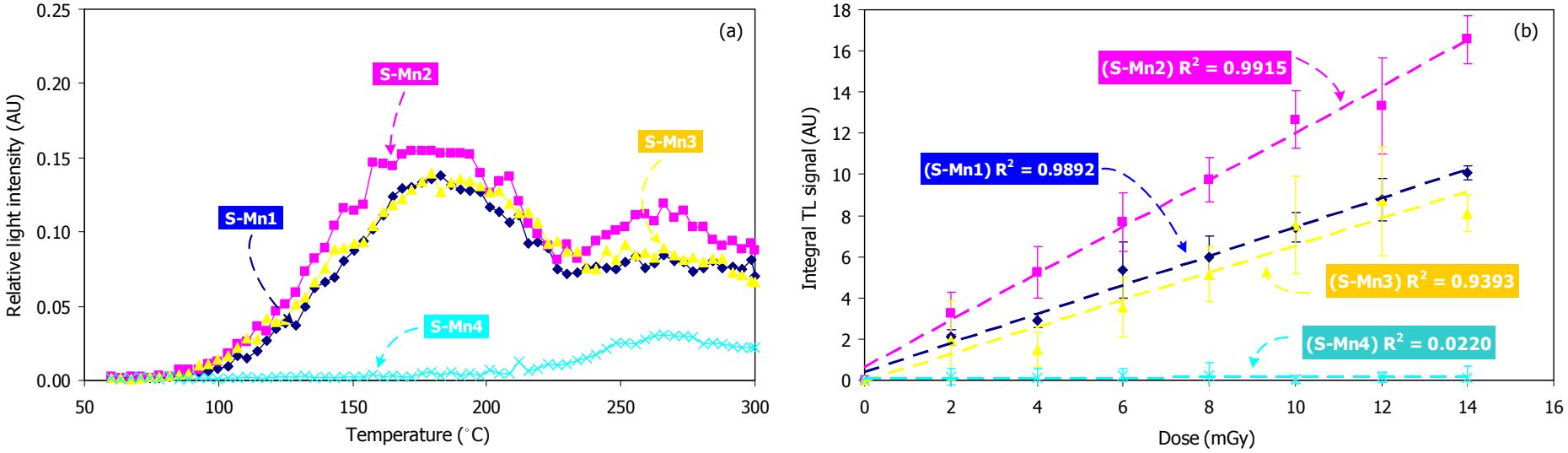

Figure 13 (a) Glow curve of the glass samples (doped with MnO_2) irradiated with X-ray photon energy of 100 keV at dose of 14 mGy, **(b)** linear relationship between TL response and irradiation dose of glass samples (doped with MnO_2).

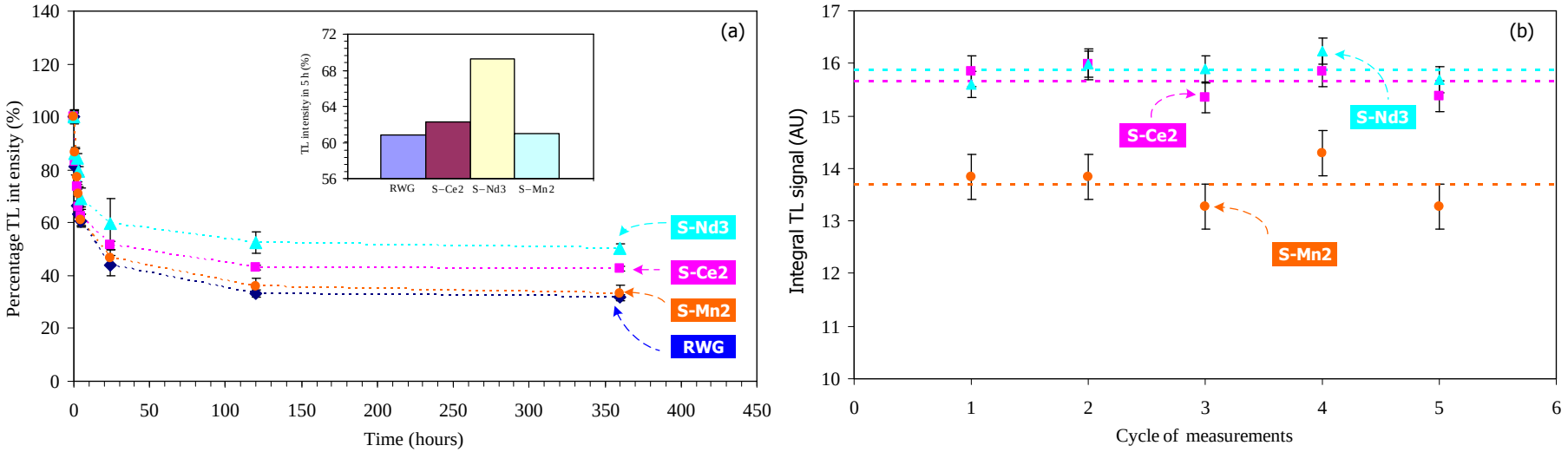

Figure 14 (a) Fading of glass samples irradiated with X-ray photon energy of 100 keV at dose of 14 mGy at room temperature and it was compared with the window glass (RWG) [35] and subscript with TL intensity of glass samples in 5 h, **(b)** Reproducibility of glass samples with 14 mGy for five cycles (dash line is average values of each samples). Error bars correspond to one standard deviation.

Table 6 Data on various trap depth parameters of selected glass samples.

Glass Type	T_m (°C)		τ (°C)		δ (°C)		μ		E_τ (eV)		E_δ (eV)		$S \times 10^6$ (s^{-1})	
	Peak 1	Peak 2	Peak 1	Peak 2	Peak 1	Peak 2	Peak 1	Peak 2	Peak 1	Peak 2	Peak 1	Peak 2	Peak 1	Peak 2
S – Ce2	180	-	44	-	45	-	0.506	-	0.576	-	0.597	-	32.415	-
S – Nd3	195	-	43	-	37	-	0.463	-	0.577	-	0.512	-	8.396	-
S – Mn2	185	266	45	48	48	47	0.516	0.495	0.585	0.834	0.625	0.803	60.328	445.002

The most important problems in TL technique applied to different fields of dosimetry, such as personal, environmental and clinical dosimetry, are related to the loss of the stored TL signal after irradiation, generally called thermal fading. Figure 14 (a) shows the stability of TL signals of the $S-Ce2$, $S-Nd3$ and $S-Mn2$ glass samples after a storage period of 360 h at a dose of 14 mGy, compared with the window glass (RWG) [35]. There were a rapid reduce in the TL signal in the initial range, (40%, 37%, 30% and 39% decreased at 0 – 5 h of the RWG, $S-Ce2$, $S-Nd3$ and $S-Mn2$ glass samples respectively). The samples fade slowly as the time passes and takes around 120 – 360 h in losing its 70%, 57%, 50% and 67% TL information of the RWG, $S-Ce2$, $S-Nd3$ and $S-Mn2$ glass samples respectively (Figure 14 (a)). This suggests that the lower loss of TL signal of the $S-Ce2$, $S-Nd3$ and $S-Mn2$ glass samples results from the higher stabilization of trapped charge effects when compared with the RWG. This will help in estimating the doses in case the sample could not be read on time due to some reason [36]. For more information, the 10 samples of the $S-Ce2$, $S-Nd3$ and $S-Mn2$ glass samples were annealed by using a dual step process, and then irradiated with 14 mGy, and the TL signal was read out. This procedure was carried out for five cycles. The results are shown in Figure 14 (b). From the results, it was found that the response does not vary by more than 4.3% over this number of cycles [6].

The best conditions from the results of the glow curve sensitivity and the linearity of the glass samples were selected to further investigate trap depth parameters, as shown in Table 6. For investigation of trap depth parameters, the general expressions for evaluating activation energy and trap depth derived by Chen are shown in Eqs. (1) to (3). The $S-Ce2$, $S-Nd3$ and $S-Mn2$ glass samples were selected for investigation of trap depth parameters due to their high sensitivity and good linearity. X-ray irradiation on the glass produces secondary electrons from sites where they are in a stable state, which now have excess energy and also non-bridging oxygens (NBOs). These electrons traverse through the glass lattice depending upon their energy and the composition of the glass network. They are finally trapped, forming colour centres. Alternatively, they may form excitons with energy states in the forbidden gap at the inherent structural defects. This mechanism leads to the formation of (i) electron centres, (ii) non-bridging oxygen hole centres and (iii) oxygen hole centres. Thermoluminescence occurs from the radiative recombination between the electrons released by heating from the electron centre, and anti-bonding molecular orbital of the nearest oxygen hole centre. The possible reactions under X-ray irradiation are:

(i) $R^{m+} \rightarrow R^{(m-1)+} + h^{+}$

(ii) $R^{m+} \rightarrow R^{m+} + h^{+} + e^{-}$

where R^{m+} are ions of CeO_2, Nd_2O_3 and MnO_2. For reaction (i), a hole trapped at a lattice site during irradiation recombines with $R^{(m-1)+}$ and produces a TL signal when the material is heated. For reaction (ii), the electrons and holes created in the lattice in the vicinity of R^{m+} ions during irradiation recombine at R^{m+} ion sites as the material is heated and emit a TL signal. Therefore, the ions of CeO_2, Nd_2O_3 and MnO_2 play important roles in improving the sensitivity and response to radiation dose of glass samples by trapping the excited electrons from X-ray irradiation. To be more accurate, the SiO_4 groups, irradiated with X-rays are changed to $[SiO_{3/2}O]^{-}$, $[SiO_{2/2}O_2]^{2-}$, $[SiO_{1/2}O_3]^{3-}$ and interstitial oxygen ions $\left(O_i^{-} \text{ ions}\right)$. During thermal excitation O_i^{-} ions distribute back to the silicate groups and excite them. This excitation is then transferred to the nearby modifier ions (R^{m+} ions) and produces TL emission as shown by the reaction below [37]:

$$O_i^{-} \xrightarrow{h\upsilon} [SiO_{v/2}O_u]^{u-} \rightarrow \left([SiO_{v/2}O_u]^{u-}\right)^{*} \rightarrow R^{m+} + h\upsilon[SiO_{v/2}O_u]^{u-}$$

where $u = 1, 2, 3$ and $v = 1, 2, 3$. During this process the local O_i^{-} ions compensate by capturing electrons from an $[SiO_{v/2}O_u]^{u-}$ site to form $R^{(m-1)+}$ ions, releasing electrons that will later recombine with silicate complexes. This excitation may encourage silicate complexes to dissociate and form different silicate groups and oxygen ions. The mechanism of this process can be represented as reaction [37]:

$$[SiO_{3/2}O]^{-} \xrightarrow{h\upsilon} [SiO_{2/2}O_2]^{2-} + e^{-} \quad \text{then} \quad R^{m+} + e^{-} \rightarrow R^{(m-1)+}$$

after the material is heated the $R^{(m-1)+}$ ions release an electron as reactions,

$$R^{(m-1)+} \rightarrow R^{m+} + e^{-} \quad \text{then} \quad [SiO_{2/2}O_2]^{2-} + e^{-} \rightarrow \left([SiO_{3/2}O]^{-}\right)^{*} \rightarrow \left([SiO_{2/2}O_2]^{2-} + O^{-}\right) / R^{m+} + h\upsilon$$

The mechanisms above show that the activation energy directly depends on the ability of electron trapping and/or release of dopant ions (R^{m+}) added to the structure units. The activation energies $\left(E_\tau \text{ and } E_\delta\right)$ are shown in Table 6. The frequency factor (S) is proportional to the frequency of the collisions of electrons with the lattice phonons and is a constant characteristic of the electron trap. The frequency factor is shown in Table 6, and is clearly

related to the type of dopant ions. Moreover, the value of the trap depths indicates that the lifetime (τ) of electrons in these traps is of the order of several months [38].

The result shows that the 3+ valency of modifiers ions are interesting on the TL properties. Therefore, the same conditions of experimental details were used with the glass samples was added Dy_2O_3. According to all of above, Dy^{3+} ion doping has been shown to cause significant increases in TL. The sensitivity of the TL signal was normalized with respect to the weights of each condition of the glass samples at a dose of 14 mGy and shown in Figure 15.

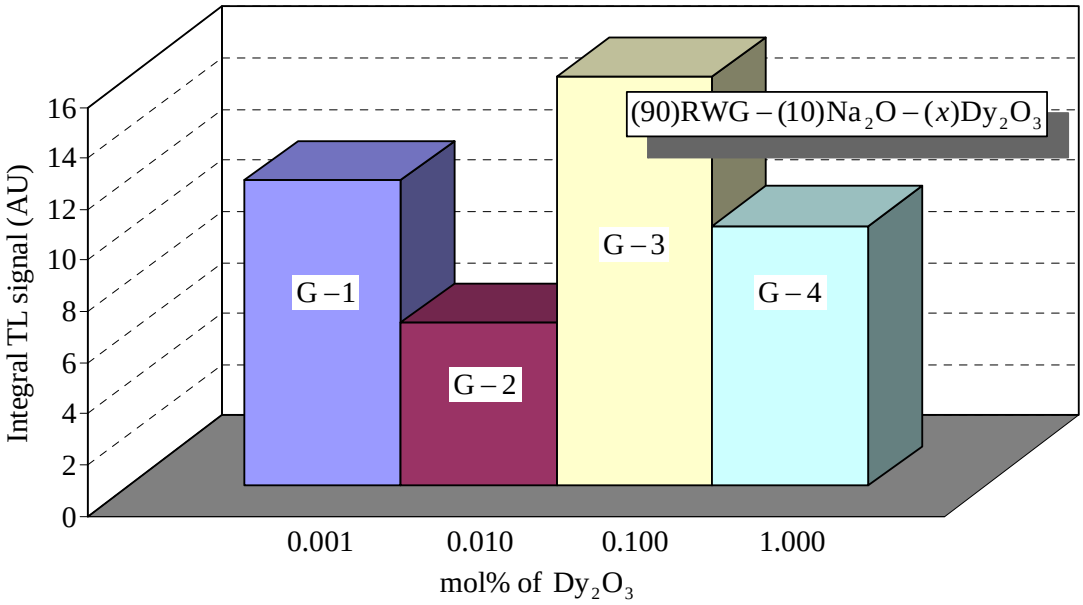

Figure 15 Integral TL signal of $(90)\mathrm{RWG}-(10)\mathrm{Na_2O}-(x)\mathrm{Dy_2O_3}$ glass system irradiated with X-ray photon energy of 100 keV at dose of 14 mGy. The sensitivity of TL signal was normalized with respect to the respective weights of the samples.

Wani et al. [39] reported that RE^{3+} ion doping resulted in increased sensitization of TL. The important role of Dy^{3+} ions in TL emission is the trap filling process that may arise through the direct transfer of electrons from the excited state of Dy^{3+} to trap centres. TL sensitivity slightly increased after Dy^{3+} doping as shown in Figure 15. This suggested that the impurities in the composition of RWG were strongly related to the intrinsic defects attributed to well-known concentration quenching phenomena and tallied with the results obtained by Hashim et al. [40]. Results showed that the highest integrated TL signal of the glass samples was for 0.100 mol% of Dy_2O_3, with all giving improved TL sensitivity after Dy^{3+} doping.

Figure 16 shows the stability of TL signals of the $G-3$ glass sample after a storage period of 720 hours at a dose of 14 mGy, compared with the window glass (RWG). There was a rapid decrease in the TL signal in the initial range, (45% and 65% decreased at 0-200 hours of the $G-3$ glass sample and RWG respectively). This suggests that the lower loss of TL signal of the $G-3$ glass sample results from the higher stabilization of trapped charge effects when compared with RWG. These results are supported by the fact that the stability and sensitivity of TL signals improved after Dy^{3+} doping. A brief description of this mechanism is presented in Figure 17.

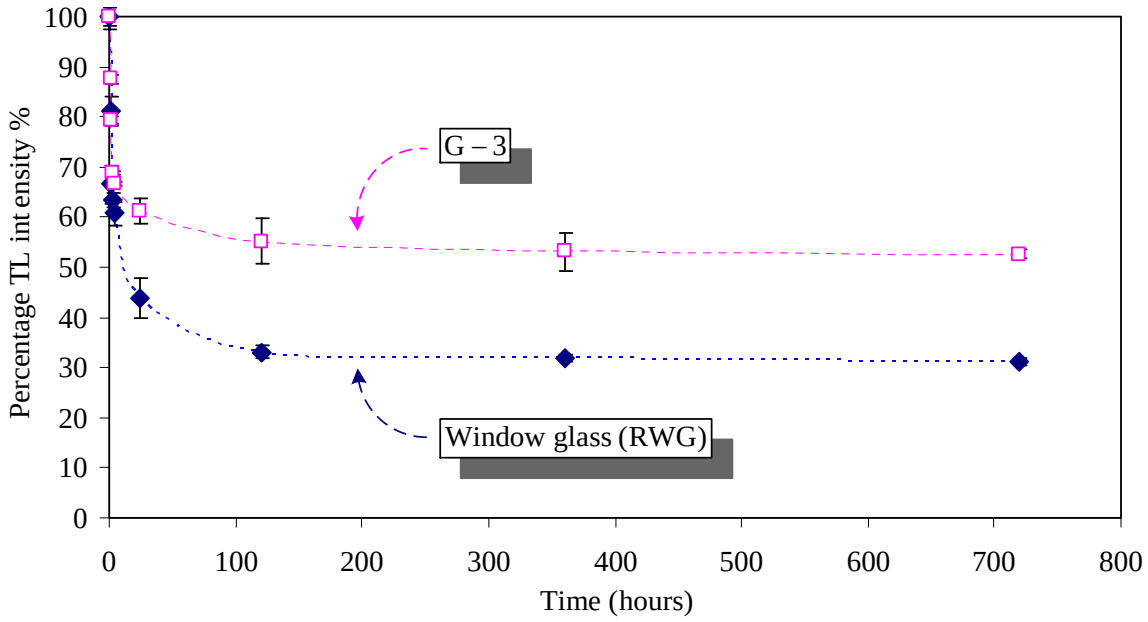

Figure 16 Fading of $G-3$ glass sample irradiated with X-ray photon energy of 100 keV at dose of 14 mGy at room temperature and it was compared with the window glass (RWG).

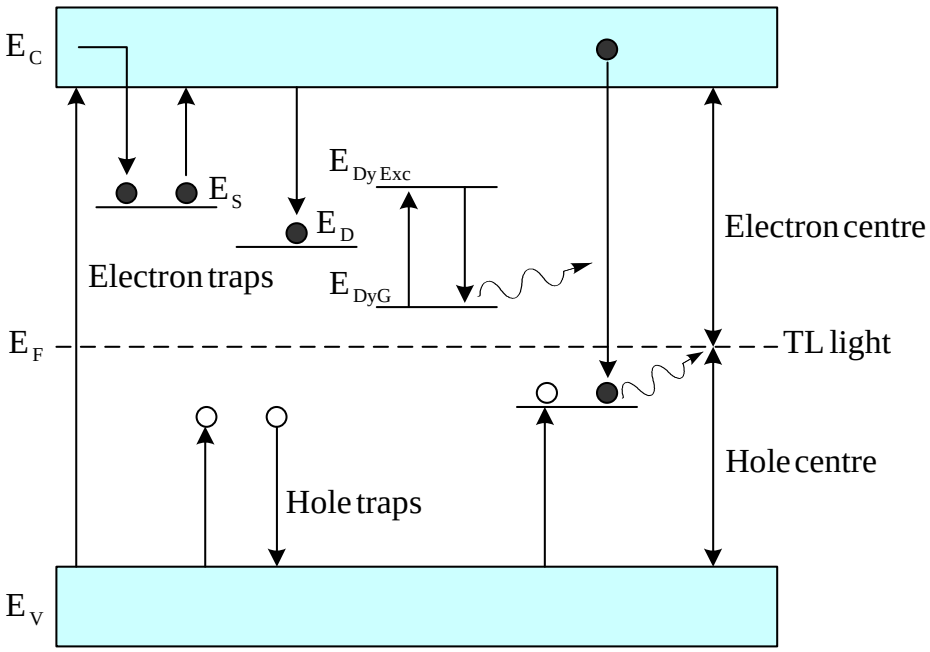

Figure 17 Brief description of TL mechanism in $RWG-Na_2O:Dy^{3+}$ glasses. Due to the X-ray irradiation electrons and hole become trapped at electron and hole defect energy trapping levels, respectively. E_S represents shallow traps while E_D represents deeper traps of electrons from where the probability of escaping is very less. In this study, E_D may be taken as the energy levels of electron traps surrounded in the vicinity of AlO_4 structural units (as part of the chemical composition of RWG). Due to thermal stimulation of the irradiated samples the electrons at the E_S level gain sufficient energy, escape and recombine with holes giving TL emission. E_{Dy} represents electron trap levels of Dy^{3+} ions.

5.3 Optical absorption properties

The results of window glass doped with Dy_2O_3 are interesting. For more information, the optical absorption properties of the glass samples were investigated. From Figure 18, the optical absorption spectra of the glass samples ($G-0$ to $G-4$), recorded at room temperature in the wavelength region of $300-900$ nm exhibited the following standard electronic transitions of Dy^{3+} ions [41]:

$^4F_{9/2} \rightarrow {}^6H_{15/2}$ (blue $\Rightarrow$ 500 nm)

$^4F_{9/2} \rightarrow {}^6H_{13/2}$ (yellow $\Rightarrow$ 580 nm)

$^4F_{9/2} \rightarrow {}^6H_{11/2}$ (red $\Rightarrow$ 670 nm)

The results in Figure 18 show that the absorption intensity increases with increasing mol% of dopants. It is also well documented that the $^4F_{9/2} \rightarrow {}^6H_{15/2}$ (blue) transition scarcely varies with the environment, whereas the $^4F_{9/2} \rightarrow {}^6H_{13/2}$ (yellow) is the hypersensitive transition, which is strongly influenced by the ligand environment. The relative intensities of these two bands depend strongly on the local symmetry of Dy^{3+} ions. The effect of concentration quenching mechanism on the $^4F_{9/2} \rightarrow {}^6H_{15/2}$ (blue) and $^4F_{9/2} \rightarrow {}^6H_{13/2}$ (yellow) transitions of Dy^{3+} ions in glass samples has been attributed to the exchange interaction among the exited Dy^{3+} ions at higher concentrations [41].

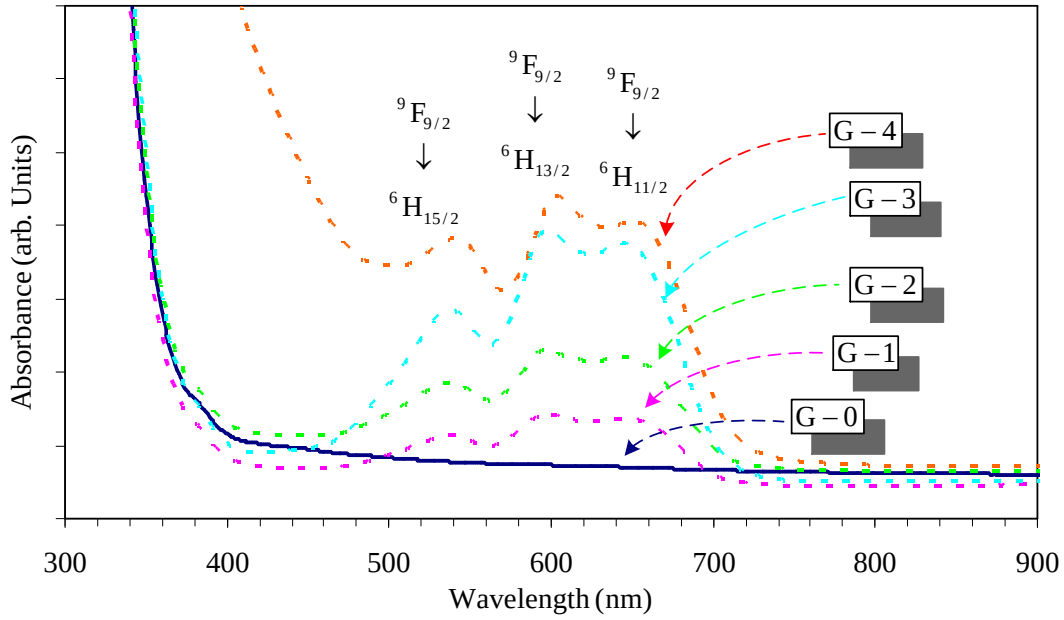

Figure 18 Optical absorption spectra of glass samples recorded at room temperature.

5.4 Effective atomic numbers

In an above study, the effective atomic number (Z_{eff}) of RWG as a function of photon energy was calculated. It is particularly interesting to study the effect of dopants on the change in the effective atomic number of the glass samples. Keep considering condition in thermoluminescence properties, the Z_{eff} of $S-Ce2$, $S-Nd3$ and $S-Mn2$ were calculated as shown in Figure 19. It is clear that Z_{eff} is dominant in the concentration of dopants as the effective atomic number of $S-Nd3$ is higher than $S-Ce2$ and $S-Mn2$, whereas the

effective atomic numbers of $S-Ce2$ and $S-Mn2$ are closed. For a material to be accepted as a tissue alternate for photon interaction, the radiation absorption and scattering acquired for a specified material must be the same as that experienced by the tissue, under similar conditions. A suitable way of comparing the interaction with radiation of a given tissue and the specified tissue equivalent material, is to consider either the photo mass attenuation coefficient and mass energy absorption coefficient, or the effective atomic number [42]. To verify that the glass samples are tissue equivalent, the ratio of Z_{eff} for selected glass samples and the Z_{eff} for soft tissue was considered. Alajerami et al. [29] reported that for human tissue Z_{eff} is 7.42. Therefore, the effective atomic numbers of selected glass samples were compared with the effective atomic number of human tissue. The ratios $\left(R = \frac{Z_{eff}\ \text{of sample}}{Z_{eff}\ \text{of human tissue}}\right)$ are 1.698, 2.294 and 1.696 (at studied energy) for $S-Ce2$, $S-Nd3$ and $S-Mn2$ respectively. These values show that the effective atomic numbers of selected glass samples are significantly higher than the effective atomic numbers of human tissue. However, the selected glass samples show good thermoluminescence properties the terms of sensitivity and linearity at low doses of radiation (0 to 14 mGy). Therefore the R $\left(\text{where } R = \frac{Z_{eff}\ \text{of sample}}{Z_{eff}\ \text{of human tissue}}\right)$ values $(R < 2.3)$ of the selected glass samples are acceptable and can be considered for potential radiation dosimetric materials.

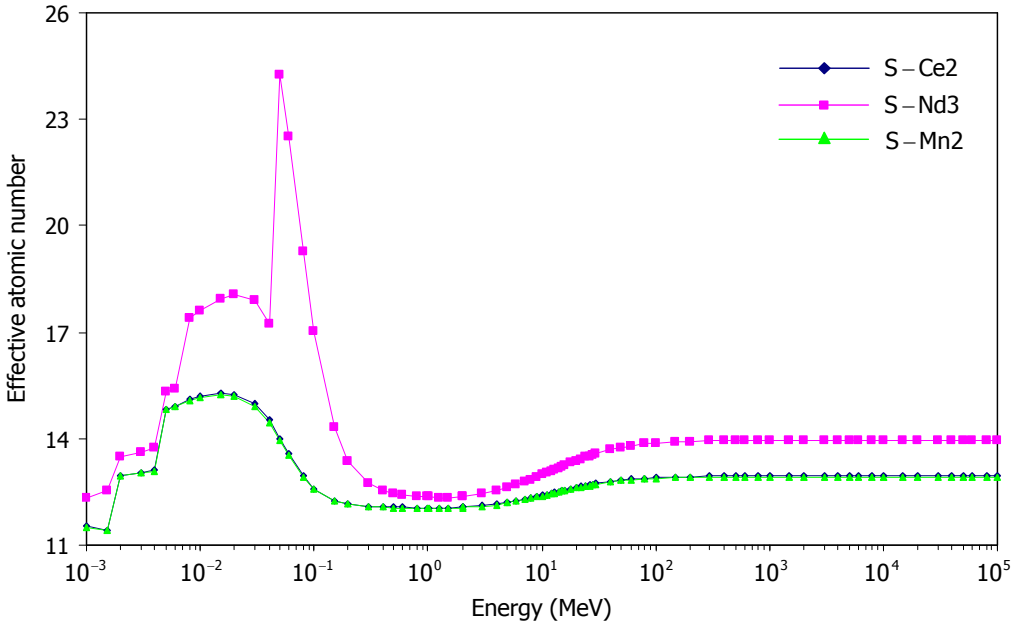

Figure 19 Effective atomic numbers (Z_{eff}) with energy of photon for glass samples

5.5 Physical properties

Physical properties are very important and interesting for a material. They give an insight into the atomic arrangement of the network structure of the material. The physical properties of the glass samples are shown in Table 7.

5.5.1 Density and molar volume

The density of the glass increased with increasing mol% of the dopants. This results from the addition of CeO_2, Nd_2O_3 and MnO_2 (molecular weights 172.1148, 336.4782 and 86.9368 $g \cdot mol^{-1}$, respectively), into the glass matrix (molecular weight of SiO_2 is 60.0843 $g \cdot mol^{-1}$). The molar volumes of the glass samples are shown in Table 7, defined as the volume occupied by the unit mass. The molar volume increased with increasing of concentration of dopants. According to Shelby [43], molar volume depends on the ionic radius of the modifier. These results are easily explained; they are due to the modifier ions ionic radii (Ce^{4+}, Nd^{3+} and Mn^{4+} ionic radii are 1.01, 1.12 and 0.67 Å, respectively), which are larger than the network structure interstices (the ionic radius of Si^{4+} is 0.54 Å).

5.5.2 Ion concentrations

Ion concentrations clearly increased with the mol% of dopants (Table 7). This indicated that the oxide of the dopants added into the glass network was in the form of the ions (R^{m+}) or non-bridging oxygens (NBOs). Moreover, the increase in the ion concentration of R^{m+} showed that R^{m+} ions are uniformly spread throughout the glass network [44]. Polaron radius and interatomic distance showed an inverse relation with dopant concentration (Table 7). The increase of ion concentration (R^{m+}) resulting from the distance between the positive and negative ion core decreased. Therefore, the decrease in Polaron radius could be due to an increase in the concentration of dopants. Moreover, the observed decrease in the interatomic distance with the increase in concentration of dopants eventually led to a more compact glass network [45], crowded with modifier interstices. Thus, the average oxygen bonding distance $(R-O)$ decreased. As a result the $R-O$ bond strength increased, producing a stronger field strength (F) around the modifier ions (Table 7) [46].

Table 7 Physical properties of glass samples.

Measurements	Glass samples											
	S – Ce1	S – Ce2	S – Ce3	S – Ce4	S – Nd1	S – Nd2	S – Nd3	S – Nd4	S – Mn1	S – Mn2	S – Mn3	S – Mn4
Density, $\rho\ (g \cdot cm^{-3})$	2.562	2.563	2.567	2.612	2.572	2.570	2.575	2.656	2.558	2.557	2.560	2.581
Molar volume, $V_a\ (cm^3 \cdot mol^{-1})$	23.402	23.399	23.422	23.615	23.313	23.340	23.416	23.838	23.190	23.247	23.264	23.377
Ion concentration, $N\ (\times 10^{21}\ ion \cdot cm^{-3})$	0.026	0.257	2.570	25.492	0.026	0.258	2.571	25.254	0.026	0.259	2.588	25.751
Polaron radius, $r_P\ (\mathring{A})$	13.649	6.335	2.942	1.369	13.632	6.330	2.941	1.373	13.608	6.321	2.935	1.364
Interatomic distance, $r_i\ (\mathring{A})$	33.876	15.723	7.300	3.398	33.833	15.710	7.300	3.408	33.773	15.689	7.284	3.386
Field strength, $F\ (\times 10^{16}\ cm^{-2})$	0.016	0.075	0.347	1.601	0.016	0.075	0.347	1.591	0.016	0.075	0.348	1.611
Longitudinal velocity, $v_L\ (m \cdot s^{-1})$	5818	5816	5808	5797	5838	5814	5791	5660	5814	5825	5838	5891
Shear velocity, $v_S\ (m \cdot s^{-1})$	3611	3605	3543	3539	3592	3570	3557	3520	3389	3428	3449	3589
Longitudinal modulus, $L_{Exp}\ (GPa)$	86.71	86.69	86.59	87.76	87.64	86.87	86.35	85.09	86.46	86.77	87.26	89.57
Longitudinal modulus, $L_{Th}\ (GPa)$	93.52	93.36	96.08	91.89	99.54	99.11	98.44	94.71	104.72	103.24	101.91	91.86
Shear modulus, $G_{Exp}\ (GPa)$	33.28	33.30	32.14	32.78	33.18	32.75	32.58	32.91	29.37	30.05	30.45	33.24
Shear modulus, $G_{Th}\ (GPa)$	33.68	33.59	34.33	30.87	37.16	37.00	36.76	35.47	37.62	37.03	36.07	29.76
Bulk modulus, $K_{Exp}\ (GPa)$	42.33	42.28	43.74	44.05	43.39	43.21	42.92	41.21	47.29	46.71	46.66	45.26
Bulk modulus, $K_{Th}\ (GPa)$	48.73	48.68	50.42	50.83	50.12	49.90	49.55	47.53	54.69	53.99	53.93	52.25
Young's modulus, $E_{Exp}\ (GPa)$	79.11	79.13	77.45	78.80	79.33	78.43	78.00	77.98	73.00	74.22	75.02	80.10
Young's modulus, $E_{Th}\ (GPa)$	82.12	81.93	83.94	77.03	89.38	89.00	88.41	85.21	91.80	90.42	88.49	75.07

5.5.3 Ultrasonic velocity and elastic moduli

This part is presents the results and discussion of ultrasonic measurements and elastic properties. The properties of glasses are closely related to the inter-atomic forces and potentials in the lattice structure. Thus, change in lattice structure due to doping can be directly noted. The elastic properties are of great interest to investigate the linear and anomalous variations as a function of the composition of the glass and these have been interpreted in terms of the structure in the glass network [8,47]. To better understand the structure of oxide glasses, the coordination number of the network former, and the change in the oxygen bonds of the framework induced by cation modifiers, an ultrasonic pulse echo technique was used. This is a versatile tool for investigating the change in microstructure and the deformation process and mechanical properties of materials [48-49]. The decrease of ultrasonic velocity is related to the increase in the number of non-bridging oxygens (NBOs) which leads to the decrease in the connectivity of the glass network [43]. From Table 7, the longitudinal and shear velocity are almost constant, showing only slight change with the increase of dopant concentrations. The maximum percentage differences of ultrasonic velocities were calculated as 0.316 %, 0.773 % and 1.324 % for the longitudinal velocities of glass samples doped with CeO_2, Nd_2O_3 and MnO_2 respectively, and 1.994 %, 2.330 % and 5.901 % for the shear velocities. The maximum percentage difference was less than 6 %. Therefore, adding the dopants induced small damage or change in the glass network and the structure remained strong. The variations of experimental elastic moduli (longitudinal, shear, bulk and Young's modulus) with different concentration and type of modifier are shown in Table 7. The elastic modulus represents the resistance to deformation of a network structure when external force is applied. The higher the elastic moduli when compared with others [50-54] indicated that the glass samples were highly stable to the external applied force. The theoretical bond compression model was used to confirm the results from the experimental elastic moduli and these are shown in Figure 20 and Table 7. The experimental elastic moduli show a fair agreement with the theoretical values. The uncertainties for the experimental and theoretical values were acquired from the maximum different of the data (percents). The estimated error in this result was lass than 22%.

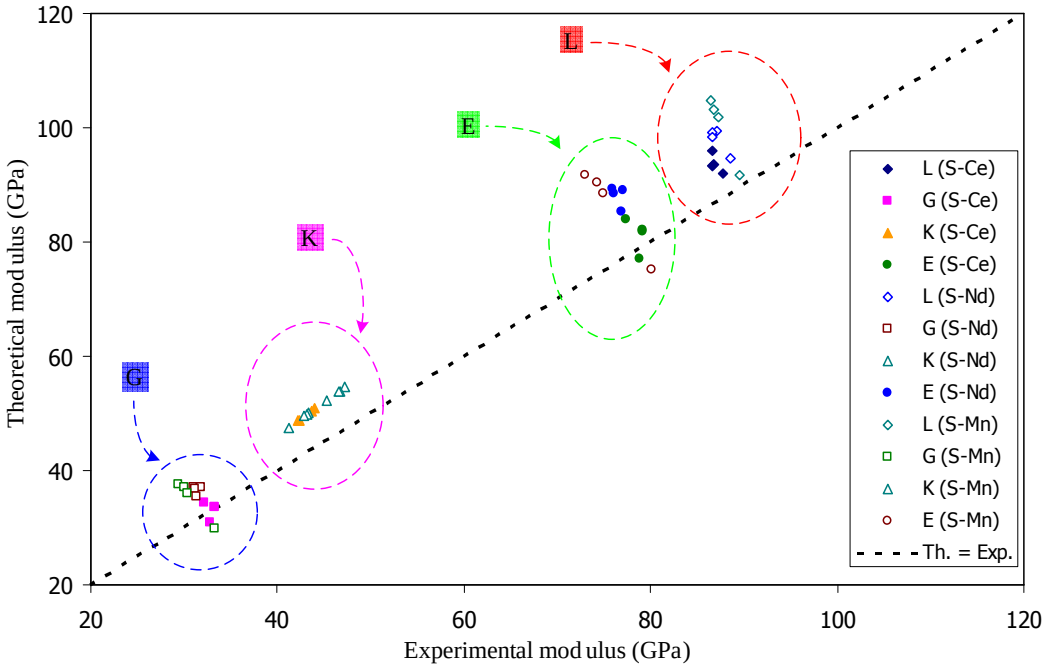

Figure 20 Variation of theoretical modulus (Th.) vs. experimental modulus (Exp.) of the glass samples

From the results, Soda lime glasses improved by adding CeO_2, Nd_2O_3, Dy_2O_3 and MnO_2, were prepared for investigation of their thermoluminescence and physical properties to design for radiation dosimetric measurement. The results of the thermoluminescence testing showed that the glass samples doped with CeO_2 0.010 mol%, Nd_2O_3 0.100 mol%, Dy_2O_3 0.100 mol% and MnO_2 0.010 mol% had the highest integrated TL signals and linearity. Therefore, the glass samples were selected to calculate trap depth parameters. The activation energy depends directly on the ability of electron trapping and/or release of dopant ions (R^{m+}). The effective atomic numbers of selected glass samples were significantly higher than the effective atomic numbers of human tissue. However, the R $\left(\text{where } R = \dfrac{Z_{eff} \text{ of sample}}{Z_{eff} \text{ of human tissue}}\right)$ values $(R < 2.3)$ of the selected glass samples were acceptable to consider for potential radiation dosimetric materials, as they showed good thermoluminescence properties in terms of sensitivity and linearity at low dose levels of radiation. Moreover, the high elastic moduli of the glass samples indicated high rigidity and stability of the glass matrix structure. There was a fair agreement between the theoretically calculated and experimental elastic moduli for the glass samples.

5.5.4 Radiation effects

This section is reported that the radiation effects on structural properties of the glass samples. The selected glass sample is the RWG doped with Nd_2O_3 due to the glass samples shows good TL properties and the glasses containing rare-earth ions have attracted a great deal of interest due to their important properties. For examples, the glasses are heat-resistant, present interesting optical and magnetic behaviour [55-57]. At first, the effect of gamma irradiation on the density of the glass samples is shown in Figure 21 and exacted values are shown in Table 8.

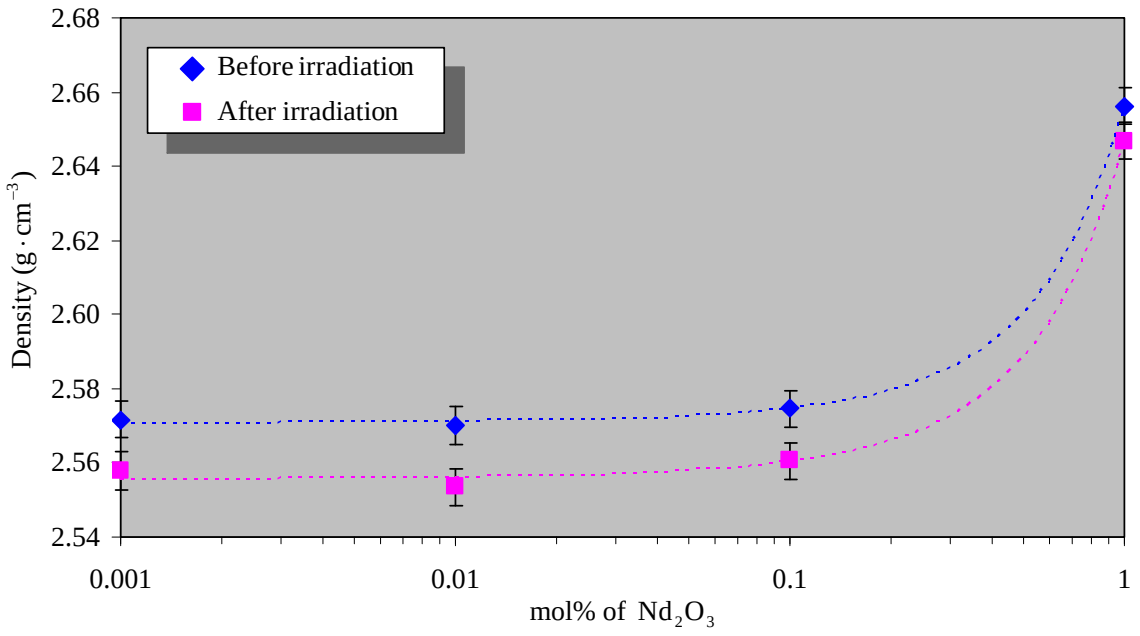

Figure 21 Variation of densities (ρ) before and after irradiation with γ-radiation of the glass samples with the difference of doping (lines are drawn as guides to the eyes).

The results shows that the densities of the glass samples increase with increasing the concentration of Nd_2O_3 but decrease after irradiated by gamma radiation. The decreased of the density of the glass can be attributed to three factors, namely [58]:

(i) transformation of the main glass network structure from triagonal (Q_4) to tetrahedral (Q_3),

(ii) decrease in the molecular mass of the glass because of the glass because of the higher atomic weight of the modifier, and

(iii) decrease of the bridging oxygen (BO) ratio in the glass composition, due to the adding of modifier and/or irradiation.

From mentioned above, damage by an irradiation species can create displacement of atoms and/or breaks in the network bonds, leading to a rise of the number of non-bridging oxygens (NBOs) and/or transformation of the main glass network structure from tetrahedral (Q_4) to triagonal (Q_3) and resulting in a decrease of the densities of the glass samples after irradiation [59-60]. The molar volume is defined as the volume occupied by the unit mass of the glass, molar volume can be used as a parameter to identify an open structure [61].

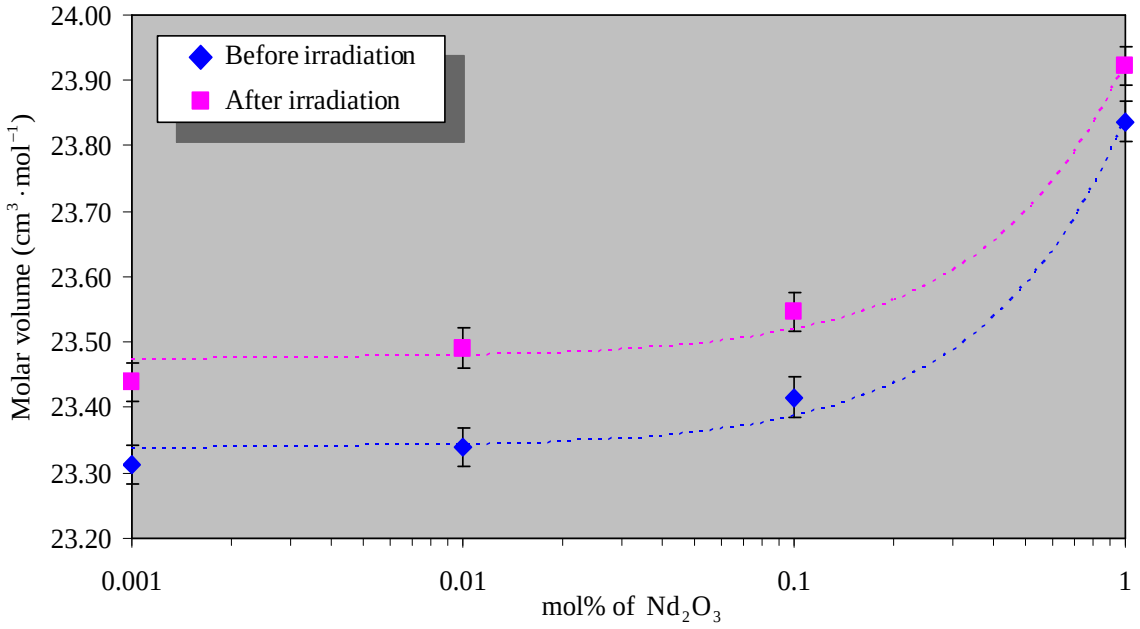

Figure 22 Variation of molar volume (V_a) before and after irradiation with γ-radiation of the glass samples with the difference of doping (lines are drawn as guides to the eyes).

Figure 22 shows that the molar volume increases with increasing Nd_2O_3 concentrations and after gamma irradiation. These results are easily explained; they are due to the modifier ions ionic radius (the Nd^{3+} ionic radius is 1.123 Å), which is larger than the network structure interstices (the ionic radius of Si^{4+} is 0.400 Å). The modifier ion attraction to oxygen ions can yield a grater interstices size and molar volume. Irradiation with gamma rays is assumed to create displacement of atoms, electronic defects and/or breaks in the network bonds, which allow the structure to relax and fill the relatively large interstices in the interconnected silicon and/or boron and oxygen atom network, which produces volume expansion followed by compaction [59]. To confirm this results the packing density of the glasses were calculated and shown in Table 1. The packing density is the ratio between the minimum theoretical volume occupied by the ions and the corresponding effective volume of the glass. Therefore, the increase of packing density with increases concentration of Nd_2O_3 due to the volume occupied

by the ions increase (the ionic radius of Nd^{3+} is large). Adding Nd_2O_3 into the glass matrix resulting to produces volume expansion followed by compaction. Therefore, the molar volume increases with the mol% of Nd_2O_3. After irradiation, the packing density was decreases in all samples. This is due to the increase of the effective volume of the glass matrix. The damage of radiation can create the opens structure lead to increase of molar volume of the glass samples. Moreover, this results good agree with the transformation of the main glass network structure from tetrahedral (Q_4) to triagonal (Q_3) after irradiation.

Table 8 Glass composition, density (ρ), molar volume (V_a) and packing density (V_t) of the glass samples before and after gamma irradiation.

Sample No.	Composition (mol%)			$\rho\ (g\cdot cm^{-3})$ ± 0.001		$V_a\ (cm^3\cdot mol^{-1})$ ± 0.021		$V_t \times 10^{-6}\ (m^3)$ ± 0.0013	
	RWG	Na_2O	Nd_2O_3	Before	After	Before	After	Before	After
$G-0$	90	10	0	2.567	2.565	23.351	23.3747	0.4592	0.4588
$G-1$	89.999	10	0.001	2.572	2.558	23.313	23.4391	0.4609	0.4584
$G-2$	89.990	10	0.01	2.570	2.554	23.340	23.4911	0.4690	0.4660
$G-3$	89.900	10	0.1	2.575	2.560	23.416	23.5458	0.5530	0.5500
$G-4$	89	10	1	2.656	2.647	23.837	23.9225	1.3838	1.3789

The plots before and after irradiation of longitudinal (v_L) and shear (v_S) velocities in the glass samples with the concentration of Nd_2O_3 are shown in Figure 23 and 24, respectively and exact values are shown in Table 9. In addition, elastic moduli $(L, G, K \text{ and } E)$, Poisson's ratio (σ), micro-hardness (H), Debye temperature (θ_D) and softening temperature (T_s) of the glass samples are shown in Table 10. The ultrasonic velocities $(v_L \text{ and } v_S)$ in the glasses decrease as the mol% of the dopant increase and after irradiation. The changes in geometrical configuration, co-ordination number, cross-link density and dimension of interstitial space of glass determine the ultrasonic velocity and, therefore, ultrasonic velocity is an appropriate tool in revealing the degree of the structural change in the glass [20]. In general, the decrease of ultrasonic velocity is related to the increase in the number of non-bridging oxygens (NBOs) and, consequently, the decrease in connectivity of the glass network [62]. Therefore, the decrease in ultrasonic velocities is due to the fact that Nd^{3+} ions are involved in the glass network as modifiers by breaking up the tetrahedral bond of SiO_4 units. Moreover, damage by an irradiation species can create displacement of atoms and/or breaks in the network bonds, leading to a rise of the number of NBOs. Hence, the ultrasonic velocities decrease with mol% of Nd_2O_3 increases and after gamma-irradiation. Moreover, difference of ultrasonic velocity before and

after irradiation as shown in Table 9 (%different). The results indicated that highest damage of irradiation on the structure is occurred in $G-3$ glass sample.

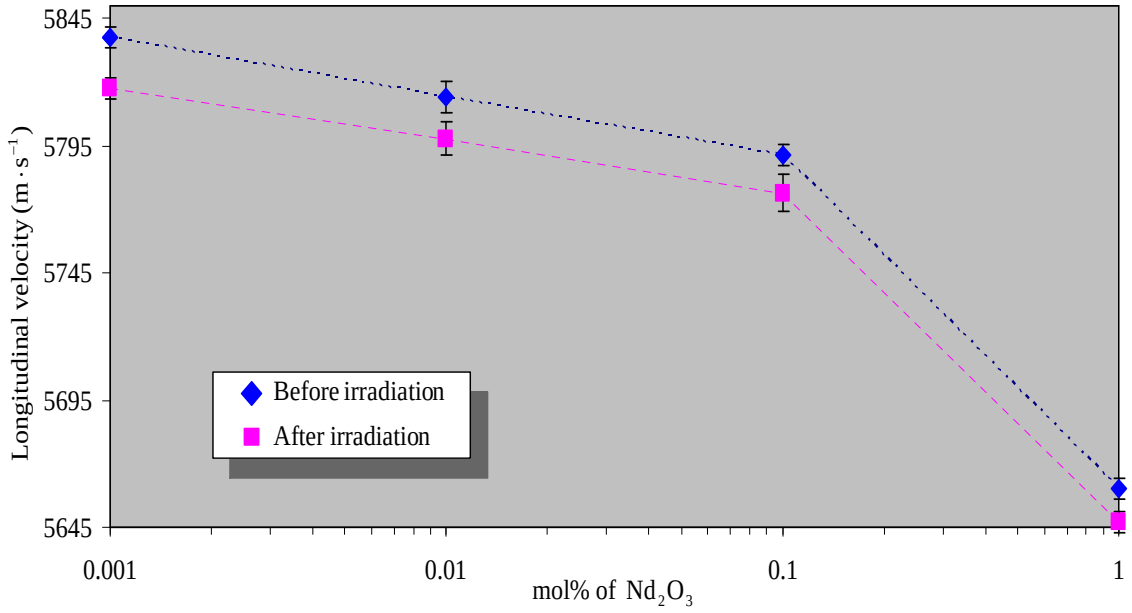

Figure 23 Variation of longitudinal velocity (v_L) before and after irradiation with γ-radiation of the glass samples with the difference of doping.

Table 9 Longitudinal (v_L), shear (v_S) and mean (v_m) velocities of the glass samples before and after gamma irradiation.

Sample No.	v_L $(m\cdot s^{-1}) \pm 7$			v_S $(m\cdot s^{-1}) \pm 14$			v_m $(m\cdot s^{-1}) \pm 11$	
	Before	After	%different	Before	After	%different	Before	After
$G-0$	5842	5827	0.257	3646	3635	0.302	4017	4005
$G-1$	5838	5817	0.348	3592	3577	0.427	3964	3947
$G-2$	5814	5798	0.281	3570	3549	0.565	3940	3919
$G-3$	5791	5776	0.259	3557	3484	2.062	3926	3852
$G-4$	5660	5647	0.230	3520	3502	0.516	3880	3861

In the asseveration of these results, the number of bonds per unit volume (n_b) is calculated by using a theoretical bond compression model is shown in Table 11. From the results, all samples show the decrease in the number of bonds per unit volume with increase of the mol% of dopants. Furthermore, the decrease of bonds per unit volume of glass samples after irradiation due to the greater the formation of non-bridging oxygens (NBOs). These results supported our discussions of the ultrasonic velocities of glass samples.

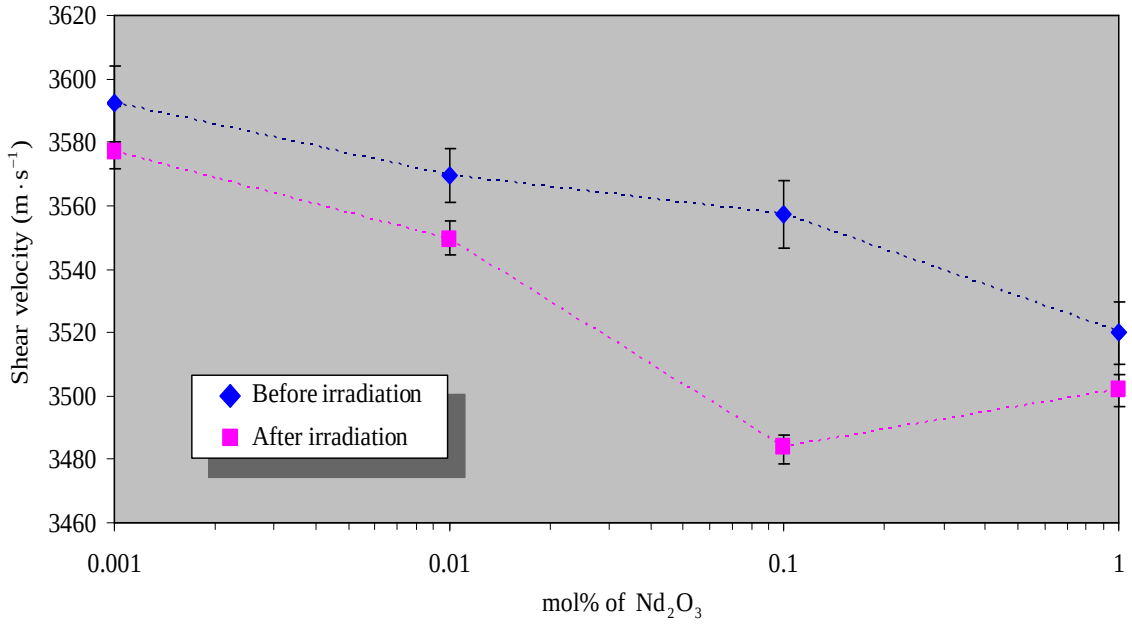

Figure 24 Variation of shear velocity (v_S) before and after irradiation with γ-radiation of the glass samples with the difference of doping.

The elastic moduli $(L, G, K \text{ and } E)$ as shown in Table 9 decrease with the increase of Nd_2O_3 concentrations and after irradiation. All of the elastic moduli are related to the average strength of the bond. The average strength of the bond depends on the value of cation-anion forces. For a given A-O-A bond angle, the A-A separation would be directly proportional to the stretching force constant $(\overline{F})$ of the glass network [63]. As the A-O-A bond force constants decrease, the energy required to produce a given degree of bond angle or length distortion and/or bond distortion decreases which leads to the decrease in the average strength of the bond.

Table 10 Longitudinal (L), shear (G), bulk (K), Young's (E) modulus, Poisson's ratio (σ), micro-hardness (H), Debye (θ_D) and softening (T_s) temperature of the glass samples before and after gamma irradiation.

Sample No.	L (GPa) ± 0.03		G (GPa) ± 0.01		K (GPa) ± 0.02		E (GPa) ± 0.04		$\sigma \pm 0.003$		H (GPa) ± 0.01		θ_D (K) ± 2		T_s (K) ± 5	
	Before	After	Before	After	Before	After	Before	After	Before	After	Before	After	Before	After	Before	After
G – 0	87.63	87.10	34.13	33.89	42.12	41.91	80.62	80.09	0.181	0.181	7.26	7.20	354	353	612	609
G – 1	87.64	86.56	33.18	32.73	43.39	42.93	79.33	78.28	0.195	0.196	6.74	6.63	349	347	593	591
G – 2	86.87	85.83	32.75	32.17	43.21	42.94	78.43	77.22	0.198	0.200	6.60	6.43	347	344	586	583
G – 3	86.35	85.43	32.58	31.08	42.92	44.00	78.00	75.46	0.197	0.214	6.58	5.92	345	338	584	563
G – 4	85.09	84.39	32.91	32.46	41.21	41.12	77.98	77.09	0.185	0.188	6.92	6.76	339	337	582	578

Table 11 Average cross-link density ($\bar{n}_c$), calculation of Poisson' ratio (σ_{cal}), number of vibrating atoms per unit volume (N/V), average stretching force constant ($\bar{F}$), average ring diameter (ℓ) of the glass samples. Theoretical bond compression bulk modulus (K_{bc}), number of bonds per unit volume (n_b) and K_{bc}/K_{exp} ratio of the glass samples before and after gamma irradiation.

Sample No.	$\bar{n}_c$	σ_{cal}	$\frac{N}{V}\times 10^{21}$ (cm^{-3})	$\bar{F}$ (N/m)	ℓ (nm)	K_{bc} (GPa)		$n_b \times 10^{22}$ (cm^{-3})		K_{bc}/K_{exp}
						Before	After	Before	After	
G – 0	3.6364	0.2028	7.7341	377.96	0.5424	170.99	170.81	14.9526	14.9375	4.0595
G – 1	3.6365	0.2028	7.7467	377.95	0.5382	171.26	170.34	14.9770	14.8966	3.9471
G – 2	3.6375	0.2027	7.7390	377.89	0.5388	171.08	169.98	14.9611	14.8651	3.9593
G – 3	3.6479	0.2026	7.7256	377.29	0.5396	170.70	169.76	14.9268	14.8443	3.9772
G – 4	3.7500	0.2012	7.7026	371.42	0.5431	169.33	168.72	14.7990	14.7464	4.1088

To confirm these results, the stretching force constants $(\overline{F})$ are calculated by using a theoretical bond compression model, the exact values were collected in Table 11. The stretching force constants decrease with the increase of the mol% of the dopant. These results indicate that the glass doped with Nd_2O_3 leads to the decrease in the average strength of the bond (elastic moduli were decreased). While the elastic moduli decrease after gamma irradiation can be speculate that the bond distortion occurred by irradiation.

Variation of Poisson's ratio and micro-hardness of the glass samples as a function of the dopants are listed in Table 3. Point to influence of Nd_2O_3 on Poisson's ratio can be seen that the Poisson's ratio nearly constant with concentration of Nd_2O_3 from 0.001 mol% to 0.1 mol% ($G-1$ to $G-3$) and then decreases with increasing of mol% dopants from 0.1 mol% to 1.0 mol% ($G-3$ to $G-4$). The variation of Poisson's ratio related to cross-link density. Poisson's ratio decrease as the cross-link density increases. At low concentration of dopants, effect of modifier is insignificant as a result the nearly constant of Poisson's ratio. However, when the concentration of modifier reach to 0.1 mol% or higher resulting to the decrease of Poisson's ratio due to the increase of cross-link density in the glass network. After irradiation, the Poisson's ratio is higher than the before irradiation especially at 0.1 mol% ($G-3$ glass sample) indicate that the highest effects of irradiation occurred in $G-3$ glass sample. These results support our discussion of the ultrasonic velocities. In addition, the average numbers of cross-link density $(\overline{n}_c)$ was calculated by using the theoretical bond compression model for confirm the effects of Nd_2O_3 on Poisson's ratio and are shown in Table 11. The average numbers of cross-link density $(\overline{n}_c)$ extremely increase when the mol% of the dopant increase from 0.1 to 1.0 mol%. These results strongly support the results of Poisson's ratio. Moreover, the theoretical of Poisson's ratio (σ_{cal}) was calculated to compare the results (Table 11). It is observed that a theoretical of Poisson's ratio is in a good agreement with the experimental values. The micro-hardness is defined as the resistance of a material to permanent indentation or penetration [12]. It can be seen that (Table 9) the micro-hardness decrease with increase concentration of dopant reach to 0.1 mol% and then it is return to increase at 1.0 mol% of dopant. The micro-hardness decrease of all samples after irradiated with gamma ray. These results show that the rigidity and/or compactness of the sample depend on the concentration and irradiation. The results good agreement with the results of molar volume as was described.

Debye temperature (θ_D) and softening temperature (T_s) before and after irradiation of the glass samples are listed in Table 10. Debye temperature is an important parameter of a solid, describes the properties arising from atomic vibration and is directly proportional to the mean ultrasonic velocity (v_m). The variations of the mean ultrasonic velocity are shown in

Table 9. Debye temperature represents the temperature at which all the high-frequency “lattice” vibrational modes are excited [64]. Softening temperature is another important parameter defined as the temperature point at which viscous flow changes to plastic flow [62,65]. It can be observed that the decrease of the Debye temperature, softening temperature and mean ultrasonic velocity with adding Nd_2O_3 and after irradiation are mainly contributed from the increase in formation of NBOs as a direct effect of the insertion of Nd_2O_3 and effect of irradiation. For clarity of obtained results, the dependence of Debye temperature could be discussed on the basis of the number of vibrating atoms per unit volume [24]. Therefore, the number of vibrating atoms per unit volume $\left(\frac{N}{V}\right)$ was calculated and shown in Table 11. The number of vibrating atoms per unit volume was found to decrease with the increasing mol% of the Nd_2O_3.

The values of average ring diameter (ℓ), theoretical bond compression bulk modulus (K_{bc}) and K_{bc}/K_{exp} ratio are shown in Table 11. From Table 11, it is rather clear that the values of the theoretical bond compression bulk modulus (K_{bc}) decrease when the content of Nd_2O_3 increases and decrease after irradiation. This indicates that adding Nd_2O_3 to the pure composition of the glass plays a major role in the average coordination of the network structure [66] or the average stretching force constant which was found as a similar trend with the theoretical bond compression bulk modulus (K_{bc}). In general, the ratio of K_{bc}/K_{exp} is a measure of the extent to which bond bending is governed by the configuration of the network bonds. The variation of K_{bc}/K_{exp} ratio increase with increase of concentration of dopant. This indicates that the network bonds are expanding of extent. This ratio is assumed to be directly proportional to the average ring diameter. The average ring diameter is shown in the Table 11. It is very clear that the average ring diameter increase with increase of the concentration of Nd_2O_3.

Comparison of experimental estimated elastic moduli $(K, G, L \text{ and } E)$ with those obtained theoretically by using bond compression model are shown in Figure 25. From the Figure 25, the calculated elastic moduli are in the range of the experimental values. It is observed that a theoretical bond compression model is in a good agreement with the experimental values of elastic moduli.

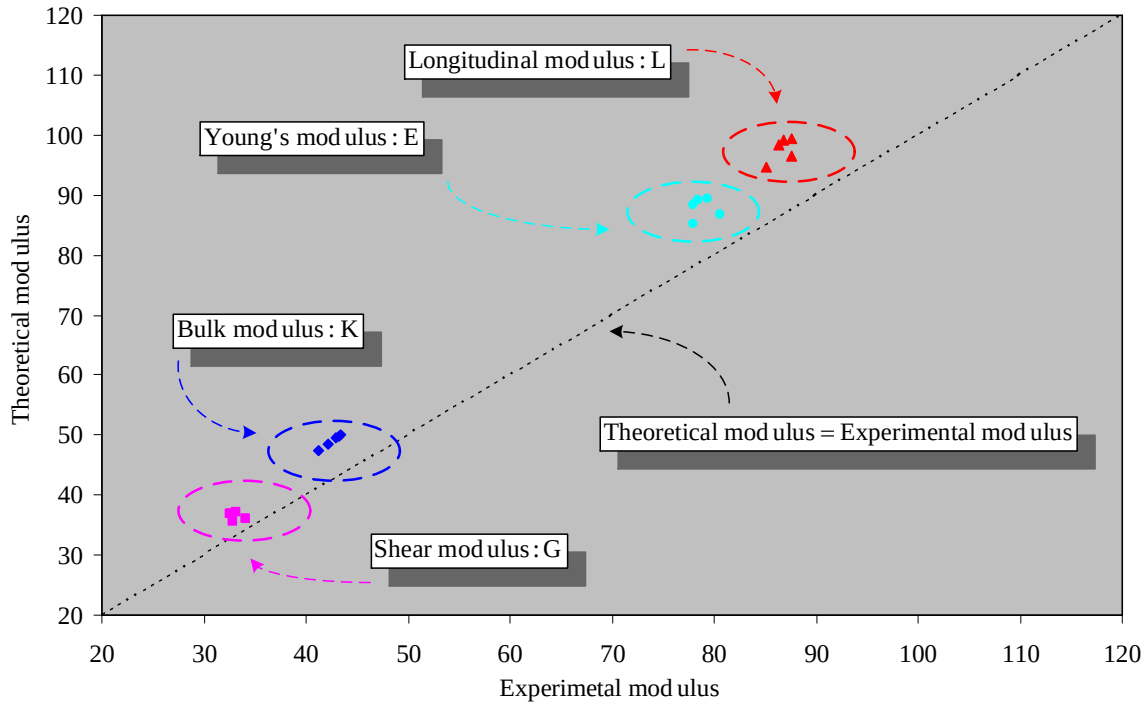

Figure 25 Variation of theoretical modulus vs experimental modulus of the glass samples with the difference of doping.

5.5.5 FTIR measurements

FTIR spectral curves in $400-4000\ \mathrm{cm}^{-1}$ region of the glass samples before and after irradiation are illustrated in Figures 26 (a) and (b), respectively. The water groups are indicated by frequency bands over $2000\ \mathrm{cm}^{-1}$. The main absorption band and corresponding vibration modes of FTIR spectrum of glass samples are shown in Table 12. The frequency bands from the glasses network vibrations appear in the range $400-1500\ \mathrm{cm}^{-1}$ [67-68]. The FTIR absorption spectra for the glass samples examined herein have four main frequency bands. Figure 26 (a) shows apparently decrease of $\mathrm{Si-O-Si}$ unti-asymmetric stretching of BOs within tetrahedral ($995-1050\ \mathrm{cm}^{-1}$) peak when the mol% of Nd_2O_3 increases. Furthermore, the $\mathrm{Si-O-Si}$ bending vibrations ($470-485\ \mathrm{cm}^{-1}$) peak and the $\mathrm{Si-O-Si}$ and $\mathrm{O-Si-O}$ symmetrical stretching of BOs between tetrahedral ($650-780\ \mathrm{cm}^{-1}$) peak shows decrease of absorption with mol% of Nd_2O_3 increases. The results from FTIR spectroscopy support our discussion on the transformation of SiO_4 tetrahedral units from Q_4 to Q_3 with consequent rising in NBO when mol% of Nd_2O_3 increases. Figure 26 (b) shows decrease of FTIR absorption bands at $470-485$, $650-780$ and $995-1050\ \mathrm{cm}^{-1}$ all samples after irradiation. These results reveal that the formation of NBOs occurred when the glass sample were irradiated with

gamma ray. The results of the FTIR spectra are evidence of the discussion the change in structure of the glass network was added Nd_2O_3 and after irradiated.

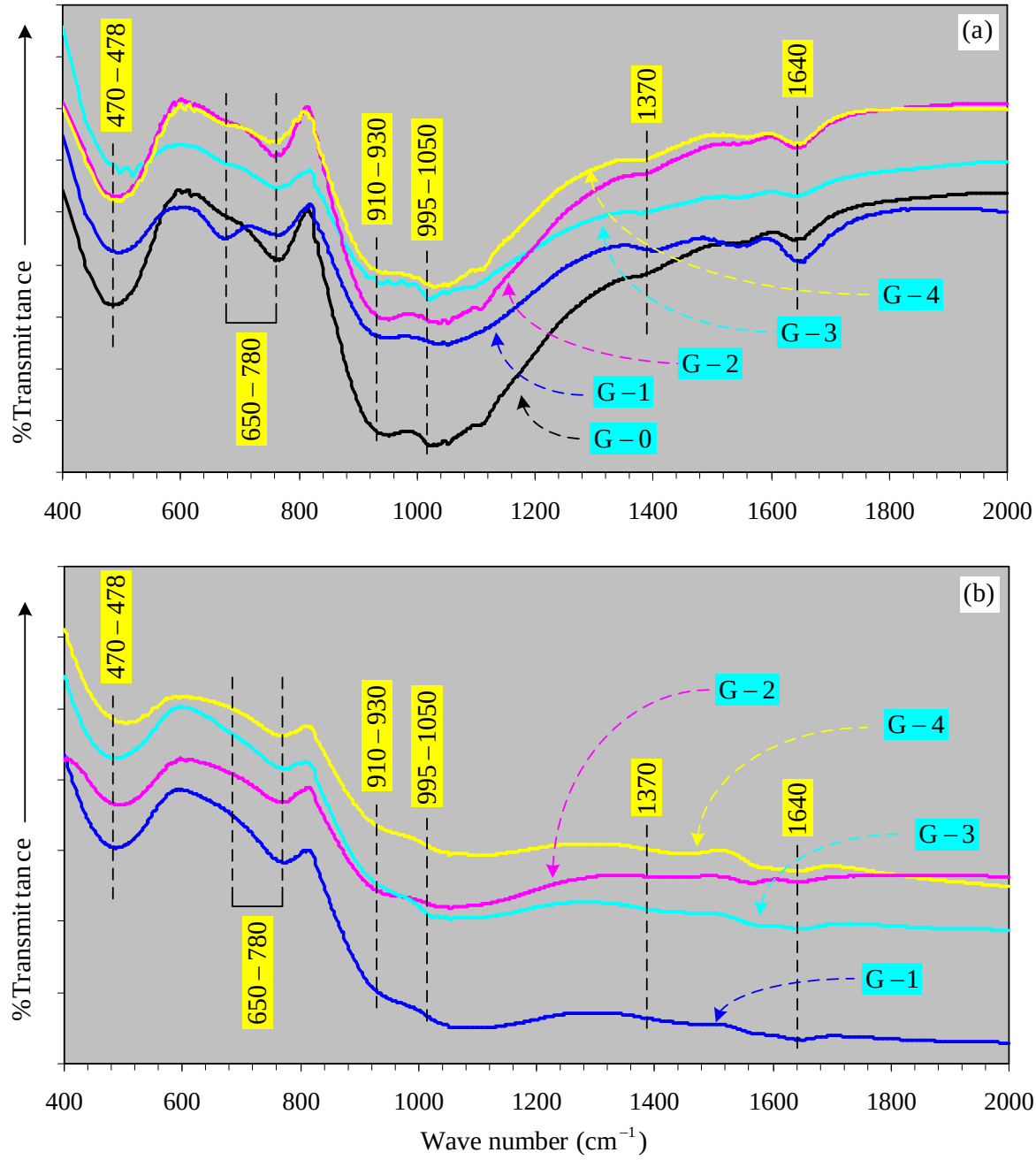

Figure 26 FTIR spectra of the glass samples before (a) and after (b) gamma irradiation.

Table 12 Main absorption band and corresponding vibration modes of FTIR spectrum of glass samples in $400-2000\ \mathrm{cm}^{-1}$ region.

Wave number (cm^{-1})	Assignment	References
$470-485$	$\mathrm{Si-O-Si}$ Bending vibrations	[67,69]
$650-780$	$\mathrm{Si-O-Si}$ and $\mathrm{O-Si-O}$ symmetrical stretching of BOs between tetrahedra	[67,69]
$910-930$	$\mathrm{Si-O-Si}$ stretching of NBOs	[69]
$995-1050$	$\mathrm{Si-O-Si}$ unti-asymmetric stretching of BOs within tetrahedra	[67,69]
1370	Carbonate group	[69]
1640	Molecular water vibrations	[67]

5.5.6 Effects of dopants for other glass systems on the structural properties

For more comprehensive study, the effects of dopants for the others glass systems on the structural properties have been investigated. It can be separated study on concentrations and types on the network structure of the host glasses. However, the study in this part are summarizing mentioned. Borosilicate glasses have high chemical and mechanical resistance, very low electrical conductivity and thermal expansion coefficient. Thus, they are widely used in laboratory, optical, heat-resistant, fiber, pharmaceutical and sealing glasses applications, and even for nuclear waste immobilization. Therefore, the elastic moduli of borosilicate glasses have been discussed. The elastic moduli and structure of the glass samples have been investigated as a function of compositions (different contents of TiO_2, BaO and Bi_2O_3) by measuring ultrasonic velocities. The lowest longitudinal, shear, bulk and Young's moduli of these glasses were 73.65, 27.26, 37.31 and 65.76 GPa, respectively for the composition 5 mol% of TiO_2 glass samples. The highest longitudinal, shear, bulk and Young's moduli of these glasses were 102.18, 37.73, 52.36 and 90.82 GPa, respectively for the composition 5 mol% of Bi_2O_3, 3 mol% of Bi_2O_3, 5 mol% of Bi_2O_3 and 3 mol% of Bi_2O_3 glass samples, respectively. The number of bonds per unit volume, the average stretching force constant, the average cross-link density, the average ring diameter and the theoretical bond compression bulk modulus were calculated by using a theoretical bond compression model for asseveration of the obtained results. The agreement between the theoretically calculated and experimental elastic moduli is excellent for the studied samples. Moreover, the results showed good agreement when the number of bonds per unit volume, average crosslink density, ring diameter and stretching force constant of SiO_2 is compared with those of TeO_2. These results indicate the reliability of the experimental data [70]. The plots of elastic moduli of the glass samples are shown in Figures 27-29.

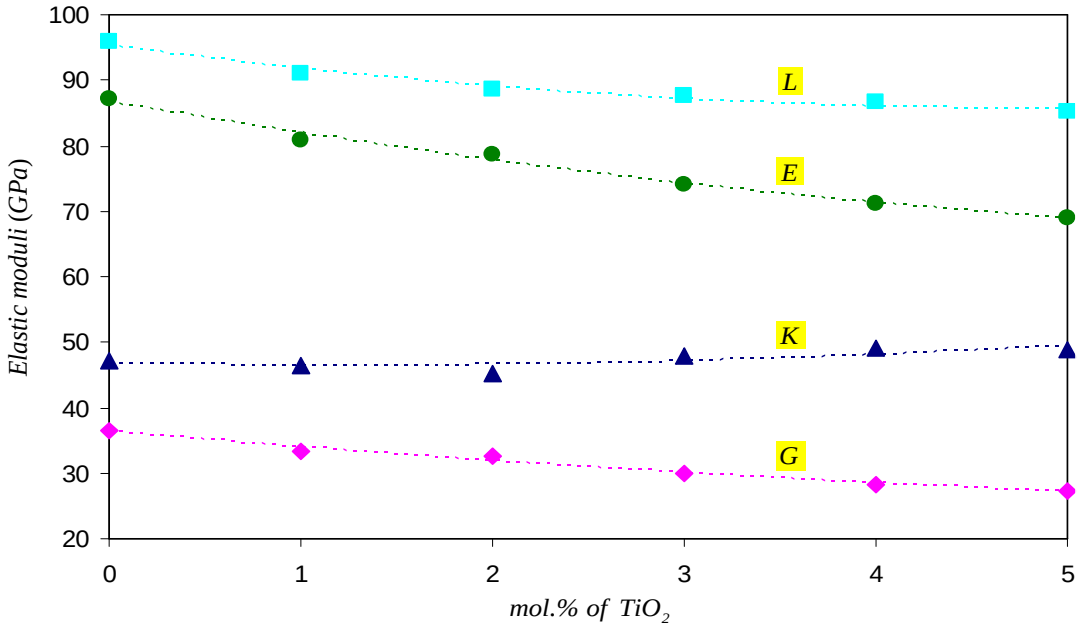

Figure 27 Variation of elastic moduli of glass samples with difference mol.% of TiO_2. The error bar is contained within the symbol size (lines are drawn as guides to the eyes).

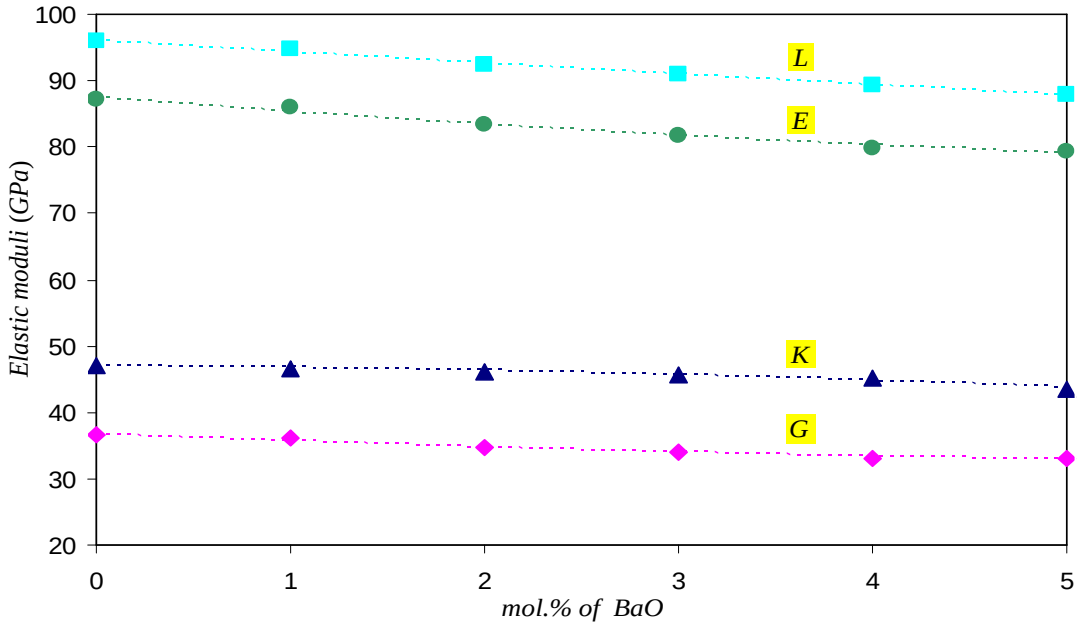

Figure 28 Variation of elastic moduli of glass samples with difference mol.% of BaO. The error bar is contained within the symbol size (lines are drawn as guides to the eyes).

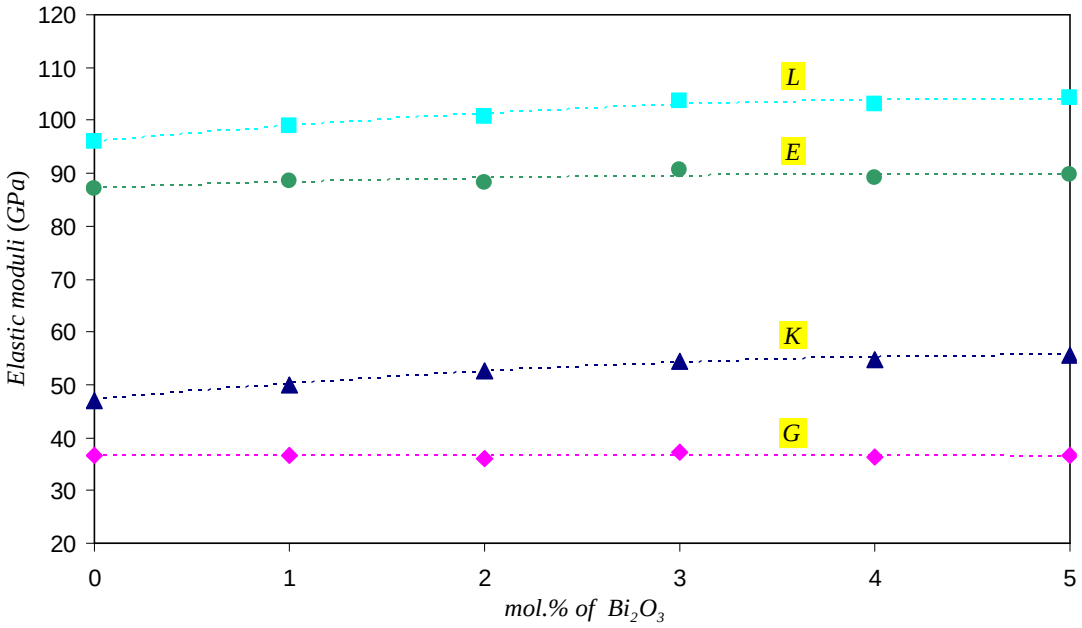

Figure 29 Variation of elastic moduli of glass samples with difference mol.% of Bi_2O_3. The error bar is contained within the symbol size (lines are drawn as guides to the eyes).

In addition, the local sand (was acquired from Moon River in Ubon Ratchathani province, Thailand) was used as starting materials for a comparative study with pure silica (SiO_2). A comparison between local sand and SiO_2 with different compositions of CeO_2 on the structural properties of glasses after successive irradiation was carried out by using ultrasonic techniques and FTIR spectroscopy. The ultrasonic velocities were measured by the pulse echo technique, with a frequency of 4 MHz and at room temperature. From these obtained velocities and densities, various elastic moduli, micro-hardness and Poisson's ratio were calculated. The results indicate that local sand is more affected with gamma irradiation than SiO_2. These results are due to a higher iron impurity in local sand leading to the more information of non-bridging oxygens (NBO) [71]. The results of radiation effects on elastic moduli (bulk and Young's modulus) are shown in Figure 30.

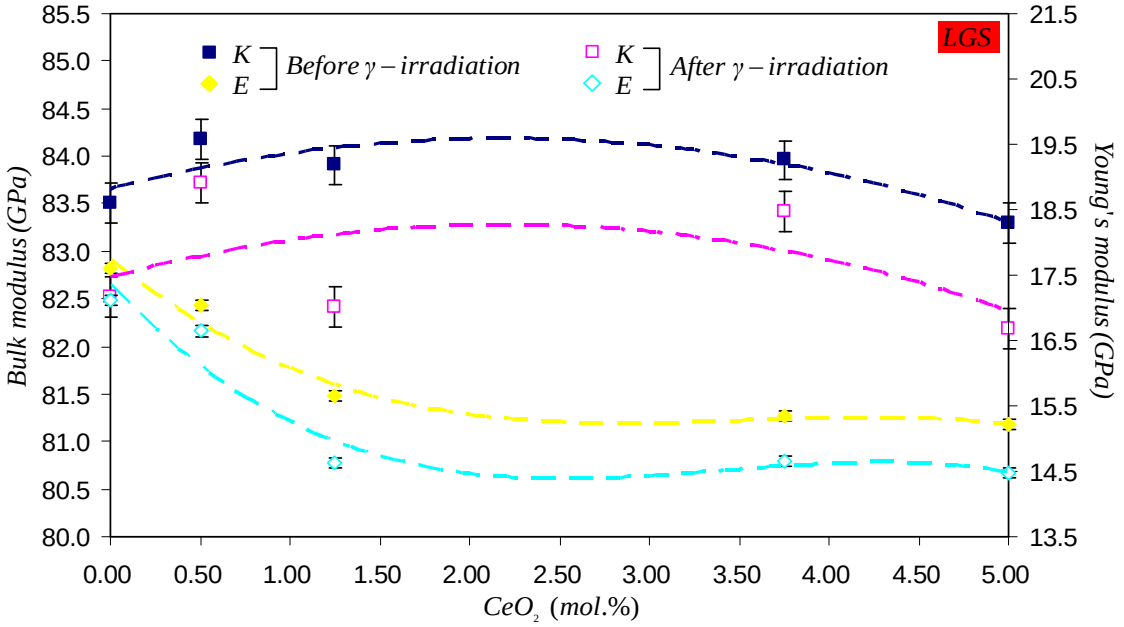

Figure 30 Bulk (K) and Young's (E) modulus before and after successive gamma irradiation of the local sand (LGS) glass samples with concentration of CeO_2. Lines are fitting plots of the data. The uncertainty in the measurement of the bulk and Young's modulus are ± 0.21 GPa and ± 0.08 GPa , respectively.

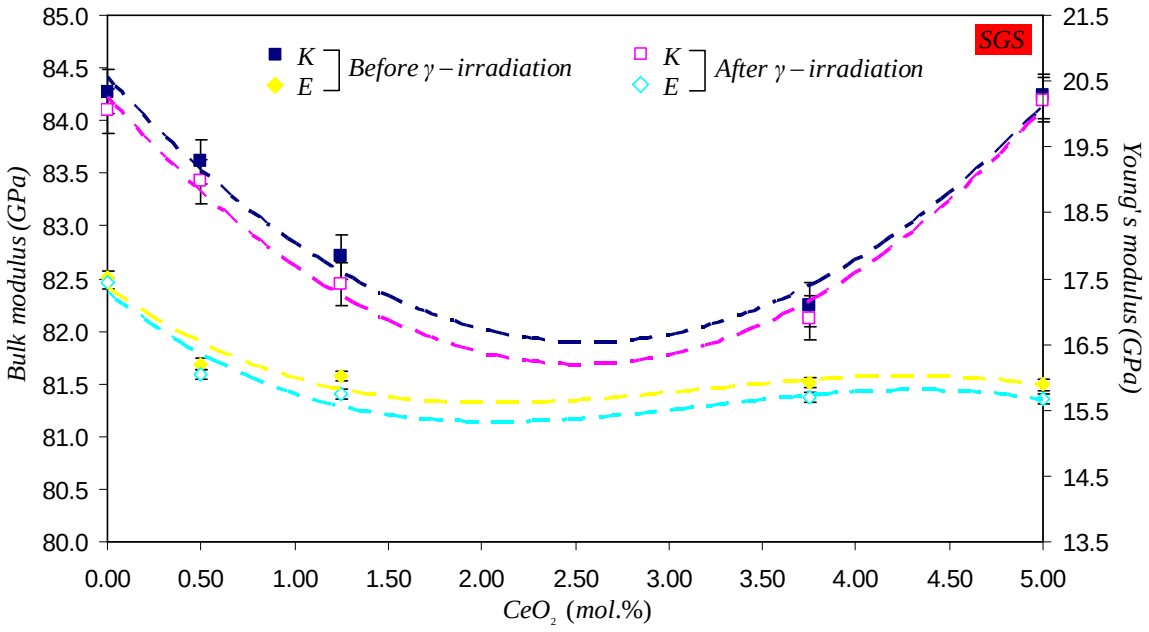

Figure 31 Bulk (K) and Young's (E) modulus before and after successive gamma irradiation of the SGS glass samples with concentration of CeO_2. Lines are fitting plots of the data. The uncertainty in the measurement of the bulk and Young's modulus are ± 0.21 GPa and ± 0.08 GPa , respectively.

The ultrasonic velocity of the alkali-borosilicate with different transition metal oxides (TMOs) has been studied using the pulse echo technique. The elastic moduli such as elastic constant and bulk modulus have been obtained from the experimental data. Changes in the structure with different gamma irradiation dose have been investigated by using FTIR spectroscopy and ultrasonic studies. The results show that structural change in the BO_3 to BO_4 due to TMOs (V_2O_5, TiO_2 and ZnO) and irradiation are obtained [72]. The results of bulk modulus on the effects of irradiation are shown in the Figure 32.

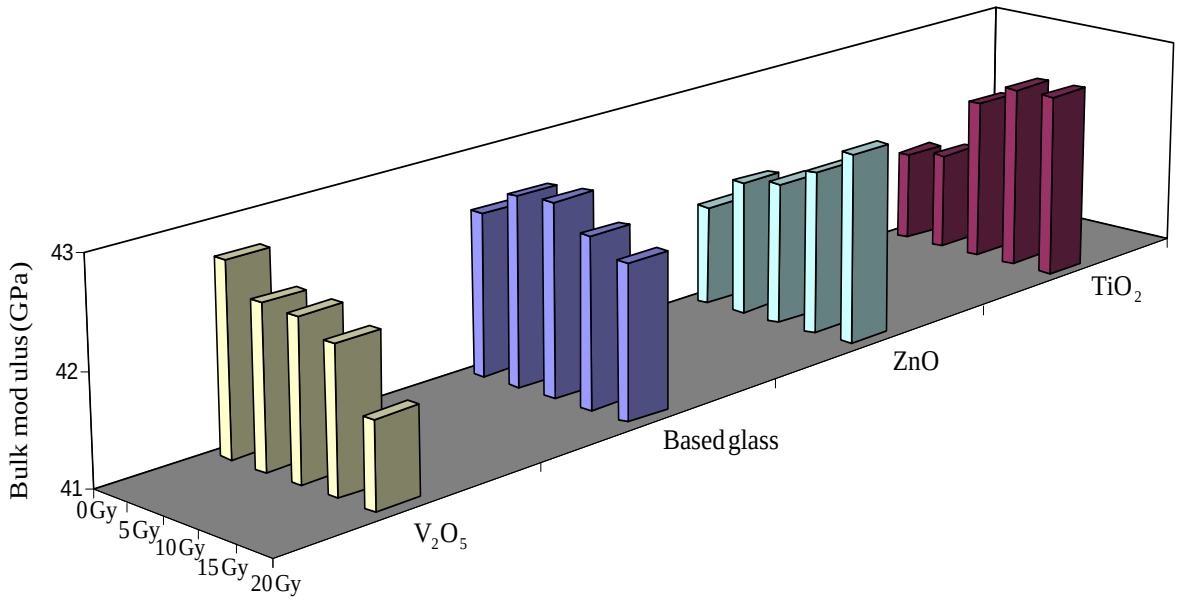

Figure 32 Variation of bulk modulus (K) of the alkali-borosilicate samples doped TMOs with different gamma irradiation dose

Moreover, the borosilicate glasses doped with Co_2O_3 and Fe_2O_3 have been studied under the influence of gamma irradiation. The results from this study show that glass with Co_2O_3 added is more responsive to irradiation than glass with Fe_2O_3 added. The structural response upon irradiation was a change from a triangular to tetrahedral structure ($BO_3 \rightarrow BO_4$ and $SiO_4^- \rightarrow SiO_4$). In addition, the irradiation effect was lower with higher TMO concentrations [73]. The effects of irradiation on the mean ultrasonic velocity are shown in the Figure 33.

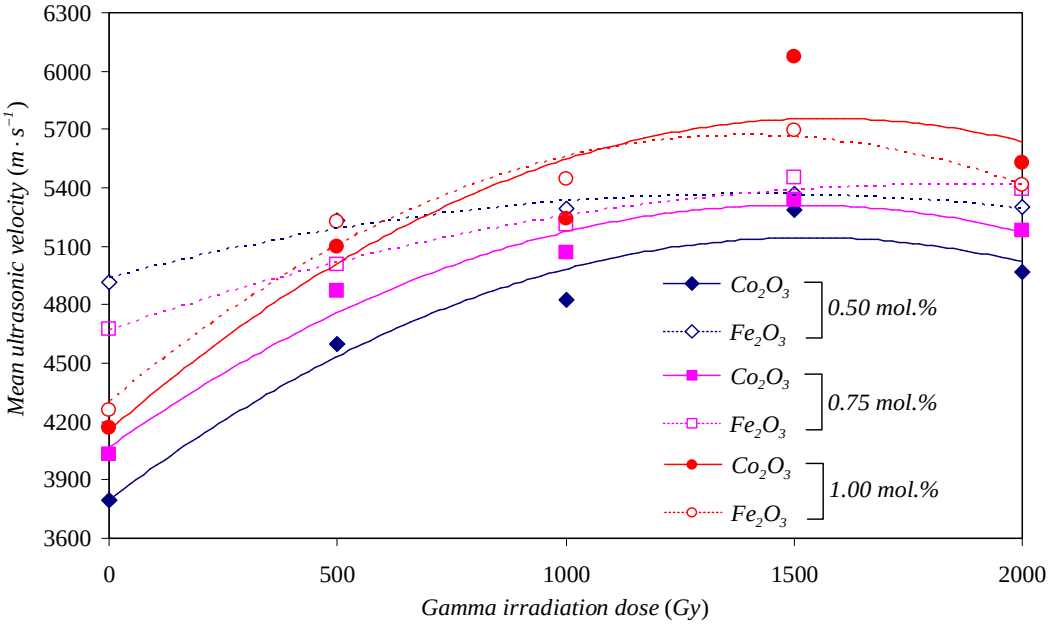

Figure 33 The mean ultrasonic velocity (v_m) of glass samples with different gamma irradiation dose

6. Conclusions

The $(100-x)\mathrm{RWG}-(x)\mathrm{Na_2O}$ glass system with different concentrations of Na_2O was prepared and their integrated TL signals were recorded. The results indicated that the $(90)\mathrm{RWG}-(10)\mathrm{Na_2O}$ glass sample produced the highest TL intensity, thus this glass was selected as base glass ($\mathrm{G}-0$). The $(90)\mathrm{RWG}-(10)\mathrm{Na_2O}$ glass system was doped with different concentrations of CeO_2, Nd_2O_3, Dy_2O_3 and MnO_2. From the results, Soda lime glasses improved by adding CeO_2, Nd_2O_3, Dy_2O_3 and MnO_2, were prepared for investigation of their thermoluminescence and physical properties to design for radiation dosimetric measurement. The results of the thermoluminescence testing showed that the glass samples doped with CeO_2 0.010 mol%, Nd_2O_3 0.100 mol%, Dy_2O_3 0.100 mol% and MnO_2 0.010 mol% had the highest integrated TL signals and linearity. Therefore, the glass samples were selected to calculate trap depth parameters. The activation energy depends directly on the ability of electron trapping and/or release of dopant ions (R^{m+}). The effective atomic numbers of selected glass samples were significantly higher than the effective atomic numbers of human tissue. However, the R $\left(\text{where } \mathrm{R}=\dfrac{\mathrm{Z_{eff}\ of\ sample}}{\mathrm{Z_{eff}\ of\ human\ tissue}}\right)$ values $(\mathrm{R}<2.3)$ of the selected glass samples were

acceptable to consider for potential radiation dosimetric materials, as they showed good thermoluminescence properties in terms of sensitivity and linearity at low dose levels of radiation. Moreover, the high elastic moduli of the glass samples indicated high rigidity and stability of the glass matrix structure. There was a fair agreement between the theoretically calculated and experimental elastic moduli for the glass samples. The optical absorption testing of glass samples ($G-0$ to $G-4$) was carried out. Results show that the transitions of Dy^{3+} ions in the glass samples is attributed to the exchange interaction among the exited Dy^{3+} ions at higher concentrations. In addition, the results from adding the dopants and effects of irradiation on some host glasses (such as borosilicate glasses, silicate glasses and local sand) shows that the types and concentrations of dopants directly change in structural properties of the glasses as well as the radiation effects.

References

[1] V. Kortov, Materials for thermoluminescent dosimetry: Current status and future trends, Radiation Measurements 42 (2007) 576-581.

[2] E.M. Yoshimura, E.G. Yukihara, Optically stimulated luminescence: Searching for new dosimetric materials, Nuclear Instruments and Methods in Physics Research B 250 (2006) 337-341.

[3] P. Olko, Advantages and disadvantages of luminescence dosimetry, Radiation Measurements 45 (2010) 506-511.

[4] V. Correcher, J. Garcia-Guinea, T. Rivera, Thermoluminescence sensitivity of daily-use materials, Radiation Effects & Defects in Solids 164 (2009) 232-239.

[5] B. Engin, C. Aydas, H. Demirtas, Study of the thermoluminescence dosimetric properties of window glass, Radiation Effects & Defects in Solids 165 (2010) 54-64.

[6] F.A. Balogun, F.O. Ogundare, M.K. Fasasi, TL response of sodalime glass at high doses, Nuclear Instruments and Methods in Physics Research A 505 (2003) 407-410.

[7] M.H. Kharita, S. Yousef, S. Bakr, The use of commercial glass as a potential gamma accidental dosimeter through the absorption spectra, Nuclear Instruments and Methods in Physics Research B 278 (2012) 50-57.

[8] G. Sharma, V. Rajendran, K.S. Thind, G. Singh, A. Singh, Structural investigation of bismuth borate glasses under the influence of γ-irradiation through ultrasonic studies, Physica B 404 (2009) 3371-3378.

[9] R. Laopaiboon, C. Bootjomchai, M. Chanphet, J. Laopaiboon, Elastic properties investigation of gamma-radiated barium lead borosilicate glass using ultrasonic technique, Ann. Nucl. Energy 38 (2011) 2333-2337.

[10] C. Bootjomchai, J. Laopaiboon, S. Nontachat, U. Tipparach, R. Laopaiboon, Structural investigation of borosilicate recycled-barium-bismuth glasses under the influence of gamma-irradiation through ultrasonic and FTIR studies, Nuclear Engineering and Design 248 (2012) 28-34.

[11] R. Chen, On the calculation of activation energies and frequency factors from glow curves, J. Appl. Phys. 40 (1969) 570.

[12] A. Abd El-Moneim, I.M. Youssof, L. Abd El-Latif, Structural role of RO and Al_2O_3 in borate glasses using an ultrasonic technique, Acta Mater. 54 (2006) 3811-3819.

[13] I.Z. Hager, Effect of Er_2O_3 and ErF_3 on the structural and elastic properties of sodium oxyfluoroborate glasses. J. Alloys Compd. 539 (2012) 256-263.

[14] K. Singh, H. Singh, V. Sharma, R. Nathuram, A. Khanna, R. Kumar, S.S. Bhatti, H.S. Sahota, Gamma-ray attenuation coefficients in bismuth borate glasses, Nucl. Instrum. Methods Phys. Res. B 194 (2002) 1-6.

[15] L. Gerward, N. Guibert, K.B. Jensen, H. Levring, WinXcom – a program for calculating X-ray attenuation coefficients, Radiat. Phys. Chem. 71 (2004) 653-654.

[16] R.J. Amjad, M.R. Sahar, S.K. Ghoshal, M.R. Dousti, R. Arifin, Synthesis and characterization of Dy^{3+} doped zinc-lead-phosphate glass, Opt. Mater. 35 (2013) 1103-1108.

[17] Y.S.M. Alajerami, S. Hashim, W.M.S.W. Hassan, A.T. Ramli, A. Kasim, Optical properties of lithium magnesium borate glasses doped with Dy^{3+} and Sm^{3+} ions, Phys. B 407 (2012) 2398-2403.

[18] R. El-Mallawany, N. El-Khoshkhany, H. Afifi, Ultrasonic studies of $(TeO_2)_{50}$-$(V_2O_5)_{50-x}$-$(TiO_2)_x$ glasses. Mater. Chem. Phys. 95 (2006) 321-327.

[19] M.A. Sidkey, M.S. Gaafar, Ultrasonic studies on network structure of ternary TeO_2-WO_3-K_2O glass system. Phys. B 348 (2004) 46-55.

[20] S.Y. Marzouk, Ultrasonic and infrared measurements of copper-doped sodium phosphate glasses. Mater. Chem. Phys. 114 (2009) 188-193.

[21] B. Bridge, A.A Higazy, Model of the compositional dependence of the elastic moduli of polycomponent oxide glasses. Phys. Chem. Glasses 27 (1986) 1-14.

[22] A. Abd El-Moneim, Quantitative analysis of elastic moduli and structure of B_2O_3-SiO_2 and Na_2O-B_2O_3-SiO_2 glasses. Phys. B 325 (2003) 319-332.

[23] R. El-Mallawany, Structural interpretations on tellurite glasses. Mater. Chem. Phys. 63 (2000) 109-115.

[24] R. El-Mallawany, H. Afifi, Elastic moduli and crosslinking of some tellurite glass systems. Mater. Chem. Phys. 143 (2013) 11-14.

[25] S.W.S. McKeever, M. Moscovitch, P.D. Townsend, Thermoluminescence dosimetry materials: Properties and uses. Nuclear Technology Publishing 1995.

[26] R. El-Mallawany, H.M. Diab, Improving dosimetric properties of tellurite glasses. Physica B 407 (2012) 3580-3585.

[27] A. Un, Investigation of dopant effect on some TL dosimeters containing boron, Radiat. Phys. Chem. 85 (2013) 23-35.

[28] ICRU (1989), Tissue Substitutes in Radiation Dosimetry and Measurement, Report 44 of the International Commission on Radiation Units and Measurements (Bethesda, MD).

[29] Y.S.M. Alajerami, S. Hashim, A.T. Ramli, M.A.S. Saleh, T. Kadni, Thermoluminescence characteristics of the Li_2CO_3-K_2CO_3-H_3BO_3 glass system co-doped with CuO and MgO. J. Lumin. 143 (2013) 1-4.

[30] B.J.R. Swamy, B. Sanyal, Y. Gandhi, R.M. Kadam, V.N. Rajan, P.R. Rao, N. Veeraiah, Thermoluminescence study of MnO doped borophosphate glass samples for radiation dosimetry, J. Non-Cryst. Solids 368 (2013) 40-44.

[31] G.V. Rao, P.Y. Reddy, N. Veeraiah, Thermoluminescence studies on Li_2O-CaF_2-B_2O_3 glasses doped with manganese ions, Mater. Lett. 57 (2002) 403-408.

[32] S. Mohan, K.S. Thind, G. Sharma, Effect of Nd^{3+} concentration on the physical and absorption properties of sodium-lead-borate glasses, Brazilian J. Phys. 37 (2007) 1306-1313.

[33] N.H. Yaakob, H. Wagiran, I. Hossain, A.T. Ramli, D.A. Bradley, S. Hashim, H. Ali, Electron irradiation response on Ge and Al-doped SiO_2 optical fibres, Nucl. Instrum. Methods Phys. Res. A 637 (2011) 186-189.

[34] V. Pagonis, G. Kitis, C. Furetta, Numerical and practical exercises in thermoluminescence, Springer+Business Media, Inc., 233 Spring Street, New York. 2006.

[35] C. Bootjomchai, R. Laopaiboon, Thermoluminescence dosimetric properties and effective atomic numbers of window glass, Nucl. Instrum. Methods Phys. Res. B 323 (2014) 42-48.

[36] P. Narayan, K.R. Senwar, S.G. Vaijapurkar, D. Kumar, P.K. Bhatnagar, Application of commercial glasses for high dose measurement using the thermoluminescent technique, Appl. Radiat. Isot. 66 (2008) 86-89.

[37] M. Sundara Rao, B. Sanyal, K. Bhargavi, R. Vijay, I.V. Kityk, N. Veeraiah, Influence of induced structural change on thermoluminescence characteristics of γ-ray irradiated PbO-Al_2O_3-SiO_2: Dy^{3+} glasses, J. Mol. Struct. 1073 (2014) 174-180.

[38] R.K. Gartia, L. Rey, Th. Tejkumar Singh, Th. Basanta Singh, Thermoluminescence of alkali halides and its implications, Nucl. Instrum. Methods Phys. Res. B 274 (2012) 129-134.

[39] J.A. Wani, M.S. Atone, N.S. Dhoble, S.J. Dhoble, Effect of rare earth ions on TL of $CaSO_4$:Dy, P phosphor, J. Lumin. 134 (2013) 640-648.

[40] S. Hashim, Y.S.M. Alajerami, A.T. Ramli, S.K. Ghoshal, M.A. Saleh, A.B. Abdul Kadir, M.I. Saripan, K. Alzimami, D.A. Bradley, M.H.A. Mhareb, Thermoluminescence dosimetry properties and kinetic parameters of lithium potassium borate glass co-doped with titanium and magnesium oxides, App. Radiat. Isotopes 91 (2014) 126-130.

[41] G.V.L. Reddy, L.R. Moorthy, B.C. Jamalaiah, T. Sasikala, Preparation, structural and luminescent properties of $YAl_3(BO_3)_4$:Dy^{3+} phosphor for white light-emission under UV excitation, Ceram. Inter. 39 (2013) 2675-2682.

[42] T.K. Kumar, V.K. Reddy, Effective atomic numbers for materials of dosimetric interest, Radiat. Phys. Chem. 50 (1997) 545-553.

[43] J.E. Shelby, Introduction to Glass Science and Technology. Royal Society of Chemistry, Cambridge. 1997.

[44] S.A. Azizan, S. Hashim, N.A. Razak, M.H.A. Mhared, Y.S.M. Alajerami, N.Tamchek, Physical and Optical properties of Dy^{3+}: Li_2O-K_2O-B_2O_3 glasses, J. Mol. Struct. 1076 (2014) 20-25.

[45] T.Y. Lim, H. Wagiran, R. Hussin, S. Hashim, M.A. Saeed, Physical and optical properties of dysprosium ion doped strontium borate glasses, Phys. B 451 (2014) 63-67.

[46] R.S. Gedam, D.D. Ramteke, Influence of CeO_2 addition on the electrical and optical properties of lithium borate glasses, J. Phys. Chem. Solids 74 (2013) 1399-1402.

[47] V. Rajendran, N. Palanivelu, P. Palanichamy, T. Jayakumar, B. Raj, B.K. Chaudhuri, Ultrasonic characterization of ferroelectric $BaTiO_3$ doped lead bismuth oxide semiconducting glasses, J. Non-Cryst. Solids 296 (2001) 39-49.

[48] R. El-Mallawany, A. Abousehly, A.A. El-Rahamani, E. Yousef, Radiation effect on the ultrasonic attenuation and internal friction of tellurite glasses, Mater. Chem. Phys. 52 (1998) 161-165.

[49] H. Doweidar, Y.B. Saddeek, FTIR and ultrasonic investigation on modified bismuth borate glasses, J. Non-Cryst. Solids 355 (2009) 348-354.

[50] Y.B. Saddeek, I.S. Yahia, K.A. Aly, W. Dobrowolski, Spectroscopic, mechanical and magnetic characterization of some bismuth borate glasses containing gadolinium ions, Solid State Sci. 12 (2010) 1426-1434.

[51] Y.B. Saddeek, L. Abd El Latif, Effect of TeO_2 on the elastic moduli of sodium borate glasses, Phys. B 348 (2004) 475-484.

[52] A. Abd El-Moneim, I.M. Youssof, M.M. Shoaib, Elastic moduli prediction and correlation in SiO_2-based glasses, Mater. Chem. Phys. 52 (1998) 258-262.

[53] B. Eraiah, R.V. Anavekar, Elastic properties of silver-phospho-vanadate glasses, J. Alloys Compd. 489 (2010) 325-327.

[54] T.Y. Wei, Y. Hu, L.G. Hwa, Structure and elastic properties of low-temperature sealing phosphate glasses, J. Non-Cryst. Solids 288 (2001) 140-147.

[55] A.G. Clare, Key engineering materials, in: J.E. Shelby et al. (Eds.), Rare Elements in Glasses. Trans Tech Publications, Switzerland 94-95, 1994. pp. 161-180.

[56] N.J. Clayden, S. Esposito, A. Aronne, Solid state ^{27}Al NMR and FTIR study of lanthanum aluminosilicate glasses. J. Non-Cryst. Solids 258 (1999) 11-19.

[57] H. Lemercier, T. rouxel, D. Fargeot, J.L. Besson, B. Piriou, Yttrium SiAlON glasses: structure and mechanical properties elasticity and viscosity. J. Non-Cryst. Solids 201 (1996) 128-145.

[58] Y.S.M. Alajerami, S. Hashim, S.K. Ghoshal, A.T. Ramli, M.A. Saleh, Z. Ibrahim, T. Kadni, D.A. Bradley, Luminescence characteristics of Li_2CO_3-K_2CO_3-H_3BO_3 glasses co-doped with TiO_2/MgO. App. Radiat. Isotopes 82 (2013) 12-19.

[59] F.M. Ezz El-Din, N.A. El-Alaily, H.A. El-Batal, Density and refractive index of some γ-irradiated alkali silicate glasses. J. Radioanal. Nucl. Chem. 163 (2) (1992) 267-275.

[60] M.O. Prado, N.B. Messi, T.S. Plivelic, I.L. Torriani, A.M. Bevilacqua, M.A. Arribére, The effects of radiation on the density of an aluminoborosilicate glass. J. Non-Cryst. Solids 289 (2001) 175-184.

[61] H. Singh, K. Singh, L. Gerward, K. Singh, H.S. Sahota, R. Nathuram, ZnO-PbO-B_2O_3 glasses as gamma-ray shielding materials. Nucl. Instr. and Meth. B 207 (2003) 257-262.

[62] S.Y. Marzouk, M.S. Gaafar, Ultrasonic study on some borosilicate glasses doped with different transition metal oxides. Solid State Commun. 144 (2007) 478-483.

[63] A.A. Higazy, B. Bridge, Elastic constants and structure of the vitreous system Co_3O_4-P_2O_5. J. Non-Cryst. Solids 72 (1985) 81-108.

[64] M.S. Gaafar, H.A. Afifi, M.M. Mekawy, Structural studies of some phosphor-borate glasses using ultrasonic pulse-echo technique, DSC and IR spectroscopy. Phys. B 404 (2009) 1668-1673.

[65] M.S. Gaafar, S.Y. Marzouk, Mechanical and structural studies on sodium borosilicate glasses doped with Er_2O_3 using ultrasonic velocity and FTIR spectroscopy. Phys. B 388 (2007) 294-302.

[66] D.J.M. Burkhard, Elastic properties of alkali silicate glasses with iron oxide: relation to glass structure. Solid State Commun. 101 (1997) 903-907.

[67] M. Wang, M. Li, J. Cheng, F. He, Structure and viscosity of soda lime silicate glasses with varying Gd_2O_3 content. J. Mol. Struct. 1063 (2014) 139-144.

[68] F.H. ElBatal, A.M. Abdelghany, H.A. ElBatal, Characterization by combined optical and FT infrared spectra of 3d-transition metal ions doped-bismuth silicate glasses and effects of gamma irradiation. Spectrochimica Acta A 122 (2014) 461-468.

[69] R.R. Zahran, Effect of γ-irradiation on the ultrasonic and structural properties of polyoxymethylene. Mater. Lett. 37 (1998) 83-89.

[70] C. Bootjomchai, R. Laopaiboon, S. Pencharee, J. Laopaiboon, Elastic moduli of borosilicate glasses doped with heavy metal oxides, J. Non-Cryst. Solids 388 (2014) 37-45.

[71] R. Laopaiboon, C. Bootjomchai, Radiation effects on structural properties of glass by using ultrasonic techniques and FTIR spectroscopy: A comparison between local sand and SiO_2, Ann. Nucl. Energy 68 (2014) 220-227.

[72] R. Laopaiboon, S. Nontachat, S. Pencharee, J. Laopaiboon, C. Bootjomchai, Structural investigation of glasses with doped some transition metal oxides under the influence of gamma irradiation, Radiat. Eff. Defects Solids 169 (2014) 862-873.

[73] R. Laopaiboon, C. Bootjomchai, Glass structure responses to gamma irradiation using infrared absorption spectroscopy and ultrasonic techniques: A comparative study between Co_2O_3 and Fe_2O_3, Appl. Radiat. Isot. 89 (2014) 42-46.

7. Output (Acknowledge the Thailand Research Fund)

- **Cherdsak Bootjomchai***, Raewat Laopaiboon, *Thermoluminescence dosimetric properties and effective atomic numbers of window glass*, **Nuclear Instruments and Methods in Physics Research B** 323 (2014) 42-48.

- Raewat Laopaiboon, **Cherdsak Bootjomchai***, *Radiation effects on structural properties of glass by using ultrasonic techniques and FTIR spectroscopy: A comparison between local sand and SiO_2*, **Annals of Nuclear Energy** 68 (2014) 220-227.

- R. Laopaiboon, **C. Bootjomchai***, *Glass structure responses to gamma irradiation using infrared absorption spectroscopy and ultrasonic techniques: A comparative study between Co_2O_3 and Fe_2O_3*, **Applied Radiation and Isotopes** 89 (2014) 42-46.

- **Cherdsak Bootjomchai***, Raewat Laopaiboon, Somkid Pencharee, Jintana Laopaiboon, *Elastic moduli of borosilicate glasses doped with heavy metal oxides*, **Journal of Non-Crystalline Solids** 388 (2014) 37-45.

- R. Laopaiboon, S. Nontachat, S. Pencharee, J. Laopaiboon, **C. Bootjomchai***, *Structural investigation of glasses with doped some transition metal oxides under the influence of gamma irradiation*, **Radiation Effects & Defects in Solids** 169 (2014) 862-873.

- **C. Bootjomchai***, *Comparative studies between theoretical and experimental of elastic properties and irradiation effects of soda lime glasses doped with neodymium oxide*, **Radiation Physics and Chemistry** 110 (2015) 96-104.

- Raewat Laopaiboon, **Cherdsak Bootjomchai***, *Thermoluminescence studies on alkali-silicate glass doped with dysprosium oxide for use in radiation dosimetry measurement*, **Journal of Luminescence** 158 (2015)275-280.

- R. Laopaiboon, **C. Bootjomchai***, *Physical properties and thermoluminescence of glasses designed for radiation dosimetry measurements*, **Materials and Design** (2015), doi: http://dx.doi.org/10.1016/j.matdes.2015.05.002

Appendix

(Publications)

Nuclear Instruments and Methods in Physics Research B 323 (2014) 42–48

Contents lists available at ScienceDirect

Nuclear Instruments and Methods in Physics Research B

journal homepage: www.elsevier.com/locate/nimb

Thermoluminescence dosimetric properties and effective atomic numbers of window glass

Cherdsak Bootjomchai *, Raewat Laopaiboon

Glass Technology Excellent Center (GTEC), Department of Physics, Faculty of Science, Ubon Ratchathani University, Ubon Ratchathani 34190, Thailand

ARTICLE INFO

Article history:
Received 27 October 2013
Received in revised form 14 January 2014
Available online 7 February 2014

Keywords:
Glass
Thermoluminescence
Effective atomic number

ABSTRACT

This work presents the main thermoluminescence (TL) dosimetric characteristics of commercial Thai transparent window glass. The amorphous structure of window glass was investigated by XRD. The glow curve revealed a peak (T_m) at 235 °C. The thermoluminescence response of window glass was studied after irradiation with photons in the absorb dose range of 0–14.05 mGy, which is of interest for the personal protection level of dosimetry. A linear response was obtained after both the first irradiation and the second irradiation. The minimum detectable dose of window glass was 0.15 mGy. The effective atomic number of window glass as a function of photon energy was calculated. The obtained results for the effective atomic number showed that it is very close to that of human biological tissues (Z_{eff} = 6.7–8.4 at studied energy).

1. Introduction

The search for materials which are universally available and can be used as dosimeters in case of an accidental radiological emergency has become a research issue for many researchers around the world [1–3]. Many kinds of thermoluminescence (TL) materials used as detectors in the fields of medicine, industry, environmental monitoring and space research are accessible commercially. The main advantages of thermoluminescence dosimeters (TLD) are their extensive functional dose range, small physical size, reusability and tissue equivalence [4]. For a material to be accepted as a tissue alternate for photon interaction, the radiation absorption and scattering acquired for a specified material must be the same as that experienced by the tissue under similar conditions. A suitable way of comparing the interaction with radiation of a given tissue and the specified tissue equivalent material is to consider either the photon mass attenuation coefficient and mass energy absorption coefficient or the effective atomic number [5]. Glass materials have valuable properties such as easy handling, chemical inertness, rigidity and excellent transparency. The advantages of glass are its easy fabrication, good homogeneity and the fact that its structural properties can be improved by the addition of oxides in the glass formula. Moreover, a dosimeter made from glass possesses several advantages over other dosimeters, not least of which is its Z_{eff}, which is very close to that of human biological tissues (Z_{eff} = 7.42 for soft tissue) [6–8].

The possibility of using biological tissue and inorganic materials in radiation-dose measurements and in particular in accident dosimetry has been investigated. One of the reasons why window glass was considered was because it is common in most laboratories, houses and other building constructions and can easily be used after a radiation accident to estimate the radiation dose. Engin et al. [9] investigated the thermoluminescence dosimetric properties of commercial Turkish transparent window glass. They reported that the window glass may be proposed as reliable TL material for measuring high gamma doses. In addition, Kharita et al. [10] used commercial glass (ordinary window glass in Syria) as a potential gamma accidental dosimeter. They found that the common glass can be used to estimate the irradiation dose. However, the use of commercial window glass in Thailand for radiation dosimetry has not yet appeared although an accident involving gamma radiation from Co-60 occurred in Thailand in 2000 [11].

Therefore, the main objective of this work is to investigate the TL properties of commercial window glass in Thailand and to evaluate its possible use for gamma radiation dose measurements in accident dosimetry. The window glass or sodalime glass is a common material in almost all the laboratories and therefore if comprehensively studied and developed for radiation dose measurements, it will become a consistent means of estimating the doses of personnel who may be accidentally irradiated [12–13].

2. Experimental

The window glass samples were used for the TL analysis before and after exposure to an X-ray exposure machine. All of the samples were taken from the same window glass plate. The window

* Corresponding author. Tel.: +66 853078883; fax: +66 45288381.
E-mail addresses: cherdsak_per@hotmail.co.th, cherdsak2303@gmail.com (C. Bootjomchai).

0168-583X/$ - see front matter © 2014 Elsevier B.V. All rights reserved.
http://dx.doi.org/10.1016/j.nimb.2014.01.008

glass was common window glass sold in Ubon Ratchathani, Thailand. The chemical composition analyses of the window glass were carried out by using the WDXRF method and are shown in Table 1. The window glass was cleaned and cut into small pieces of dimensions $5 \times 5 \times 2\ mm^3$ for the TL and XRD measurements. X-ray diffraction studies were carried out to confirm the amorphous structure of the window glass. A Philips X'Pert PANalytical diffractrometer was used during the investigations. The radiation used was CuKα and the pattern was recorded at a scanning rate of 4°/min and an angular range (2θ) of 5–80°. The absence of crystallization peaks in the XRD data showed that the window glass was amorphous (Fig. 1).

All samples were annealed at 400 °C for 1 h and 100 °C for 2 h (dual step technique) before being irradiated with X-ray photon energy of 100 keV at dose range 0–14.05 mGy to determine the thermoluminescence response and glow curve. The photon energy dependence was studied at photon energies of 25, 50, 100 and 110 keV, respectively. TL light emitted from window glass was detected by a TLD Reader (Harshaw/Bicron Model 3500 Manual). The glow curves were recorded from room temperature up to a maximum temperature of 300 °C, at heating rates of 10 °C/s and the second reading with the same profile. A region of interest facility available in the TLD Reader was used to evaluate the responses of different glow peaks resulting from the Computerized Glow Curve Deconvolution (CGCD) procedure. The estimation of glow peaks was carried out by copying the American Standard Code for Information Interchange (ASCII) files from the TLD Reader to the Excel program. Each data point observed in the figures was obtained by an average of five measurements. The effective atomic number (Z_{eff}) for all types of materials, compounds as well as mixtures, can be written in terms of the fraction abundance as [14]:

$$Z_{eff} = \frac{\sum_i f_i A_i (\mu/\rho)_i}{\sum_j f_j \frac{A_j}{Z_j} (\mu/\rho)_j} \quad (1)$$

where $f_i = \frac{n_i}{\sum_j n_j}$ is the fractional abundance of constituent element i, n_i is the total number of atoms and $\sum_j n_j$ is the total number of atoms present in the molecular formula, A_i and Z_i are the atomic weight and atomic number, respectively. $(\mu/\rho)_i$ is the mass attenuation coefficient obtained from the WinXCom program.

3. Results and discussion

Table 1 shows the condition of quantitative measurement of the chemical composition of recycled window glass (RWG) by using the WDXRF method. The major components of window glass are SiO_2, Na_2O, CaO, MgO, Al_2O_3, Fe_2O_3, TiO_2 and K_2O respectively. The thermoluminescence samples irradiated with 100 keV photon energy at doses of 2.01, 4.07, 6.00, 8.03, 10.06 and 14.05 mGy were measured and are shown in Fig. 2. From observations, the glow curves centered at about 235 °C and the relative light intensity of TL signals increased with increasing irradiation dose. The investigation of the dependence of the TL signal on irradiation dose was carried out on window glass samples exposed to photons for doses between 0 and 14.05 mGy. The average integrated TL signals of each dose were recorded and the relative standard deviations were calculated.

Fig. 3 shows the experimental trend obtained and the corresponding calibration line of best fit resulting from the processing of the experimental points. The correlation coefficient (R^2) was calculated to confirm the linearity of the dose response in the investigated dose range. The minimum detectable dose (MMD) value of window glass samples was determined as a dose of 3 times the corresponding value of the standard deviations of 10 un-irradiated samples. The estimated value of MMD obtained was about 0.15 mGy. Hence thermoluminescence intensities of the window glass were shown as likely to be used for low radiation doses. Fig. 4 shows the reproducibility of the window glass (annealing → irradiation → readout). Data from Fig. 4 reveal that the calibration lines for the first and the second irradiation are

Table 1
Condition of quantitative measurement of chemical composition of recycled window glasses (RWG) by using WDXRF method.

Chemical	Line	Crystal	Detector	Collimator (μm)	kV	mA	Concentration (%)
Na_2O	K_α	PX1	Flow	4000	24	125	15.1700
MgO	K_α	PX1	Flow	4000	24	125	3.4030
SiO_2	K_α	PE002	Flow	300	24	125	73.3900
Al_2O_3	K_α	PE002	Flow	300	24	125	0.5866
CaO	K_α	LiF200	Flow	300	24	125	7.3390
Fe_2O_3	K_α	LiF200	Duplex	300	50	60	0.0635
TiO_2	K_α	LiF200	Flow	300	125	125	0.0263
K_2O	K_α	LiF200	Flow	300	125	125	0.0238

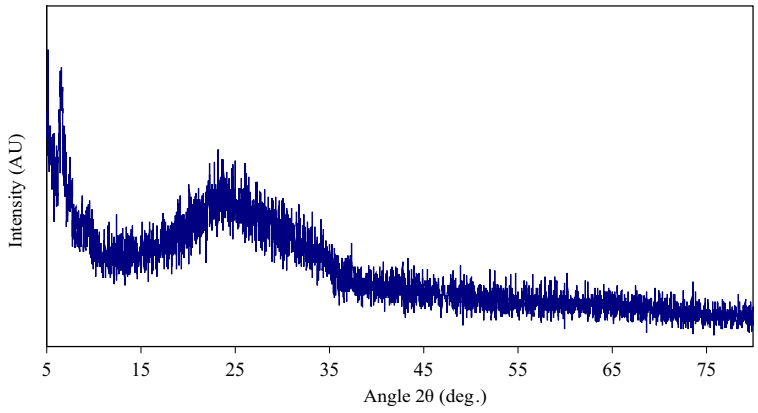

Fig. 1. XRD pattern of window glasses.

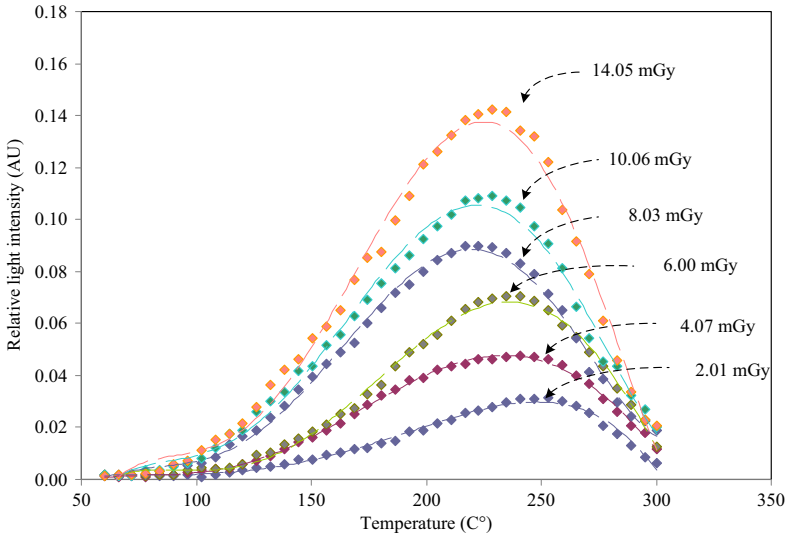

Fig. 2. Glow curve of window glass irradiated with different doses.

matching at low doses. For more information, the 10 samples were annealed by using a dual step process, and then irradiated with 10.08 mGy, and the TL signal was read out. This procedure was carried out for five cycles. The experimental values obtained are reported in Table 2 and the average values are shown in Fig. 5. The results indicated that after the reproducibility procedure the sensitivity increased as shown in Fig. 4. This was due to the improvement of the electron trap by heat treatment [15]. The statistical analysis to represent the reproducibility used the coefficients of variation analysis method. Covariance (CV) is a measure of how much two random variables change together. The following coefficients of variation can be defined [15] as:

The system variability index (SVI) or $\%\overline{CV} = \frac{SD}{\bar{X}} \times 100$; this is the mean value of percent standard deviations of each TL detector. This quantity gives a measure of the reproducibility of the whole system. The variation of SVI is 3.6% (Table 3).

The reader variability index (RVI) or $\%CV = \frac{SD}{mean} \times 100$; this is the percent standard deviations of the mean values of each cycle of readings. This quantity gives a measure of the long-term reader reproducibility. The variation of RVI is 1.8% (Table 4).

The detector variability index (DVI); this quantity gives a measure of the reproducibility of the TL detectors (samples), and is defined as:

$$DVI = \sqrt{(SVI)^2 - (RVI)^2} = 3.1\%$$

The DVI values indicated the high reproducibility of samples. However, the reproducibility of window glass samples required improvement when compared with the initial read out (Fig. 5). The author suggests that electron trapping should be improved by adding the modifier for constant trapping in the structure of the glass. This point is worthy of further investigation in the near future.

The most important problems in TL technique applied to different fields of dosimetry, such as personal, environmental and clinical dosimetry, are related to the loss of the stored TL signal after irradiation, generally called thermal fading (trapped charge effects), and to its evaluation [16]. Fig. 6 shows the average integrated TL intensity after a storage period of 1440 h at a dose of 14.05 mGy. This figure demonstrates a large decrease in the TL signal in the initial range (about 65% decreased at 0–200 h). These results suggest that the high loss of TL signal is due to un-stabilization of trapped charge effects. However, the TL signals become constant after a storage period of 200 h. Fig. 7 shows the average integrated TL intensity after the irradiation of window glass at 6.00 mGy with different radiation energies (25, 50, 75, 100 and 110 keV, respectively) which predict the energy dependent

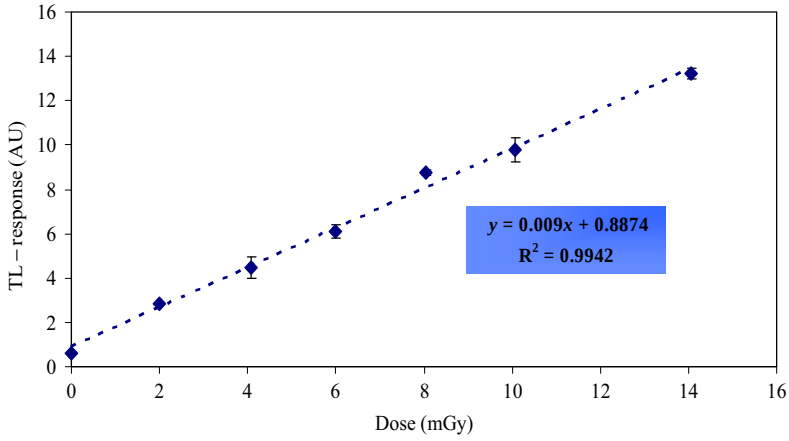

Fig. 3. Linear relationship between TL-response and irradiation dose of window glass.

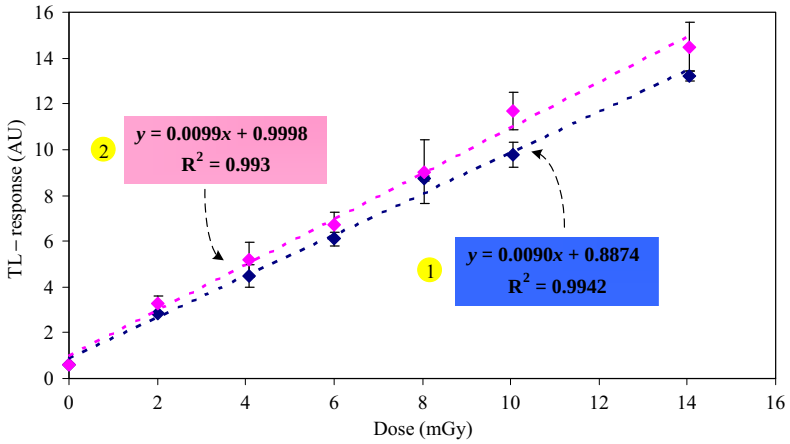

Fig. 4. Reproducibility of window glasses with blue line (1) is first irradiation and pink line and (2) is second irradiation. (For interpretation of the references to color in this figure legend, the reader is referred to the web version of this article.)

Table 2
Data for reproducibility of TLD measurement of recycled window glasses (RWG).

Chip No.	1st Reading	2nd Reading	3rd Reading	4th Reading	5th Reading
1	12.550	12.010	12.780	12.320	12.220
2	11.850	12.720	12.580	12.310	12.340
3	9.656	10.150	10.530	9.231	10.100
4	12.390	11.940	12.110	12.320	12.430
5	13.930	12.430	13.210	12.780	13.560
6	11.580	10.750	11.570	11.120	11.780
7	11.440	10.600	11.330	10.450	11.250
8	11.060	10.880	11.420	10.970	10.190
9	7.435	7.971	8.190	7.952	8.342
10	8.585	8.933	9.112	8.631	9.210

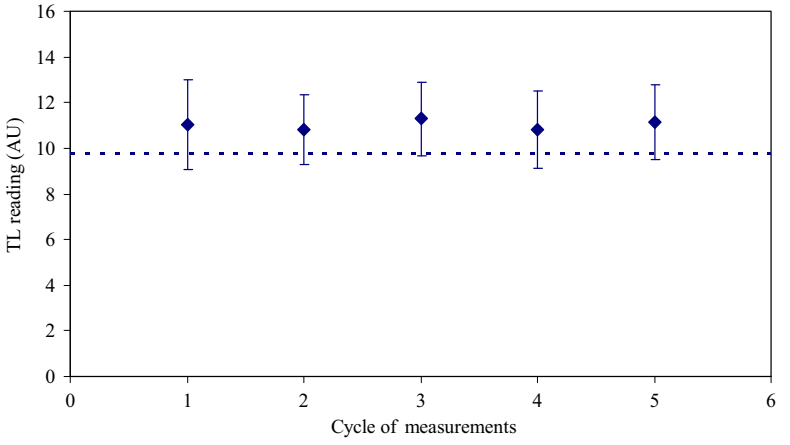

Fig. 5. Reproducibility of window glass samples with 10.08 mGy for five cycles (dash line is initial read out). Error bars correspond to one standard deviation.

behavior of the window glass. The energy dependence for window glass may be highly related with the value of effective atomic number (Z_{eff}) [9]. Fig. 8 shows the effective atomic numbers of window glass. It has been observed that the effective atomic numbers decrease with incident photon energy up to 15 keV. Then, effective atomic numbers suddenly increase with incident photon energy up to 150 keV. After that, effective atomic numbers become relatively constant with incident photon energy in the range 200–7000 keV. Effective atomic numbers slightly decrease with photon energy in the range 8–50 MeV. Then, effective atomic numbers become independent of the incident photon energy in the range 60–100000 MeV. The investigated energy range from 25 to 110 keV shows a linear increase of effective atomic number. This can be explained on the basis of dominance of the photoelectric process. For the photoelectric interaction near the K-edge of the elements with the high Z numbers [4] (Table 1), the effect of impurity of the window glass on the photoelectric effect is higher than the Compton effect in the studied energy range. Moreover, the effective atomic numbers obtained in this study show that it is very close to human biological tissues (Z_{eff} = 6.7–8.4 at studied energy). To confirm these results, the mass energy absorption coefficients were calculated by comparison between window glass and soft tissue. The mass attenuation coefficients of window glass were obtained from the WinXCom program. The mass energy absorption

Table 3
Calculation of system variability index (SVI). The average values of the five reading calculated from Table 2.

Chip No.	Average values of the five reading: $\bar{X}$	Standard deviation: SD	Covariance: CV = $\bar{X}$/SD
1	12.376	0.298	0.024
2	12.360	0.332	0.027
3	9.933	0.500	0.050
4	12.238	0.207	0.017
5	13.182	0.598	0.045
6	11.360	0.418	0.037
7	11.014	0.455	0.041
8	10.904	0.449	0.041
9	7.978	0.344	0.043
10	8.894	0.280	0.031
$\overline{CV}$			0.036
SVI = $\overline{CV} \times 100$			3.6%

Table 4
Calculation of reader variability index (RVI). The values of each reading are average of TL signal of all Chip No. in Table 2.

1st Reading	2nd Reading	3rd Reading	4th Reading	5th Reading	Mean	SD	RVI = $\frac{SD}{mean} \times 100$
11.048	10.838	11.283	10.808	11.142	11.024	0.202	1.8%

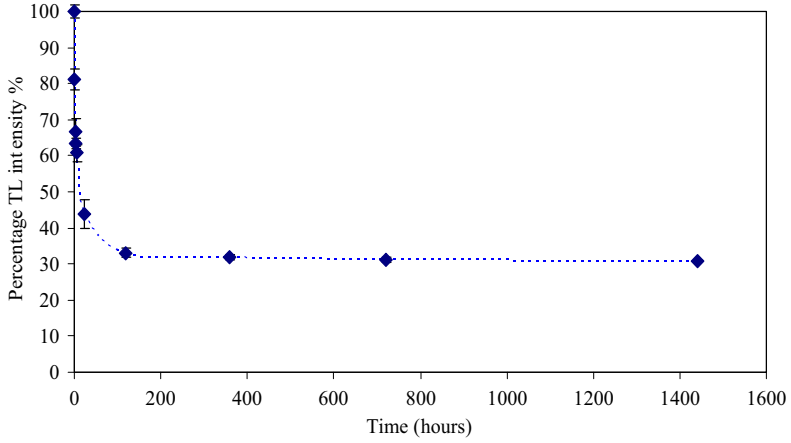

Fig. 6. Fading of irradiated window glass at room temperature.

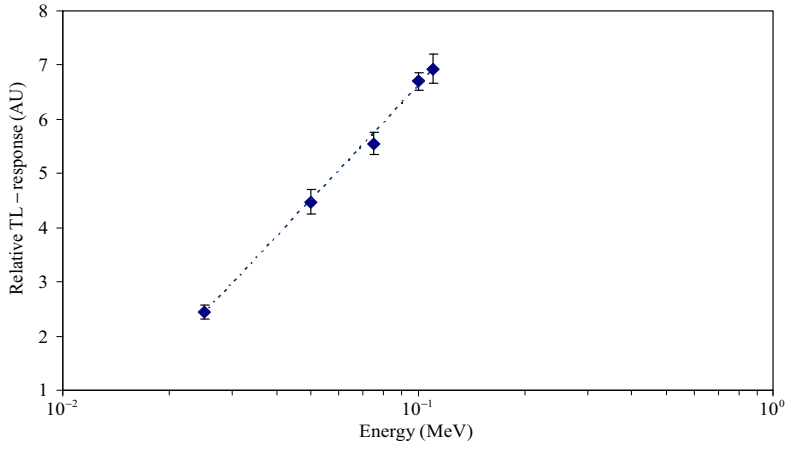

Fig. 7. The photon energy dependence of window glasses.

coefficients of soft tissue were obtained from ICRU-44 [17]. The results are shown in Fig. 9, with good agreement of trend lines of mass energy absorption coefficients between samples and soft tissue. In order to verify that the window glass is tissue equivalent, the ratio of Z_{eff} for window glass and the Z_{eff} for soft tissue was considered. Alajerami et al. reported that the human tissue Z_{eff} is 7.42. Therefore, the effective atomic number of window glass was compared with the Z_{eff} of human tissue [8]. The ratio

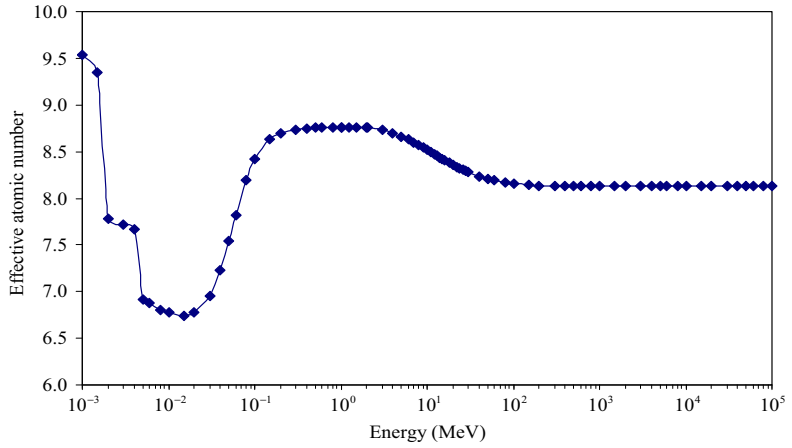

Fig. 8. The effective atomic number of window glasses with difference photon energy.

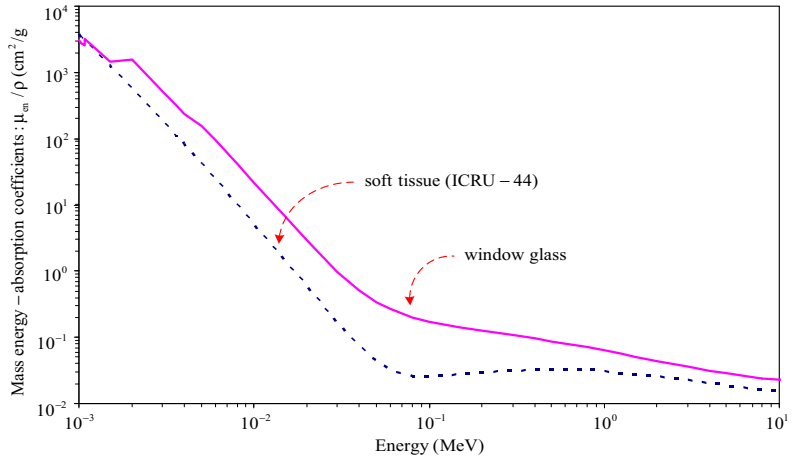

Fig. 9. Comparison mass energy-absorption coefficients between window glass and soft tissue (ICRU-44).

($R = \frac{Z_{\text{eff}} \text{ of sample}}{Z_{\text{eff}} \text{ of human tissue}}$) is in the range of 0.9–1.1 (at studied energy) which is close to 1. The result was sufficient to state that the window glass is tissue equivalent.

4. Conclusions

The results obtained in this paper show that the window glass sold in Ubon Ratchathani province, Thailand, is potentially a good candidate for retrospective dosimetry or personal dosimetry due to its common materials, easy sample preparation, linearity of TL response and because its effective atomic number is close to that of human biological tissues. However, the results also show differences in reproducibility and a high fading of the TL signal of window glass. Therefore, the improvements of TL properties of window glass as starting materials would provide an interesting study in the future.

Acknowledgements

Financial support of this study has been provided by The Thailand Research Fund (TRF), Office of the Higher Education Commission (OHEC) and Ubon Ratchathani University (UBU). The results and comments on this article are those of the authors. The TRF, OHEC and UBU are unnecessary always agree.

References

[1] M. Marrale, A. Longo, A. Bartolotta, S. Basile, M.C. D'Oca, E. Tomarchio, G.A.P. Cirrone, F. Di Rosa, F. Romano, G. Cuttone, M. Brai, Thermoluminescence response of sodalime glass irradiated with proton and neutron beams, Nucl. Instr. Meth. B 292 (2012) 55–58.
[2] M. Marrale, A. Longo, A. Bartolotta, M.C. D'Oca, M. Brai, Preliminary application of thermoluminescence and single aliquot regeneration method for dose reconstruction in soda lime glass, Nucl. Instr. Meth. B 297 (2013) 58–63.
[3] M. Ignatovych, M. Fasoli, A. Kelemen, Thermoluminescence study of Cu, Ag and Mn doped lithium tetraborate single crystals and glasses, Radiat. Phys. Chem. 81 (2012) 1528–1532.
[4] A. Un, Investigation of dopant effect on some TL dosimeters containing boron, Radiat. Phys. Chem. 85 (2013) 23–35.
[5] T.K. Kumar, V.K. Reddy, Effective atomic numbers for materials of dosimetric interest, Radiat. Phys. Chem. 50 (1997) 545–553.
[6] M.M. Elkholy, Thermoluminescence of B_2O_3–Li_2O glass system doped with MgO, J. Lumin. 130 (2010) 1880–1892.
[7] R. Sharma, V. Sharma, P.S. Singh, T. Singh, Effective atomic numbers for some calcium–strontium–borate glasses, Ann. Nucl. Energy 45 (2012) 144–149.
[8] Y.S.M. Alajerami, S. Hashim, A.T. Ramli, M.A.S. Saleh, T. Kadni, Thermoluminescence characteristics of the Li_2CO_3–K_2CO_3–H_3BO_3 glass system co-doped with CuO and MgO, J. Lumin. 143 (2013) 1–4.
[9] B. Engin, C. Aydaş, H. Demirtaş, Study of the thermoluminescence dosimetric properties of window glass, Radiat. Eff. Defects Solids 165 (2010) 54–64.
[10] M.H. Kharita, S. Yousef, S. Bakr, The use of commercial glass as a potential gamma accidental dosimeter through the absorption spectra, Nucl. Instr. Meth. B 278 (2012) 50–57.
[11] N. Ya-anant, K. Tiyapun, K. Saiyut, Radiological accident and incident in Thailand: lesson to be learned, Radiat. Prot. Dosimetry 146 (2011) 111–114.
[12] F.A. Balogun, F.O. Ogundare, M.K. Fasasi, TL response of sodalime glass at high doses, Nucl. Instr. Meth. A 505 (2003) 407–410.

[13] A. Bartolotta, M. Brai, V. Caputo, M.C. D'Oca, A. Longo, M. Marrale, Thermoluminescence response of sodalime glass irradiated with photon and electron beams in the 1–20 Gy range, Radiat. Meas. 46 (2011) 975–977.
[14] K. Singh, H. Singh, V. Sharma, R. Nathuram, A. Khanna, R. Kumar, S.S. Bhatti, H.S. Sahota, Gamma-ray attenuation coefficients in bismuth borate glasses, Nucl. Instr. Meth. B 194 (2002) 1–6.
[15] S.W.S. McKeever, M. Moscovitch, P.D. Townsend, Thermoluminescence Dosimetry Materials: Properties and Uses, Nuclear Technology Publishing, 1995.
[16] R. El-Mallawany, H.M. Diab, Improving dosimetric properties of tellurite glasses, Phys. B 407 (2012) 3580–3585.
[17] ICRU, Tissue Substitutes in Radiation Dosimetry and Measurement, Report 44 of the International Commission on Radiation Units and Measurements, Bethesda, MD, 1989.

Annals of Nuclear Energy 68 (2014) 220–227

Contents lists available at ScienceDirect

Annals of Nuclear Energy

journal homepage: www.elsevier.com/locate/anucene

Radiation effects on structural properties of glass by using ultrasonic techniques and FTIR spectroscopy: A comparison between local sand and SiO_2

Raewat Laopaiboon, Cherdsak Bootjomchai *

Glass Technology Excellent Center (GTEC), Department of Physics, Faculty of Science, Ubon Ratchathani University, Ubon Ratchathani 34190, Thailand

ARTICLE INFO

Article history:
Received 12 September 2013
Received in revised form 14 January 2014
Accepted 19 January 2014
Available online 8 February 2014

Keywords:
Glass
Ultrasonic techniques
Gamma irradiation
Local sand
FTIR spectra

ABSTRACT

A comparison between local sand and SiO_2 with different compositions of CeO_2 with respect to the structural properties of glasses after successive irradiation was carried out by using ultrasonic techniques and FTIR spectroscopy. The ultrasonic velocities were measured by the pulse echo technique, with a frequency of 4 MHz and at room temperature. From these obtained velocities and densities, various elastic moduli, micro-hardness and Poisson's ratio were calculated. The results indicate that local sand is more affected by gamma irradiation than SiO_2. These results are due to a higher iron impurity in local sand leading to the occurrence more non-bridging oxygen (NBO).

1. Introduction

Borosilicate glass is a technologically important material because it generally has good chemical resistance and high dielectric strength thanks to its low thermal expansion (ElBatal et al., 2007; Baccaro et al., 2007; Baydogan and Tugrul, 2012). Therefore, the structure of borosilicate glass has been extensively studied by using several techniques, as this system has a wide variety of technological applications such as; optical lenses, nuclear waste materials, shielding materials and use in the electronics industry (Fayon et al., 1998, 1999; Stentz et al., 2001). In addition, borosilicate is extensively used in semiconductor microelectronics for obtaining passive and insulating layers (Parchinskii, 2002). For this reason, it is important to study the influences of various external factors, in particular the effect of irradiation upon the structural properties of this glass system (Malchukova et al., 2005; Arora et al., 2009; Prymak et al., 2012; Deschanels et al., 2007; Bootjomchai et al., 2012). The knowledge of the glass structure before and after irradiation is a prerequisite for understanding the structural evolution of glass under long term irradiation (Ollier et al., 2004; De Bonfils et al., 2010; Prado et al., 2001; Aygun et al., 2012). The investigation of radiation effects leads to a better understanding of the intrinsic structure as well as the alterations, which result from the interaction with radiation. For this reason, it is important to study the influences of irradiation on borosilicate glass. Moreover, glass containing rare-earth ions has been the subject of various investigations, due to its potential as optical-fibre, amplifiers and scintillating glass (Weber, 1980; Marzouk, 2010).

The properties of glass are closely related to the inter-atomic forces and potentials in the lattice structure. Thus, changes in the lattice, due to doping and/or irradiation, can be directly noted. The elastic properties, micro-hardness, Poisson's ratio, and other related parameters are of great interest, in order to investigate the linear and anomalous variations as a function of composition of glass, and have been interpreted in terms of the structure or transformation of cross-linkages in the glass network (Sharma et al., 2009; Rajendran et al., 2001). To study the structure of oxide glass, the coordination number of the network former and the change of oxygen bonds in the frame work, induced by the cation modifiers, need to be investigated. This information can be obtained from FTIR spectroscopy. Furthermore, many author's studies on borosilicate glass have been reported for irradiation effects on structural properties of glass, by using ultrasonic techniques (Bootjomchai et al., 2012; Sharma et al., 2009; Zahran, 1998; El-Mallawany et al., 1998). Therefore, the ultrasonic technique is a versatile tool for investigating the change in microstructure, the deformation process and the structural properties of materials after successive irradiation.

In my previous work, I reported that the comparisons of structural properties between the glass, prepared from local sand (LGS)

* Corresponding author. Tel.: +66 853078883; fax: +66 45288381.
E-mail addresses: cherdsak_per@hotmail.co.th, cherdsak2303@gmail.com (C. Bootjomchai).

http://dx.doi.org/10.1016/j.anucene.2014.01.026
0306-4549/

and pure silica (SGS), revealed that the glass samples were prepared from Moon River sand, Ubon Ratchathani province, Thailand, may substitute the pure chemicals (SiO_2) by considering terms the of elastic properties (Laopaiboon and Bootjomchai, 2013). It is particularly interesting to study the effects of gamma irradiation on the structural properties of the glass (Comparison between LGS and SGS glass samples). Therefore, the present work has been investigating the effects of gamma irradiation on the structural properties of glass with different compositions of CeO_2, by using ultrasonic techniques and FTIR studies (comparison between local sand and pure silica).

2. Materials and methods

2.1. Sample preparation

The rectangular shaped glass samples of the $x$$CeO_2$–20$Na_2O$–1$Al_2O_3$–13$B_2O_3$–6.5CaO–1.5PbO–(58–$x$) local sand (LGS glass samples) and $x$$CeO_2$–20$Na_2O$–1$Al_2O_3$–13$B_2O_3$–6.5CaO–1.5PbO–(58–$x$)$SiO_2$ (SGS glass samples) (where x is mol.%) were prepared by using the melt-quenching method. The oxides of cerium, sodium, aluminium, boron, calcium, lead and silicon used in this work were analytical regent grades. The local sand was acquired from Moon River in Ubon Ratchathani province, Thailand. The qualitative and quantitative data of local sand were defined by using the wavelength dispersive X-ray fluorescence (WDXRF) technique (The condition of quantitative measurements and the chemical composition of local sand has been presented in previous work) (Laopaiboon and Bootjomchai, 2013). The quantities of chemicals and local sand were used as starting materials, and weighed using an electronic balance and having accuracy in the order of 0.0001 g. The starting materials were mixed thoroughly in alumina crucibles. The mixtures were melted in an electrical furnace at 1250 °C to ensure homogeneity. Then the melted glass was poured into a preheated stainless steel mold and annealed at 450 °C. The glass samples were cut and polished by using different grades of silicon carbide. The thickness measurement was carried out by a micrometer.

2.2. Density and molar volume measurements

The variation of density of each sample was measured by using the Archimedes's principle with n-hexane as the immersion liquid. The experiments were repeated three times for accurate value of the density. The estimated error in these measurements was approximately ±0.005 g cm^{-3}. The molar volume (V_a) was calculated for each glass from the expression; $V_a = M/\rho$, where M is the molecular weight of the glass, calculated according to the relation (Abd El-Moneim et al., 2006)

$$M = \sum_i x_i M_i \quad (1)$$

where x_i is the mole fraction of the component oxide i and M_i is its molecular weight. The estimated error in molar volume measurements was about ±0.021 cm^3 mol^{-1}.

2.3. Gamma-ray irradiation

The glass samples were irradiated by an exposure machine (THERATRON 780C) using a Co-60 gamma-ray source at a dose rate of 1.16 Gy min^{-1} and field size of 30 × 30 cm^2, at a distance of 30 cm from the source, and at room temperature. The samples were irradiated for sufficiently long enough to achieve the overall dose of 2 kGy. The diagram of the geometry is shown in Fig. 1.

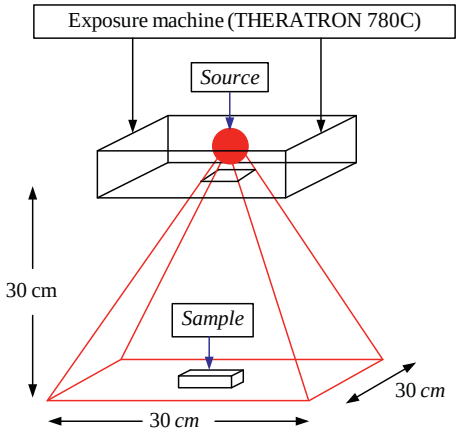

Fig. 1. Geometrical arrangement of gamma irradiation.

2.4. Ultrasonic velocity measurements

An ultrasonic flaw detector, SONATEST Sitescan 230, was employed to measure ultrasonic velocity. The ultrasonic waves were generated from a ceramic transducer (Probe model: SA04-45 for shear velocity and SLG4-10 for longitudinal velocity) with a resonant frequency of 4 MHz, and acting as transmitter–receiver at the same time. The ultrasonic wave velocity (v) can be calculated by following equation (El-Mallawany et al., 2006):

$$v = \frac{2x}{\Delta t} \quad (\text{cm s}^{-1}) \quad (2)$$

where x is the sample thickness (cm) and Δt is the time interval (s). The measurements were repeated three times to check the reproducibility of the data. The estimated errors in velocity measurements were ±11 m s^{-1} and ±8 m s^{-1} for longitudinal and shear velocities, respectively.

2.5. FTIR measurements

FTIR spectra of powdered glass samples were recorded in the range of 400–4000 cm^{-1}, using the KBr technique at room temperature. A recording spectrometer from Perkin–Elmer was used to reveal the absorption spectra with a resolution of 4 cm^{-1}.

3. Determination of elastic constants

The elastic strain produced by a small stress can be described as two independents; the elastic constants, C_{11} and C_{44} (Eraiah et al., 2010). The elastic moduli were calculated using the following standard relations (Eraiah et al., 2010):

Longitudinal modulus $C_{11} = L = \rho v_L^2$ (3)

Shear modulus $C_{44} = G = \rho v_S^2$ (4)

Bulk modulus $K = L - \left(\frac{4}{3}G\right)$ (5)

Young's modulus $E = (1+\sigma)2G$ (6)

Poisson's ratio $\sigma = \frac{L-2G}{2(L-G)}$ (7)

Micro-hardness $H = \frac{(1-2\sigma)E}{6(1+\sigma)}$ (8)

4. Results and discussion

4.1. Density and molar volume

The results of density were carefully mentioned in previous work. However, in this work the values of density were taken to calculate the molar volume. Therefore, the density overview is mentioned again. Fig. 2 shows the variations of the density and molar volumes with CeO_2 mol.%. For the LGS glass samples, it is clear that the density increases with increasing CeO_2 mol.%. This is due to the replacement of all the SiO_2 and B_2O_3 (molecular weights are 60.084 and 69.615 g mol^{-1}, respectively) with CeO_2 (molecular weight is 172.118 g mol^{-1}) (El-Mallawany et al., 2006; Eraiah et al., 2010; Gaafar and Marzouk, 2007; Veeranna Gowda et al., 2007; Reddy et al., 2008). For the SGS glass samples, the densities increase slowly with 0.00–1.25 mol.% of CeO_2, and then the densities increase rapidly with 1.25–5.00 mol.% of CeO_2. The initial increase of density (0.00–1.25 mol.% of CeO_2) suggests that CeO_2 gets into the order structure with random distribution. The concentration of the CeO_2 increases (1.25–5.00 mol.% of CeO_2) results in the structure becoming compact leading to a rapid increase of density.

The molar volume is defined as the volume occupied by the unit mass of the glass, Molar volume can be used as a parameter to identify an open structure (Singh et al., 2003). For LGS glass samples, the molar volume increases with increasing CeO_2 mol.%. This is due to the LGS glass samples having had high impurities in their structure. Adding the CeO_2 into the network structure leads to a more open structure of the glass. On the other hand, the SGS glass samples had low impurities in their structure. Initially, with 0.00–1.25 mol.% of CeO_2, the molar volume decreases due to the addition of CeO_2 in order to fill the interstices of the glass network. After that, when the interstices are filled, the greater addition of CeO_2 leads to a breakdown in the ring type structure of the glass samples, resulting in a rapidly increasing molar volume (1.25–5.00 mol.% of CeO_2). The exact values of density and molar volume are shown in the Table 1.

Table 1
Density (ρ) and molar volume (V_a) of the glass samples with different mol.% of CeO_2.

CeO_2 (mol.%)	ρ (g cm^{-3}) ±0.005		V_a (cm^3 mol^{-1}) ±0.021	
	Local sand (LGS)	Silica (SGS)	Local sand (LGS)	Silica (SGS)
0.00	2.839	2.863	23.731	23.812
0.50	2.882	2.857	23.870	23.695
1.25	2.894	2.874	24.037	23.687
3.75	3.014	2.975	24.059	24.138
5.00	3.030	3.099	24.102	24.211

4.2. Ultrasonic velocity and elastic moduli

The influences of concentration of CeO_2 have been described in previous work (Laopaiboon and Bootjomchai, 2013). Therefore, the present work will only discuss the influences of gamma-irradiation. Figs. 3 and 4 show plots of the longitudinal (v_L) and shear (v_S) wave velocities before and after successive gamma-irradiation against CeO_2 mol.% of LGS and SGS glass samples, respectively. From the figures, it is found that the ultrasonic velocities (both longitudinal and shear) decreased after gamma-irradiation, and the exact values are shown in Table 2. The changes in geometrical configuration, co-ordination number, cross-link density and dimensions of interstitial space of glass determine the ultrasonic velocity and, therefore, ultrasonic velocity is a tool in revealing the degree of the structural change in the glass (Marzouk, 2009). In general, the decrease of ultrasonic velocity is related to the increase in the number of non-bridging oxygen (NBO) and, consequently, the decrease in connectivity of the glass network (Gaafar and Marzouk, 2007). Moreover, irradiation with gamma-rays is assumed to create displacements, electronic defects and/or breaks in the network bonds, which allow the structure to relax and fill the relatively large interstices that exist in the interconnected network of boron and/or silicon and oxygen atoms, causing expansion followed by compaction of the volume (Ezz Eldin et al., 1992). Damage by an irradiation species can create displacement of atoms and/or breaks in the network bonds, leading to a rise of the number of non-bridging oxygens (NBO) and resulting in a decrease of ultrasonic wave velocities (Prado et al., 2001). In addition, the LGS glass samples were much more affected by gamma irradiation than the SGS glass samples. ElBatal et al. have reported that gamma irradiation produces induced defects and/or breaks in the network bonds generated from collective combinations of trace iron impurities (ElBatal et al., 2009). The LGS glass samples had higher iron impurities (Laopaiboon and Bootjomchai, 2013) leading to more information about non-bridging oxygens than the SGS glass samples. Hence, the ultrasonic velocities of the LGS glass samples clearly decrease when compared to the SGS glass samples.

Figs. 5 and 6 show the variations of elastic moduli (bulk and Young's modulus values are listed in Table 3) before and after successive gamma irradiation of the LGS and SGS glass samples,

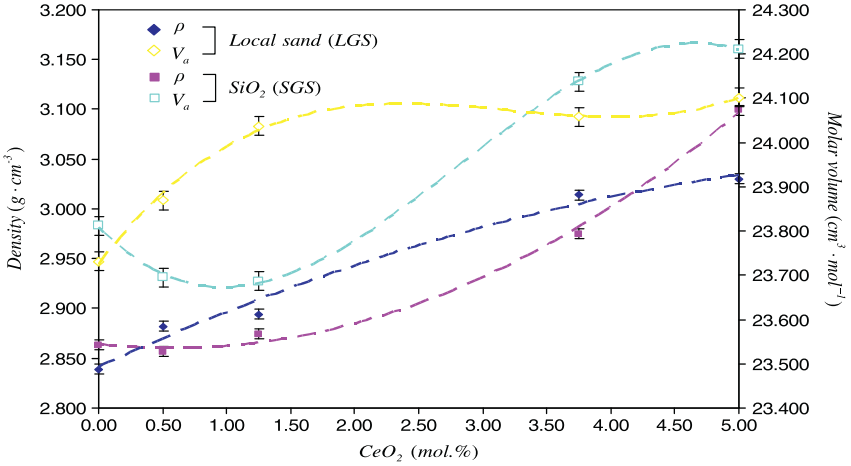

Fig. 2. Densities (ρ) and molar volume (V_a) of the glass samples with concentration of CeO_2. Lines are fitting plots of the data. The uncertainty in the measurement of the densities and molar volume are ±0.005 g cm^{-3} and ±0.021 cm^3 mol^{-1}, respectively.

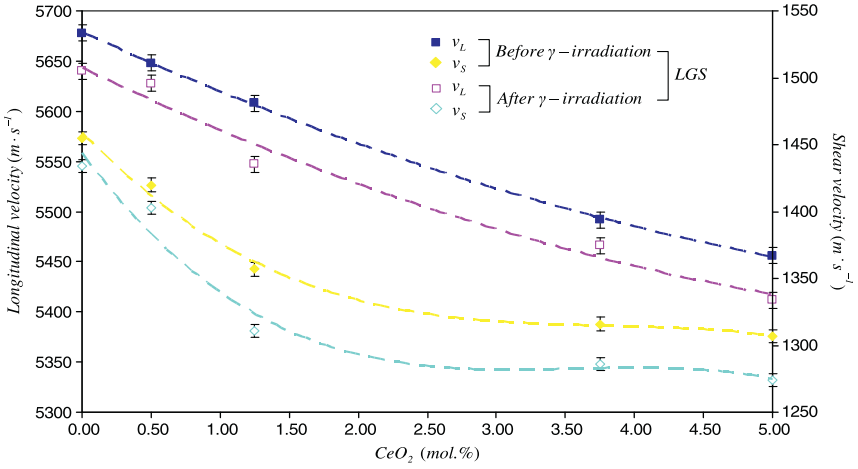

Fig. 3. Longitudinal (v_L) and shear (v_S) velocities before and after successive gamma irradiation of the LGS glass samples with concentration of CeO_2. Lines are fitting plots of the data. The uncertainty in the measurement of the longitudinal and shear velocity are ±11 m s^{-1} and ±8 m s^{-1}, respectively.

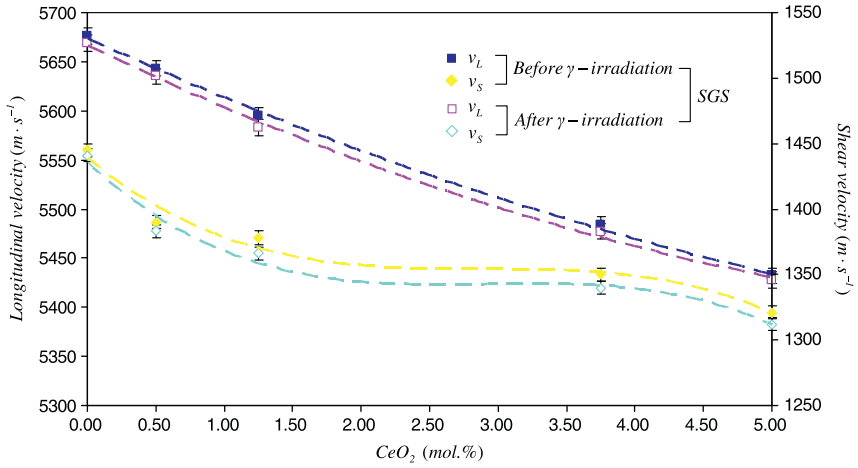

Fig. 4. Longitudinal (v_L) and shear (v_S) velocities before and after successive gamma irradiation of the SGS glass samples with concentration of CeO_2. Lines are fitting plots of the data. The uncertainty in the measurement of the longitudinal and shear velocity are ±11 m s^{-1} and ±8 m s^{-1}, respectively.

Table 2
Longitudinal (v_L) and shear (v_S) velocities before and after gamma irradiation of glass samples with different mol.% of CeO_2.

CeO_2 (mol.%)	LGS glass samples				SGS glass samples			
	v_L (m s^{-1}) ±11		v_S (m s^{-1}) ±8		v_L (m s^{-1}) ±11		v_L (m s^{-1}) ±11	
	Before	After	Before	After	Before	After	Before	After
0.00	5678	5640	1455	1434	5676	5669	1445	1441
0.50	5648	5628	1420	1403	5643	5635	1390	1383
1.25	5608	5547	1357	1311	5595	5583	1378	1366
3.75	5492	5466	1316	1286	5484	5477	1350	1340
5.00	5456	5412	1307	1274	5432	5428	1321	1312

respectively. From the figures, the elastic moduli (both bulk and Young's modulus) of the glass decrease after (both LGS and SGS glass samples) irradiated with gamma rays. It is believed that the behavior of both bulk and Young's modulus are associated with the change in the cross-linkage and coordination of the glass network (Gaafar and Marzouk, 2007). Therefore, the decrease of bulk and Young's modulus of the LGS and SGS glass samples after gamma irradiation suggests that the greater formation of NBO results in a decrease in the cross-linkage and coordination of the glass network. Furthermore, there is an apparent decrease of bulk and Young's modulus after gamma irradiation in the LGS glass samples when compared to the SGS glass samples. This result indicated that the LGS glass samples have a greater reduction of cross-linkage due to a higher amount of non-bridging oxygens than in the SGS glass samples. The results supported our discussion in that gamma irradiation produces NBO from a collective combination of iron impurities. Figs. 7 and 8 show the variation of Poisson's ratio and the micro-hardness of the LGS and SGS glass samples before and after successive irradiation, respectively, and the exact values are listed in Table 4. Both LGS and SGS glass samples show an increase in Poisson's ratio after successive gamma irradiation. The variation of Poisson's ratio is a measure of cross-link density and it decreases

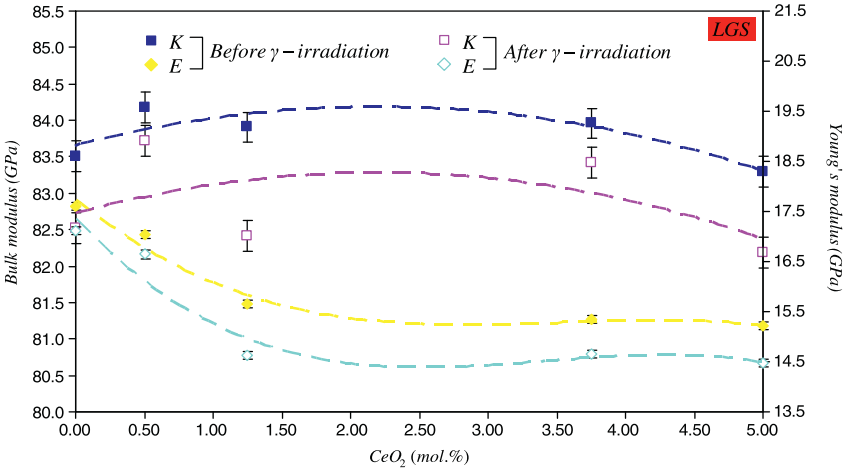

Fig. 5. Bulk (K) and Young's (E) modulus before and after successive gamma irradiation of the LGS glass samples with concentration of CeO_2. Lines are fitting plots of the data. The uncertainty in the measurement of the bulk and Young's modulus are ±0.21 GPa and ±0.08 GPa, respectively.

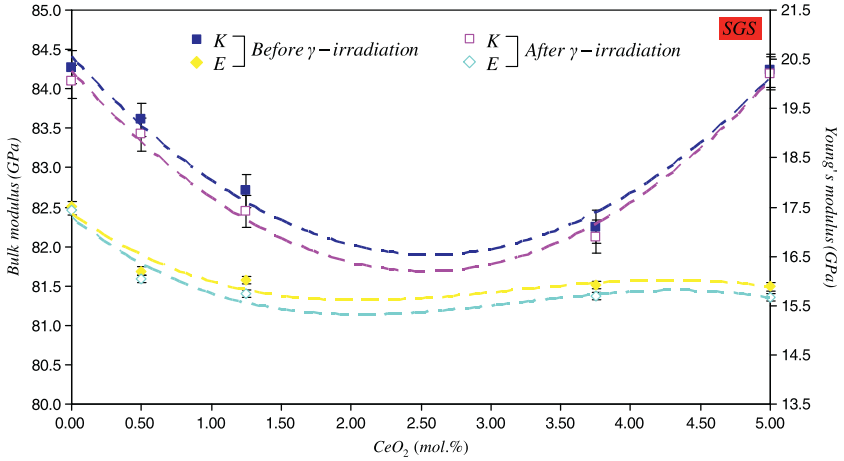

Fig. 6. Bulk (K) and Young's (E) modulus before and after successive gamma irradiation of the SGS glass samples with concentration of CeO_2. Lines are fitting plots of the data. The uncertainty in the measurement of the bulk and Young's modulus are ±0.21 GPa and ±0.08 GPa , respectively.

Table 3
Experimentally estimated values of the elastic moduli: bulk modulus (K) and Young's modulus (E) before and after successive gamma irradiation of glass samples with different mol.% of CeO_2.

CeO_2 (mol.%)	LGS glass samples				SGS glass samples			
	K (GPa) ±0.21		E (GPa) ±0.08		K (GPa) ±0.21		E (GPa) ±0.08	
	Before	After	Before	After	Before	After	Before	After
0.00	83.51	82.52	17.61	17.11	84.27	84.09	17.52	17.43
0.50	84.18	83.71	17.04	16.64	83.61	83.42	16.20	16.04
1.25	83.91	82.41	15.66	14.63	82.70	82.45	16.02	15.75
3.75	83.96	83.41	15.34	14.66	82.24	82.12	15.92	15.69
5.00	83.30	82.19	15.21	14.47	84.23	84.20	15.88	15.67

with an increase in the cross-link density. Therefore, the increase in Poisson's ratio shows that the reduction of the cross-link density, due to a rising amount of non-bridging oxygens after irradiation with gamma rays. The decrease in hardness after irradiation by gamma is related to the decrease of the rigidity of the glass (Gaafar et al., 2009). This indicates that irradiation with gamma rays attributes to defects created in the glass network (Mansour et al., 2011). Moreover, the results of Poisson's ratio and microhardness are in good agreement with our discussion about iron impurities having a greater affect upon LGS glass samples. For confirmation of these studies, the information obtained from FTIR spectroscopy is important.

4.3. Infrared absorption measurements

The IR spectra obtained for the studied glass samples are shown in Figs. 9–13. Each figure (Figs. 9–13) shows the comparison between the LGS and SGS glass samples before and after gamma irradiation with 0.00, 0.50, 1.25, 3.75 and 5.00 mol.%, respectively. The results obtained will be discussed in this section. The presence of

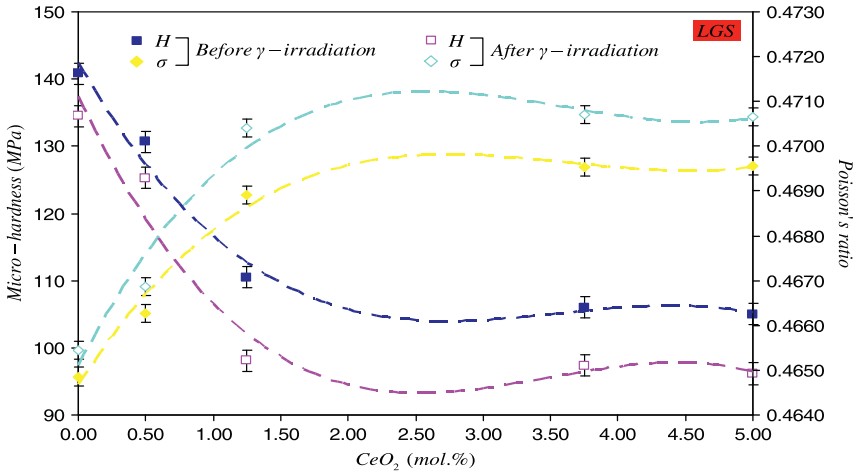

Fig. 7. Micro-hardness (H) and Poisson's ratio (σ) before and after successive gamma irradiation of the LGS glass samples with concentration of CeO_2. Lines are fitting plots of the data. The uncertainty in the measurement of the bulk and Young's modulus are ±1.6 MPa and ±0.0002, respectively.

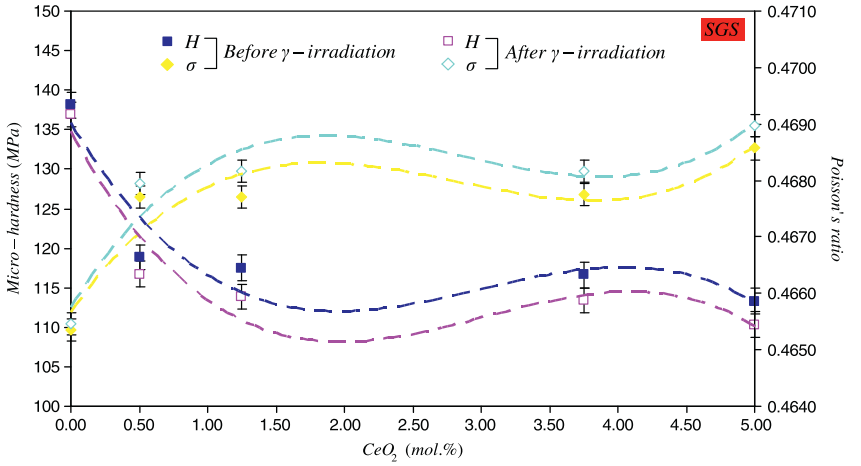

Fig. 8. Micro-hardness (H) and Poisson's ratio (σ) before and after successive gamma irradiation of the SGS glass samples with concentration of CeO_2. Lines are fitting plots of the data. The uncertainty in the measurement of the bulk and Young's modulus are ±1.6 MPa and ±0.0002, respectively.

Table 4
Experimentally estimated values of the Poisson's ratio (σ) and micro-hardness (H) before and after successive gamma irradiation of glass samples with different mol.% of CeO_2.

CeO_2 (mol.%)	LGS glass samples				SGS glass samples			
	σ ± 0.0002		H (MPa) ±1.6		σ ±0.0002		H(MPa) ± 1.6	
	Before	After	Before	After	Before	After	Before	After
0.00	0.4649	0.4654	140.80	134.50	0.4653	0.4655	138.11	136.89
0.50	0.4663	0.4669	130.69	125.29	0.4677	0.4680	118.84	116.74
1.25	0.4689	0.4704	110.47	98.09	0.4677	0.4682	117.50	113.85
3.75	0.4695	0.4707	106.00	97.37	0.4677	0.4682	116.60	113.38
5.00	0.4696	0.4707	105.04	96.17	0.4686	0.4690	113.31	110.34

water groups is marked by the presence of bands above 2000 cm^{-1}. From the figures (Figs. 8–12), the band arising from the vibrations of the borosilicate network appears in the range 400–1500 cm^{-1}. The signal around 470 cm^{-1} is assigned to Si–O–Si and O–Si–O bending modes of bridging oxygens (Q_4). The peak, at roughly 680 cm^{-1}, is assigned to curve vibrations of Si–O–B bridges (Handke et al., 2003). The absorption bands in the regions extending from 800 cm^{-1} to 1200 cm^{-1} are observed at 954, 1012, 1054 and 1120 cm^{-1}. These bands are assigned to the stretching vibrations of the B–O bonds in the structural groups, consisting of BO_4 units in the di-, tri-, tetra- and penta- borate groups (Kaur et al., 2012). Particularly, the region of 1000–1120 cm^{-1} can arise from overlapping contributions of silicate (vibrations of NBO of SiO_4^-) and borate groups containing BO_3 and BO_4 units (Kaur et al., 2012). The individual contribution of silicate and borate groups cannot be separated, and is assumed to depend on the concentration of each component in the glass system. The peak at around 1460 cm^{-1} is assigned to stretching vibrations of NBO of BO_3 triangles. A small absorption edge at around 1625 cm^{-1} is assigned to Si–OH stretching the surface of silanol hydrogen bonds into molecular water. All samples show a similar presence of broad bands.

It can be observed from Figs. 9–13 that the IR absorption spectra of investigated glass have four main absorption bands at around 470, 680, 800–1200 and 1460 cm^{-1}. The absorption of these

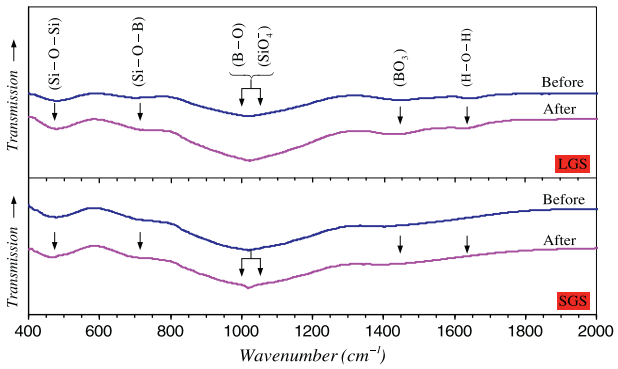

Fig. 9. Comparison of IR spectra between LGS and SGS glass samples with 0 mol.% of CeO_2 before and after successive gamma irradiation.

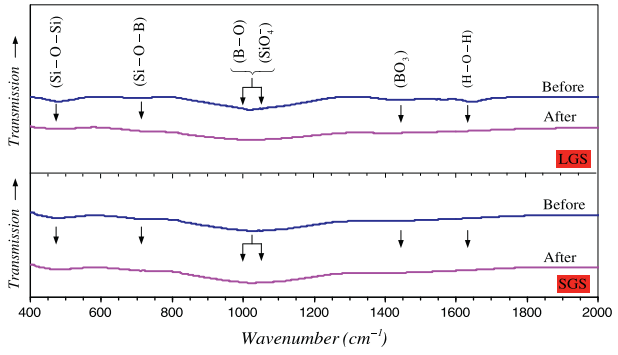

Fig. 10. Comparison of IR spectra between LGS and SGS glass samples with 0.5 mol.% of CeO_2 before and after successive gamma irradiation.

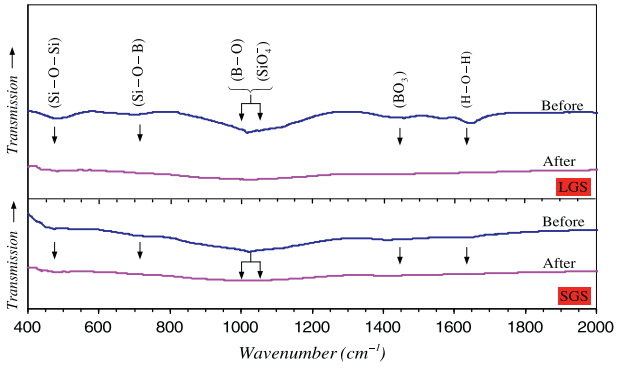

Fig. 11. Comparison of IR spectra between LGS and SGS glass samples with 1.25 mol.% of CeO_2 before and after successive gamma irradiation.

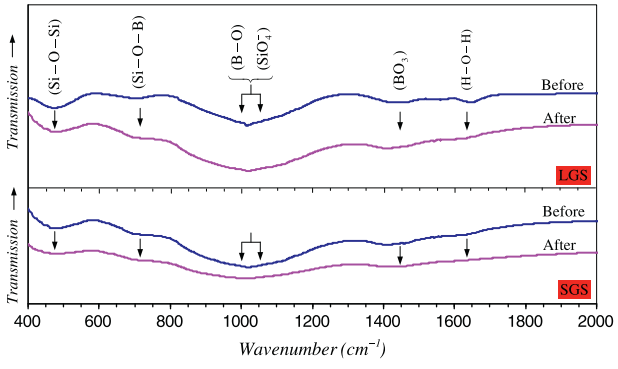

Fig. 12. Comparison of IR spectra between LGS and SGS glass samples with 3.75 mol.% of CeO_2 before and after successive gamma irradiation.

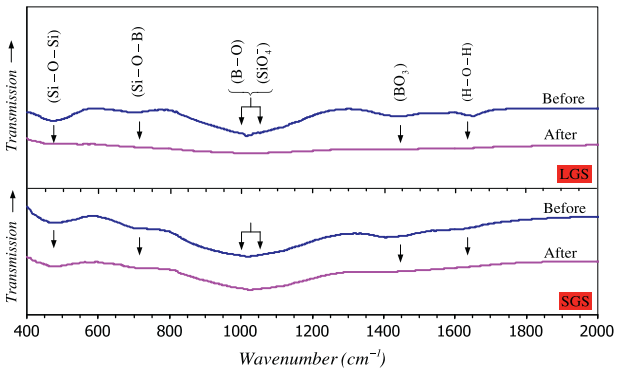

Fig. 13. Comparison of IR spectra between LGS and SGS glass samples with 5.00 mol.% of CeO_2 before and after successive gamma irradiation.

frequency bands decreases after successive gamma irradiation. This result is due to the photon of gamma rays perhaps destroying the associate of the silicon and/or boron with oxygen, creating non-bridging oxygens (NBO). In addition, the absorption bands observed for LGS glass samples seriously decrease in comparison to the SGS glass samples. This indicates that the LGS glass samples were more affected by irradiation than the SGS glass samples. The results of the FTIR spectra are evidence of the results and discussion of the ultrasonic velocities.

5. Conclusions

From the studies both composition (Laopaiboon and Bootjomchai, 2013) and radiation effects found that changes in ultrasonic velocity and elastic moduli are related to a change in the structure of the glass. In this work, the results indicate that gamma irradiation produces the formation of non-bridging oxygens in the network structure of the glass. Moreover, the SGS glass samples shows obvious shielding effect towards successive gamma irradiation exposure. The FTIR spectra also support the structural changes resulting from irradiation effects. Finally, the properties of local sand acquired from Moon River, in Ubon Ratchathani province (Thailand), is very interesting because its properties are similar to the pure chemicals. Furthermore, it is more affected by irradiation than the pure chemicals. In this point, it is an interesting investigation into the radiation response.

Acknowledgements

Financial support of this study has been provided by The Thailand Research Fund (TRF), Office of the Higher Education Commission (OHEC) and Ubon Ratchathani University (UBU). The results and comments on this article are those of the authors. The TRF, OHEC and UBU are unnecessary always agree. The author gratefully expresses his appreciation to the Department of Radiotherapy, Ubon Ratchathani Cancer Centre for the use of exposure machine.

References

Abd El-Moneim, A., Youssof, I.M., Adb El-Latif, L., 2006. Structural role of RO and Al_2O_3 in borate glasses using an ultrasonic technique. Acta Mater. 54, 3811–3819.

Arora, M., Baccaro, S., Sharma, G., Singh, D., Thind, K.S., Singh, D.P., 2009. Radiation effects on $PbO–Al_2O_3–B_2O_3–SiO_2$ glasses by FTIR spectroscopy. Nucl. Instrum. Methods Phys. Res. B 267, 817–820.

Aygun, Z., Aygun, M., Karabulut, B., Karabulut, A., 2012. Investigation of non-irradiated and gamma-irradiated Trommel Sieve Waste (TSW) with EPR technique. Ann. Nucl. Energy 40, 84–86.

Baccaro, S., Monika, Sharma., Thind, G., Devinder Singh, K.S., Cecillia, A., 2007. Analysis of structural modification in -irradiated $PbO–B_2O_3–SiO_2$ glasses by FTIR spectroscopy. Nucl. Instrum. Methods Phys. Res. B 260, 613–618.

Baydogan, N., Tugrul, A.B., 2012. Borosilicate glass for gamma irradiation fields. Solid State Sci. 14, 1692–1697.
Bootjomchai, C., Laopaiboon, J., Nontachat, S., Tipparach, U., Laopaiboon, R., 2012. Structural investigation of borosilicate recycled-barium-bismuth glasses under the influence of gamma-irradiation through ultrasonic and FTIR studies. Nucl. Eng. Des. 248, 28–34.
De Bonfils, J., Peuget, S., Panczer, G., De Ligny, D., Henry, S., Noël, P.-Y., Chenet, A., Champagnon, B., 2010. Effect of chemical composition on borosilicate glass behavior under irradiation. J. Non-Cryst. Solids 356, 388–393.
Deschanels, X., Peuget, S., Cachia, J.N., Charpentier, T., 2007. Plutonium solubility and self-irradiation effects in borosilicate glass. Prog. Nucl. Energy 49, 623–634.
ElBatal, F.H., Selim, M.S., Marzouk, S.Y., Azooz, M.A., 2007. UV–vis absorption of the transition metal-doped SiO_2–B_2O_3–Na_2O glasses. Phys. B 398, 126–134.
ElBatal, F.H., Hamdy, Y.M., Marzouk, S.Y., 2009. UV–visible and infrared absorption spectra of transition metals-doped lead phosphate and the effect of gamma irradiation. J. Non-Cryst. Solids 355, 2439–2447.
El-Mallawany, R., Abousehly, A., El-Rahamani, A.A., Yousef, E., 1998. Radiation effect on the ultrasonic attenuation and internal friction of tellurite glasses. Mater. Chem. Phys. 52, 161–165.
El-Mallawany, R., El-Khoshkhany, N., Afifi, H., 2006. Ultrasonic studies of $(TeO_2)_{50}$–$(V_2O_5)_{50-x}$–$(TiO_2)_x$ glasses. Mater. Chem. Phys. 95, 321–327.
Eraiah, B., Smitha, M.G., Anavekar, R.V., 2010. Elastic properties of lead–phosphate glasses doped with samarium trioxide. J. Phys. Chem. Solids 71, 153–155.
Ezz Eldin, F.M., El-Alaily, N.A., Elbatal, H.A., 1992. Density and refractive index of some -irradiated alkali silicate glasses. J. Radioanal. Nucl. Chem. 163 (2), 267–275.
Fayon, F., Bessada, C., Massiot, D., Farnan, I., Coutures, J.P., 1998. ^{29}Si and ^{207}Pb NMR study of local order in lead silicate glasses. J. Non-Cryst. Solids 232–234, 403–408.
Fayon, F., Landron, C., Sakurai, K., Bessada, C., Massiot, D., 1999. Pb^{2+} environment in lead silicate glasses probed by Pb-L_{III} edge XAFS and ^{207}Pb NMR. J. Non-Cryst. Solids 243, 39–44.
Gaafar, M.S., Marzouk, S.Y., 2007. Mechanical and structural studies on sodium borosilicate glasses doped with Er_2O_3 using ultrasonic velocity and FTIR spectroscopy. Phys. B 388, 294–302.
Gaafar, M.S., Afifi, H.A., Mekawy, M.M., 2009. Structural studies of some phosphoborate glasses using ultrasonic pulse-echo technique, DSC and IR spectroscopy. Phyisca B 404, 1668–1673.
Handke, M., Sitaz, M., Rokita, M., Galuskin, E., 2003. Vibrational spectra of phosphate–silicate biomaterials. J. Mol. Struct. 651, 39–54.
Kaur, R., Singh, S., Pandey, O.P., 2012. FTIR structural investigation of gamma irradiated BaO–Na_2O–B_2O_3–SiO_2 glasses. Phys. B 407, 4765–4769.
Laopaiboon, R., Bootjomchai, C., 2013. Influence of CeO_2 on structural properties of glasses by using ultrasonic technique: comparison between the local sand and SiO_2. Ultrasonics 53, 907–912.
Malchukova, E., Boizot, B., Ghaleb, D., Petite, G., 2005. Optical properties of pristine and -irradiated Sm doped borosilicate glasses. Nucl. Instrum. Methods Phys. Res. A 537, 411–414.
Mansour, E., El-Damrawi, G., Fetoh, R.E., Doweidar, H., 2011. Structure-properties changes in ZnO–PbO–GeO_2 glasses. European Phys. J. B 83, 133–141.
Marzouk, S.Y., 2009. Ultrasonic and infrared measurements of copper-doped sodium phosphate glasses. Mater. Chem. Phys. 114, 188–193.
Marzouk, S.Y., 2010. The acoustic properties of borosilicate glass affected by oxide of rare earth gadolinium. Phys. B 405, 3395–3400.
Ollier, N., Boizot, B., Reynard, B., Ghaleb, D., Petite, G., 2004. Irradiation in borosilicate glasses: the role of the mixed alkali effect. Nucl. Instrum. Methods Phys. Res. B 218, 176–182.
Parchinskii, P.B., 2002. The effect of radiation on the electrical properties of passive coatings based on lead borosilicate glasses. Tech. Phys. Lett. 28, 932–934.
Prado, M.O., Messi, N.B., Plivelic, T.S., Torriani, I.L., Bevilacqua, A.M., Arribére, M.A., 2001. The effects of radiation on the density of an aluminoborosilicate glass. J. Non-Cryst. Solids 289, 175–184.
Prymak, M.V., Axhniuk, Yu.M., Solomon, A.M., Krasilinets, V.M., Lopushansky, V.V., Bodnar, I.V., Gomonnai, A.V., Zahn, D.R.T., 2012. Effect of X-ray irradiation on the optical absorption of $CdSe_{1-x}Te_x$ nanocrystals embedded in borosilicate glass. Radiat. Phys. Chem. 81, 766–770.
Rajendran, V., Palanivelu, N., Palanichamy, P., Jayakumar, T., Raj, B., Chaudhuri, B.K., 2001. Ultrasonic characterization of feroelectric $BaTiO_3$ doped lead bismuth oxide semiconducting glasses. J. Non-Cryst. Solids 296, 39–49.
Reddy, C.N., Veeranna Gowda, V.C., Sreekanth Chakradhar, R.P., 2008. Elastic properties and structural studies on lead-boro-vanadate glasses. J. Non-Cryst. Solids 354, 32–40.
Sharma, G., Rajendran, V., Thind, K.S., Singh, G., Singh, A., 2009. Structural investigation of bismuth borate glasses under the influence of -irradiation through ultrasonic studies. Phys. B 404, 3371–3378.
Singh, H., Singh, K., Gerward, L., Singh, K., Sahota, H.S., Nathuram, R., 2003. ZnO–PbO–B_2O_3 glasses as gamma-ray shielding materials. Nucl. Instrum. Methods Phys. Res. B 207, 257–262.
Stentz, Dale., Blair, Sarah., Goater, Cole., Feller, Steve., Affatigato, Mario., 2001. Analysis of the structure of lead borosilicate glasses using laser ionization time of flight mass spectroscopy. J. Non-Cryst. Solids 293–295, 416–421.
Veeranna Gowda, V.C., Narayana Reddy, C., Radha, K.C., Anavekar, R.V., Etourneau, J., Rao, K.J., 2007. Structural investigations of sodium diborate glasses containing PbO, Bi_2O_3 and TeO_2: elastic property measurements and spectroscopic studies. J. Non-Cryst. Solids 353, 1150–1163.
Weber, M.J., 1980. Glass for neodymium fusion lasers. J. Non-Cryst. Solids 42, 189–196.
Zahran, R.R., 1998. Effect of -irradiation on the ultrasonic and structural properties of polyoxymethylene. Mater. Lett. 37, 83–89.

Applied Radiation and Isotopes 89 (2014) 42–46

Contents lists available at ScienceDirect

Applied Radiation and Isotopes

journal homepage: www.elsevier.com/locate/apradiso

Glass structure responses to gamma irradiation using infrared absorption spectroscopy and ultrasonic techniques: A comparative study between Co_2O_3 and Fe_2O_3

R. Laopaiboon, C. Bootjomchai *

Glass Technology Excellent Center (GTEC), Department of Physics, Faculty of Science, Ubon Ratchathani University, 34190 Thailand

HIGHLIGHTS

- Changes in $BO_3 \rightarrow BO_4$ and $SiO_4^- \rightarrow SiO_4$ due to the effect of radiation.
- Structural changes in $BO_3 \rightarrow BO_4$ and $SiO_4^- \rightarrow SiO_4$ have a more compactness structure.
- FTIR were adequate supporting our discussion in the structural changes.

ARTICLE INFO

Article history:
Received 25 April 2013
Received in revised form
7 February 2014
Accepted 7 February 2014
Available online 15 February 2014

Keywords:
Glasses
FTIR
Ultrasonic technique
Irradiation effects

ABSTRACT

The response of glass to radiation was investigated using ultrasonic and FTIR spectroscopy. New materials were prepared from borosilicate-based glass with different cobalt and iron oxide compositions. The results indicate that the glass structures were most responsive to irradiation at 1500 Gy. Moreover, the results show that the radiation effect decreases when the cobalt and iron oxide compositions increase. These results are relevant to studies on high-dose processing, radio-pharmacy and storage.

1. Introduction

Radiation and its application have become indispensable to modern society, through uses such as nuclear power plants and radiotherapy. However, radiation can be dangerous in accidents, such as the Chernobyl disaster in 1986 and, recently, at Fukushima Dai-Ichi in 2011. Therefore, radiation damage in materials must be studied. Understanding the effect of radiation on the structural properties of matter is important in evaluating radiation shielding materials and dosimetric materials (Singh et al., 2008; Han et al., 2009; Abd El-Malak, 2002; Baccaro et al., 2007; Arora et al., 2009; Prado et al., 2001; Sharma et al., 2009; Soliman et al., 2013). Studies on radiation-induced defective centers in glass have been an interesting subject recently because such studies aid in examining the suitability of glass for radiation dosimetry applications. Many studies are available in the literature on the activating or modifying effect of radiation on structural properties due to certain transition metal ions (TMOs), such as Fe^{3+} and Co^{3+}, in amorphous materials (Srinivasarao and Veeraiah, 2001; Dance et al., 1986). In addition, glass doped with multivalent ions, such as Fe^{3+} and Co^{3+}, have been used for many applications, such as semiconducting glass, active oxide catalysts to oxidize CO and hydrocarbons, and glassy behavior in manganites (Mao et al., 2011; Vasilyeva et al., 2010; Tran et al., 2013; Azianty et al., 2012).

Borosilicate-based glass has certain remarkable features, such as high chemical stability and low thermal expansion coefficients, which render the glass resistant to thermal shock; this glass is also excellent for transmission to visible light. Thus, this glass has been used in application such as coatings, semiconductor microelectronics, optical lenses, scintillation detectors, glass–ceramic cement, and hard nuclear waste materials (Arora et al., 2009; Sharma et al., 2009; Ramkumar et al., 2008; Sawvel et al., 2005). In addition, glass doped with and/or with added transition metal oxide (TMOs) exhibits interesting optical, magnetic, and electrical properties due to possible TMOs ions in two or more valence or coordination states (Shelby, 1997).

The glass properties are closely related to the lattice structure inter-atomic forces and potentials. Therefore, lattice changes due to composition change and/or irradiation can be directly detected.

* Corresponding author: Tel.: +66853078883; fax: +6645288381.
E-mail address: cherdsak_per@hotmail.co.th (C. Bootjomchai).

http://dx.doi.org/10.1016/j.apradiso.2014.02.008
0969-8043

The coordination number of the former network and change in oxygen bonds for the network by cation modifiers and/or irradiation are helpful for better understanding the glass structure; these data are generated through ultrasonic techniques and FTIR spectroscopy (Baccaro et al., 2007; Arora et al., 2009). Ultrasonic techniques and FTIR spectroscopy are versatile tools for investigating microstructure change, structural deformation and materials' mechanical properties due to a change in composition and/or irradiation (Sharma et al., 2009; El-Mallawany et al., 1998; Doweidar and Saddeek, 2009).

The aforementioned concerns led to this study, wherein the authors report the effects of TMOs composition (Co_2O_3 and Fe_2O_3) and side effects from irradiation on structural properties. The results herein were generated to consider the available materials for high-dose processing, radio-pharmacy and storage.

2. Experimental details

2.1. Glass preparation

The glass samples were prepared in rectangular shapes from the $(Co_2O_3)_x\,(Na_2O)_{20}\,(Al_2O_3)_1\,(B_2O_3)_{13}\,(CaO)_{6.5}\,(PbO)_{1.5}\,(SiO_2)_{58-x}$ and $(Fe_2O_3)_x\,(Na_2O)_{20}\,(Al_2O_3)_1\,(B_2O_3)_{13}\,(CaO)_{6.5}\,(PbO)_{1.5}\,(SiO_2)_{58-x}$ glass systems (x is the mol%) using the melt-quenching method. The oxides used herein were analytical regent grade (more than 99% pure). The raw materials were weighed using an electronic balance with accuracy on order of 0.1 mg; they were mixed and calculated to yield a 50 g sample. Next, the starting materials were mixed carefully in alumina crucibles. To ensure homogeneity, the mixtures were melted at 1250 °C in an electrical furnace that was constructed at the Department of Physics, Faculty of Science, Ubon Ratchathani University. The melted glass was then poured into pre-heated stainless steel molds and annealed at 450 °C. The glass samples were cut and polished using different silicon carbide grades. The sample thicknesses were measured to the micrometer.

2.2. Density and molar volume measurements

The density of each sample was measured using Archimedes' principle and n-hexane as the immersion liquid as well as applying the following equation (Marzouk and Gaafar, 2007):

$$\rho = \rho_L\left(\frac{W_a}{W_a - W_b}\right) \tag{1}$$

where ρ_L is the immersion liquid density; W_a and W_b are the sample weights in air and the immersion liquid, respectively. The experiments were repeated three times for an accurate density value. The molar volume (V_a) was calculated using the expression $V_a = M/\rho$, where M is the molecular weight of the glass, which was calculated using the following equation: $M = \sum_i x_i M_i$ (Abd El-Malak, 2002), where x_i is the mole fraction of the component oxides i and M_i is its molecular weight.

2.3. Gamma-ray irradiation

The glass samples were irradiated with gamma ray using an exposure machine (THERATRON 780C) and Co-60 as the gamma-ray source at the dose rate 1.16 Gy min^{-1} and the field size 30×30 cm^2 at room temperature 30 cm from the source. The samples were irradiated with gamma rays for a sufficiently long time to receive the doses 500, 1000, 1500 and 2000 Gy.

2.4. Fourier transform infrared absorption measurements

Infrared absorption spectra for the powdered glass were recorded in the range 400–4000 cm^{-1} using the KBr technique at room temperature. A spectrometer from Perkin-Elmer was used to measure the absorption spectra; the measurements were at a 4 cm^{-1} resolution (Chahine et al., 2004). The FTIR measurements were measured immediately after irradiation by gamma rays (Sharma et al., 2009).

2.5. Ultrasonic velocity measurements

To measure the mean ultrasonic velocity of the glass samples, an ultrasonic flaw detector, the SONATEST Sitescan 230, was used (Table 2). The ultrasonic waves were generated from a ceramic transducer at the resonant frequency 4 MHz, which simultaneously acted as a transmitter and receiver. The mean ultrasonic velocity was calculated using the following equation (Marzouk, 2009):

$$v_m = \left[\frac{3v_L^3 v_S^3}{v_L^3 + v_S^3}\right]^{1/3} \tag{2}$$

where v_L and v_s are the longitudinal and shear velocities, respectively. The estimated error in the velocities measurement was ± 14.0 m s^{-1} for the longitudinal velocity and ± 10.0 m s^{-1} for the shear velocity.

3. Results and discussion

3.1. Density and molar volume

The glass sample density and molar volumes were calculated, and the exact values are listed in Table 1. The density variations with different TMO compositions (Co_2O_3 and Fe_2O_3) are shown in Fig. 1. The densities increase with increasing TMO concentrations because SiO_2 (molecular weight is 60.084 g mol^{-1}) is replaced with Co_2O_3 and Fe_2O_3 (molecular weight are 165.863 and 159.687 g mol^{-1}, respectively) (Eraiah, et al., 2010; Laopaiboon and Bootjomchai, 2013; Gaafar and Marzouk, 2007; Veeranna Gowda et al., 2007). Moreover, the density of the glass samples with the added Co_2O_3 was higher than the glass samples with the added Fe_2O_3 because Co_2O_3 has a higher molecular weight than Fe_2O_3. However, the glass samples with Co_2O_3 and Fe_2O_3 added yielded densities with small differences.

Table 1
Density (ρ) and molar volume (V_a) of glass samples with different concentration of Co_2O_3 and Fe_2O_3, respectively.

mol%	Co_2O_3		Fe_2O_3	
	ρ (g cm^{-3})	V_a (cm^3 mol^{-1})	ρ (g cm^{-3})	V_a (cm^3 mol^{-1})
0.00	2.6885 ± 0.0011	24.2183 ± 0.4990	2.6882 ± 0.0010	24.2384 ± 0.6512
0.50	2.7286 ± 0.0015	30.3544 ± 0.7082	2.7019 ± 0.0012	32.1901 ± 0.3100
0.75	2.7324 ± 0.0012	36.5082 ± 0.6760	2.7124 ± 0.0016	37.1804 ± 0.9983
1.00	2.7468 ± 0.0020	54.8988 ± 0.9683	2.7125 ± 0.0013	56.2714 ± 0.8593

Table 2
Mean ultrasonic velocity (v_m) of glass samples (each concentration) with different dose of gamma irradiation.

Dose of gamma irradiation (Gy)	v_m (m s^{-1}): Co_2O_3			v_m (m s^{-1}): Fe_2O_3		
	0.50 mol%	0.75 mol%	1.00 mol%	0.50 mol%	0.75 mol%	1.00 mol%
0	3795	4030	4165	4920	4678	4259
500	4598	4871	5097	5237	5011	5226
1000	4827	5071	5244	5292	5213	5443
1500	5290	5338	6075	5369	5451	5696
2000	4973	5180	5528	5299	5389	5417

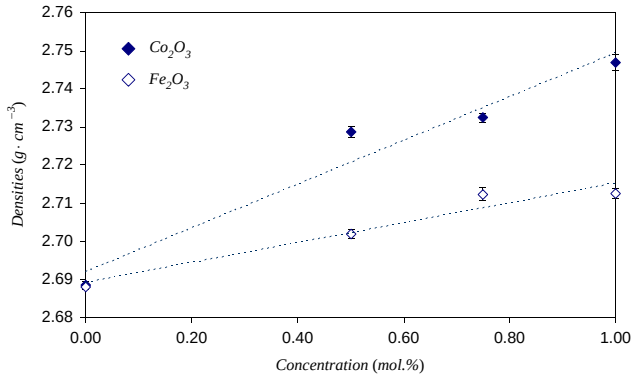

Fig. 1. Densities (ρ) of the glass samples with different of concentration of TMOs.

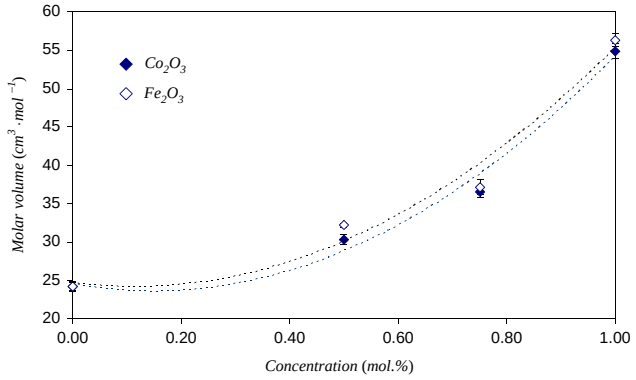

Fig. 2. Molar volume (V_a) of glass samples with different concentration of TMOs.

According to Shelby (1997), molar volume describes the volume occupied by the unit mass of the glass, and it depends on the ionic radius of the modifier. Fig. 2 shows that the molar volume increases with increasing TMO concentrations (Co_2O_3 and Fe_2O_3). These results are easily explained; they are due to the modifier ions ionic radii (the Co^{3+} and Fe^{3+} ionic radii are 0.545 and 0.550 Å, respectively), which are larger than the network structure interstices (the ionic radius of Si^{4+} is 0.400 Å). The modifier ion attraction to oxygen ions can yield a grater interstices size and molar volume.

3.2. Ultrasonic velocity

Fig. 3 shows plots for the mean ultrasonic velocity (0.50, 0.75 and 1.00 mol% of TMOs, respectively) with different gamma irradiation doses. The mean ultrasonic velocity increased with increasing gamma irradiation doses from 0 to 1500 Gy. The mean ultrasonic velocity then decreased with increasing gamma irradiation doses from 1500 to 2000 Gy. Moreover, the results show that,

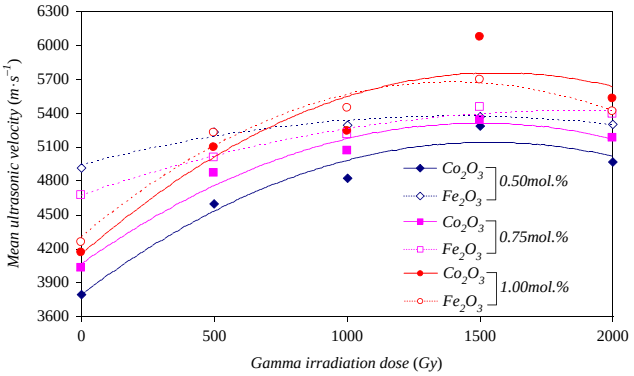

Fig. 3. The mean ultrasonic velocity (v_m) of glass samples with different gamma irradiation dose.

for the low TMO concentrations (0.50–0.75 mol%), the mean ultrasonic velocity for glass samples with Co_2O_3 added were more responsive than the samples with Fe_2O_3 due to a change in mean ultrasonic velocity after irradiation. However, for high TMO concentrations (1.00 mol%), the glass samples with Co_2O_3 and Fe_2O_3 added did not yield distinctive mean velocities. To explain the variations observed, the change in glass geometrical configuration, co-ordination number, cross-link density and interstitial space dimensions determine the ultrasonic velocity; therefore, ultrasonic velocity is a tool for discerning the level of change in glass structure (Marzouk, 2009). Generally, an ultrasonic velocity decrease is related to an increase in the number of non-bridging oxygens (NBO) and, consequently, lower glass network connectivity (Gaafar and Marzouk, 2007). Abd El-Malak (2002) reported that increased ultrasonic velocities with increasing radiation doses are primarily due to the glass sample compactness and, consequently, its glass network hardness and atom rearrangement. Irradiation with gamma rays is assumed to create displacements, electronic defects and/or breaks in the network bonds, which allow the structure to relax and fill the relatively large interstices in the interconnected silicon and/or boron and oxygen atom network, which produces volume expansion followed by compaction (Ezz Eldin et al., 1992). Damage by an irradiating species can produce compaction in a borosilicate structure by breaking bonds between triagonal (BO_3) elements, which facilitate tetrahedral (BO_4) formation and/or changes SiO_4^- to SiO_4. The tetrahedral groups (BO_4 and SiO_4) are more strongly bonded than the triangular groups (BO_3 and SiO_4^-) and a compact structure is expected to increase the mean ultrasonic velocities. Therefore, increases in mean ultrasonic velocity with an increasing gamma irradiation dose from 0 to 1500 Gy are due to a change from a triangular to tetrahedral structure ($BO_3 \rightarrow BO_4$ and $SiO_4^- \rightarrow SiO_4$). At a high gamma irradiation dose (2000 Gy), the irradiation can displace atoms and/or produce breaks in the network bonds, which increases the number of non-bridging oxygens (NBO) and decreases the mean ultrasonic velocity (Prado et al., 2001). The results indicate that the glass structure with added Co_2O_3 is more responsive to irradiation than glass with added Fe_2O_3. Moreover, effect of irradiation was lower with high TMO concentrations due to a dominant composition effect. To confirm these results, information from FTIR spectroscopy is important.

3.3. Fourier transform infrared absorption (FTIR)

The FTIR spectra for the glass with Co_2O_3 and Fe_2O_3 added at the concentrations 0.50, 0.75 and 1.00 mol% are shown in Figs. 4–6, respectively. The water groups are indicated by frequency bands over 2000 cm^{-1}. The frequency bands from the glasses network vibrations

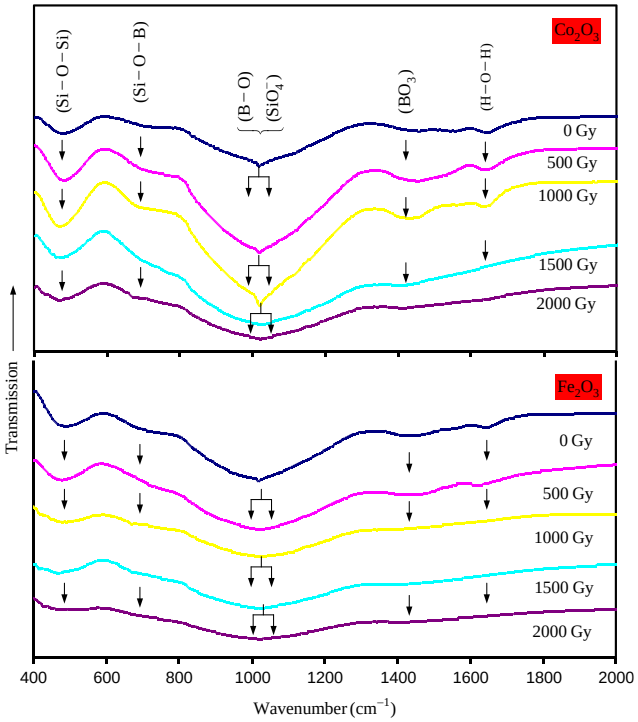

Fig. 4. The IR spectra of the glass samples at 0.50 mol% with different gamma irradiation dose comparative between Co_2O_3 and Fe_2O_3.

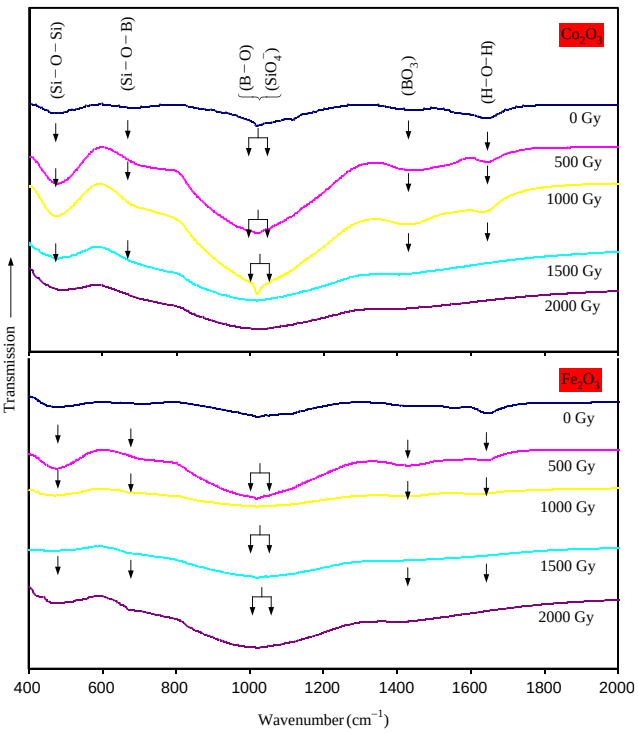

Fig. 5. The IR spectra of the glass samples at 0.75 mol% with different gamma irradiation dose comparative between Co_2O_3 and Fe_2O_3.

appear in the range 400–1500 cm^{-1}. The first vibration signals near 470 cm^{-1} are assigned to the Si–O–Si and O–Si–O bending modes of the SiO_4 (Q_4) bridging oxygens. The peaks near 680 cm^{-1} are assigned to the Si–O–B bridges frequency vibrations (Handke et al., 2003). The absorption bands in the region from 800 to 1200 cm^{-1} are at

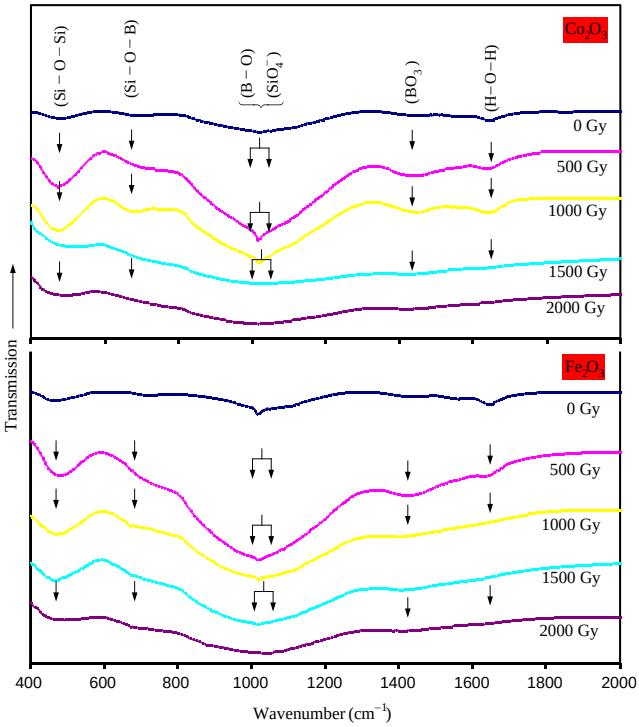

Fig. 6. The IR spectra of the glass samples at 1.00 mol% with different gamma irradiation dose comparative between Co_2O_3 and Fe_2O_3.

954, 1012, 1054 and 1120 cm^{-1}. These regions are assigned to the B–O bonds stretching vibrations in the structural groups with BO_4 units in di-, tri-, tetra- and penta- borate groups (Kaur et al., 2012). The individual contributions from silicate and borate groups cannot be separated, and they are assumed to depend on the concentration of each component in the glass system (Laopaiboon and Bootjomchai, 2013). The signal at approximately 1460 cm^{-1} corresponds to the BO_3 NBO triangle stretching vibrations. A small vibration at approximately 1625 cm^{-1} is due to Si–OH stretching of a surface silanol hydrogen bond with molecular water. The samples (Figs. 4–6) show a similar frequency band.

Figs. 4–6 show that the IR absorption spectra for the glass examined herein have four main frequency bands at approximately 470, 680, 800–1200 and 1460 cm^{-1}. In each sample, the peak at approximately 470 cm^{-1} indicates increased absorption bands with increasing irradiation doses (0–1500 Gy) and, thus increased SiO_4 formation with irradiation from 0 to 1500 Gy. Moreover, the peak at approximately 1460 cm^{-1} decreases with increasing irradiation from 0 to 1500 Gy. The results show that BO_3 transforms into BO_4 upon irradiation from 0 to 1500 Gy. The results compare glass with Co_2O_3 and Fe_2O_3 added. The results from FTIR spectroscopy support our discussion on the change from a triangular to tetrahedral structure ($BO_3 \rightarrow BO_4$ and $SiO_4^- \rightarrow SiO_4$).

4. Conclusions

The results from this study show that glass with Co_2O_3 added is more responsive to irradiation than glass with Fe_2O_3 added. The structural response upon irradiation was a change from a triangular to tetrahedral structure ($BO_3 \rightarrow BO_4$ and $SiO_4^- \rightarrow SiO_4$). In addition, the irradiation effect was lower with higher TMO concentrations. Finally, future studies should include the luminescence properties of the glass.

Acknowledgments

Financial support of this study has been provided by The Thailand Research Fund (TRF), Office of the Higher Education Commission (OHEC) and Ubon Ratchathani University (UBU). The results and comments on this article are those of the authors. The TRF, OHEC and UBU are unnecessary always agree. The author is grateful to Ubon Ratchathani Cancer Center for the facility support and use of the Co-60 gamma-ray source.

References

Abd El-Malak, N.A., 2002. Ultrasonic studies on irradiated sodium borate glasses. Mater. Chem. Phys. 73, 156–161.

Arora, M., Baccaro, S., Sharma, G., Singh, D., Thind, K.S., Singh, D.P., 2009. Radiation effects on PbO–Al_2O_3–B_2O_3–SiO_2 glasses by FTIR spectroscopy. Nucl. Instrum. Methods B 267, 817–820.

Azianty, S., Yahya, A.K., Halimah, M.K., 2012. Effects of Fe_2O_3 replacement of ZnO on elastic and structural properties of $80TeO_2$–$(20-x)$ZnO–xFe_2O_3 tellurite glass system. J. Non-Cryst. Solids 358, 1562–1568.

Baccaro, S., G., Monika Sharma, Thind, K.S., Singh, Devinder, Cecillia, A., 2007. Analysis of structural modifications in γ-irradiated PbO–B_2O_3–SiO_2 glasses by FTIR spectroscopy. Nucl. Instrum. Methods B 260, 613–618.

Chahine, A., Et-tabirou, M., Pascal, J.L., 2004. FTIR and Raman spectra of the Na_2O–CuO–Bi_2O_3–P_2O_5 glasses. Mater. Lett. 58, 2776–2780.

Dance, J.-M., Videau, J.-J., Portier, J., 1986. EPR of transition metal ions (Mn^{2+}, Cu^{2+}, Cr^{3+}, Fe^{3+}) in fluoroaluminate glasses. J. Non-Cryst. Solids 86, 88–93.

Doweidar, H., Saddeek, Y.S., 2009. FTIR and ultrasonic investigation on modified bismuth borate glasses. J. Non-Cryst. Solids 355, 248–354.

El-Mallawany, R., Abousehly, A., El-Rahamani, A.A., Yousef, E., 1998. Radiation effect on the ultrasonic attenuation and internal friction of tellurite glasses. Mater. Chem. Phys. 52, 161–165.

Eraiah, B., Smitha, M.G., Anavekar, R.V., 2010. Elastic properties of lead–phosphate glasses doped with samarium trioxide. J. Phys. Chem. Solids 71, 153–155.

Ezz Eldin, F.M., El-Alaily, N.A., Elbatal, H.A., 1992. Density and refractive index of some γ-irradiated alkali silicate glasses. J. Radioanal. Nucl. Chem. 63 (2), 267–275.

Gaafar, M.S., Marzouk, S.Y., 2007. Mechanical and structural studies on sodium borosilicate glasses doped with Er_2O_3 using ultrasonic velocity and FTIR spectroscopy. Physica B 388, 294–302.

Handke, M., Sitaz, M., Rokita, M., Galuskin, E., 2003. Vibrational spectra of phosphate silicate biomaterials. J. Mol. Struct. 651, 39–54.

Han, I., Demir, L., Sahin, M., 2009. Determination of mass attenuation coefficients, effective atomic and electron numbers for some natural minerals. Radiat. Phys. Chem. 78, 760–764.

Kaur, R., Singh, S., Pandey, O.P., 2012. FTIR structural investigation of gamma irradiated BaO–Na_2O–B_2O_3–SiO_2 glasses. Physica B 407, 4765–4769.

Laopaiboon, R., Bootjomchai, C., 2013. Influence of CeO_2 on structural properties of glasses by using ultrasonic technique: comparison between the local sand and SiO_2. Ultrasonics 53, 907–912.

Mao, J., Sui, Y., Wang, X., Yang, Yiyun, Zhang, X., Wang, Yang, Wang, Y., Liu, W., 2011. Spin-glass behavior and exchange bias in phase-separated $Nd_{0.85}Sr_{0.15}CoO_3$. J. Alloys Compd. 509, 4950–4953.

Marzouk, S.Y., Gaafar, M.S., 2007. Ultrasonic study on some borosilicate glasses doped with different transition metal oxides. Solid State Commun. 144, 478–483.

Marzouk, S.Y., 2009. Ultrasonic and infrared measurement of copper-doped sodium phosphate glasses. Mater. Chem. Phys. 114, 188–193.

Prado, M.O., Messi, N.B., Plivelic, T.S., Torriani, I.L., Bevilacqua, A.M., Arribére, M.A., 2001. The effects of radiation on the density of an aluminoborosilicate glass. J. Non-Cryst. Solids 289, 175–184.

Ramkumar, J., Sudarsan, V., Chandramouleeswaran, S., Shrikhande, V.K., Kothiyal, G. P., Ravindran, P.V., Kulshreshtha, S.K., Mukherjee, T., 2008. Structural studies on boroaluminosilicate glasses. J. Non-Cryst. Solids 354, 1591–1597.

Sawvel, A.M., Chinn, S.C., Bourcier, W.L., Maxwell, R.S., 2005. Local structure of amorphous $(PbO)_x[(B_2O_3)_{1-z}(Al_2O_3)_z]_y(SiO_2)_y$ dielectric materials by multinuclear solid state NMR. Chem. Mater. 17, 1493–1500.

Sharma, G., Rajendran, V., Thind, K.S., Singh, G., Singh, A., 2009. Structural investigation of bismuth borate glasses under the influence of γ-irradiation through ultrasonic studies. Physica B 404, 3371–3378.

Shelby, J.E., 1997. Introduction to Glass Science and Technology. Royal Society of Chemistry, Cambridge

Singh, S., Kumar, A., Singh, D., Thind, K.S., Mudahar, G.S., 2008. Barium-borate-flyash glasses: as radiation shielding materials. Nucl. Instrum. Methods B 266, 140–146.

Soliman, Y.S., Beshir, W.S., Abdel-Fattah, A.A., Abdel-Rehim, F., 2013. Dosimetric studies for gamma radiation validation of medical devices. Appl. Ratiat. Isot. 71, 21–28.

Srinivasarao, G., Veeraiah, N., 2001. Study on various physical properties of PbO–As_2O_3 glasses containing manganese ions. J. Alloys Compd. 327, 52–65.

Tran, H., Mehta, T., Zeller, M., Jarman, R.H., 2013. Synthesis and characterization of mixed phases in the Ca–Co–O system using the Pechini method. Mater. Res. Bull. , http://dx.doi.org/10.1016/j.materresbull.2013.02.060

Vasilyeva, M.S., Rudnev, V.S., Ustinov, A.Yu., Korotenko, I.A., Modin, E.B., Voitenko, O.V., 2010. Cobalt-containing oxide layers on titanium, their composition, morphology, and catalytic activity in CO oxidation. Appl. Surf. Sci. 257, 1239–1246.

Veeranna Gowda, V.C., Naraynan Reddy, C., Radha, K.C., Anavekar, R.V., Etoumeau, J., Rao, K.J., 2007. Structural investigations of sodium diborate glasses containing PbO, Bi_2O_3 and TeO_2: elastic property measurements and spectroscopic studies. J. Non-Cryst. Solids 353, 1150–1163.

Journal of Non-Crystalline Solids 388 (2014) 37–45

Contents lists available at ScienceDirect

Journal of Non-Crystalline Solids

journal homepage: www.elsevier.com/ locate/ jnoncrysol

Elastic moduli of borosilicate glasses doped with heavy metal oxides

Cherdsak Bootjomchai *, Raewat Laopaiboon, Somkid Pencharee, Jintana Laopaiboon

Glass Technology Excellent Center (GTEC), Department of Physics, Faculty of Science, Ubon Ratchathani University, Ubon Ratchathani 34190, Thailand

ARTICLE INFO

Article history:
Received 16 September 2013
Received in revised form 21 January 2014
Available online 7 February 2014

Keywords:
Amorphous materials;
Glasses;
Structural materials;
Ultrasonic measurements;
Elastic properties

ABSTRACT

Comparative studies on the theoretical and experimental values of elastic moduli of the borosilicate glasses (70-*x*) SiO_2–$30B_2O_3$–*x*HMOs glass system, where HMOs (heavy metal oxides) are TiO_2, BaO and Bi_2O_3 with 0, 1, 2, 3, 4 and 5 mol% of each HMO, were investigated. Elastic moduli were assessed by measuring the ultrasonic velocities. The number of network bonds per unit volume, the average of a stretching force constant, the average of cross-link density, the average of ring diameter and the theoretical bond compression bulk modulus were calculated by using a theoretical bond compression model to confirm the obtained results from the experiments. The results show that changes in the structure of the glass depend on a type and concentration of HMOs. Moreover, the experimental elastic moduli are in good agreement with the theoretical values.

1. Introduction

Glass is a solid material of interest because it is transparent to visible light and is a good insulator. Of specific interest for a glass material, borosilicate glasses have high chemical and mechanical resistance, very low electrical conductivity and thermal expansion coefficient. Thus, they are widely used in laboratory, optical, heat-resistant, fiber, pharmaceutical and sealing glass applications, and even for nuclear waste immobilization [1–4].

Elastic properties are very informative regarding the structures of glasses and they are directly related to the interatomic potentials. The glasses are isotropic and have only two independent elastic constants: longitudinal and shear moduli. These parameters are obtained from calculating the longitudinal and shear velocities and the densities of the glasses. The bulk modulus, Young's modulus and Poisson's ratio can also be deduced. The elastic moduli of borosilicate glasses containing transition, rare earth and/or heavy metal oxide (HMO) depend on ultrasonic waves at room temperature and were previously reported by several groups [4–15].

The glasses based on heavy metal oxides (HMOs) such as BaO, Bi_2O_3, PbO, TiO_2, Ag_2O, etc. have always been an area of interest because of their characteristic structural and physical properties such as high refractive index, high thermal expansion, high density, low transformation temperature and excellent infrared transmission (IR). Therefore, these glasses have been desirable aspirants for potential applications in IR technologies, design of laser devices and non-linear optics [16,17]. Among HMO glasses, bismuth and/or barium borosilicate glasses are the subject of growing and intense research. The glasses containing BaO and/or Bi_2O_3 have attracted considerable attention because of their vast range of applications in the fields of radiation shielding, glass-ceramics, reflecting windows, thermal and mechanical sensors, etc. [18–20]. In addition, the glasses containing significant concentrations of transition metal oxides (TMOs) such as TiO_2, ZnO, Fe_2O_3, V_2O_5, MnO_2, etc. are of continuing interest because of their applicability in memory switching, electrical threshold, optical switching devices, etc. [21–25].

In this work, the elastic moduli of borosilicate glasses will be discussed. Information regarding the number of network bonds per unit volume, the average of stretching force constant, the average of ring size diameter and the average of the cross-link density will be examined and discussed. The theoretical values of bond compression bulk modulus and elastic moduli will be calculated and compared with the experimental values.

2. Materials and methods

2.1. Preparation of glass samples

Rectangular shaped glass samples of the (70-*x*)SiO_2–$30B_2O_3$–*x*HMOs glass system (where HMOs are TiO_2, BaO and Bi_2O_3 with 0, 1, 2, 3, 4 and 5 mol% of each HMO) were prepared by the conventional melting technique. The oxides of SiO_2, B_2O_3, TiO_2, BaO and Bi_2O_3 used in this work were of an analytical regent grade. To prepare the glass samples, appropriate amounts of SiO_2, B_2O_3, TiO_2, BaO and Bi_2O_3 were weighed using an electronic balance with the accuracy of the order of 0.0001 g. The homogeneous mixtures were placed in ceramic crucible and melted in an electric furnace until homogeneity of the glass melt was ensured. The melted glasses were poured into graphite molds and annealed for 2 h before naturally cooling down to room temperature.

* Corresponding author.
E-mail address: cherdsak_per@hotmail.co.th (C. Bootjomchai).

0022-3093/$ – see front matter © 2014 Elsevier B.V. All rights reserved.
http://dx.doi.org/10.1016/j.jnoncrysol.2014.01.039

2.2. Density and molar volume measurements

The densities of the glass samples were determined by Archimedes' principle, using n-hexane as an immersion liquid and applying the relationship (1) [6]

$$\rho = \rho_L\left(\frac{W_a}{W_a - W_b}\right) \tag{1}$$

where ρ_L is density of the immersion liquid, and where W_a and W_b are the sample weights in air and in the immersion fluid, respectively. The experiment was repeated three times to obtain an accurate value for the density. The estimated error in these measurements was about ± 0.015 g cm^{-3} (shown in Table 1). The molar volume (V_a) was calculated from the expression $V_a = \frac{M}{\rho}$, where M is the molecular weight of the glass, which was calculated according to the relationship $M = \sum x_i M_i$ [26], where x_i is the mole fraction of the component oxide i and M_i is its molecular weight. The glass packing density can be calculated from the following Eqs. (2)–(3) [7]

$$V_t = \frac{\rho}{M}\sum_i x_i V_i \tag{2}$$

where V_i is given by,

$$V_i = \frac{4\pi N_A}{3}\left(x r_M^3 + y r_O^3\right) \tag{3}$$

where N_A is Avogadro's number, and where r_M and r_O are the ionic radii of the cation and anion of the oxide M_xO_y, respectively. The uncertainties in molar volume and packing density were acquired from experiments repeated three times of densities. The estimated error in these results was about ± 0.200 cm^3·mol^{-1} and $\pm 0.003 \times 10^{-6}$ m^3, respectively (shown in Table 1).

2.3. Ultrasonic measurements and determination of elastic moduli

To measure the ultrasonic velocity in the glass samples, an ultrasonic flaw detector, SONATEST Sitescan 230, was used. The ultrasonic wave was generated from a ceramic transducer with a resonant frequency at 4 MHz and acting as a transmitter–receiver at the same time. The ultrasonic wave velocity (v) can be calculated using the following Eq. (4) [5]:

$$v = \frac{2x}{\Delta t} \quad \left(cm{\cdot}s^{-1}\right) \tag{4}$$

where x is the sample thickness (cm) and Δt is the time interval (s). The measurements were repeated three times to check the reproducibility of the data. The estimated error in the velocity measurements was ± 23 m·s^{-1} for the longitudinal velocity and ± 11 m·s^{-1} for the shear velocity. The elastic strain produced by a small stress can be described by two independent elastic constants, C_{11} and C_{44} [27]. Elastic moduli were calculated using the following standard relations (5)–(10) [27]:

$$\text{Longitudinal modulus } C_{11} = L = \rho v_L^2, \tag{5}$$

$$\text{Shear modulus } C_{44} = G = \rho v_S^2, \tag{6}$$

$$\text{Bulk modulus } K = L - \frac{4}{3}G, \tag{7}$$

$$\text{Young's modulus } E = (1+\sigma)2G, \tag{8}$$

$$\text{Poisson's ratio } \sigma = \frac{L-2G}{2(L-G)}, \tag{9}$$

$$\text{Microhardness } H = \frac{(1-2\sigma)E}{6(1+\sigma)}, \tag{10}$$

Debye temperature calculated from Eq. (11) [28]

$$\theta_D = \left(\frac{h}{k_B}\right)\left(\frac{3zN_A}{4\pi V_a}\right)^{1/3} v_m, \tag{11}$$

where v_L and v_S are longitudinal and transverse velocities, respectively. h is Planck's constant, k_B is Boltzmann's constant, N_A is Avogadro's number, z is the number of atoms in the chemical formula and v_m is the mean ultrasonic velocity defined by the relationship (12) [29].

$$v_m = \left[\frac{3v_L^3 v_S^3}{v_L^3 + v_S^3}\right]^{1/3} \tag{12}$$

Softening temperature T_s is related to the ultrasonic velocity of shear waves v_S by Eq. (13) [4]

$$T_s = \frac{v_S M}{C^2 Z} \tag{13}$$

where Z is the number of atoms in the chemical formula and C is the constant of proportionality and equals 507.4 $m{\cdot}s^{-1}{\cdot}K^{1/2}$. The

Table 1
Glass composition, density (ρ), molar volume (V_a) and packing density (V_t) of the glass samples.

Sample no.	SiO_2 (mol%)	B_2O_3 (mol%)	TiO_2 (mol%)	BaO (mol%)	Bi_2O_3 (mol%)	ρ (g·cm^{-3})	V_a (cm^3·mol^{-1})	$V_t \times 10^{-6}$ (m^3)
S0	70	30	0	0	0	2.548	24.704	0.485
S1–TiO_2	70	30	1	0	0	2.547	24.287	0.498
S2–TiO_2	70	30	2	0	0	2.572	23.821	0.512
S3–TiO_2	70	30	3	0	0	2.594	23.390	0.526
S4–TiO_2	70	30	4	0	0	2.614	22.985	0.540
S5–TiO_2	70	30	5	0	0	2.634	22.585	0.555
S1–BaO	70	30	0	1	0	2.582	24.933	0.485
S2–BaO	70	30	0	2	0	2.600	25.023	0.488
S3–BaO	70	30	0	3	0	2.630	25.189	0.489
S4–BaO	70	30	0	4	0	2.647	25.381	0.489
S5–BaO	70	30	0	5	0	2.671	25.503	0.491
S1–Bi_2O_3	70	30	0	0	1	2.676	24.132	0.501
S2–Bi_2O_3	70	30	0	0	2	2.800	23.645	0.516
S3–Bi_2O_3	70	30	0	0	3	2.947	23.020	0.535
S4–Bi_2O_3	70	30	0	0	4	3.021	22.996	0.540
S5–Bi_2O_3	70	30	0	0	5	3.123	22.767	0.551
The uncertainty						±0.015	±0.200	±0.003

Table 2
Longitudinal (v_L), shear (v_S) and mean (v_m) velocities, longitudinal (L), shear (G), bulk (K) and Young's (E) modulus, Poisson's ratio (σ), microhardness (H), Debye (θ_D) and softening (T_s) temperature of the glass samples.

Sample no.	v_L (m/s)	v_S (m/s)	v_m (m/s)	L (GPa)	G (GPa)	K (GPa)	E (GPa)	σ	H (GPa)	θ_D (K)	T_s (K)
S0	6134	3788	4178	95.87	36.56	47.12	87.15	0.1918	7.51	361	699
S1–TiO_2	5925	3619	3996	89.41	33.36	44.94	80.22	0.2025	6.62	347	632
S2–TiO_2	5783	3557	3925	86.02	32.54	42.63	77.82	0.1957	6.60	343	599
S3–TiO_2	5521	3393	3744	79.07	29.86	39.25	71.47	0.1965	6.04	330	535
S4–TiO_2	5399	3290	3634	76.20	28.29	38.47	68.17	0.2047	5.57	322	494
S5–TiO_2	5288	3217	3554	73.65	27.26	37.31	65.76	0.2062	5.34	316	464
S1–BaO	6057	3737	4122	94.73	36.06	46.65	86.01	0.1927	7.39	355	681
S2–BaO	5963	3655	4035	92.45	34.73	46.14	83.30	0.1991	6.97	347	656
S3–BaO	5879	3594	3968	90.90	33.97	45.60	81.64	0.2016	6.76	341	636
S4–BaO	5811	3537	3907	89.38	33.11	45.23	79.86	0.2057	6.50	335	621
S5–BaO	5734	3524	3889	87.82	33.17	43.59	79.38	0.1965	6.71	333	619
S1–Bi_2O_3	6034	3725	4109	97.43	37.13	47.92	88.53	0.1921	7.62	358	685
S2–Bi_2O_3	5938	3633	4011	98.73	36.96	49.45	88.76	0.2009	7.37	352	660
S3–Bi_2O_3	5865	3578	3952	101.37	37.73	51.07	90.82	0.2036	7.45	350	643
S4–Bi_2O_3	5791	3522	3891	101.31	37.47	51.35	90.42	0.2065	7.33	344	641
S5–Bi_2O_3	5720	3459	3824	102.18	37.37	52.36	90.56	0.2117	7.18	340	628
The uncertainty	±23	±11	±16	±0.9	±0.4	±0.6	±0.7	±0.0012	±0.08	±2	±4

uncertainties in elastic moduli, Poisson' ratio, micro-hardness, Debye temperature and softening temperature were acquired from experiments repeated three times of the densities and the ultrasonic velocities. The estimated errors in these results are shown in Table 2.

2.4. Theoretical bond compression model

A bond compression model is a useful guide for structures containing only one type of bond. For a three dimensional polycomponent oxide glass, the bond compression bulk modulus is given by Eq. (14) [30]

$$K_{bc} = \frac{n_b \overline{F}}{9} r^2 \tag{14}$$

where r is the bond length between cation and anion and n_b is the number of network bonds per unit volume of the glass given by Eq. (15) [30]

$$n_b = \frac{N_A}{V_a} \sum_i \left(x n_f\right)_i \tag{15}$$

where x is the mole fraction of the component oxide i. $\overline{F}$ is the average of stretching force constant and can be calculated from Eq. (16) [31]

$$\overline{F} = \frac{\sum \left(x n_f F\right)_i}{\sum \left(x n_f\right)_i} \tag{16}$$

where n_f is the coordination number of the cation and F is the stretching force constant of the oxide. The average atomic ring size (l) of a structure consisting of a three-dimensional network according to the ring deformation model is expressed in the form of Eq. (17) [32].

$$l = \left[0.0106 \frac{\overline{F}}{K_{exp}}\right]^{0.26} \tag{17}$$

The theoretical Poisson's ratio for the polycomponent oxide glasses according to the bond compression model is given by Eq. (18) [30]

$$\sigma_{cal} = 0.28(\overline{n}_c)^{-0.25} \tag{18}$$

where $\overline{n}_c$ is the average cross-link density of the glass network and is given by Eq. (19) [30]

$$\overline{n}_c = \frac{1}{\eta} \sum_i (n_c)_i (N_c)_i \tag{19}$$

where n_c is the number of cross-links per cation (number of bridging bonds per cation minus two) in oxide i. N_c is the number of cations per glass formula unit and $\eta = \Sigma(N_c)_i$ is the total number of cations per glass formula unit. The theoretical bulk modulus (K_{cal}) can be calculated from Eq. (20) [31].

$$K_{cal} = 1.062 \times 10^{-29} \overline{F} l^{-4.0022} \tag{20}$$

The other theoretical elastic moduli can be obtained from the bulk modulus and Poisson's ratio for each glass system as Eqs. (21)–(23) [30].

$$G_{cal} = 1.5 K_{cal} \left[\frac{1-2\sigma_{cal}}{1+\sigma_{cal}}\right] \tag{21}$$

$$L_{cal} = K_{cal} + 1.33 G_{cal} \tag{22}$$

$$E_{cal} = 2(1+\sigma_{cal}) G_{cal} \tag{23}$$

3. Results and discussion

3.1. Density and molar volume

The glass composition, density, molar volume and packing density are given in Table 1. The density and molar volume increase when the content of doping (TiO_2, BaO and Bi_2O_3) increases as shown in Fig. 1. The density increases with the content of doping in all the glasses. Moreover, the density of the glass samples doped with Bi_2O_3 was higher than that of the glass samples doped with BaO and TiO_2. This is due to the adding of TiO_2, BaO and Bi_2O_3 (molecular weights of 79.866, 153.326 and 465.959 $g \cdot mol^{-1}$, respectively) into the glass matrix [7].

The results of molar volume as shown in Fig. 1 revealed that the molar volumes of the glass samples decreased with the increase of content of Bi_2O_3 and TiO_2, whereas the molar volume of the glass samples doped with BaO slightly increases. The molar volume is defined as the volume occupied by the unit mass. To explain the results of molar volume the variations of packing density or compactness of the glasses

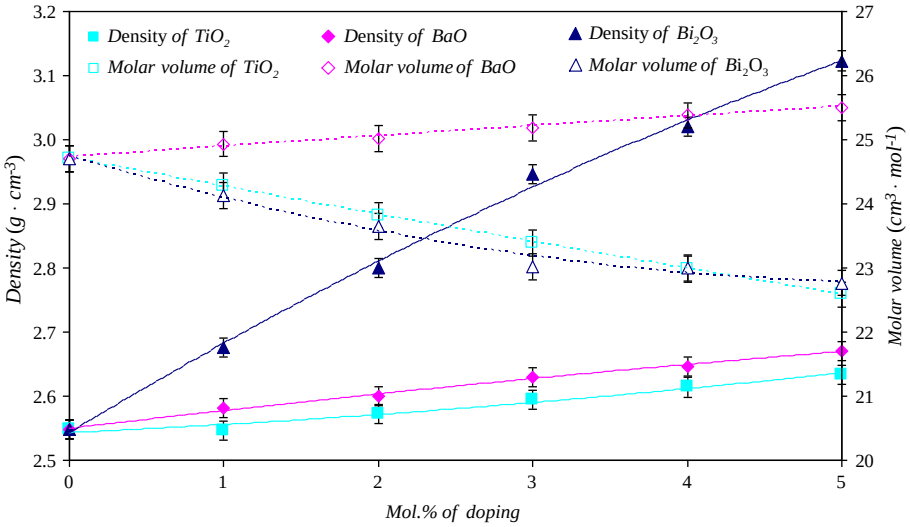

Fig. 1. Variation of densities (ρ) and molar volume (Va) of glass samples with the difference of doping (lines are drawn as guides to the eyes).

were calculated and shown in Fig. 2. The glass packing density is the ratio between the minimum theoretical volume occupied by the ions and the corresponding effective volume of the glass. The packing density or compactness of the glasses doped with Bi_2O_3 and TiO_2 shows large increase with increasing mol% of the dopant as shown in Fig. 2. These results indicate that the compactness of the glass matrix increases with the increase of the content of Bi_2O_3 and TiO_2. Therefore, the molar volume decreases with the mol% of Bi_2O_3 and TiO_2 increase. However, the compactness of the glass doped with BaO slightly increases with the increase of the content of BaO. These results suggested that the glass compactness depends on the ionic radius of the modifier. The ionic radius of the Ba^{2+} (1.49 Å) is larger than the ionic radii of Bi^{3+} and Ti^{4+} (1.17 and 0.745 Å, respectively) which can lead to an increase in the size of the interstices and increase in the molar volume [33]. Therefore, the glass doped with BaO shows the smaller increase of packing density than the glass doped with Bi_2O_3 and TiO_2. Moreover, the larger ionic radius results in increasing of the molar volume.

3.2. Ultrasonic velocity and elastic moduli

The plots of longitudinal (v_L) and shear (v_S) wave velocities in the borosilicate glasses with the mol% of the dopants are shown in Fig. 3 and exact values are shown in Table 2. It is observed that the ultrasonic wave velocities, v_L and v_S, in the glasses decrease as the mol% of the dopants (TiO_2, BaO and Bi_2O_3) increase. Preferably, the glasses doped with TiO_2 showed significant decreases of both v_L and v_S velocities with the increase of concentration of TiO_2. In general, the decrease of ultrasonic velocity is related to the increase in the number of non-bridging oxygens (NBOs) resulting in decrease in connectivity of the glass network [28]. For these reasons, adding the modifier (TiO_2, BaO and Bi_2O_3) leads to structural changes by creating the formation of NBOs. The lower sound velocity with doped TiO_2 indicates that adding TiO_2 leads to higher formation of NBOs than that of BaO and Bi_2O_3. Therefore, the decrease in ultrasonic wave velocities is due to the fact that HMO ions are involved in the glass network as modifiers by breaking up the tetrahedral bond of SiO_4 units [6]. In the asseveration of these results, the number of bonds per unit volume (n_b) is calculated by using a theoretical bond compression model and exact values are given in Table 3. It can be seen that all the samples show the decrease in the number of bonds per unit volume with the increase of the mol% of the dopants. In addition, the lower the number of bonds per unit volume of the glass doped with TiO_2, the greater the formation of non-bridging oxygens (NBOs). These results supported our discussions of the ultrasonic wave velocities of glass samples.

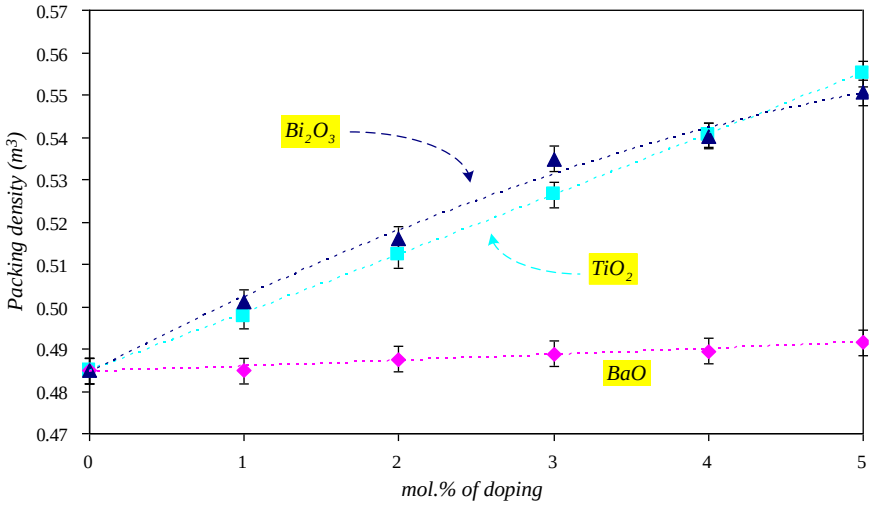

Fig. 2. Variation of packing density (Vt) of glass samples with the difference of doping (lines are drawn as guides to the eyes).

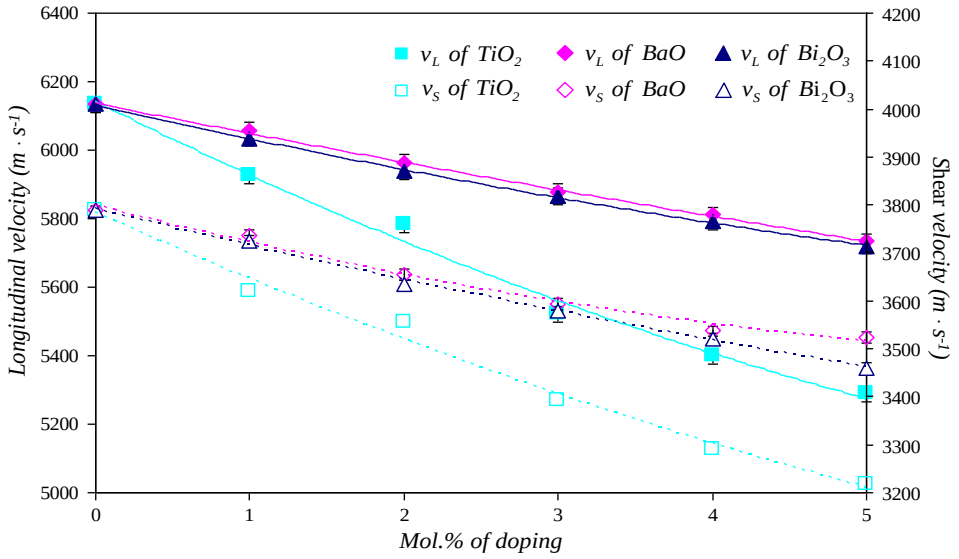

Fig. 3. Variation of longitudinal (vL) and shear (vS) velocity of glass samples with the difference of doping. The error bar is contained within the symbol size (lines are drawn as guides to the eyes).

As seen from Figs. 4–6 and Table 2, all elastic moduli values (L, G, K and E) decrease with the increase of TiO_2 and BaO concentrations while they increase with the increase of Bi_2O_3 concentration. All of the elastic moduli are related to the average strength of the bond. The average strength of the bond depends on the value of the cation–anion forces. For a given A–O–A bond angle, the A–A separation would be directly proportional to the stretching force constant ($\overline{F}$) of the glass network [34]. As the A–O–A bond force constants decrease, the energy required to produce a given degree of bond angle or length distortion and/or bond distortion decreases which leads to the decrease in the average strength of the bond. To verify these results, the stretching force constants ($\overline{F}$) are calculated by using a theoretical bond compression model, and the exact values are shown in Table 3. From the table, the average stretching force constants ($\overline{F}$) for the glass doped with TiO_2 and BaO decrease with the increase of the mol% of the dopant (TiO_2 and BaO). On the other hand, the average stretching force constants ($\overline{F}$) for the glass doped with Bi_2O_3 show the increase with the increase of the mol% of the dopant (Bi_2O_3). These results indicate that the glass doped with TiO_2 and BaO leads to the decrease in the average strength of the bond (elastic moduli were decreased) while the average strength of the bond increases when doped with Bi_2O_3 (elastic moduli were increased).

Table 3
E/G ratio, average cross-link density ($\overline{n}_c$), average stretching force constant ($\overline{F}$), average ring diameter (l), theoretical bond compression bulk modulus (K_{bc}), number of network bonds per unit volume (n_b) and K_{bc}/K_{exp} ratio of the glass samples.

Sample no.	E/G	$\overline{n}_c$	$\overline{F}$ (N/m)	l (nm)	K_{bc} (GPa)	$n_b \times 10^{22}$ (cm^{-3})	K_{bc}/K_{exp}
S0	2.384	2.615	431.5	0.5453	152.02	14.68	3.226
S1—TiO_2	2.421	2.667	429.2	0.5513	176.22	12.37	3.483
S2—TiO_2	2.421	2.657	426.8	0.5581	171.22	12.36	3.788
S3—TiO_2	2.483	2.647	424.5	0.5694	166.34	12.33	4.238
S4—TiO_2	2.516	2.636	422.3	0.5716	161.45	12.29	4.451
S5—TiO_2	2.530	2.626	420.1	0.5754	156.50	12.27	4.723
S1—BaO	2.385	2.595	430.7	0.5465	151.21	14.39	3.242
S2—BaO	2.398	2.576	429.8	0.5478	151.25	13.99	3.278
S3—BaO	2.403	2.556	429.0	0.5491	150.84	13.59	3.308
S4—BaO	2.411	2.537	428.2	0.5500	150.27	13.19	3.322
S5—BaO	2.393	2.519	427.3	0.5550	150.12	12.79	3.444
S1—Bi_2O_3	2.411	2.583	425.0	0.5449	156.52	13.88	3.266
S2—Bi_2O_3	2.440	2.552	426.3	0.5421	160.64	13.67	3.248
S3—Bi_2O_3	2.444	2.522	427.6	0.5372	165.93	13.57	3.249
S4—Bi_2O_3	2.458	2.493	428.9	0.5323	167.03	13.14	3.253
S5—Bi_2O_3	2.462	2.464	430.2	0.5312	169.64	12.80	3.240

Fig. 7 shows the variation of Poisson's ratio and micro-hardness of the glass samples as a function of the dopants and the exact values are listed in Table 2. Poisson's ratio of all samples increases as the mol% of the dopants increases. The variation of Poisson's ratio related to cross-link density decreases as the cross-link density increases. Therefore, the increase of Poisson's ratio shows that the cross-link density decreases due to the increase in the number of non-bridging oxygens after adding TiO_2, BaO and Bi_2O_3, respectively. To confirm the results, the average number of cross-links density ($\overline{n}_c$) was calculated by using the theoretical bond compression model and shown in Table 3. The average number of cross-links density ($\overline{n}_c$) decreased when the mol% of the dopants increases. These results strongly support the increase of Poisson's ratio with the increase of the mol% of the dopants because of the occurrence of non-bridging oxygens (NBOs). Moreover, these results support our explanation of the ultrasonic velocities. The micro-hardness (H) of the glass samples as a content of the dopants is shown in Fig. 7. It is defined as the resistance of a material to permanent indentation or penetration [35]. It can be seen that the micro-hardness has the same characteristic as the ultrasonic velocities with the increase of the mol% of the dopants. Therefore, it is evident that the decrease in micro-hardness is related to the decrease in the rigidity of the glass network due to the occurrence of non-bridging oxygens (NBOs) [36].

Debye temperature (θ_D) and softening temperature (T_s) of the glasses are listed in Table 2 and the plots of Debye temperature (θ_D) and softening temperature (T_s) are shown in Fig. 8. Debye temperature (θ_D) is an important parameter of a solid, describes the properties arising from atomic vibration and is directly proportional to the mean ultrasonic velocity (v_m). The variations of the mean ultrasonic velocity are shown in Table 2 [29]. Softening temperature (T_s) is another important parameter defined as the temperature point at which viscous flow changes to plastic flow [6,28]. It can be observed from Fig. 8 that both the Debye and softening temperature decrease as the mol% of the dopants increases. The decreases in the mean of ultrasonic velocity, Debye temperature and softening temperature are mainly contributed by the increase in formation of non-bridging oxygens (NBOs) as a direct effect of the insertion of HMO ions (ions of TiO_2, BaO and Bi_2O_3) into the glass network structures [6,28].

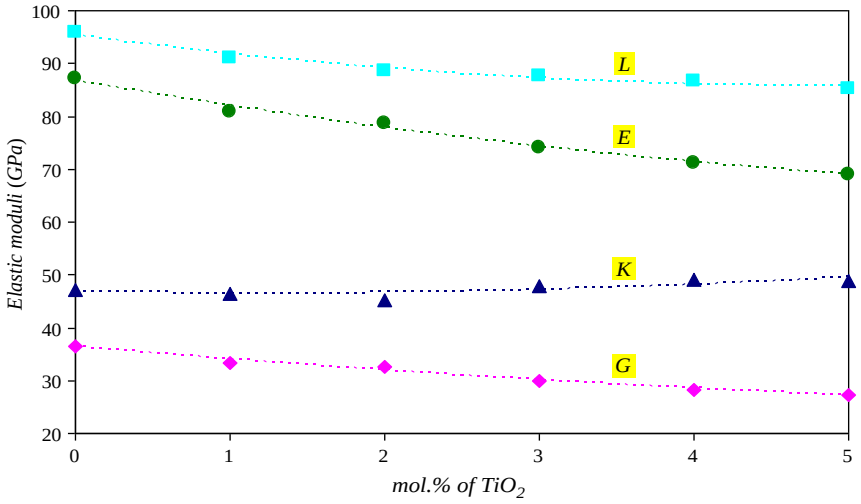

Fig. 4. Variation of elastic moduli of glass samples with different mol% of TiO2. The error bar is contained within the symbol size (lines are drawn as guides to the eyes).

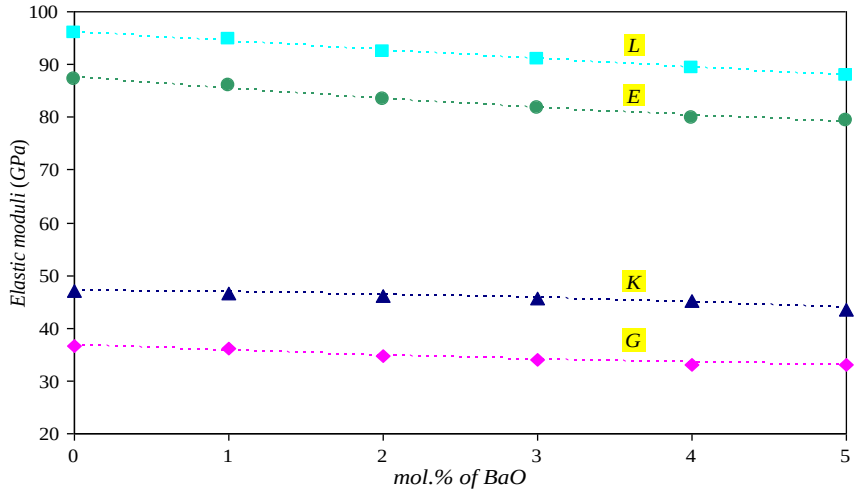

Fig. 5. Variation of elastic moduli of glass samples with different mol% of BaO. The error bar is contained within the symbol size (lines are drawn as guides to the eyes).

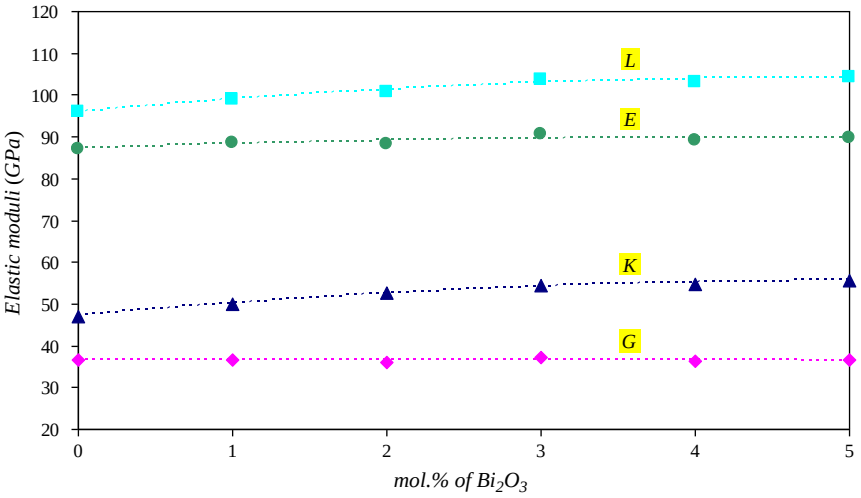

Fig. 6. Variation of elastic moduli of glass samples with different mol% of Bi2O3. The error bar is contained within the symbol size (lines are drawn as guides to the eyes).

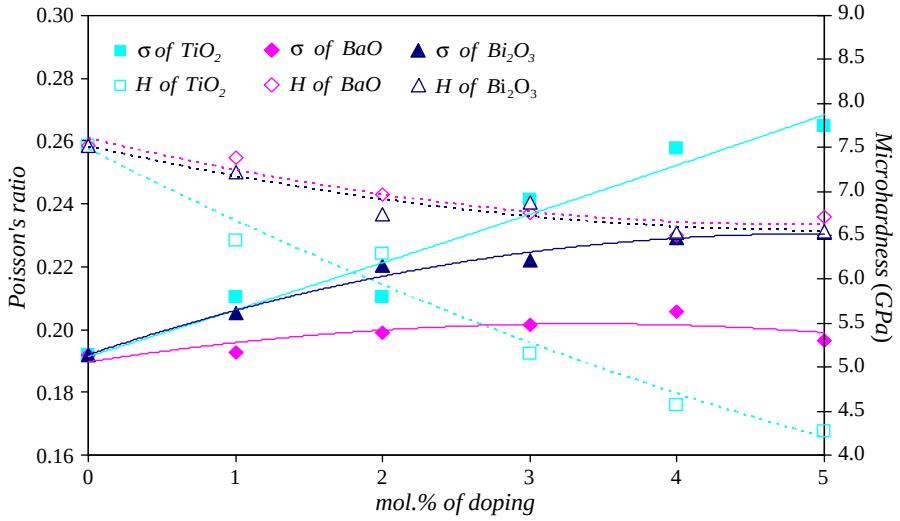

Fig. 7. Variation of Poisson's ratio (σ) and microhardness (H) of glass samples with different mol% of doping. The error bar is contained within the symbol size (lines are drawn as guides to the eyes).

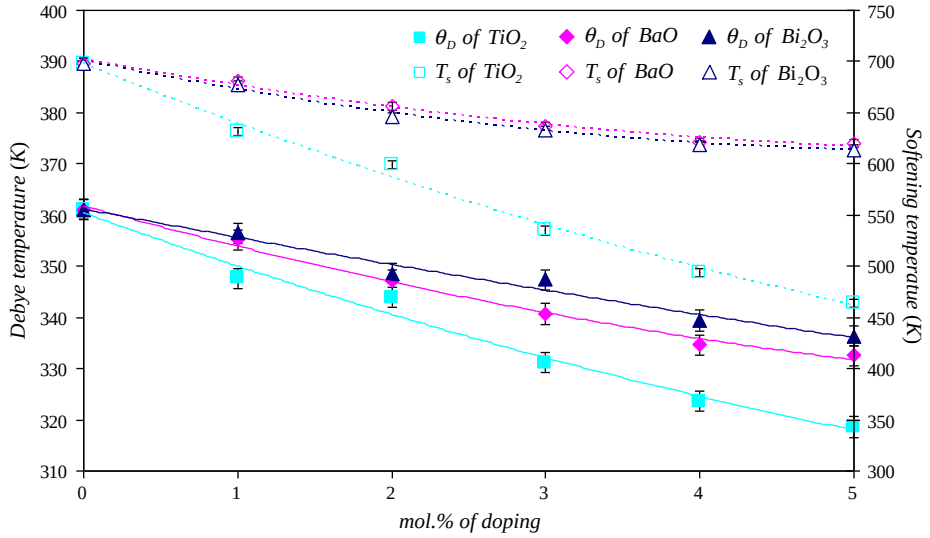

Fig. 8. Variation of Debye (θD) and softening (H) temperature of glass samples with different mol% of doping (lines are drawn as guides to the eyes).

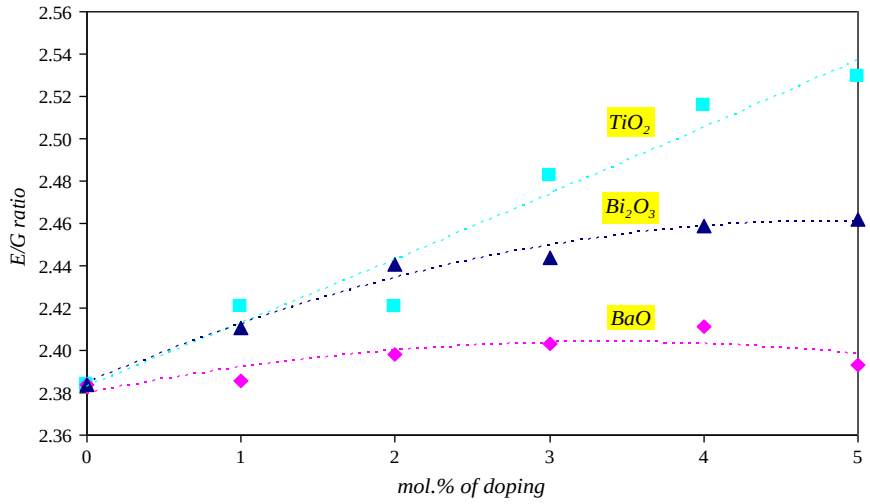

Fig. 9. Variation of E/G ratio of glass samples with different mol% of doping (lines are drawn as guides to the eyes).

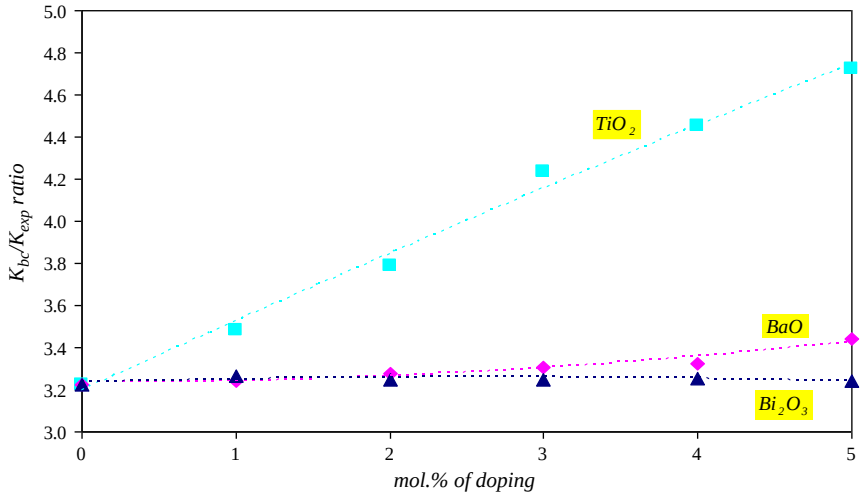

Fig. 10. Variation of Kbc/Kexp ratio of glass samples with different mol% of doping (lines are drawn as guides to the eyes).

The values of E/G, average ring diameter (l), theoretical bond compression bulk modulus (K_{bc}) and K_{bc}/K_{exp} ratio are shown in Table 3. The values of E/G were derived from the Poisson's ratio of the glasses. The relationship between E/G ratio and Poisson's ratio was related to the three chain network of the glass matrix [34]. From Table 3 and Fig. 9, it is clear that the tendency of the E/G ratio is likely the same as that of the behavior of Poisson's ratio with the increase of the mol% of the dopants. From Table 3, it is quite clear that the values of the theoretical bond compression bulk modulus (K_{bc}) decrease when the content of TiO_2 or BaO increases while K_{bc} increases with the increase of the content of Bi_2O_3. This indicates that adding HMOs to the pure composition of the glass plays a major role in the average coordination of the network structure [37] or the average stretching force constant which was found as a similar trend with the K_{bc}. In general, the ratio of K_{bc}/K_{exp} is a measure of the extent to which bond bending is governed by the configuration of the network bonds. This ratio is assumed to be directly proportional to the average ring diameter. The values of the K_{bc}/K_{exp} ratio and average ring diameter are shown in Figs. 10 and 11, respectively. From the figures, the variation of the K_{bc}/K_{exp} ratio increases as TiO_2 dopant increases while it slightly increases as the BaO dopant increases, yet it slightly decreases when the Bi_2O_3 dopant increases. Moreover, the variation of the K_{bc}/K_{exp} ratio has a similar trend to average ring diameter as shown in Fig. 11. These results of the K_{bc}/K_{exp} ratio and average ring diameter confirm the results for elastic moduli of the glass samples. Furthermore, the change in average ring diameter supports our discussion of the change of average strength of the bonds of the glass matrix with differently doped HMOs.

Table 4 shows the theoretically calculated from a theoretical bond compression model and experimental values of the elastic moduli (L, G, K and σ) for the glass samples. From the table, the calculated elastic moduli are in the range of the experimental values. It is observed that a theoretical bond compression model is in a good agreement with the experimental values of elastic moduli.

El-Mallawany et al. [32,38–41] studied the structure of TeO_2 glass which also has tetrahedral single bonds. The number of bonds per unit volume (n_b), average crosslink density ($\bar{n}_c$), ring diameter (l) and stretching force constant ($\bar{F}$) of SiO_2 are compared with those of TeO_2. These values of TeO_2 glass are listed in Table 5. The results show that the changes in the number of bonds per unit volume (n_b), average crosslink density ($\bar{n}_c$), ring diameter (l) and stretching force constant ($\bar{F}$) of TeO_2 depend on the type and the concentration of the modifiers. These results show good agreement between the changes in the structure of SiO_2 and TeO_2.

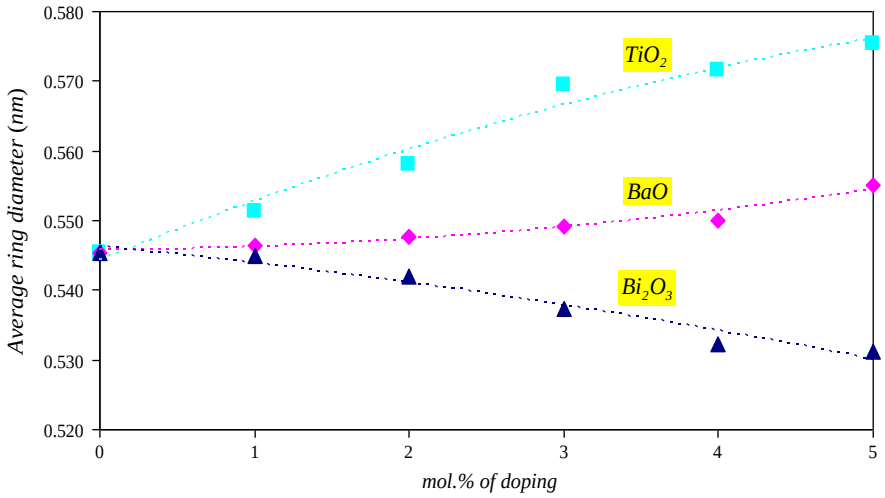

Fig. 11. Variation of average ring diameter (l) of glass samples with different mol% of doping (lines are drawn as guides to the eyes).

Table 4
Comparison of experimental estimated elastic moduli (L, G, K and σ) with those obtained theoretically by using bond compression model.

Sample No.	L_{exp} (GPa)	L_{cal} (GPa)	G_{exp} (GPa)	G_{cal} (GPa)	K_{exp} (GPa)	K_{cal} (GPa)	σ_{exp}	σ_{cal}
S0	95.87	104.02	36.56	37.37	47.12	54.32	0.1918	0.2202
S1—TiO_2	89.41	99.07	33.36	35.61	44.94	51.71	0.2025	0.2200
S2—TiO_2	86.02	93.84	32.54	33.75	42.63	48.96	0.1957	0.2197
S3—TiO_2	79.07	86.17	29.86	31.01	39.25	44.94	0.1965	0.2195
S4—TiO_2	76.20	84.45	28.29	30.40	38.47	44.02	0.2047	0.2193
S5—TiO_2	73.65	81.85	27.26	29.48	37.31	42.64	0.2062	0.2191
S1—BaO	94.73	102.84	36.06	36.91	46.65	53.75	0.1927	0.2206
S2—BaO	92.45	101.59	34.73	36.43	46.14	53.14	0.1991	0.2210
S3—BaO	90.90	100.29	33.97	35.93	45.60	52.51	0.2016	0.2214
S4—BaO	89.38	99.35	33.11	35.56	45.23	52.06	0.2057	0.2219
S5—BaO	87.82	95.54	33.17	34.16	43.59	50.11	0.1965	0.2223
S1—Bi_2O_3	97.43	103.88	37.13	37.26	47.92	54.32	0.1921	0.2209
S2—Bi_2O_3	98.73	105.58	36.96	37.81	49.45	55.29	0.2009	0.2215
S3—Bi_2O_3	101.37	108.95	37.73	38.96	51.07	57.13	0.2036	0.2222
S4—Bi_2O_3	101.31	112.52	37.47	40.18	51.35	59.08	0.2065	0.2228
S5—Bi_2O_3	102.18	113.02	37.37	40.29	52.36	59.43	0.2117	0.2235

Table 5
The number of bonds per unit volume (n_b), average crosslink density ($\overline{n}_c$),average ring diameter (l) and average stretching force constant ($\overline{F}$) of TeO_2 with different compositions [32,38–41].

Glass	$n_b \times 10^{22}$ (cm^{-3})	$\overline{n}_c$	l (nm)	$\overline{F}$ (N/m)
TeO_2	7.740	2.000	0.500	216
$80TeO_2$–$5TiO_2$–$10WO_3$–$5Nb_2O_5$	9.950	2.480	–	–
$80TeO_2$–$5TiO_2$–$12WO_3$–$3Nd_2O_3$	9.499	2.450	–	–
$80TeO_2$–$5TiO_2$–$10WO_3$–$5Nd_2O_3$	9.648	2.480	–	–
$80TeO_2$–$5TiO_2$–$10WO_3$–$5Er_2O_3$	9.684	2.480	–	–
$80TeO_2$–$20MoO_3$	8.600	–	0.512	219
$80TeO_2$–$20V_2O_5$	7.560	–	0.535	231

4. Conclusions

The elastic moduli and structure of the glass samples have been investigated as a function of compositions (different contents of TiO_2, BaO and Bi_2O_3) by measuring ultrasonic velocities. The lowest longitudinal, shear, bulk and Young's moduli of these glasses were 73.65, 27.26, 37.31 and 65.76 GPa, respectively for the composition S5—TiO_2 glass samples. The highest longitudinal, shear, bulk and Young's moduli of these glasses were 102.18, 37.73, 52.36 and 90.82 GPa, respectively for the composition S5—Bi_2O_3, S3—Bi_2O_3, S5—Bi_2O_3 and S3—Bi_2O_3 glass samples, respectively. The number of bonds per unit volume, the average stretching force constant, the average cross-link density, the average ring diameter and the theoretical bond compression bulk modulus were calculated by using a theoretical bond compression model for the asseveration of the obtained results. The agreement between the theoretically calculated and experimental elastic moduli is excellent for the studied samples. Moreover, the results showed good agreement when the number of bonds per unit volume, average crosslink density, ring diameter and stretching force constant of SiO_2 are compared with those of TeO_2. These results indicate the reliability of the experimental data.

Acknowledgments

Financial support of this study has been provided by the Thailand Research Fund (TRF), Office of the Higher Education Commission (OHEC) and Ubon Ratchathani University (UBU). The results and comments on this article are those of the authors. The TRF, OHEC and UBU are unnecessary always agree. The authors thank Dr. Udom Tipparach for editing and reading the proof.

References

[1] R.H. Doremus, Glass Science, 2nd ed., John Wiley & Son. Inc., NewYork, 1994.
[2] A.K. Varshneya, Fundamentals of Inorganic Glasses, AcademicPress, NewYork, 1994.
[3] H.G. Pfaerder, Schott Guide to Glass, Chapman and Hall, London, 1996.
[4] S.Y. Marzouk, Physica B 405 (2010) 3395–3400.
[5] R. El-Mallawany, N. El-Khoshkhany, H. Afifi, Mater. Chem. Phys. 95 (2006) 321–327.
[6] S.Y. Marzouk, M.S. Gaafar, Solid State Commun. 144 (2007) 478–483.
[7] I.Z. Hager, J. Alloys Compd. 539 (2012) 256–263.
[8] K.A. Matori, M.H.M. Zaid, S.Hj.A. Aziz, H.M. kamari, Z.A. Wahab, J. Non-Cryst. Solids 361 (2012) 78–81.
[9] G.E. El-Falaky, M.S. Gaafar, N.S. Abd El-Aal, Curr. Appl. Phys. 12 (2012) 589–596.
[10] F. Benmeddour, G. Villain, O. Abraham, M. Choinska, Constr. Build. Mater. 37 (2012) 934–942.
[11] A. Benhammou, Y. El Hafiane, L. Nibou, A. Yaacoubi, J. Soro, A. Smith, J.P. Bonnet, B. Tanouti, Ceram. Int. 39 (2013) 21–27.
[12] G.S. Rao, B.K. Sudhakar, N.R. Chand, B. Johnson, P.V.S. Sai Ram, P.S. Sastry, V. Devasahayam, Mater. Lett. 68 (2012) 21–23.
[13] El Sayed Yousef, Badriah Al-Qaisi, Solid State Sci. 19 (2013) 6–11.
[14] S. Laila, S.N. Supardan, A.K. Yahya, J. Non-Cryst. Solids 367 (2013) 14–22.
[15] M.S. Gaafar, S.Y. Marzouk, H.A. Zayed, L.I. Soliman, A.H. Serag El-Deen, Curr. Appl. Phys. 13 (2013) 152–158.
[16] R. Kaur, S. Singh, K. Singh, O.P. Pandey, Radiat. Phys. Chem. 86 (2013) 23–30.
[17] G. Upender, V.G. Sathe, V.C. Mouli, Physica B 405 (2010) 1269–1273.
[18] C. Bootjomchai, J. Laopaiboon, C. Yenchai, R. Laopaiboon, Radiat. Phys. Chem. 81 (2012) 785–790.
[19] C. Bootjomchai, J. Laopaiboon, S. Nontachat, U. Tipparach, R. Laopaiboon, Nucl. Eng. Des. 248 (2012) 28–34.
[20] A. Khanna, A. Saini, B. Chen, F. González, C. Pesquera, J. Non-Cryst. Solids 373–374 (2013) 34–41.
[21] S. Azianty, A.K. Yahya, M.K. Halimah, J. Non-Cryst. Solids 358 (2012) 1562–1568.
[22] Z. Huang, C. Chen, C. Lv, S. Chen, J. Alloys Compd. 564 (2013) 158–161.
[23] T.G.V.M. Rao, A.R. Kumar, K. Neeraja, N. Veeraiah, M.R. Reddy, J. Alloys Compd. 557 (2013) 209–217.
[24] T.G.V.M. Rao, A.R. Kumar, N. Veeraiah, M.R. Reddy, J. Phys. Chem. Solids 74 (2013) 410–417.
[25] P. Martín, M.L. López, C. Pico, M.L. Veiga, Mater. Chem. Phys. 140 (2013) 535–542.
[26] N.A. Abd El-Malak, Mater. Chem. Phys. 73 (2002) 156–161.
[27] B. Eraiah, M.G. Smitha, R.V. Anavekar, J. Phys. Chem. Solids 71 (2010) 153–155.
[28] M.S. Gaafar, S.Y. Marzouk, Physica B 388 (2007) 294–302.
[29] S.Y. Marzouk, Mater. Chem. Phys. 114 (2009) 188–193.
[30] B. Bridge, A. Higazy, Phys. Chem. Glasses 27 (1986) 1–14.
[31] A. Abd El-Moneim, Physica B 325 (2003) 319–332.
[32] R. El-Mallawany, Mater. Chem. Phys. 63 (2000) 109–115.
[33] J.E. Shelby, Density and molar volume, Introduction to Glass Science and Technology, The Royal Society of Chemistry, UK, 1997. 137–142.
[34] A.A. Higazy, B. Bridge, J. Non-Cryst. Solids 72 (1985) 81–108.
[35] A. Abd El-Moneim, I.M. Youssof, L. Abd El-Latif, Acta Mater. 54 (2006) 3811–3819.
[36] M.S. Gaafar, H.A. Afifi, M.M. Mekawy, Physica B 404 (2009) 1668–1673.
[37] D.J.M. Burkhard, Solid State Commun. 101 (1997) 903–907.
[38] R. El-Mallawany, H. Afifi, Mater. Chem. Phys. 143 (2013) 11–14.
[39] R. El-Mallawany, J. Mater. Res. 5 (1990) 2218–2222.
[40] R. El-Mallawany, J. Appl. Phys. 73 (1993) 4878–4880.
[41] R. El-Mallawany, A. Abousehly, E. Yousef, J. Mater. Sci. Lett. 19 (2000) 409–411.

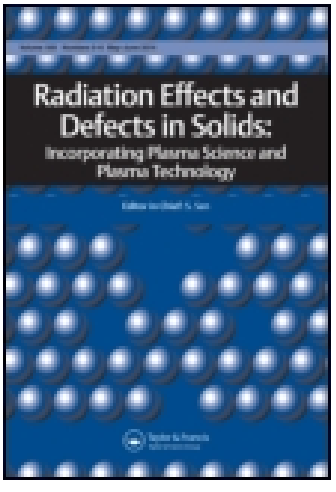

Radiation Effects and Defects in Solids: Incorporating Plasma Science and Plasma Technology
Publication details, including instructions for authors and subscription information:
http://www.tandfonline.com/loi/grad20

Structural investigation of glasses with doped some transition metal oxides under the influence of gamma irradiation

R. Laopaiboon[a], S. Nontachat[b], S. Pencharee[a], J. Laopaiboon[a] & C. Bootjomchai[a]

[a] Glass Technology Excellent Center (GTEC), Department of Physics, Faculty of Science, Ubon Ratchathani University, Ubon Ratchathani 34190, Thailand

[b] Department of Radiotherapy, Ubon Ratchathani Cancer Centre, Ubon Ratchathani 34190, Thailand

Published online: 29 Sep 2014.

To cite this article: R. Laopaiboon, S. Nontachat, S. Pencharee, J. Laopaiboon & C. Bootjomchai (2014) Structural investigation of glasses with doped some transition metal oxides under the influence of gamma irradiation, Radiation Effects and Defects in Solids: Incorporating Plasma Science and Plasma Technology, 169:10, 862-873, DOI: 10.1080/10420150.2014.958746

To link to this article: http://dx.doi.org/10.1080/10420150.2014.958746

Radiation Effects & Defects in Solids, 2014
Vol. 169, No. 10, 862–873, http://dx.doi.org/10.1080/10420150.2014.958746

Structural investigation of glasses with doped some transition metal oxides under the influence of gamma irradiation

R. Laopaiboon[a], S. Nontachat[b], S. Pencharee[a], J. Laopaiboon[a] and C. Bootjomchai[a]*

[a]*Glass Technology Excellent Center (GTEC), Department of Physics, Faculty of Science, Ubon Ratchathani University, Ubon Ratchathani 34190, Thailand;* [b]*Department of Radiotherapy, Ubon Ratchathani Cancer Centre, Ubon Ratchathani 34190, Thailand*

(*Received 30 April 2014; final version received 23 August 2014*)

The ultrasonic velocity of the alkali-borosilicate with different transition metal oxides (TMO) has been studied using the pulse echo technique. The elastic moduli such as elastic constant and bulk modulus have been obtained from the experimental data. Changes in the structure with different gamma irradiation doses have been investigated by using FTIR spectroscopy and ultrasonic studies. The results show that structural changes in the BO_3 to BO_4 due to TMO and irradiation are obtained.

Keywords: damage; gamma; radiation

1. Introduction

Several glasses have been developed for nuclear engineering application because they accomplish the double task of allowing visibility while absorbing radiation such as gamma rays and neutron, this is protection of the observer (*1*,*2*). Recently, the use of nuclear energy and radiation is indispensable in modern society such as nuclear power plants and radiotherapy. The knowledge of gamma-ray interaction with materials is very important in the field of radiation protection and/or nuclear safety. The most significant types of radiation for which shielding is required in a nuclear reactor are primary neutrons and gamma rays originating within the core itself and secondary gamma rays produced by neutron interactions with materials external to the reactor core, example reflector, pressure vessel, shield, etc. (*3*). As mentioned above, many researchers have studied the application of glass materials in radiation field. The technological affinity of glasses has led to greater efforts to determine their structures, particularly effect of modifiers and irradiation. The information was designed to gain a deep insight into the structure–properties association that can be exploited for the design of new glassy materials (*4*–*9*). Borosilicate glass is a type of glass with the main glass-forming constituents of silica (silicate) and boron (borate) oxide (*10*). The new glassy materials from alkali borosilicate glasses with high ionic conductivity are receiving considerable attention because of their unique properties and their potential applications such as used in the processing of high-level radioactive waste disposal, where the waste is immobilized in the glass (*11*–*14*). The role of alkali (such as Na_2O and K_2O)

*Corresponding author. Email: cherdsak_per@hotmail.co.th

in the B_2O_3 network is to modify the host structure through the transformation of the structural units of the borate network from BO_3 to BO_4. The sodium or potassium diborate is a type of borate glass that consists of one-third sodium or potassium oxide and two-thirds boron oxide. This type of borate glass draws great attention because of their improved electrical and optical properties (*15*–*17*).

Oxide glasses containing transition metal oxides (TMOs) are of technological interest because of the semiconducting properties that arise from the electron hopping between two TM ions having different valence states in these glasses (*18*). The optical absorption spectra of vanadium ions in various cabal, silicate and borate glasses before and after gamma irradiation have been reported by several investigators (*19*, *20*). Vanadium is believed to exist in glasses in three possible valences, namely, the trivalent, tetravalent and pentavalent states. The addition of TiO_2 to glasses contributes to an improved glass-forming ability, chemical durability and stabilization of the glass structure (*21*). TiO_2 has attractive characteristics, such as chemical stability and high refractive index, and it is sometimes used as a photocatalyst. In recent years, ZnO and the materials based on it are drawing more attention due to their interesting optical, electrical and magnetic properties in combination with its non toxicity, non-hygroscopic nature and low cost.

The properties of glasses are closely related to inter-atomic forces and potentials in the lattice structure. Thus, any change in lattice due to doping and/or irradiation can be directly noted. The elastic properties are important material properties to investigate the linear and anomalous variation as a function of the composition of glass and have been interpreted in terms of the structure or transformation of cross-linkages in the glass network (*22*). To study the structure of oxide glasses, the coordination number of the network former and the change of oxygen bonds of the framework induced by the cation modifiers need to be investigated. This information can be obtained from FTIR spectroscopy. The majority of structural investigations on glasses before irradiation in the past have been made using vibrational spectroscopy and ultrasonic studies (*23*–*25*). The ultrasonic technique is a versatile tool for investigating the change in microstructure, the deformation process and mechanical properties of materials (*26*). Many authors have studied the structural modifications in gamma irradiation dose of glasses by ultrasonic and FTIR spectroscopy. The experimental results clearly indicate that after irradiation a significant change in the structure of borosilicate glass network is observed (*7*, *27*–*31*).

In all of the above, the authors are producing new materials from borosilicate-based glass with doped V_2O_5, TiO_2 and ZnO. Then, the new glass materials were tested for stability of the structural properties using gamma irradiation by using the ultrasonic technique. In addition, an attempt has been made to do the same type of correlation between the changes in ultrasound velocities and elastic properties of the anticipated structural changes in the borosilicate glass network using FTIR spectroscopy. The obtained results were considered the possibility to materials of choices for applied in the fields of retrospective dosimetry materials.

2. Experimental details

2.1. *Sample preparation*

The alkali borosilicate glasses with doped TMOs (V_2O_5, TiO_2 and ZnO) were prepared using the melt-quenching technique. The chemical compositions of all these glasses are given in Table 1. The oxides of sodium, potassium, vanadium, titanium and zinc used in this work were of analytical reagent grade. The borosilicate glasses used in this work was waste glass from a laboratory. The chemical compositions of the borosilicate glasses are given in Table 2. The method of preparation of recycling glass from the laboratory to be used in the work is to thoroughly clean and grind to a powder form. The quantities of chemical powder and borosilicate glass powder were

Table 1. Composition and density ($\rho \pm 0.07\, kg/m^3$) of glass samples.

Samples	Composition (mol%)				Density (kg/m^3)
	Borosilicate	Na_2O	K_2O	TMOs	
Base glass	70	25	5	Undoped	2538.54
V_2O_5	70	25	5	0.1 (V_2O_5)	2541.85
ZnO	70	25	5	0.1 (ZnO)	2539.87
TiO_2	70	25	5	0.1 (TiO_2)	2539.55

Table 2. Chemical composition of borosilicate glasses.

Compound	Percentage
B_2O_3	20.20
Na_2O	8.21
Al_2O_3	17.35
SiO_2	48.51
K_2O	5.73

weighed using an electronic balance having an accuracy of the order of 0.0001 g. The chemicals and powders of borosilicate glass were mixed thoroughly in a crucible. The mixtures were melted in an electrical furnace at 1250°C to ensure homogeneity. Then the melted glass was poured into a preheated stainless steel mold and annealed at 500°C. The glass samples were cut and polished using different grades of silicon carbide. The thickness measurement was carried out using a micrometer.

2.2. *Gamma-ray irradiation*

The glass samples were irradiated by an exposure machine (THERATRON 780C) using a Co-60 gamma-ray source at a dose rate of 1.16 Gy/min and a field size of 15 × 15 cm^2 at a distance of 80 cm from the source at room temperature. The samples were irradiated sufficiently long enough to achieve an overall dose of 5, 10, 15 and 20 Gy. The diagram of the geometry is shown in Figure 1.

2.3. *Infrared absorption measurements*

Infrared (IR) absorption spectra of powdered glass samples were recorded in the range of 400–4000 cm^{-1} using the KBr technique at room temperature. A recording spectrometer from PerkinElmer was used to reveal the absorption spectra and all measurements were at 4 cm^{-1} resolution. Optical measurements were taken immediately after irradiation.

2.4. *Density measurement*

The density of each sample was measured by Archimedes' principle using *n*-hexane as the immersion liquid and applying the relation (*32*)

$$\rho = \rho_L \left(\frac{W_a}{W_a - W_b} \right), \quad (1)$$

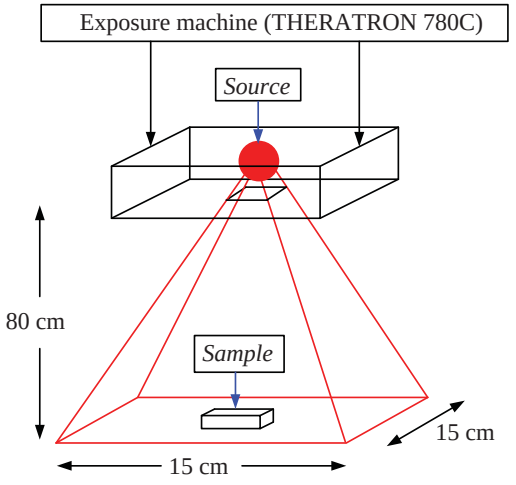

Figure 1. Geometrical arrangement of gamma irradiation.

where ρ_L is the density of the immersion liquid, W_a and W_b are the sample weights in air and in the immersion fluid, respectively. The experiment was repeated three times to get an accurate value of the density. The relative errors in these measurements were about ± 0.07 kg/cm^3.

2.5. *Ultrasonic velocity measurements*

For the measurement of ultrasonic velocity in the glass samples, an ultrasonic flaw detector, SONATEST Sitescan 230, was used. The ultrasonic wave was generated from a ceramic transducer with a resonant frequency of 4 MHz and acts as transmitter–receiver at the same time. The ultrasonic wave velocity (v) can be calculated per the following equation (*33*):

$$v = \frac{2x}{\Delta t}, \tag{2}$$

where x is the sample thickness (cm) and Δt is the time interval (s). The measurements were repeated three times to check the reproducibility of the data. The estimated error in velocity measurements was ± 12.0 m/s for the longitudinal velocity and ± 8.0 m/s for the shear velocity.

2.6. *Determination of elastic moduli*

The elastic strain produced by a small stress can be described by two independent elastic constants (C_{11} and C_{44}) and bulk modulus (K). Elastic moduli were calculated using the following standard relations (*34*):

$$\text{Longitudinal modulus } C_{11} = L = \rho v_L^2, \tag{3}$$

$$\text{Shear modulus } C_{44} = G = \rho v_S^2, \tag{4}$$

$$\text{Bulk modulus } K = L - \tfrac{4}{3}G. \tag{5}$$

3. Results and discussion

3.1. *Density results*

Experimental values of density of the investigated glasses are given in Table 1. The density of pure alkali borosilicate glass (based glass) is 2538.54 kg/m^3. The values of the densities of doped glasses with transition metals (V_2O_5, ZnO and TiO_2) are slightly higher than that of pure alkali borosilicate glass. This is due to the direct addition of 0.1 mol% of transition metals to the pure composition. Moreover, the density of the glass was doped with TMO depending on the molecular weight of TMO (V_2O_5 is 181.878 g/mol, ZnO is 81.379 g/mol and TiO_2 is 79.856 g/mol, respectively) (*7*). The variations of the densities are shown in Figure 2.

3.2. *Ultrasonic velocity and elastic moduli*

Figures 3 and 4 show the variation of longitudinal (v_L) and shear (v_S) wave velocities with different gamma-irradiation doses and the extracted values are given in Table 3. For the pure composition (based glass), both longitudinal (v_L) and shear (v_S) wave velocities increase from 5773 to 5812 m/s, and 3527 to 3578 m/s, respectively, with increasing gamma-irradiation dose from 0 to 20 Gy. In general, the increase in ultrasonic velocities is related to the decrease in the number of non-bridging oxygens (NBO) and consequently the increase in connectivity of the glass network (*35*). According to Abd El-Malak (*36*) the increase in velocities with increasing radiation dose is mainly due to the compactness of the glass sample and consequently to its hardness and rearrangement of the atoms in the glass network (*36*). Irradiation with gamma rays is assumed to create displacements, electronic defects and/or breaks in the network bonds, which allow the structure to relax and fill the relatively large interstices that exist in the interconnected network of boron and oxygen atoms causing expansion followed by compaction of the volume (*37*). Shelby (*38*) suggested that the boron–oxygen bond is more likely to be affected by irradiation. Damage by an irradiation species can cause the compaction of B_2O_3 by the breaking of bonds between trigonal elements, allowing the formation of tetrahedral (BO_4). The tetrahedral groups (BO_4) are more strongly bonded than the triangular (BO_3) and a compactness structure in them is expected to lead to an increase in ultrasonic velocities. For the glass doped with

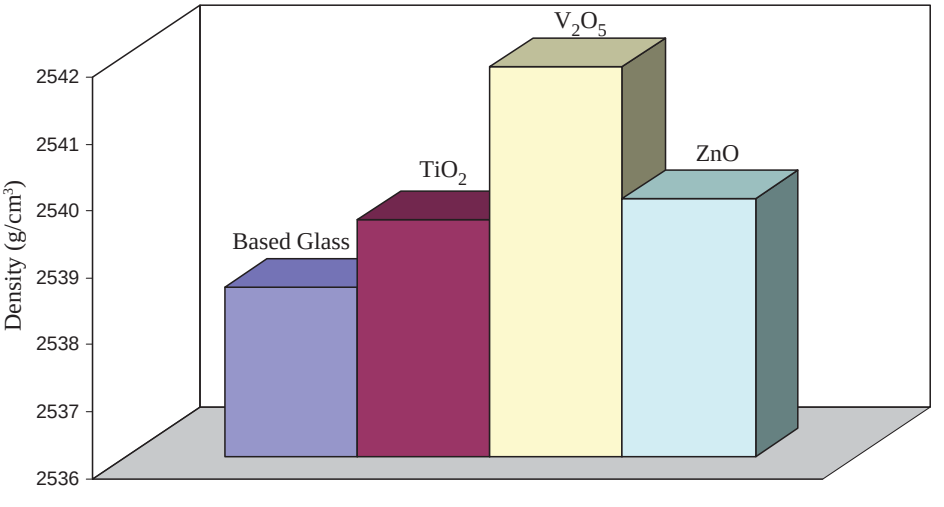

Figure 2. Variation of density of glass samples.

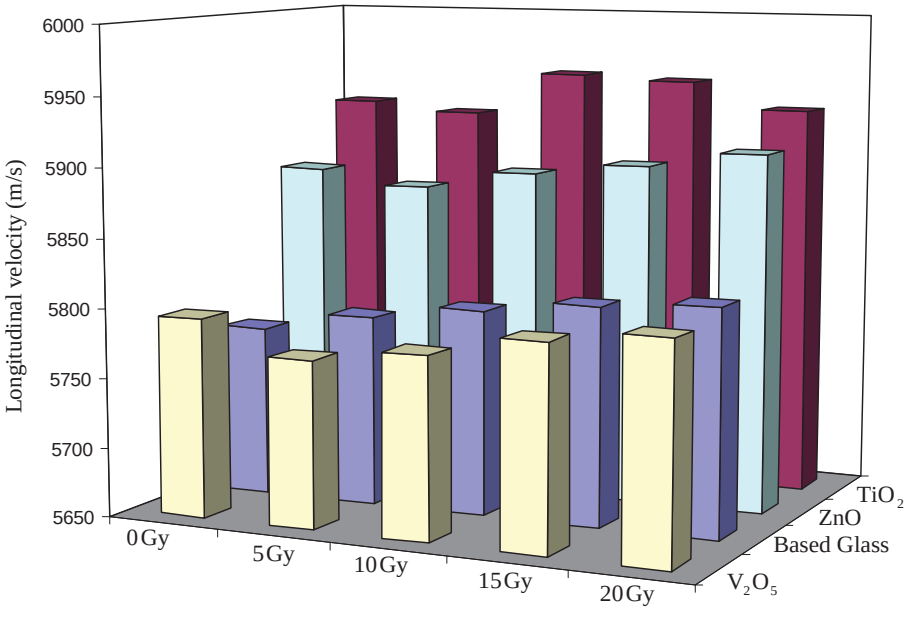

Figure 3. Variation of longitudinal velocity (v_L) of glass samples with different gamma irradiation doses.

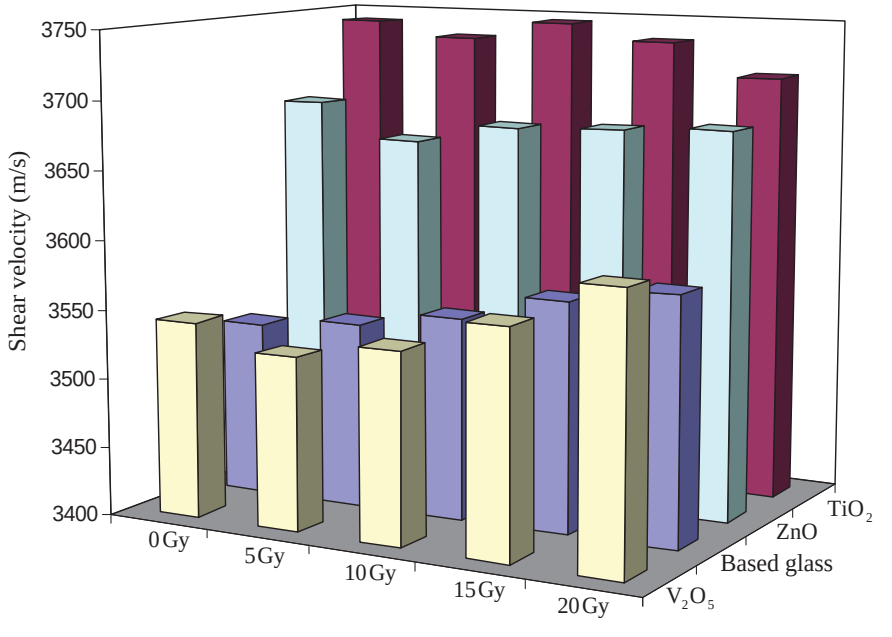

Figure 4. Variation of shear velocity (v_S) of glass samples with different gamma irradiation doses.

TMO, considering a 0 Gy of gamma-irradiation dose, both longitudinal and shear wave velocities increased with the addition of 0.1 mol% of V_2O_5, ZnO and TiO_2, respectively. For most of the materials, ultrasonic wave velocities will increase as the density or compactness and/or connectivity of the glass network increases. The increase in wave velocities of the present glasses may be attributed to the increase in ionic radii of the TMO ions from vanadium (V^{5+} is 68 pm), titanium (Ti^{4+} is 74.5 pm) and zinc (Zn^{2+} is 88 pm) which fill the interstices of the glass network.

Table 3. Longitudinal ($v_L \pm 12$ m/s) and shear ($v_S \pm 8$ m/s) velocities of glass samples with different gamma irradiation doses.

	Base glass		V_2O_5		ZnO		TiO_2	
Dose (Gy)	v_L(m/s)	v_S(m/s)	v_L(m/s)	v_S(m/s)	v_L(m/s)	v_S(m/s)	v_L(m/s)	v_S(m/s)
0	5773	3527	5793	3542	5883	3685	5928	3742
5	5787	3534	5770	3525	5873	3660	5922	3732
10	5798	3546	5780	3538	5887	3674	5954	3746
15	5807	3566	5796	3563	5896	3677	5951	3734
20	5812	3578	5805	3596	5908	3681	5932	3711

However, the TiO_2 and ZnO glass samples show the opposite phenomenon. This is because the density was necessary to considered. As for the effects of gamma-irradiation dose, both longitudinal and shear velocities decrease at 5 Gy and then come back gradually increasing from 10 to 20 Gy. As a form of explanation, the initial decreases in sound velocities were suggested to be due to the accumulated stress in the network structure as a result of addition of the TMO resulting in bending of the bond. This result causes the weakening of the glass network and leads to a breakdown of the ring-type structure of the glass network by gamma irradiation. The sound velocities coming back with the increase in gamma-irradiation dose between 10 and 20 Gy were suggested to be due to competition between bridging oxygen ($BO_3 \rightarrow BO_4$) in the cross-linkage direction and NBO ions in the glass network (*38*).

As seen from Table 4 and Figures 5 and 6, the elastic moduli (longitudinal and shear modulus) values show increases due to the irradiation effect. In general, the elastic moduli increase when the density or ultrasonic velocity increases (*39*). In this work, the elastic moduli have the same trend as observed for ultrasonic wave velocities in Figures 3 and 4. From our observations, the increase in these moduli is due to the decrease in the formation of NBO atoms ($BO_3 \rightarrow BO_4$) that cause the formation of a compactness structure (*40*). Figure 7 shows the bulk modulus of all glass samples with different gamma-irradiation doses. The behavior of bulk modulus is associated with the change in the cross-linkage and coordination of the glass network (*35*). For pure glass composition (based glass), the bulk modulus remains constant with different gamma-irradiation doses. The obtained results indicate that the irradiation dose has a little effect on the cross-linkage. For the glass doped with TMO, the TiO_2 and ZnO glass samples show increases with an increase in the irradiation dose. This is due to the increase in the formation of bridging oxygens (BO) in all directions of the glass network. For the V_2O_5 glass sample, the bulk modulus decreases with an increase in the irradiation dose. This result we suggested is due to the increase in the formation of cross-linkage direction more than longitudinal direction ($K = L - 4/3\,G$).

Table 4. Longitudinal (L $\pm$ 0.85 GPa), shear (G $\pm$ 0.41 GPa) and bulk (K $\pm$ 0.32 GPa) modulus of glass samples with different gamma irradiation doses.

Dose	Base glass			V_2O_5			ZnO			TiO_2		
(Gy)	L (GPa)	G (GPa)	K (GPa)	L (GPa)	G (GPa)	K (GPa)	L (GPa)	G (GPa)	K (GPa)	L (GPa)	G (GPa)	K (GPa)
0	84.60	31.58	42.50	85.20	31.85	42.73	87.93	34.50	41.93	89.28	35.57	41.85
5	85.01	31.70	42.74	84.53	31.55	42.46	87.63	34.03	42.25	89.10	35.38	41.92
10	85.34	31.92	42.78	84.82	31.78	42.45	88.05	34.29	42.32	90.06	35.65	42.53
15	85.60	32.28	42.56	85.29	32.23	42.31	88.32	34.35	42.52	89.97	35.42	42.74
20	85.75	32.50	42.42	85.55	32.83	41.78	88.68	34.42	42.78	89.40	34.99	42.75

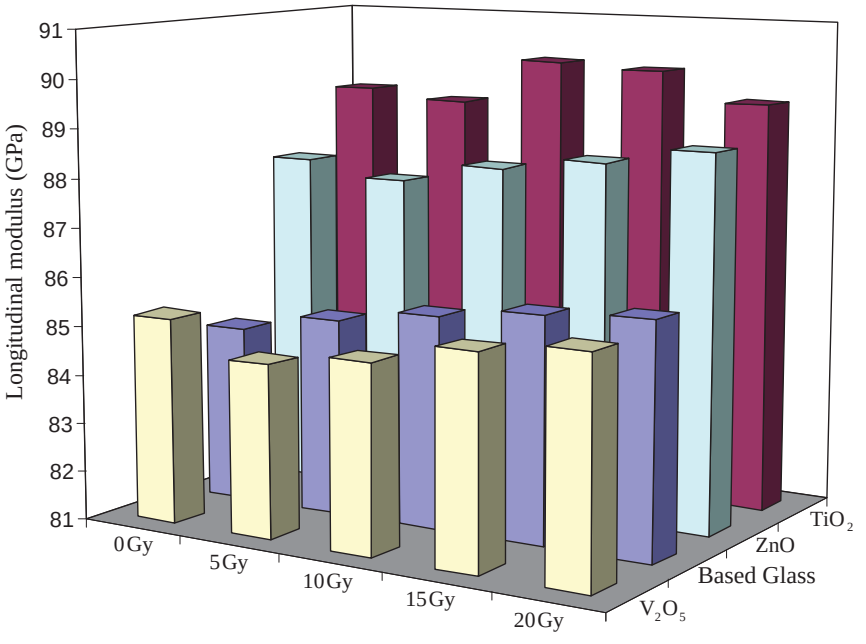

Figure 5. Variation of longitudinal modulus (L) of glass samples with different gamma irradiation doses.

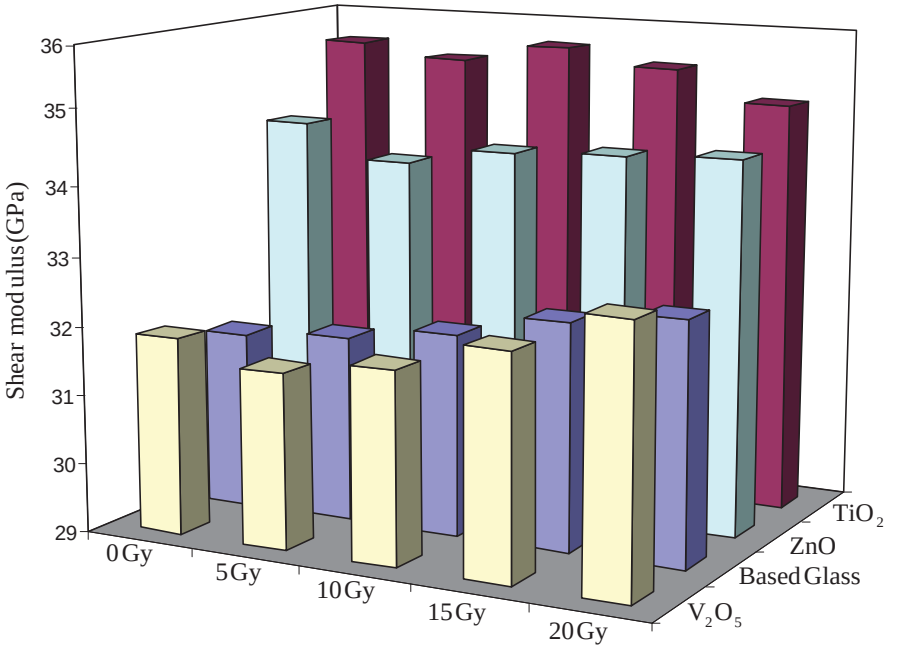

Figure 6. Variation of shear modulus (G) of glass samples with different gamma irradiation doses.

3.3. *IR absorption*

The FTIR spectra obtained for the studied glass samples are shown in Figures 8–11 (based glass, V_2O_5, ZnO and TiO_2 glass samples, respectively). The presence of water groups is marked by

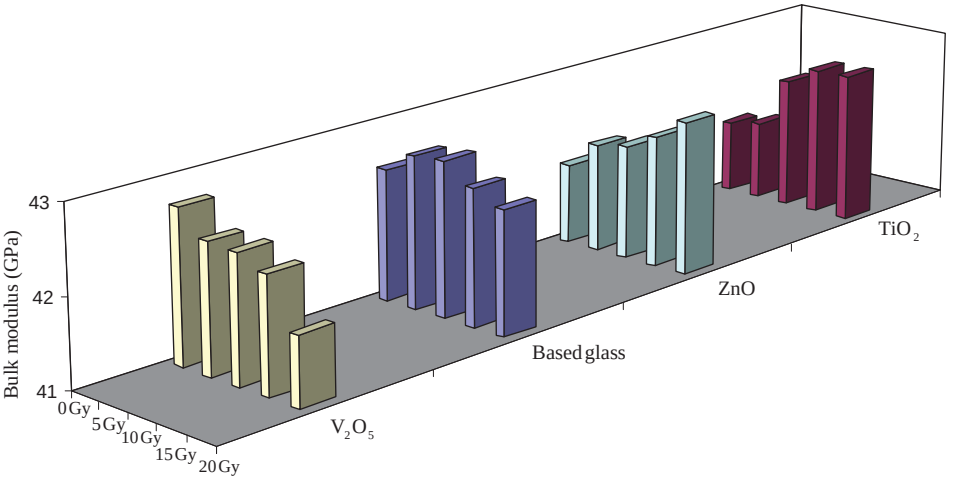

Figure 7. Variation of bulk modulus (K) of glass samples with different gamma irradiation doses.

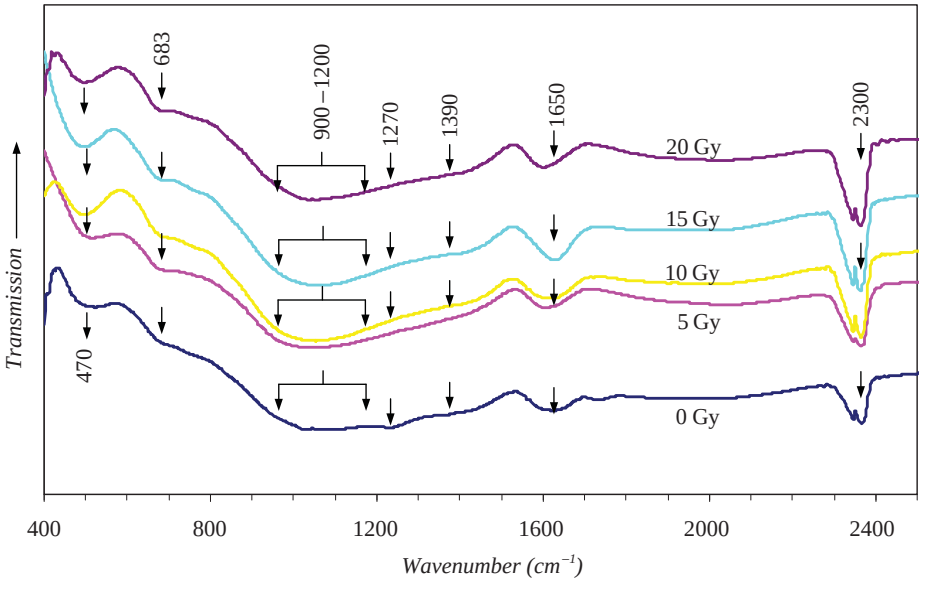

Figure 8. The IR spectra of based glass with different gamma irradiation doses.

the presence of bands above 2500 cm^{-1}. The signal around 1600–1650 cm^{-1} is due to the deformation modes of O–H groups and absorbed water molecules (*41*). The band arising from the vibrations of the borosilicate network appears in the range 1500–400 cm^{-1}. The signal at around 470 cm^{-1} is assigned to Si–O–Si and O–Si–O bending modes of bridging oxygens (Q_4) overlapped with B–O–B linkages. The peak at roughly 683 cm^{-1} is assigned to curve vibrations of Si–O–B bridges (*42*). The absorption bands in the region extending from 900 to 1200 cm^{-1} are observed at 954, 1012, 1054 and 1120 cm^{-1}. These bands are assigned to the stretching vibrations of the B–O bonds in the structural groups consisting of BO_4 units in di-, tri-, tetra- and penta-borate groups (*43*). Particularly, the region of 1000–1120 cm^{-1} can arise from overlapping contributions of silicate (vibrations of NBO of SiO_4^-) and borate groups containing BO_3 and BO_4 units (*43*). The individual contribution of silicate and borate groups cannot be separated and is

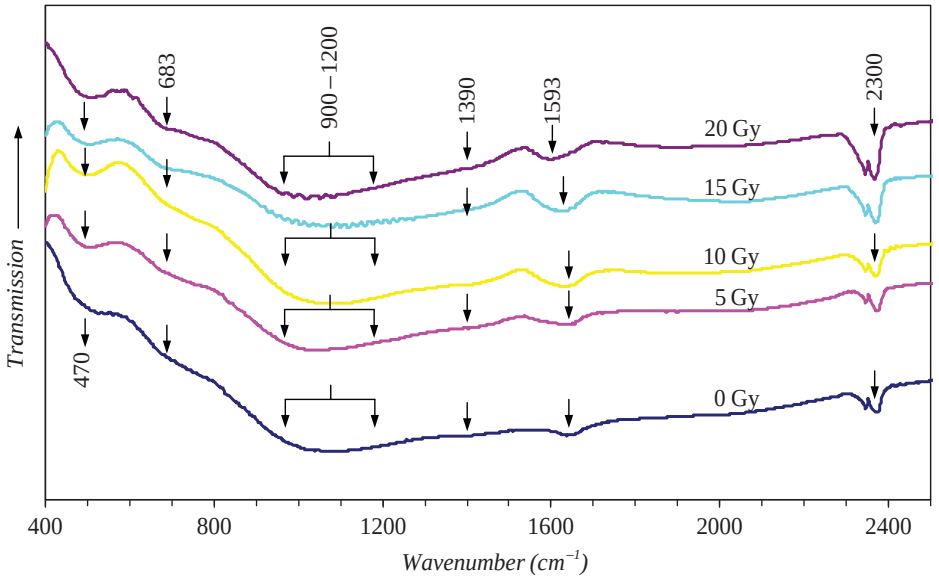

Figure 9. The IR spectra of glasses doped V_2O_5 with different gamma irradiation doses.

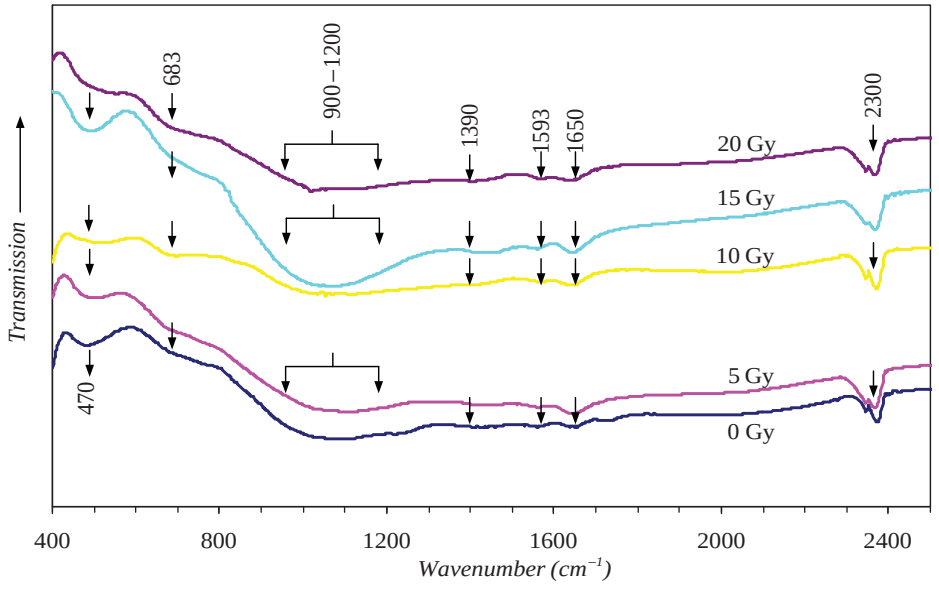

Figure 10. The IR spectra of glasses doped ZnO with different gamma irradiation doses.

assumed to depend on the concentration of each component in the glass system. The bands in the region 1200–1500 cm^{-1} are due to the presence of BO_3 structural units in the glass. The component bands in this region appear at 1270 and 1390 cm^{-1} which can be attributed to stretching vibrations of NBOs of trigonal BO_3 units in metaborate chains and rings, pyro and ortho borate groups (*44*). All samples (based glass, V_2O_5, ZnO and TiO_2 glass samples, respectively) show a similar presence of broad bands.

It can be observed from Figures 8 to 11 that the IR absorption spectra of investigated glass have four main absorption bands at around 470, 683, 900–1200 and 1200–1500 cm^{-1}. From

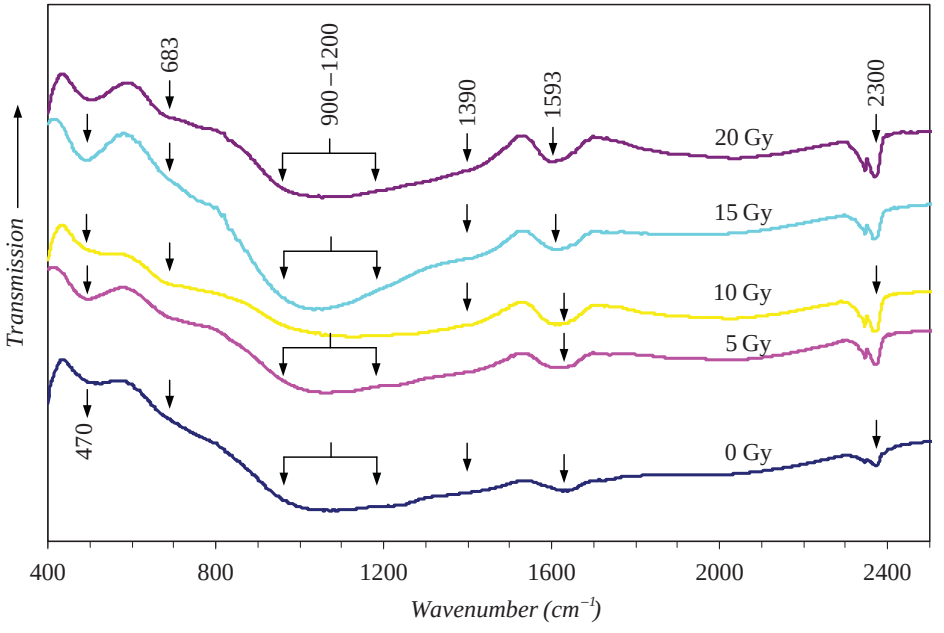

Figure 11. The IR spectra of glasses doped TiO_2 with different gamma irradiation doses.

Figure 8, the absorption frequency at 470 and 683 cm^{-1} increases with an increase in the gamma-irradiation dose. Moreover, the absorption frequency at regions 1270 and 1390 cm^{-1} decreases with an increase in the gamma-irradiation dose. The results obtained show an increase in the formation of BO due to the BO_3 transform to BO_4. Figures 9–11 show the similar trend of absorption bands. The absorption frequency at region 470 and 683 cm^{-1} shows decreased absorption when irradiation of gamma dose is at 5 Gy and switch to increased absorption when irradiation of gamma dose increases from 5 to 20 Gy. However, the changes are not pronounced by observations from the absorption bands at around 1200–1500 cm^{-1}. Notwithstanding, the results obtained from FTIR were adequate in supporting our discussion in ultrasonic wave velocities.

4. Conclusions

The observed change in ultrasonic velocity and elastic moduli is related to change in the structure of the glass matrix due to the composition effect as well as the irradiation effect. The acoustical properties of present glasses indicate that the addition of TMO leads to change in the structure of the glass network and influences of gamma irradiation at low dose. In addition, the FTIR spectra are also good evidence of the irradiation effect. The observed results reveal that ultrasonic studies can be used as a tool in exploring the stability of the glass exposed to radiation.

Acknowledgements

Financial support of this study has been provided by the Thailand Research Fund (TRF), Office of the Higher Education Commission (OHEC) and Ubon Ratchathani University (UBU). The results and comments on this article are those of the authors. The TRF, OHEC and UBU are unnecessary always agree.

References

(1) Singh, K.; Singh, H.; Sharma, V.; Nathuram, R.; Khanna, A.; Kumar, R.; Bhatti, S.S.; Sahota, H.S. *Nucl. Instrum. Methods B.* **2002,** *194,* 1–6.
(2) Singh, N.; Singh, K.J.; Singh, K.; Singh, H. *Nucl. Instrum. Methods B.* **2004,** *225,* 305–309.
(3) Singh, K.J.; Singh, N.; Kaundal, R.S.; Singh, K. *Nucl. Instrum. Methods B.* **2008,** *266,* 944–948.
(4) Kaur, R.; Singh, S.; Singh, K.; Pandey, O.P. *Radiat. Phys. Chem*. **2013,** *86,* 23–30.
(5) Du, J.; Wu, J.; Zhao, L.; Song, L. *Radiat. Phys. Chem*. **2013,** *86,* 59–63.
(6) Prymak, M.V.; Azhniuk, Y.M.; Solomon, A.M.; Krasilinets, V.M.; Lopushansky, V.V.; Bodnar, I.V.; Gomonnai, A.V.; Zahn, D.R.T. *Radiat. Phys. Chem*. **2012,** *81,* 766–770.
(7) Bootjomchai, C.; Laopaiboon, J.; Nontachat, S.; Tipparach, U.; Laopaiboon, R. *Nucl. Eng. Des*. **2012,** *248,* 28–34.
(8) Saddeek, Y.B. *Physica B*. **2005,** *363,* 19–24.
(9) Schirmer, H.; Keding, R.; Rüssel, C. *J. Non-Cryst. Solids*. **2004,** *336,* 37–43.
(10) Varshneya, A.K. *Fundamentals of Inorganic Glasses*; Academic Press: New York, **1994**.
(11) Balkanski, M.; Wallis, R.F.; Deppe, J. *Mater. Sci. Eng. B*. **1992,** *12,* 281–298.
(12) Swenson, J.; Börjesson, L. *Phys. Rev. B*. **1998,** *57,* 13514–13526.
(13) Wollenhaupt, M.; Ahrens, H.; Fröbel, P.; Bärner, K.; Giessinger, E.R. *J. Non-Cryst. Solids*. **1996,** *194,* 191–197.
(14) Ramadevudu, G.; Shareefuddin, Md.; Sunitha Bai, N.; Lakshmipathi Rao, M.; Narasimha Chary, M. *J. Non-Cryst. Solids* **2000,** *278,* 205–212.
(15) Joseph, C.M.; Binu, P.R.; Shreekrishnakumar, K.; Menon, C.S. *Mater. Lett*. **2002,** *53,* 326–328.
(16) Petit, L.; Cardinal, T.; Videau, J.J.; Le Flem, G.; Guyot, Y.; Boulon, G.; Couzi, M.; Buffeteau, T. *J. Non-Cryst. Solids*. **2002,** *298,* 76–88.
(17) Culea, E.; Bratu, I. *Act. Mater*. **2001,** *49,* 123–125.
(18) Khattak, G.D.; Salim, M.A.; Wenger, L.E.; Cilani, A.H. *J. Non-Cryst. Solids*. **1999,** *244,* 128–136.
(19) Nassar, A.M.A.; Ghoneim, N.A. *J. Non-Cryst. Solids*. **1981,** *46,* 181–195.
(20) Ezz-Eldin, F.M.; Elalaily, N.A.; El-Batal, H.A.; Choneim, N.A. *Radiat. Phys. Chem*. **1996,** *48,* 659–664.
(21) Abdel-Hameed, S.A.M.; Azooz, M.A. *Ceramics Inter*. **2009,** *35,* 643–648.
(22) Sharma, G.; Rajendran, V.; Thind, K.S.; Singh, G.; Singh, A. *Physica B*. **2009,** *404,* 3371–3378.
(23) Rajendran, V.; Palanivelu, N.; Modak, D.K.; Chaudhuri, B.K. *Phys. Stat. Solidi*. **2000,** *180,* 467–477.
(24) Rajendranm, V.; Palanivelum, N.; Palanichamym, P.; Jayakumarm, T.; Baldev, Raj; Chaudhurim, B.K. *J. Non-Cryst. Solids*. **2001,** *296,* 39–49.
(25) Rajendran, V.; Palanivelu, N.; Chaudhuri, B.K.; Goswami, K. *Phys. Stat. Solidi*. **2002,** *191,* 445–457.
(26) Krauthramer, J.; Krauthramer, H. *Ultrasonic Testing of Materials*, 4th ed.; Narosha: New Delhi, **1993**.
(27) Arora, M.; Baccaro, S.; Sharma, G.; Singh, D.; Thind, K.S.; Singh, D.P. *Nucl. Instrum. and Methods B*. **2009,** *267,* 817–820.
(28) Ollier, N.; Boizot, B.; Reynard, B.; Ghaleb, D.; Petite, G. *Nucl. Instrum. and Methods B*. **2004,** *218,* 176–182.
(29) De Bonfils, J.; Peuget, S.; Panczer, G.; De Ligny, D.; Henry, S.; Noel, P.-Y.; Chenet, A.; Champagnon, B. *J. Non-Cryst. Solids*. **2010,** *356,* 388–393.
(30) Prado, M.O.; Messi, N.B.; Plivelic, T.S.; Torriani, I.L.; Bevilacqua, A.M.; Arribere, M.A. *J. Non-Cryst. Solids*. **2001,** *289,* 175–184.
(31) Baccaro, S.; Monika Sharma, G.; Thind, K.S.; Devinder Singh Cecillia, A. *Nucl. Instrum. and Methods B*. **2007,** *260,* 613–618.
(32) Marzouk, S.Y.; Gaafar, M.S. *Solid Stat. Commu*. **2007,** *144,* 478–483.
(33) El-Mallawany, R.; El-Khoshkhany, N.; Afifi, H. *Mater. Chem. Phys*. **2006,** *95,* 321–327.
(34) Eraiah, B.; Smitha, M.G.; Anavekar, R.V. *J. Phys. Chem. Solids*. **2010,** *71,* 153–155.
(35) Gaafar, M.S.; Marzouk, S.Y. *Physica B*. **2007,** *388,* 294–302.
(36) Abd El-Malak, N.A. *Mater. Chem. Phys*. **2002,** *73,* 156–161.
(37) Ezz Eldin, F.M.; El-Alaily, N.A.; Elbatal, H.A. *J. Radio-Anal. Nucl. Chem.* **1992,** *63*(2), 267–275.
(38) Shelby, J.E. *Introduction to Glass Science and Technology*; The Royal Society of Chemistry: New York, **1997**, pp. 137.
(39) Yasser, B.S.; Lamia, Abd.; Latif, El. *Physica B*. **2004,** *348,* 475–484.
(40) Marzouk, S.Y. *Physica B*. **2010,** *405,* 3395–3400.
(41) Hussain, N.S.; Lopes, M.A.; Santos, J.D. *Mater. Chem. Phys*. **2004,** *88,* 5–8.
(42) Handke, M.; Sitaz, M.; Rokita, M.; Galuskin, E. *J. Mol. Struct*. **2003,** *651,* 39–54.
(43) Kaur, R.; Singh, S.; Pandey, O.P. *Physica B*. **2012,** *407,* 4765–4769.
(44) Kamitsos, E.I.; Patsis, A.P.; Karakassides, M.A.; Chryssikos, G.D. *J. Non-Cryst. Solids*. **1990,** *126,* 52–67.

Radiation Physics and Chemistry 110 (2015) 96–104

Contents lists available at ScienceDirect

Radiation Physics and Chemistry

journal homepage: www.elsevier.com/locate/radphyschem

Comparative studies between theoretical and experimental of elastic properties and irradiation effects of soda lime glasses doped with neodymium oxide

C. Bootjomchai

Glass Technology Excellent Center (GTEC), Department of Physics, Faculty of Science, Ubon Ratchathani University, Ubon Ratchathani 34190, Thailand

HIGHLIGHTS

- Results show good agreement between experimental and theoretical of elastic moduli.
- Network bonding was distorted with the Nd_2O_3 was added and irradiated.
- Transformation of the glass network structure from Q_4 to Q_3 after irradiation.

ARTICLE INFO

Article history:
Received 9 December 2014
Received in revised form
12 January 2015
Accepted 28 January 2015
Available online 29 January 2015

Keywords:
Glasses
Elastic properties
Irradiation effects
Ultrasonic measurements
FTIR

ABSTRACT

A comparative studies on the theoretical and experimental values of elastic moduli of $(90-x)$RWG – $(10)Na_2O$– $(x)Nd_2O_3$ glass system, where RWG is recycled window glass and x is 0.001, 0.01, 0.1 and 1 mol%, was investigated. The radiation effects on structural properties and elastic moduli were evaluated by measuring the ultrasonic velocities. In addition, the FTIR spectra were measured to investigate the effects of irradiation on the structure of the glass. Moreover, the theoretical bond compression model was used to confirm the obtained results from the experiments. The results show that evidently changes in the structure of the glass depend on the concentration of the neodymium oxide and gamma irradiation. Furthermore, the experimental elastic moduli are in good agreement with the theoretical values.

1. Introduction

Glasses materials are receiving extensive attention due to their unique properties such as hardness, transparency at room temperature, high strength and excellent corrosion resistance. Continued effort for the improvement of new glassy materials and the study of their properties is highly relevant because of the potential in various technological fields. Glassy systems have physical isotropy, the absence of grain boundaries, continuously variable composition and good work ability over their crystalline counterparts (Joseph et al., 2002). Moreover, the radiation damage processes which emerge in glass are generically the same as those which occur in crystals. In the simplest provision, there are three basic processes: (i) radiolysis, (ii) displacement (or knock on) damage, and (iii) electron rearrangement. In all processes, what we define as damage is the existence of after irradiation local structures (either atomic or electronic) which differ from the structure present before irradiation (Ezz-Eldin et al., 1996). Irradiation affects the structure of the glass matrix, resulting in changes in the optical, physical and electrical properties. Therefore, the scientific information of the glass structure before and after irradiation is a requirement for understanding the structural evolution of nuclear glasses under long term irradiation during storage of radioactive wastes or isotopes sources, radiation shielding, radiation detection by using glass dosimeter, etc. (Neuville et al., 2003). Studies on irradiated glasses have been previously published on simple glass systems such as silicate glasses (Devine, 1994) or on multicomponent glasses such as borosilicate glasses (Kaur et al., 2013; Abdelghany et al., 2014; AbdelAziz et al., 2014).

Glasses containing rare-earth ions have attracted a great deal of interest due to their important properties. For examples, the glasses are heat-resistant, present interesting optical and magnetic behavior (Clare, 1994; Lemercier et al., 1996; Clayden et al., 1999). The properties of rare-earth glasses include greater glass transition temperatures, greater hardness and elastic modulus, and greater chemical durability than many other glasses (Lemercier 1996; Clayden et al., 1999). Therefore, the rare-earth glasses have been successfully used as laser

E-mail address: cherdsak_per@hotmail.co.th

http://dx.doi.org/10.1016/j.radphyschem.2015.01.034
0969-806X/

ion hosts, optical lenses, seals, and vivo radiation delivery vehicles (Lin and Hwang, 1996; Shelby and Kohli, 1990). Among all the rare-earth ions doped in glasses, the neodymium (III) ion has been distinguished as on of the most efficient ones for obtaining laser emission, frequency up-conversion and optical fiber amplification (Jayasimhadir et al., 2007). Thus, the effects of gamma irradiation on structural properties of rare-earth glasses have been interested to investigation.

The properties of glass are closely related to the inter-atomic forces and potentials in the lattice structure. Therefore, changes in the lattice, due to doping and/or irradiation, can be directly noted. The elastic properties and other related parameters are of great interest, in order to study the linear and anomalous variations as a function of composition of glass, and have been interpreted in terms of the structure or transformation of cross-linkages in the glass network (Rajendran et al., 2001; Sharma et al., 2009). To study the structural properties of glass, the coordination numbers of the network structure and the change of oxygen bonds in the network former, induced by the cation modifiers and/or irradiation, need to be investigated. The information can be obtained from FTIR spectroscopy. Furthermore, many researchers use ultrasonic techniques for investigation the effects of irradiation on structural properties of glass (Sharma et al., 2009; Zahran, 1998; El-Mallawany et al., 1998; Laopaiboon and Bootjomchai 2014a, 2014b). Therefore, the ultrasonic technique is an appropriate tool for characterizing the microstructure, the deformation process and the structural properties of materials after successive irradiation. Moreover, the depth scientific results of structural properties by using bond compression model were reported (Abd El-Moneim, 2001; Marzouk and Gaafar, 2007). Thus, the theoretical values of elastic moduli were calculated by using the bond compression model to compare between the experimental and theoretical modulus (Gaafar and Marzouk, 2007; Abd El-Moneim, 2003).

Therefore, the investigation of the influence of rare-earth oxides (ROs) contents and gamma irradiation on the structural properties of silicate glasses have been interested. In this article, the effects of rare-earth oxides contents and irradiation on structural properties of glass samples were studied via ultrasonic techniques and FTIR spectroscopy. The elastic moduli of the glass samples before and after irradiation with different concentration of neodymium oxide will be discussed. Information about the structure of the glass samples can be deduced after calculating the number of network bonds per unit volume, the average cross-link density, the number of vibrating atoms per unit volume, the average stretching force constant and the average ring size. Moreover, the theoretical and experimental of elastic moduli have been compared.

2. Experimental work

2.1. Glass Preparation

The glass samples were prepared in rectangular shapes from the $(90 - x)$RWG – (10)Na_2 O– $(x)Nd_2O_3$ glass system (where RWG is recycled window glass and x are 0.001, 0.01, 0.1 and 1 mol%) using the melt-quenching method. The oxides of Na_2O and Nd_2O_3 used in this work were of an analytical regent grade. The RWG was common window glass sold in Ubon Ratchathani, Thailand. The chemical composition of RWG was determined in my previous work (Bootjomchai and Laopaiboon, 2014). Preparation of recycling glass from window glass to be used in this work is to thoroughly clean and grind until powdery. To prepare the glass samples, appropriate amounts of Na_2O, Nd_2O_3 and RWG powders were weighed using an electronic balance with the accuracy of the order of 0.0001 g. The starting materials were mixed thoroughly in ceramic crucibles. The mixture was preheated at 573 K for 1 h to remove H_2O and CO_2. The preheated mixture was then melted in an electric furnace whose temperature was controlled at 1523 K to ensure homogeneity. The melted glass was then poured into preheated stainless steel molds at about 723 K and then annealing was carried out for a period of 2 h at 773 K. Bulk glass samples of about $1.5 \times 1.5 \times 1.0\ cm^3$ were thus obtained. The glass samples were polished using different silicon carbide grades. The sample thicknesses were measured to the micrometer.

2.2. Density and molar volume measurements

The density (ρ) of each sample was measured by using Archimedes' principle with n-hexane as immersion liquid. The experiments were repeated three times for accurate value of the density. The estimated error in these measurements was approximately $\pm 0.001\ g\ cm^{-3}$. The molar volume (V_a) was calculated for each glass from the expression; $V_a = M/\rho$, where M is the molecular weight of the glass, calculated according to the relation (1) (Abd El-Moneim et al., 2006).

$$M = \sum_i x_i M_i \tag{1}$$

where x_i is the mole fraction of the component oxide i and M_i is its molecular weight. The glass packing density can be calculated from the following Eqs. (2)–(3) (Hager, 2012)

$$V_t = \frac{\rho}{M} \sum_i x_i V_i \tag{2}$$

where V_i is given by,

$$V_i = \frac{4\pi N_A}{3}\left(x r_M^3 + y r_O^3\right) \tag{3}$$

where N_A is Avogadro's number, and where r_M and r_O are the ionic radii of the cation and anion of the oxide M_xO_y, respectively. The errors in molar volume and packing density were acquired from experiments repeated three times of densities. The estimated error in these results was $\pm 0.021\ cm^3\ mol^{-1}$ and $\pm 0.0013 \times 10^{-6}\ m^3$, respectively and shown in Table 1.

Table 1
Glass composition, density (ρ), molar volume (V_a) and packing density (V_t) of the glass samples before and after gamma irradiation.

Sample no.	Composition (mol%)			ρ (g cm^{-3}) ±0.001		V_a (cm^3 mol^{-1}) ±0.021		$V_t \times 10^{-6}$ (m^3) ±0.0013	
	RWG	Na_2O	Nd_2O_3	Before	After	Before	After	Before	After
G–0	90	10	0	2.567	2.565	23.351	23.3747	0.4592	0.4588
G–1	89.999	10	0.001	2.572	2.558	23.313	23.4391	0.4609	0.4584
G–2	89.990	10	0.01	2.570	2.554	23.340	23.4911	0.4690	0.4660
G–3	89.900	10	0.1	2.575	2.560	23.416	23.5458	0.5530	0.5500
G–4	89	10	1	2.656	2.647	23.837	23.9225	1.3838	1.3789

2.3. Gamma-ray irradiation

The glass samples were irradiated by an exposure machine (THREATRON 780C) using a Co-60 gamma-ray source at a dose rate of 1.16 Gy min^{-1} and field size of 30 × 30 cm^2, at a distance of 30 cm from the gamma-ray source, and at room temperature. The samples were irradiated for sufficiently long enough to achieve to overall dose of 1 kGy.

2.4. Ultrasonic velocity measurements

An ultrasonic flaw detector, SONATEST Sitescan 230, was used to measure ultrasonic velocity. The ultrasonic waves were generated from a ceramic transducer (Probe model: SLG4-10 for longitudinal velocity and SA04-45 for shear velocity) with a resonant frequency of 4 MHz, and acting as transmitter-receiver at the same time. The ultrasonic wave velocity (v) can be calculated by the following Eq. (4) (El-Mallawany et al., 2006):

$$v = \frac{2d}{\Delta t}(\mathrm{cm\ s^{-1}}) \tag{4}$$

where d is the samples thickness (cm) and Δt is the time interval (s). The measurements were repeated three times to check the reproducibility of the data. The errors in velocity measurements were ±7 m s^{-1} for longitudinal velocity (v_L) and ±14 m s^{-1} for shear velocity (v_S).

2.5. FTIR measurements

FTIR spectra of powdered glass samples were recorded at room temperature using KBr disk technique. The spectra in the wave number range of 400 – 4000 cm^{-1} with a resolution of 4 cm^{-1} were obtained using Perkin-Elmer spectrometer.

2.6. Determination of elastic moduli

Elastic moduli include longitudinal (L), shear (G), bulk (K), and Young's (E) modulus as well as Debye temperature (θ_D), softening temperature (T_s), micro-hardness (H) and Poisson's ratio (σ) of glass samples have been determined from the measured the ultrasonic velocities and densities using the standard relations (5)–(12) (Sidkey and Gaafar, 2004):

Longitudinal modulus

$$L = \rho v_L^2 \tag{5}$$

Shear modulus

$$G = \rho v_S^2 \tag{6}$$

Bulk modulus

$$K = L - \frac{4}{3}G \tag{7}$$

Young's modulus

$$E = (1 + \sigma)2G \tag{8}$$

Poisson's ratio

$$\sigma = \frac{L - 2G}{2(L - G)} \tag{9}$$

Micro-hardness

$$H = \frac{(1 - 2\sigma)E}{6(1 + \sigma)} \tag{10}$$

Debye temperature

$$\theta_D = \left(\frac{h}{k_B}\right)\left(\frac{3zN_A}{4\pi V_a}\right)^{1/3} v_m \tag{11}$$

Softening temperature

$$T_s = \frac{v_S M}{C^2 z} \tag{12}$$

where h is Planck's constant, k_B is Boltzmann's constant, N_A is Avogadro's number, z is the number of atoms in the chemical formula, C is the constant of proportionality (equals 507.4 m s^{-1} $K^{1/2}$) and v_m is the mean ultrasonic velocity defined by the relationship (13) (Marzouk, 2009).

$$v_m = \left[\frac{3v_L^3 v_S^3}{v_L^3 + v_S^3}\right]^{1/3} \tag{13}$$

The uncertainty in mean ultrasonic velocity was shown in Table 2. The uncertainties in elastic moduli, Poisson's ratio, micro-hardness, Debye temperature and softening temperature were acquired from experiments repeated three times of the densities and the ultrasonic velocities. The estimated errors in these results are shown in Table 3.

3. Theoretical models

A bond compression model is a helpful introduce for structures containing only on type of bond. For a three dimensional multi-component oxide glass, the bond compression bulk modulus is given by Eq. (14) (Bridge and Higazy, 1986)

$$K_{bc} = \frac{n_b \bar{F}}{9} r^2 \tag{14}$$

where r is the bond length between anion and cation and n_b is the number of network bonds per unit volume of the glass given by Eq. (15) (Bridge and Higazy, 1986)

$$n_b = \frac{N_A}{V_a} \sum_i (x n_f)_i \tag{15}$$

where x is the mole fraction of the component oxide i. $\bar{F}$ is the average of stretching force constant and can be calculated from

Table 2
Longitudinal (v_L), shear (v_S) and mean (v_m) velocities of the glass samples before and after gamma irradiation.

Sample no.	v_L (m s^{-1})±7			v_S (m s^{-1})±14			v_m (m s^{-1})±11	
	Before	After	% different	Before	After	% different	Before	After
G–0	5842	5827	0.257	3646	3635	0.302	4017	4005
G–1	5838	5817	0.348	3592	3577	0.427	3964	3947
G–2	5814	5798	0.281	3570	3549	0.565	3940	3919
G–3	5791	5776	0.259	3557	3484	2.062	3926	3852
G–4	5660	5647	0.230	3520	3502	0.516	3880	3861

Table 3
Longitudinal (L), shear (G), bulk (K), Young's (E) modulus, Poisson's ratio (σ), micro-hardness (H), Debye (θ_D) and softening (T_s) temperature of the glass samples before and after gamma irradiation.

Sample no.	L (GP) ±0.03		G (GPa) ±0.01		K (GPa) ±0.02		E (GPa) ±0.04		σ ± 0.003		H (GPa) ±0.01		θ_D (K) ±2		T_s (K) ±5	
	Before	After	Before	After	Before	After	Before	After	Before	After	Before	After	Before	After	Before	After
G–0	87.63	87.10	34.13	33.89	42.12	41.91	80.62	80.09	0.181	0.181	7.26	7.20	354	353	612	609
G–1	87.64	86.56	33.18	32.73	43.39	42.93	79.33	78.28	0.195	0.196	6.74	6.63	349	347	593	591
G–2	86.87	85.83	32.75	32.17	43.21	42.94	78.43	77.22	0.198	0.200	6.60	6.43	347	344	586	583
G–3	86.35	85.43	32.58	31.08	42.92	44.00	78.00	75.46	0.197	0.214	6.58	5.92	345	338	584	563
G–4	85.09	84.39	32.91	32.46	41.21	41.12	77.98	77.09	0.185	0.188	6.92	6.76	339	337	582	578

following Eq. (16) (Abd El-Moneim, 2003)

$$\bar{F} = \frac{\sum (x n_f F)_i}{\sum (x n_f)_i} \tag{16}$$

where n_f is the coordination number of the cation and F is the stretching force constant of the oxide. The average atomic ring size (l) of a structure consisting of a three-dimensional network according to the ring deformation model is shown in the form of Eq. (17) (El-Mallawany, 2000).

$$l = \left[0.0106 \frac{\bar{F}}{K_{exp}}\right]^{0.26} \tag{17}$$

The calculation of Poisson's ratio for the multicomponent oxide glasses according to the bond compression model is given by Eq. (18) (Bridge and Higazy, 1986)

$$\sigma_{cal} = 0.28(\bar{n}_c)^{-0.25} \tag{18}$$

where $\bar{n}_c$ is the average cross-link density of the glass network and is given by Eq. (19) (Bridge and Higazy, 1986)

$$\bar{n}_c = \frac{1}{\eta} \sum_i (n_c)_i (N_c)_i \tag{19}$$

where n_c is the number of cross-links per cation (number of bridging bonds per cation minus two) in oxide i. N_c is the number of cations per glass formula unit and $\eta = \sum (N_c)_i$ is the total number of cations per glass formula unit. The theoretical bulk modulus (K_{cal}) can be calculated from Eq. (20) (Abd El-Moneim, 2003).

$$K_{cal} = 1.062 \times 10^{-29} \bar{F} l^{-4.0022} \tag{20}$$

The other theoretical elastic moduli can be obtained from the bulk modulus and Poisson's ratio for each glass system as Eqs. (21)–(23) (Abd El-Moneim, 2003).

$$G_{cal} = (1.5) K_{cal} \left[\frac{1 - 2\sigma_{cal}}{1 + \sigma_{cal}}\right] \tag{21}$$

$$L_{cal} = K_{cal} + (1.33) G_{cal} \tag{22}$$

$$E_{cal} = 2(1 + \sigma_{cal}) G_{cal} \tag{23}$$

The number of vibrating atoms per unit volume (N/V) will be expressed as follows (24) (El-Mallawany and Afifi, 2013).

$$\frac{N}{V} = \frac{N_A}{V_a} \sum_i x(n + m)_i \tag{24}$$

where $(n + m)$ is the sum of the atoms present in the i – th oxide of the chemical formula.

4. Results and discussion

4.1. Density and molar volume

The glass composition, density, molar volume and packing density are given in Table 1. The density of the glass samples are shown in Fig. 1. The results shows that the densities of the glass samples increase with increasing the concentration of Nd_2O_3 but decrease after irradiated by gamma radiation. The decreased of the density of the glass can be attributed to three factors, namely (Alajerami et al., 2013):

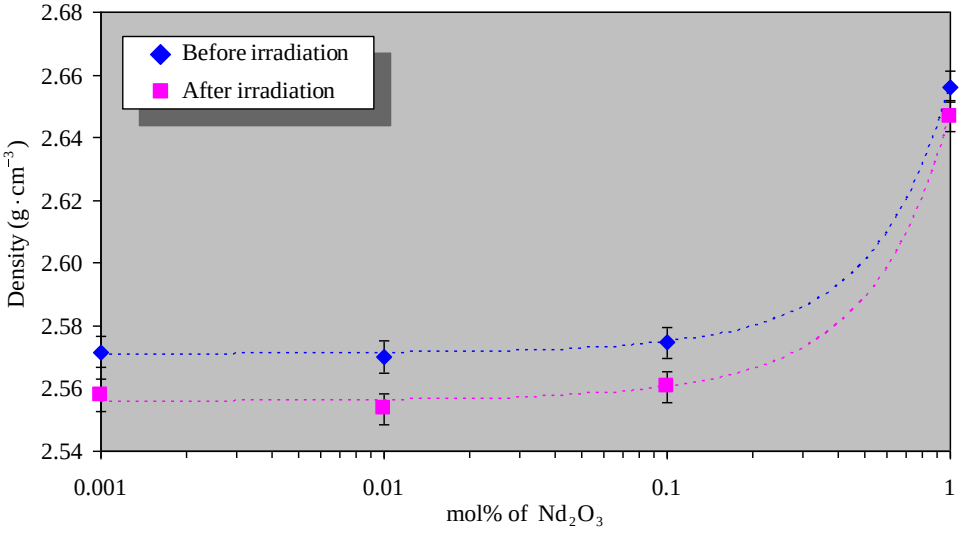

Fig. 1. Variation of densities (ρ) before and after irradiation with γ-radiation of the glass samples with the difference of doping (lines are drawn as guides to the eyes).

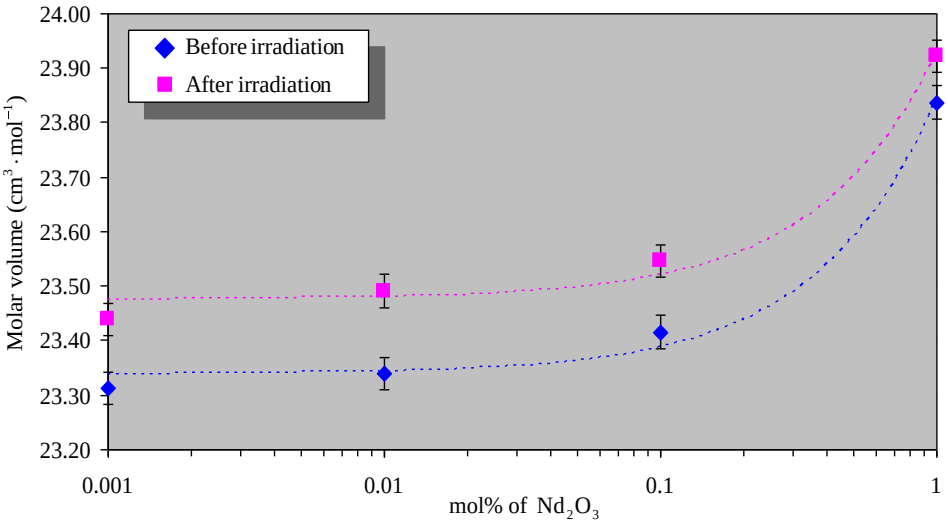

Fig. 2. Variation of molar volume (V_a) before and after irradiation with γ-radiation of the glass samples with the difference of doping (lines are drawn as guides to the eyes).

(i) transformation of the main glass network structure from triagonal (Q_4) to tetrahedral (Q_3),

(ii) decrease in the molecular mass of the glass because of the glass because of the higher atomic weight of the modifier, and

(iii) decrease of the bridging oxygen (BO) ratio in the glass composition, due to the adding of modifier and/or irradiation.

From mentioned above, damage by an irradiation species can create displacement of atoms and/or breaks in the network bonds, leading to a rise of the number of non-bridging oxygens (NBOs) and/or transformation of the main glass network structure from tetrahedral (Q_4) to triagonal (Q_3) and resulting in a decrease of the densities of the glass samples after irradiation (Ezz El-Din et al., 1992; Prado et al., 2001).

The molar volume is defined as the volume occupied by the unit mass of the glass, molar volume can be used as a parameter to identify an open structure (Singh et al., 2003). Fig. 2 shows that the molar volume increases with increasing Nd_2O_3 concentrations and after gamma irradiation. These results are easily explained; they are due to the modifier ions ionic radius (the Nd^{3+} ionic radius is 1.123 Å), which is larger than the network structure interstices (the ionic radius of Si^{4+} is 0.400 Å). The modifier ion attraction to oxygen ions can yield a grater interstices size and molar volume. Irradiation with gamma rays is assumed to create displacement of atoms, electronic defects and/or breaks in the network bonds, which allow the structure to relax and fill the relatively large interstices in the interconnected silicon and/or boron and oxygen atom network, which produces volume expansion followed by compaction (Ezz El-Din et al., 1992). To confirm this results the packing density of the glasses were calculated and shown in Table 1. The packing density is the ratio between the minimum theoretical volume occupied by the ions and the corresponding effective volume of the glass (Bootjomchai et al., 2014). Therefore, the increase of packing density with increases concentration of Nd_2O_3 due to the volume occupied by the ions increase (the ionic radius of Nd^{3+} is large). Adding Nd_2O_3 into the glass matrix resulting to produces volume expansion followed by compaction. Therefore, the molar volume increases with the mol% of Nd_2O_3. After irradiation, the packing density was decreases in all samples. This is due to the increase of the effective volume of the glass matrix. The damage of radiation can create the opens structure lead to increase of molar volume of the glass samples. Moreover, this results good agree with the transformation of the main glass network structure from tetrahedral (Q_4) to triagonal (Q_3) after irradiation.

4.2. Ultrasonic velocity and elastic moduli

The plots before and after irradiation of longitudinal (v_L) and shear (v_S) velocities in the glass samples with the concentration of Nd_2O_3 are shown in Figs. 3 and 4, respectively and exact values are shown in Table 2. In addition, elastic moduli (L, G, K and E), Poisson's ratio (σ), micro-hardness (H), Debye temperature (θ_D) and softening temperature (T_s) of the glass samples are shown in Table 3. The ultrasonic velocities (v_L and v_S) in the glasses decrease as the mol% of the dopant increase and after irradiation. The changes in geometrical configuration, co-ordination number, cross-link density and dimension of interstitial space of glass determine the ultrasonic velocity and, therefore, ultrasonic velocity is an appropriate tool in revealing the degree of the structural change in the glass (Marzouk, 2009). In general, the decrease of ultrasonic velocity is related to the increase in the number of non-bridging oxygens (NBOs) and, consequently, the decrease in connectivity of the glass network (Gaafar and Marzouk, 2007). Therefore, the decrease in ultrasonic velocities is due to the fact that Nd^{3+} ions are involved in the glass network as modifiers by breaking up the tetrahedral bond of SiO_4 units. Moreover, damage by an irradiation species can create displacement of atoms and/or breaks in the network bonds, leading to a rise of the number of NBOs. Hence, the ultrasonic velocities decrease with mol% of Nd_2O_3 increases and after gamma-irradiation. Moreover, difference of ultrasonic velocity before and after irradiation as shown in Table 2 (%different). The results indicated that highest damage of irradiation on the structure is occurred in G–3 glass sample. In the asseveration of these results, the number of bonds per unit volume (n_b) is calculated by using a theoretical bond compression model is shown in Table 4. From the results, all samples show the decrease in the number of bonds per unit volume with increase of the mol% of dopants. Furthermore, the decrease of bonds per unit volume of glass samples after irradiation due to the greater the formation of non-bridging oxygens (NBOs). These results supported our discussions of the ultrasonic velocities of glass samples.

The elastic moduli (L, G, K and E) as shown in Table 3 decrease with the increase of Nd_2O_3 concentrations and after irradiation. All of the elastic moduli are related to the average strength of the bond. The average strength of the bond depends on the value of cation-anion forces. For a given A–O–A bond angle, the A–A separation would be directly proportional to the stretching force constant ($\bar{F}$) of the glass network (Higazy and Bridge, 1985). As the A–O–A bond force constants decrease, the energy required to

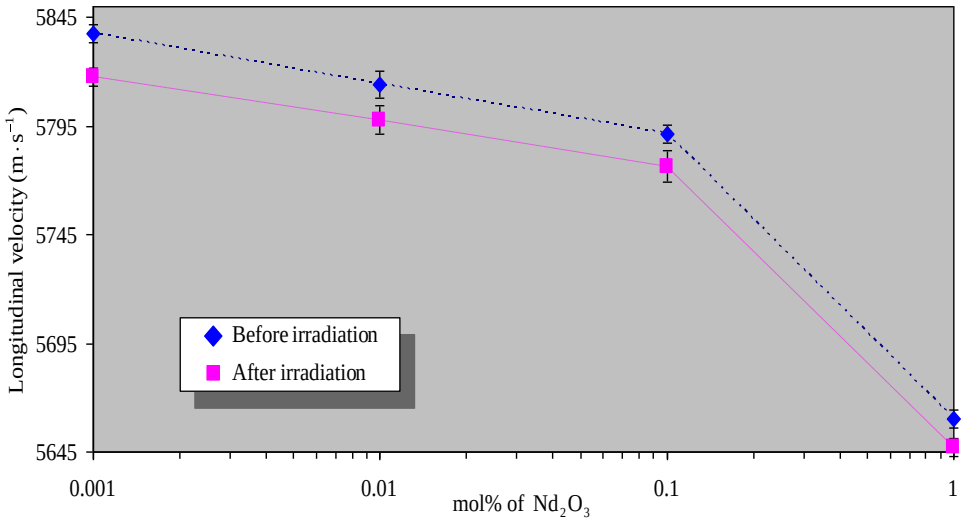

Fig. 3. Variation of longitudinal velocity (v_L) before and after irradiation with γ-radiation of the glass samples with the difference of doping.

produce a given degree of bond angle or length distortion and/or bond distortion decreases which leads to the decrease in the average strength of the bond. To confirm these results, the stretching force constants ($\bar{F}$) are calculated by using a theoretical bond compression model, the exact values were collected in Table 4. The stretching force constants decrease with the increase of the mol% of the dopant. These results indicate that the glass doped with Nd_2O_3 leads to the decrease in the average strength of the bond (elastic moduli were decreased). While the elastic moduli decrease after gamma irradiation can be speculate that the bond distortion occurred by irradiation.

Variation of Poisson's ratio and micro-hardness of the glass samples as a function of the dopants are listed in Table 3. Point to influence of Nd_2O_3 on Poisson's ratio can be seen that the Poisson's ratio nearly constant with concentration of Nd_2O_3 from 0.001 mol% to 0.1 mol% (G–1 to G– 3) and then decreases with increasing of mol% dopants from 0.1 mol% to 1.0 mol% (G–3 to G– 4). The variation of Poisson's ratio related to cross-link density. Poisson's ratio decrease as the cross-link density increases. At low concentration of dopants, effect of modifier is insignificant as a result the nearly constant of Poisson's ratio. However, when the concentration of modifier reach to 0.1 mol% or higher resulting to the decrease of Poisson's ratio due to the increase of cross-link density in the glass network. After irradiation, the Poisson's ratio is higher than the before irradiation especially at 0.1 mol% (G–3 glass sample) indicate that the highest effects of irradiation occurred in G–3 glass sample. These results support our discussion of the ultrasonic velocities. In addition, the average numbers of cross-link density ($\bar{n}_c$) was calculated by using the theoretical bond compression model for confirm the effects of Nd_2O_3 on Poisson's ratio and are shown in Table 4. The average numbers of cross-link density ($\bar{n}_c$) extremely increase when the mol% of the dopant increase from 0.1 to 1.0 mol%. These results strongly support the results of Poisson's ratio. Moreover, the theoretical of Poisson's ratio (σ_{cal}) was calculated to compare the results (Table 4). It is observed that a theoretical of Poisson's ratio is in a good agreement with the experimental values. The micro-hardness is defined as the resistance of a material to permanent indentation or penetration (Abd El-Moneim et al., 2006). It can be seen that (Table 3) the micro-hardness decrease with increase concentration of dopant reach to 0.1 mol% and then it is return to increase at 1.0 mol% of dopant. The micro-hardness decrease of all samples after irradiated with gamma ray. These results show that the rigidity and/or compactness of the sample depend on the concentration and irradiation. The results good agreement with the results of molar volume as was described.

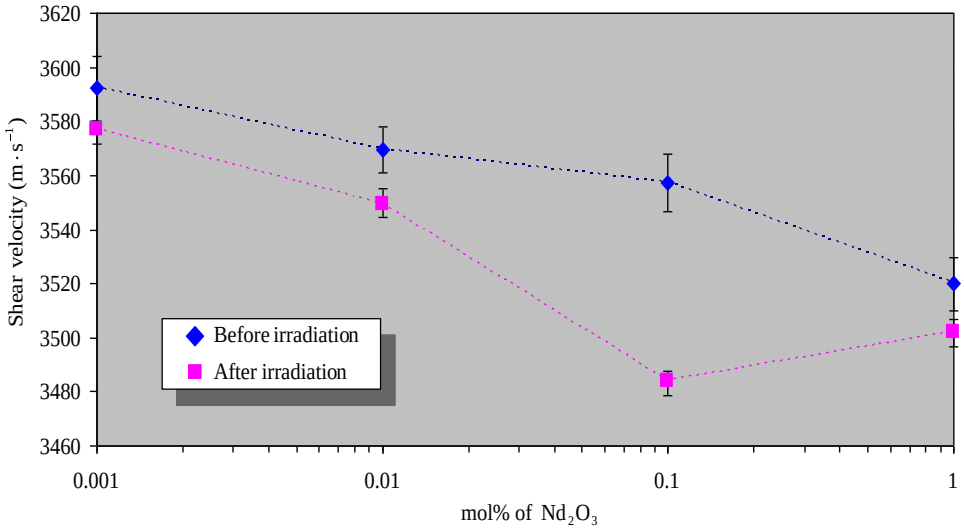

Fig. 4. Variation of shear velocity (v_S) before and after irradiation with γ-radiation of the glass samples with the difference of doping.

Table 4
Average cross-link density ($\bar{n}_c$), calculation of Poisson' ratio (σ_{cal}), number of vibrating atoms per unit volume (N/V), average stretching force constant ($\bar{F}$), average ring diameter (l) of the glass samples. Theoretical bond compression bulk modulus (K_{bc}), number of bonds per unit volume (n_b) and K_{bc}/K_{exp} ratio of the glass samples before and after gamma irradiation.

Sample no.	$\bar{n}_c$	σ_{cal}	$\frac{N}{V} \times 10^{21}(cm^{-3})$	$\bar{F}$ (N/m)	l (nm)	K_{bc} (GPa)		$n_b \times 10^{22}$ (cm^{-3})		K_{bc}/K_{exp}
						Before	After	Before	After	
G–0	3.6364	0.2028	7.7341	377.96	0.5424	170.99	170.81	14.9526	14.9375	4.0595
G–1	3.6365	0.2028	7.7467	377.95	0.5382	171.26	170.34	14.9770	14.8966	3.9471
G–2	3.6375	0.2027	7.7390	377.89	0.5388	171.08	169.98	14.9611	14.8651	3.9593
G–3	3.6479	0.2026	7.7256	377.29	0.5396	170.70	169.76	14.9268	14.8443	3.9772
G–4	3.7500	0.2012	7.7026	371.42	0.5431	169.33	168.72	14.7990	14.7464	4.1088

Debye temperature (θ_D) and softening temperature (T_s) before and after irradiation of the glass samples are listed in Table 3. Debye temperature is an important parameter of a solid, describes the properties arising from atomic vibration and is directly proportional to the mean ultrasonic velocity (v_m). The variations of the mean ultrasonic velocity are shown in Table 2. Debye temperature represents the temperature at which all the high-frequency "lattice" vibrational modes are excited (Gaafar et al., 2009). Softening temperature is another important parameter defined as the temperature point at which viscous flow changes to plastic flow (Marzouk and Gaafar, 2007; Gaafar and Marzouk, 2007). It can be observed that the decrease of the Debye temperature, softening temperature and mean ultrasonic velocity with adding Nd_2O_3 and after irradiation are mainly contributed from the increase in formation of NBOs as a direct effect of the insertion of Nd_2O_3 and effect of irradiation. For clarity of obtained results, the dependence of Debye temperature could be discussed on the basis of the number of vibrating atoms per unit volume (El-Mallawany and Afifi, 2013). Therefore, the number of vibrating atoms per unit volume (N/V) was calculated and shown in Table 4. The number of vibrating atoms per unit volume was found to decrease with the increasing mol% of the Nd_2O_3.

The values of average ring diameter (l), theoretical bond compression bulk modulus (K_{bc}) and K_{bc}/K_{exp} ratio are shown in Table 4. From Table 4, it is rather clear that the values of the theoretical bond compression bulk modulus (K_{bc}) decrease when the content of Nd_2O_3 increases and decrease after irradiation. This indicates that adding Nd_2O_3 to the pure composition of the glass plays a major role in the average coordination of the network structure (Burkhard, 1997) or the average stretching force constant which was found as a similar trend with the theoretical bond compression bulk modulus (K_{bc}). In general, the ratio of K_{bc}/K_{exp} is a measure of the extent to which bond bending is governed by the configuration of the network bonds. The variation of K_{bc}/K_{exp} ratio increase with increase of concentration of dopant. This indicates that the network bonds are expanding of extent. This ratio is assumed to be directly proportional to the average ring diameter. The average ring diameter is shown in Table 4. It is very clear that the average ring diameter increase with increase of the concentration of Nd_2O_3.

Comparison of experimental estimated elastic moduli (K, G, L and E) with those obtained theoretically by using bond compression model are shown in Fig. 5. From Fig. 5, the calculated elastic moduli are in the range of the experimental values. It is observed that a theoretical bond compression model is in a good agreement with the experimental values of elastic moduli.

4.3. FTIR measurements

FTIR spectral curves in 400 – 4000 cm^{-1} region of the glass samples before and after irradiation are illustrated in Fig. 6(a) and (b), respectively. The water groups are indicated by frequency bands over 2000 cm^{-1}. The main absorption band and corresponding vibration modes of FTIR spectrum of glass samples are shown in Table 5. The frequency bands from the glasses network

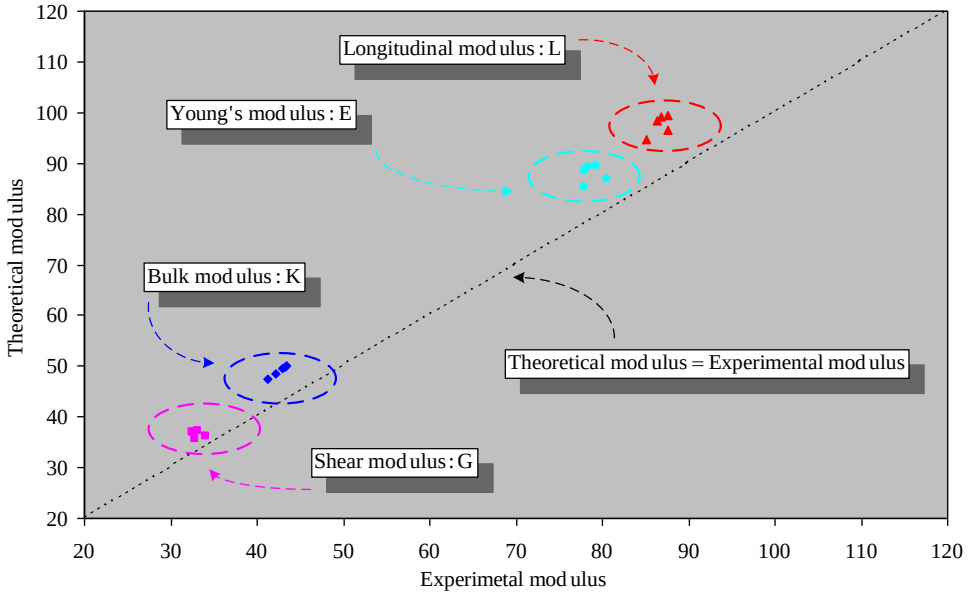

Fig. 5. Variation of theoretical modulus vs experimental modulus of the glass samples with the difference of doping.

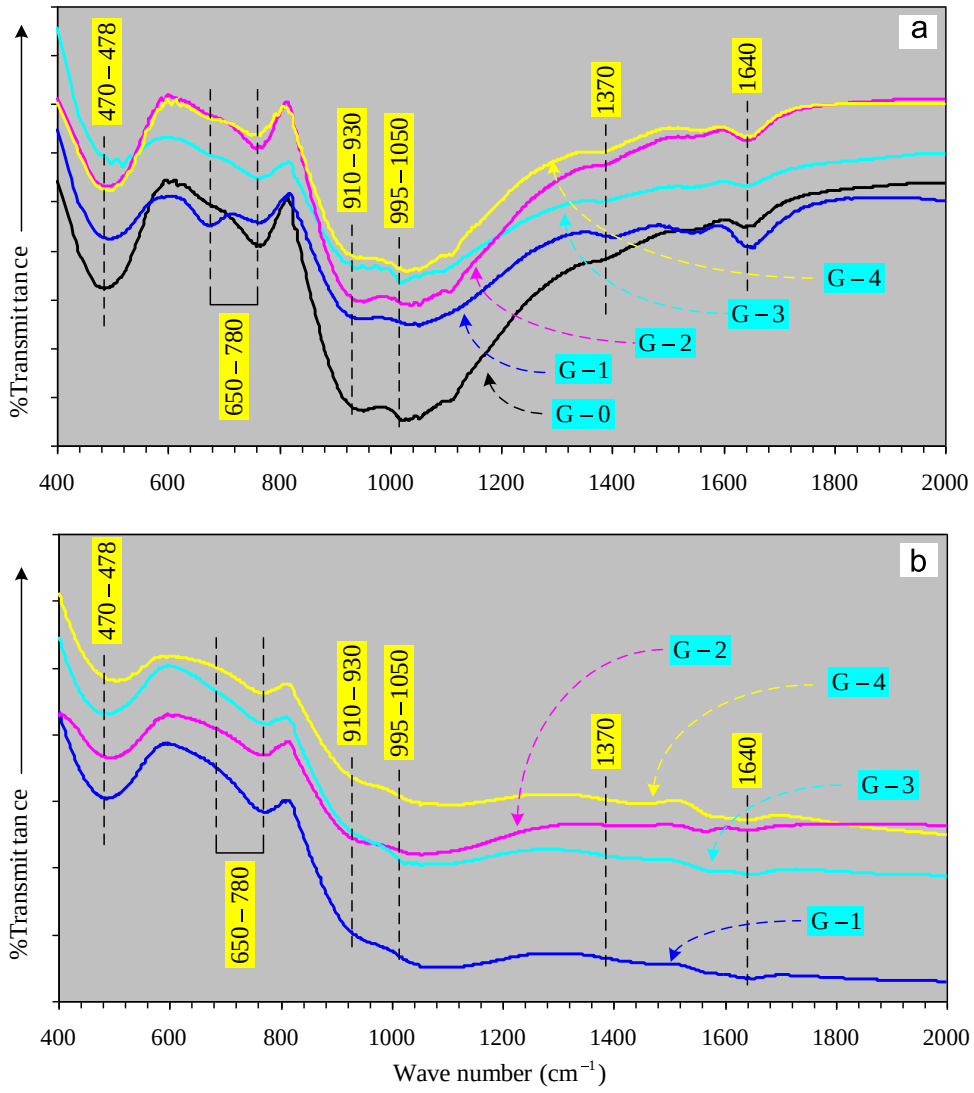

Fig. 6. FTIR spectra of the glass samples before (a) and after (b) gamma irradiation.

vibrations appear in the range 400 – 1500 cm^{-1} (Wang et al., 2014; ElBatal et al., 2014). The FTIR absorption spectra for the glass samples examined herein have four main frequency bands. Fig. 6(a) shows apparently decrease of Si – O– Si anti-asymmetric stretching of BOs within tetrahedral (995 – 1050 cm^{-1}) peak when the mol% of Nd_2O_3 increases. Furthermore, the Si – O– Si bending vibrations (470 – 485 cm^{-1}) peak and the Si – O– Si and O–Si–O symmetrical stretching of BOs between tetrahedral (650 – 780 cm^{-1}) peak shows decrease of absorption with mol% of Nd_2O_3 increases. The results from FTIR spectroscopy support our discussion on the transformation of SiO_4 tetrahedral units from Q_4 to Q_3 with consequent rising in NBO when mol% of Nd_2O_3 increases. Fig. 6(b) shows decrease of FTIR absorption bands at 470 – 485, 650 – 780 and 995 – 1050 cm^{-1} all samples after irradiation. These results reveal that the formation of NBOs occurred when the glass sample were irradiated with gamma ray. The results of the FTIR spectra are evidence of the discussion the change in structure of the glass network was added Nd_2O_3 and after irradiated.

Table 5
Main absorption band and corresponding vibration modes of FTIR spectrum of glass samples in 400 – 2000 cm^{-1} region.

Wave number (cm^{-1})	Assignment	References
470 – 485	Si – O– Si Bending vibrations	[Wang et al., 2014; Zahran, 1998]
650 – 780	Si – O– Si and O–Si–O symmetrical stretching of BOs between tetrahedra	[Wang et al., 2014; Zahran, 1998]
910 – 930	Si – O– Si stretching of NBOs	[Zahran, 1998]
995 – 1050	Si – O– Si anti-asymmetric stretching of BOs within tetrahedra	[Wang et al., 2014; Zahran, 1998]
1370	Carbonate group	[Zahran, 1998]
1640	Molecular water vibrations	[Wang et al., 2014]

5. Conclusions

The present study gives the understanding of the structural properties of soda lime glasses doped with Nd_2O_3 and effect of gamma irradiation by measuring ultrasonic velocities. Influence of Nd_2O_3 and irradiation makes the distorted network structure. The values of the theoretical bond compression model were calculated for asseveration of the obtained results. The agreement between the theoretically calculated and experimental elastic moduli is excellent for the studied samples.

Acknowledgments

The author gratefully acknowledges the financial support from the Thailand Research Fund (TRF), Office of the Higher Education Commission (CHE) and Ubon Ratchathani University (UBU). Research Grant no. MRG5680114. The author special thanks to National Research Council of Thailand (NRCT) for financial support (Fiscal year 2015).

References

AbdelAziz, T.D., EzzElDin, F.M., ElBatal, H.A., Abdelghany, A.M., 2014. Optical and FT Infrared spectral studies of vanadium ions in cadmium borate glass and effects of gamma irradiation. Spectrochim. Acta A 131, 497–501.

Abdelghany, A.M., ElBatal, F.H., ElBatal, H.A., EzzElDin, F.M., 2014. Optical and FTIR structural studies of CoO-doped sodium borate, sodium silicate and sodium phosphate glasses and effects of gamma irradiation-a comparative study. J. Mol. Struct. 1074, 503–510.

Abd El-Moneim, A., 2001. Bond compression bulk modulus and Poisson's ratio of polycomponent silicate glasses. Mater. Chem. Phys. 70, 340–343.

Abd El-Moneim, A., 2003. Quantitative analysis of elastic moduli and structure of B_2O_3–SiO_2 and Na_2O–B_2O_3–SiO_2 glasses. Physica B 325, 319–332.

Abd El-Moneim, A., Youssof, I.M., Adb El-Latif, L., 2006. Structural role of RO and Al_2O_3 in borate glasses using an ultrasonic technique. Acta Mater. 54, 3811–3819.

Alajerami, Y.S.M., Hashim, S., Ghoshal, S.K., Ramli, A.T., Saleh, M.A., Ibrahim, Z., Kadni, T., Bradley, D.A., 2013. Luminescence characteristics of Li_2CO_3–K_2CO_3–H_3BO_3 glasses co-doped with TiO_2/MgO. Appl. Radiat. Isot. 82, 12–19.

Bootjomchai, C., Laopaiboon, R., 2014. Thermoluminescence dosimetric properties and effective atomic numbers of window glass. Nucl. Instrum. Methods B 323, 42–48.

Bootjomchai, C., Laopaiboon, R., Pencharee, S., Laopaiboon, J., 2014. Elastic moduli of borosilicate glasses doped with heavy metal oxides. J. Non-Cryst. Solids 388, 37–45.

Bridge, B., Higazy, A.A., 1986. Model of the compositional dependence of the elastic moduli of polycomponent oxide glasses. Phys. Chem. Glasses 27, 1–14.

Burkhard, D.J.M., 1997. Elastic properties of alkali silicate glasses with iron oxide: relation to glass structure. Solid State Commun. 101, 903–907.

Clare, A.G., 1994. Key engineering materials. In: Shelby, J.E., et al. (Eds.), Rare Elements in Glasses, 94-95. Trans Tech Publications, Switzerland, pp. 161–180.

Clayden, N.J., Esposito, S., Aronne, A., 1999. Solid state ^{27}Al NMR and FTIR study of lanthanum aluminosilicate glasses. J. Non-Cryst. Solids 258, 11–19.

Devine, R.A.B., 1994. Macroscopic and microscopic effects of radiation in amorphous SiO_2. Nucl. Instrum. Methods B 91, 378–390.

ElBatal, F.H., Abdelghany, A.M., ElBatal, H.A., 2014. Characterization by combined optical and FT infrared spectra of 3d-transition metal ions doped-bismuth silicate glasses and effects of gamma irradiation. Spectrochim. Acta A 122, 461–468.

El-Mallawany, R., 2000. Structural interpretations on tellurite glasses. Mater. Chem. Phys. 63, 109–115.

El-Mallawany, R., Abousehly, A., El-Rahamani, A.A., Yousef, E., 1998. Radiation effect on the ultrasonic attenuation and internal friction of tellurite glasses. Mater. Chem. Phys. 52, 161–165.

El-Mallawany, R., Afifi, H., 2013. Elastic moduli and crosslinking of some tellurite glass systems. Mater. Chem. Phys. 143, 11–14.

El-Mallawany, R., El-Khoshkhany, N., Afifi, H., 2006. Ultrasonic studies of $(TeO_2)_{50}$–$(V_2O_5)_{50-x}$–$(TiO_2)_x$ glasses. Mater. Chem. Phys. 95, 321–327.

Ezz El-Din, F.M., El-Alaily, N.A., El-Batal, H.A., 1992. Density and refractive index of some γ-irradiated alkali silicate glasses. J. Radioanal. Nucl. Chem. 163 (2), 267–275.

Ezz-Eldin, F.M., Elalaily, N.A., El-Batal, H.A., Ghoneim, N.A., 1996. Formation and bleaching of induced colour centers in gamma-irradiated vanadium-containing alkali-borate glasses. Radiat. Phys. Chem. 48, 659–664.

Gaafar, M.S., Afifi, H.A., Mekawy, M.M., 2009. Structural studies of some phosphor-borate glasses using ultrasonic pulse-echo technique, DSC and IR spectroscopy. Physica B 404, 1668–1673.

Gaafar, M.S., Marzouk, S.Y., 2007. Mechanical and structural studies on sodium borosilicate glasses doped with Er_2O_3 using ultrasonic velocity and FTIR spectroscopy. Physica B 388, 294–302.

Hager, I.Z., 2012. Effect of Er_2O_3 and ErF_3 on the structural and elastic properties of sodium oxyfluoroborate glasses. J. Alloys Compd. 539, 256–263.

Higazy, A.A., Bridge, B., 1985. Elastic constants and structure of the vitreous system Co_3O_4–P_2O_5. J. Non-Cryst. Solids 72, 81–108.

Jayasimhadir, M., Rama Moorthy, L., Ravikumar, R.V.S.S.N., 2007. An investigation of the optical properties of Nd^{3+} ions in alkali tellurofluorophosphate glasses. Opt. Mater. 29, 1321–1326.

Joseph, C.M., Binu, P.R., Shreekrishnakumar, K., Menon, C.S., 2002. Preparation and physical properties of CuPc substituted sodium borate glass matrix. Mater. Lett. 53, 326–328.

Kaur, R., Singh, S., Pandey, O.P., 2013. Influence of CdO and gamma irradiation on the infrared absorption spectra of borosilicate glass. J. Mol. Struct. 1049, 409–413.

Laopaiboon, R., Bootjomchai, C., 2014a. Glass structure responses to gamma irradiation using infrared absorption spectroscopy and ultrasonic techniques: a comparative study between Co_2O_3 and Fe_2O_3. Appl. Radiat. Isot. 89, 42–46.

Laopaiboon, R., Bootjomchai, C., 2014b. Radiation effects on structural properties of glass by using ultrasonic techniques and FTIR spectroscopy: a comparison between local sand and SiO_2. Ann. Nucl. Energy 68, 220–227.

Lemercier, H., rouxel, T., Fargeot, D., Besson, J.L., Piriou, B., 1996. Yttrium SiAlON glasses: structure and mechanical properties elasticity and viscosity. J. Non-Cryst. Solids 201, 128–145.

Lin, S.L., Hwang, C.S., 1996. Structures of CeO_2–Al_2O_3–SiO_2 glasses. J. Non-Cryst. Solids 202, 61–67.

Marzouk, S.Y., 2009. Ultrasonic and infrared measurements of copper-doped sodium phosphate glasses. Mater. Chem. Phys. 114, 188–193.

Marzouk, S.Y., Gaafar, M.S., 2007. Ultrasonic study on some borosilicate glasses doped with different transition metal oxides. Solid State Commun. 144, 478–483.

Neuville, D.R., Cormier, L., Boizot, B., Flank, Anne-Marie, 2003. Structure of β-irradiated glasses studied by X-ray absorption and Raman spectroscopies. J. Non-Cryst. Solids 323, 207–213.

Prado, M.O., Messi, N.B., Plivelic, T.S., Torriani, I.L., Bevilacqua, A.M., Arribére, M.A., 2001. The effects of radiation on the density of an aluminoborosilicate glass. J. Non-Cryst. Solids 289, 175–184.

Rajendran, V., Palanivelu, N., Palanichamy, P., Jayakumar, T., Raj, B., Chaudhuri, B.K., 2001. Ultrasonic characterization of ferroelectric $BaTiO_3$ doped lead bismuth oxide semiconducting glasses. J. Non-Cryst. Solids 296, 39–49.

Sharma, G., Rajendran, V., Thind, K.S., Singh, G., Singh, A., 2009. Structural investigation of bismuth borate glasses under the influence of γ-irradiation through ultrasonic studies. Physica B 404, 3371–3378.

Shelby, J.E., Kohli, J.T., 1990. Rare-earth aluminosilicate glasses. J. Am. Ceram. Soc. 73, 39–42.

Sidkey, M.A., Gaafar, M.S., 2004. Ultrasonic studies on network structure of ternary TeO_2–WO_3–K_2O glass system. Physica B 348, 46–55.

Singh, H., Singh, K., Gerward, L., Singh, K., Sahota, H.S., Nathuram, R., 2003. ZnO-PbO-B_2O_3 glasses as gamma-ray shielding materials. Nucl. Instrum. Methods B 207, 257–262.

Wang, M., Li, M., Cheng, J., He, F., 2014. Structure and viscosity of soda lime silicate glasses with varying Gd_2O_3 content. J. Mol. Struct. 1063, 139–144.

Zahran, R.R., 1998. Effect of γ-irradiation on the ultrasonic and structural properties of polyoxymethylene. Mater. Lett. 37, 83–89.

Journal of Luminescence 158 (2015) 275–280

Contents lists available at ScienceDirect

Journal of Luminescence

journal homepage: www.elsevier.com/locate/jlumin

Thermoluminescence studies on alkali-silicate glass doped with dysprosium oxide for use in radiation dosimetry measurement

Raewat Laopaiboon, Cherdsak Bootjomchai *

Glass Technology Excellent Center (GTEC), Department of Physics, Faculty of Science, Ubon Ratchathani University, Ubon Ratchathani 34190, Thailand

ARTICLE INFO

Article history:
Received 27 June 2014
Received in revised form
13 September 2014
Accepted 8 October 2014
Available online 22 October 2014

Keywords:
Glasses
Thermoluminescence
Dose response
Optical absorption
Trap parameters

ABSTRACT

Alkali-silicate glass doped with dysprosium oxide was prepared and investigated. Recycled window glass (RWG) was substituted with pure SiO_2 chemical as starting material. Physical properties of the glass samples such as density, molar volume and ion concentrations were determined. The thermoluminescence properties such as sensitivity and linearity of the glass samples were investigated. Trap depth parameters were studied using the glow curve shape method. Moreover, the optical absorption of the glass samples was studied with the transition mechanisms of Dy^{3+} ions.

1. Introduction

Investigations of radiation induced defect centers using the thermoluminescent properties of glass have been well documented in recent years. These studies advance the knowledge of the suitability of glass in radiation dosimetry applications [1–6]. In the field of personnel monitoring, the thermoluminescence (TL) technique could be an interesting area of research to measure high dosages incurred during various radiation process applications, such as in nuclear power plants, food irradiation, radiotherapy and medical product sterilization. Amorphous systems development is therefore of paramount importance for this specific application. New materials are now being developed with more sensitivity and linearity of TL output over a broad range of dosages. Several amorphous materials such as alkali, alkaline oxy, fluoro borate, phosphates, borophosphates, silicates, alkali silicates, alkali aluminosilicates and borosilicate glasses doped with small concentrations of rare-earth ions and/or transition metal ions as activators were identified as effective [7–12].

Rare-earth doped luminescent materials play a significant part as radiation detectors in many fields of basic and applied research, for example nuclear power plants, radiotherapy, personal and environmental monitoring of ionizing radiation and even in geological dating. The added rare earth impurities in the host may cause the changes in its TL features as well as the dosage amount [13]. Recently several rare-earth doped aluminates and silicates have been presented and developed for various display and signage applications [10,14]. Among the different rare earths the Dy^{3+} ion is recognized as an active luminescence centre. The Dy^{3+} ion is identified as an f-localized trap-creating ion and found to increase the afterglow for a protracted time [15]. The Dy^{3+} ions form some electron trapping levels in the intra-band gaps of the host material. The attributed excitation of Dy^{3+} ions plays an important role in TL emission by a trap filling process that may occur through the direct transfer of electrons from the excited state of Dy^{3+} ions to trap centers and not via conduction bands, as the excitation energy is smaller than the band gap [16–18].

Previous work has studied the thermoluminescence properties of the window glass sold in Ubon Ratchathani Province, Thailand. Results showed that this window glass is potentially a good candidate for retrospective or personal dosimetry. It is a common material, has easy sample preparation, good linearity of TL response and its effective atomic number is close to that of human biological tissues [19]. However, reproducibility of the results and fading needs to be improved due to the unstable nature of trapped charge effects. From the literature reviews, Dy^{3+} ions can create electron trapping levels in the intra-band gaps of the host material. Therefore, it is particularly interesting to study the effect of dysprosium oxide powder (Dy_2O_3) on thermoluminescent properties and trap depth parameters, using recycled window glass as a starting material. This study looks at very low doses of irradiation which may be useful for clinical dosimetry.

* Corresponding author. Tel./fax: +66 45288381.
E-mail address: cherdsak_per@hotmail.co.th (C. Bootjomchai).

http://dx.doi.org/10.1016/j.jlumin.2014.10.017
0022-2313/

2. Experimental details

2.1. Preparation and determination of the final composition of based glass

Binary $(100-x)$RWG $-(x)Na_2O$ glass with different concentrations of Na_2O, where x is 5, 10, 15 and 20 mol%, was prepared using the melt-quenched technique. The sodium oxide (Na_2O) used was of analytical reagent grade. The RWG was common window glass sold in Ubon Ratchathani, Thailand. The chemical composition of the RWG has been previously determined [19]. Preparation of the recycling glass from window glass (RWG) involved a thorough cleaning and it was then ground to a powder. The quantities of Na_2O and RWG powder were weighed, using an electronic balance with accuracy of the order of 0.0001 g. They were calculated and mixed to give 50 g samples. The starting materials were mixed carefully in ceramic crucibles. To ensure homogeneity, the mixtures were melted at 1250 °C in an electrical furnace, constructed at the Glass Technology Excellent Center (GTEC), Department of Physics, Faculty of Science, Ubon Ratchathani University. The melted glasses were poured into stainless steel molds and immediately annealed at 500 °C for two hours before natural cooling to room temperature. The glass samples were cut into small pieces with dimensions $5 \times 5 \times 2$ mm^3 for TL measurements at 14 mGy. The sensitivity of the TL signal was normalized with respect to the weights of each condition of glass sample as shown in Fig. 1. Results showed that the (90)RWG $-$ (10)Na_2O glass system had the highest sensitivity; therefore this condition was selected as the base glass (G $-$ 0).

2.2. Preparation of glass samples doped with Dy_2O_3

For this study (90)RWG $-$ (10)$Na_2O-(x)Dy_2O_3$ glass systems (where x is 0.001, 0.010, 0.100 and 1.000 mol%) were prepared. For each glass, the thermal history; melting temperature, melting time, annealing temperature, annealing time and all preparation conditions were kept as similar as possible. The dysprosium oxide used was of analytical reagent grade. The details of the chemical compositions of the glass samples are shown in Table 1.

2.3. Thermoluminescence measurements

Each sample was annealed at 400 °C for one hour and then 100 °C for two hours (dual step technique), before being irradiated with X-ray photon energy of 100 keV with a dose range of 0–14 mGy, to determine the thermoluminescent response and glow curve. TL light emitted from the glass samples was detected using a TLD reader (Harshaw/Bicron Model 3500 Manual). The glow curves were recorded from room temperature up to a maximum of 300 °C, at heating rates of 10 °C/s. A region of interest facility available in the TLD reader was used to evaluate the

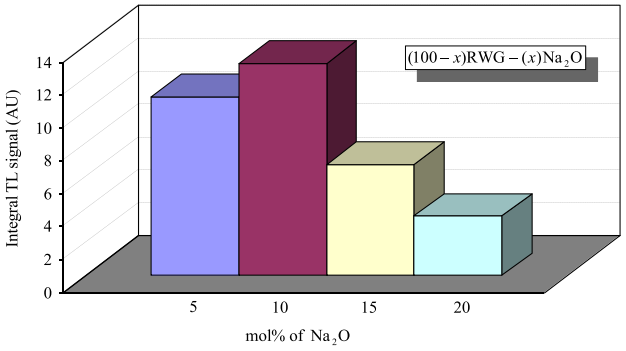

Fig. 1. Integral TL signal of $(100-x)$RWG $-(x)Na_2O$ glass system irradiated with X-ray photon energy of 100 keV at dose of 14 mGy. The sensitivity of TL signal was normalized with respect to the respective weights of the samples.

Table 1
Details of the chemical composition of the glass samples.

Glass sample	Compositions (in mol%)		
	RWG	Na_2O	Dy_2O_3
G – 0	90	10	–
G – 1	90	10	0.001
G – 2	90	10	0.010
G – 3	90	10	0.100
G – 4	90	10	1.000

responses of different glow peaks resulting from the Computerized Glow Curve Deconvolution (CGCD) procedure. The estimation of glow peaks was carried out by copying the American Standard Code for Information Interchange (ASCII) files from the TLD reader to an Excel program. Each data point observed was obtained from an average of five measurements.

2.4. UV–vis spectroscopic measurements

Absorption spectra of all the samples were recorded using the bulk form of the samples. All spectra were measured at the Chemistry Department, Ubon Ratchathani University. The spectrophotometer (Perkin Elmer Instrument, Lambda 25) results were recorded at a range of 300–900 nm with a resolution of 0.1 nm.

2.5. Density and molar volume

The variation in the density of each sample was determined by Archimedes's Principle. n-hexane (99.99% pure) was selected as an immersion liquid. For all samples the measurement was repeated three times at room temperature. The density can be calculated using the following equation:

$$\rho = \left(\frac{W_A}{W_A - W_B}\right)\rho_L \quad (1)$$

where W_A and W_B are the weights of the glass sample in air and in n-hexane respectively and ρ_L is the density of n-hexane. The estimated error in these measurements was ± 0.002 g cm^{-3}. The molar volume (V_a) was calculated using the equation $V_a = M/\rho$, where M is the average molecular weight of the glass samples, calculated according to the relationship $M = \sum x_i M_i$ [20], where x_i is the mole fraction of the component oxide i and M_i is its molecular weight. Uncertainties in molar volume were recorded by repeating the density measurements three times. The estimated error in the results was ± 0.085 cm^3 mol^{-1}.

2.6. Ion concentration

The rare-earth (RE) ion concentration can be calculated using the following equation [21]:

$$N = \frac{(\text{mol\% of RE doped})(\rho)(N_A)}{M} \quad (\text{ions cm}^{-3}) \quad (2)$$

where N_A is Avogadro's number. After determining the ion concentration, three other related physical properties can be calculated using the standard relations as shown below [21–22]:

$$\text{Polaron radius}: \quad r_p = \frac{1}{2}\left(\frac{\pi}{6N}\right)^{1/3} \quad (\text{Å}) \quad (3)$$

$$\text{Interatomic distance}: \quad r_i = \left(\frac{1}{N}\right)^{1/3} \quad (\text{Å}) \quad (4)$$

$$\text{Field strength}: \quad F = \left(\frac{Z}{r_p^2}\right) \quad (\text{cm}^{-2}) \tag{5}$$

where Z is the valence number of the rare-earth ion.

3. Results and discussion

3.1. Physical properties

The physical properties offer an insight into the atomic arrangements in a glass network. The density of the glass increased with increasing Dy_2O_3 concentration. The increase can be attributed to three factors, namely:

- Transformation of the main glass network structure from triagonal (O_3) to tetrahedral (O_4).
- Increase in the molecular mass of the glass because of the higher atomic weight of dysprosium.
- Increase of the bridging oxygen (BO) ratio in the glass composition, due to the Dy_2O_3 concentration [23].

Molar volume describes the volume occupied by the unit mass of the glass; it depends on the ionic radius of the modifier [24]. The molar volume decreases with the content of dopant (Dy_2O_3) increase as shown in Table 2. The glass system (90)RWG – (10)Na_2O, RWG has a main structure of SiO_2 (the ionic radius of Si^{4+} is 0.400 Å). When RWG was added to Na_2O (the ionic radius of Na^+ is 1.060 Å) this led to the expansion of the interstitial size of the network structure of the glass. Thus, when Dy_2O_3 (the ionic radius of Dy^{3+} is 0.912 Å) was added to the glass matrix it resulted in a decrease in the interstitial size of the network structure, which led to a decrease in the molar volume. These results showed that the glass samples increased in compactness with increasing concentrations of Dy_2O_3.

From Table 2, the ion concentrations increase with the mol% of Dy_2O_3. These results for the molar volume and the ion concentration are very promising. Clearly, the ion concentration increases as the molar volume decreases. The ion concentration is high due to the large number of mobile ions. The increase in the ion concentration of Dy^{3+} showed that Dy^{3+} ions are uniformly spread throughout the glass network [25]. An inverse relationship is observed between the dopant concentration and both the Polaron radius and interatomic distance. The Polaron radius (Table 2) decreases with increasing Dy_2O_3 concentrations. This could be due to an increase in the concentration of Dy^{3+} ions. The observed decrease in the interatomic distance (Table 2) with the increase in Dy_2O_3 concentration eventually leads to a more compact glass network [26]. It is notable that the glass network will be crowded with dysprosium interstices. Thus, the average RE-oxygen distance decreases. As a result the Dy–O bond strength increases, producing a stronger field strength (F) around the dysprosium ions [27]. This result agrees with the literature [23,28,29] and also supports the increased compactness of the glass structure as discussed above. Thus, a perfect conductivity for this glass system could be expected [30].

3.2. Thermoluminescence properties

The glass samples were irradiated with 100 keV of photon energy at doses ranging from 0 to 14 mGy. The sensitivity of the TL signal was normalized with respect to the weights of each condition of the glass samples at a dose of 14 mGy and shown in Fig. 2. The main glow curves were similar and centered for peak 1 and peak 2 for all the glass samples at 450 K and 558 K respectively. Dy^{3+} ion doping has been shown to cause significant increases in TL. Wani et al. [16] reported that RE^{3+} ion doping resulted in increased sensitization of TL. The important role of Dy^{3+} ions in TL emission is the trap filling process that may arise through the direct transfer of electrons from the excited state of Dy^{3+} to trap centers. TL sensitivity slightly increased after Dy^{3+} doping as shown in Fig. 2. This suggested that the impurities in the composition of RWG [19] were strongly related to the intrinsic defects attributed to well-known concentration quenching phenomena and tallied with the results obtained by Hashim et al. [31]. Results showed that the highest integrated TL signal of the glass samples was for 0.100 mol% of Dy_2O_3, with all giving improved TL sensitivity after Dy^{3+} doping. An investigation of the dependence of the TL signal on irradiation doses was carried out on the glass samples exposed to photons for doses between 0 and 14 mGy. The average integrated TL signal of each dose was recorded and the relative standard deviation was calculated. Fig. 3 shows the experimental trend obtained and the corresponding calibration line of best fit resulting from processing the experimental points. The correlation coefficients (R^2) were calculated to confirm the linearity of the response in the investigated dosage range. The results indicated that glass samples doped with Dy_2O_3 at 0.100 mol% (G – 3) gave the best linearity. From these results (Figs. 2 and 3), a minimum detectable dose (MMD) value of G – 3 glass sample was determined as three

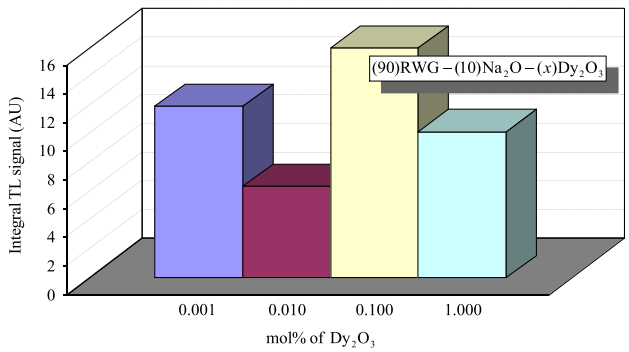

Fig. 2. Integral TL signal of (90)RWG – (10)Na_2O – (x)Dy_2O_3 glass system irradiated with X-ray photon energy of 100 keV at dose of 14 mGy. The sensitivity of TL signal was normalized with respect to the respective weights of the samples.

Table 2
Physical properties of glass samples.

Measurements	Glass samples				
	G – 0	G – 1	G – 2	G – 3	G – 4
Density, ρ (g cm^{-3})	2.567	2.572	2.585	2.602	2.682
Molar volume, V_a (cm^3 mol^{-1})	23.351	23.307	23.186	23.036	22.349
Ion concentration, N_{RE} ($\times 10^{21}$ ion cm^{-3})	–	0.026	0.258	2.577	25.359
Polaron radius, r_p (A°)	–	13.633	6.325	2.939	1.371
Interatomic distance, r_i (A°)	–	33.835	15.698	7.294	3.404
Field strength, F ($\times 10^{16}$ cm^{-2})	–	0.016	0.075	0.347	1.595

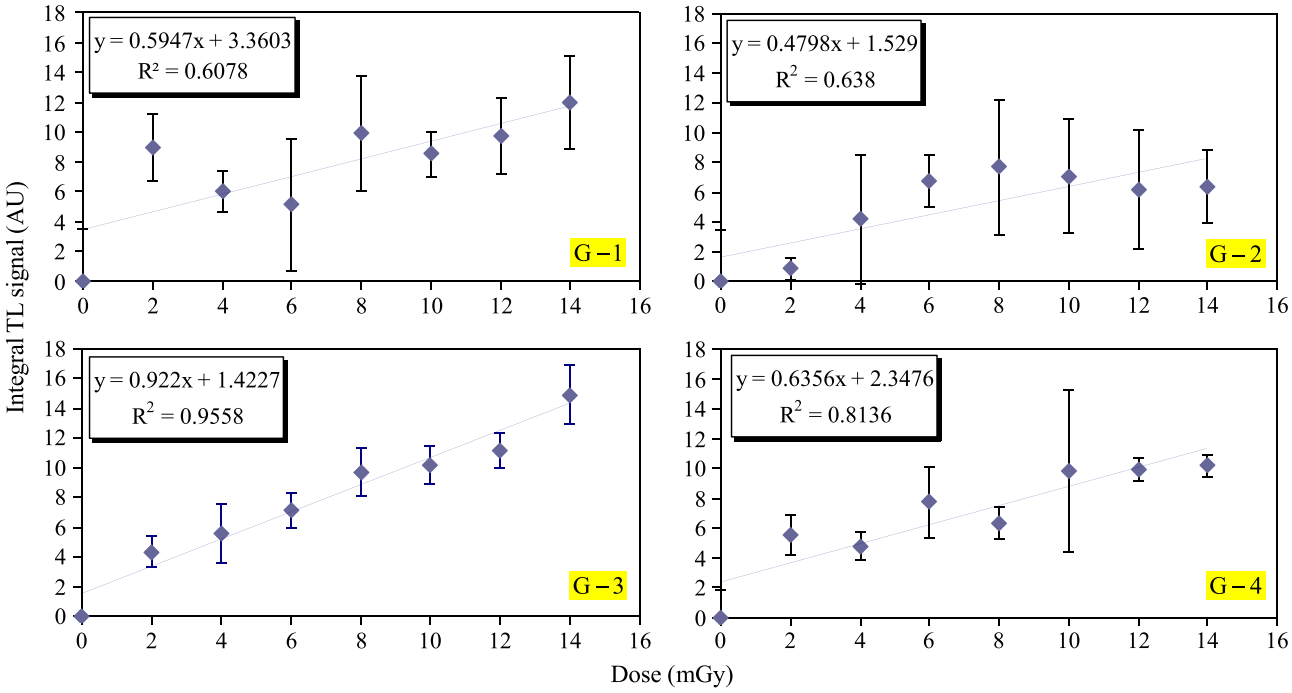

Fig. 3. Linear relationship between TL response and irradiation dose of glass samples.

times the corresponding value of the standard deviations of ten non-irradiated samples. The estimated value of MMD obtained was 3.697 mGy. Fig. 4 shows the stability of TL signals of the G – 3 glass sample after a storage period of 720 h at a dose of 14 mGy, compared with the window glass (RWG) [19]. There was a rapid decrease in the TL signal in the initial range, (45% and 65% decreased at 0–200 h of the G – 3 glass sample and RWG respectively). This suggests that the lower loss of TL signal of the G – 3 glass sample results from the higher stabilization of trapped charge effects when compared with RWG. These results are supported by the fact that the stability and sensitivity of TL signals improved after Dy^{3+} doping.

For investigation of trap depth parameters, general expressions for evaluating activation energy and trap depth were derived by Chen [32]. His method is useful for a broad range of energies ranging between 0.1 eV and 2.0 eV, and for values of the frequency factors between $10^5\ s^{-1}$ and $10^{23}\ s^{-1}$. Chen's method does not require knowledge of the kinetic order, which is found by using the symmetry factor ($\mu = T_2 - T_M / T_2 - T_1$) from the peak shape. The equations are as following:

$$E_\alpha = c_\alpha\left(\frac{KT_M^2}{\alpha}\right) - b_\alpha(2KT_M) \quad (6)$$

where K is the Boltzmann constant, T_M is the glow peak temperature, α is τ or δ ($\tau = T_M - T_1$ and $\delta = T_2 - T_M$), T_1 (rising end) and T_2 (falling end) are the temperatures at the half-widths of the glow peak. The values of c_α and b_α are summarized below.

$$c_\tau = 1.510 + 3.0(\mu - 0.42) \quad \text{and} \quad b_\tau = 1.58 + 4.2(\mu - 0.42) \quad (7)$$

$$c_\delta = 0.976 + 7.3(\mu - 0.42) \quad \text{and} \quad b_\delta = 0 \quad (8)$$

Glow curve shape is a popular method of analyzing a TL glow curve in order to ascertain the activation energies and frequency factors. The G – 3 glass sample was selected for investigation of the trap depth parameters due to its highest sensitivity and linearity. The variation of trap depth parameters of the G – 3 glass sample can be compared with G – 0 (un-doped) glass sample and window glass (RWG) as shown in Fig. 5. Data of the trap depth parameters from Fig. 5 are collected in Table 3. X-ray irradiation on the glass produces secondary electrons from the sites where they are in a

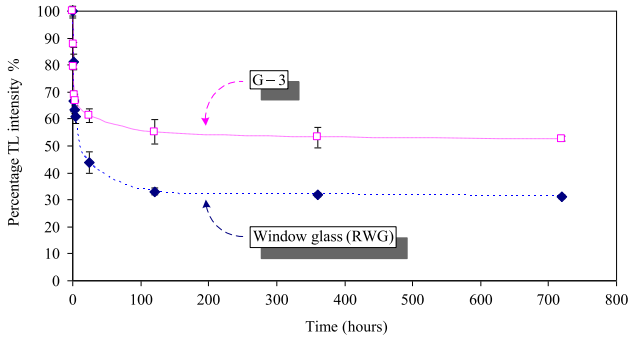

Fig. 4. Fading of G – 3 glass sample irradiated with X-ray photon energy of 100 keV at dose of 14 mGy at room temperature and it was compared with the window glass (RWG) [19].

stable state, which now have excess energy and also non-bridging oxygens (NBOs). The electrons may traverse through the glass lattice depending upon their energy and the composition of the glass network, but they are finally trapped, forming color centers. Alternatively they may form excitons with energy states in the forbidden gap at the inherent structural defects like $[SiO_{3/2}O]^-$, $[SiO_{2/2}O_2]^{2-}$ or $[SiO_{1/2}O_3]^{3-}$. This process leads to the formation of (i) electron centers, (ii) non-bridging oxygen hole centers and (iii) oxygen hole centers. Thermoluminescence is a consequence of radiative recombination between the electrons, released by heating from the electron centre and an anti-bonding molecular orbital of the nearest oxygen hole centre. Under X-ray irradiation there is also the possibility for the following reactions [33]:

$$Dy^{3+} \rightarrow Dy^{2+} + h^+$$

$$Dy^{3+} \rightarrow Dy^{3+} + h^+ + e^-$$

In the first reaction, a hole trapped at a lattice site during irradiation recombines with Dy^{2+} and produces TL when the material is heated. In the second reaction, the electrons and holes created in the lattice in the vicinity of Dy^{3+} ions during irradiation recombine at Dy^{3+} ion sites as the material is heated and emit TL.

Table 3
Data on various trap depth parameters of recycled window glass (RWG), G–0 and G–3 glass samples.

Glass type	T_m (K)		τ (K)		δ (K)		μ		E_τ (eV)		E_δ (eV)		$S \times 10^5$ (s^{-1})	
	Peak 1	Peak 2	Peak 1	Peak 2	Peak 1	Peak 2	Peak 1	Peak 2	Peak 1	Peak 2	Peak 1	Peak 2	Peak 1	Peak 2
RWG	502	–	61	–	44	–	0.420	–	0.401	–	0.482	–	2.455	–
G–0	443	558	43	32.5	47.5	19	0.525	0.369	0.564	0.990	0.621	0.853	725.487	16.983
G–3	458	558	53	40	57.5	25	0.520	0.385	0.460	0.805	0.537	0.774	38.055	1197.895

To be more precise, with X-ray irradiation the SiO_4 groups are changed to $[SiO_{3/2}O]^-$, $[SiO_{2/2}O_2]^{2-}$, $[SiO_{1/2}O_3]^{3-}$ and interstitial oxygen ions (O_i^- ions). During the thermal excitation O_i^- ions distribute back to the silicate groups and excited them. This excitation is then transferred to the nearby Dy^{3+} ions and produces TL emission as shown by the reaction below [33]:

$$O_i^- \xrightarrow{h\upsilon} [SiO_{n/2}O_m]^{m-} \rightarrow ([SiO_{n/2}O_m]^{m-})^* \rightarrow Dy^{3+} + h\upsilon[SiO_{n/2}O_m]^{m-}$$

where $m = 1,\ 2,\ 3$ and $n = 3,\ 2,\ 1$. At the same time the local O_i^- compensation captures electrons from an $[SiO_{n/2}O_m]^{m-}$ site to form Dy^{2+} ions, releasing electrons that will later recombine with silicate complexes. This excitation is either transferred to Dy^{3+} ions, to produce TL emission, or it may excite silicate complexes to dissociate and form different silicate groups and oxygen ions. The mechanism of this process can be represented as reactions [33]:

$$[SiO_{3/2}O]^- \xrightarrow{h\upsilon} [SiO_{2/2}O_2]^{2-} + e^- \quad \text{then} \quad Dy^{3+} + e^- \rightarrow Dy^{2+}$$

after the material is heated.

$$Dy^{2+} \rightarrow Dy^{3+} + e^- \quad \text{then} \quad [SiO_{2/2}O_2]^{2-} + e^- \rightarrow ([SiO_{3/2}O]^-)^* \rightarrow ([SiO_{2/2}O_2]^{2-} + O^-)/Dy^{3+} + h\upsilon$$

This results in a decrease of activation energy when the Dy^{3+} ions are added to the structure units. A brief description of this mechanism is presented in Fig. 6. The frequency factor (S) is a constant characteristic of the electron trap and is proportional to the frequency of the collisions of electrons with the lattice phonons. The frequency factor is clearly related to TL signal intensities and stimulated by temperature, as shown in Fig. 5. Moreover, the values of the trap depths indicates that the lifetime (τ) of electrons in these traps is of the order of several months [34].

3.3. Optical absorption properties

From Fig. 7, the optical absorption spectra of the glass samples (G–0 to G–4), recorded at room temperature in the wavelength region of 300–900 nm exhibited the following standard electronic transitions of Dy^{3+} ions [35]:

$^4F_{9/2} \rightarrow {}^6H_{15/2}$ (blue ⇒ 500 nm)

$^4F_{9/2} \rightarrow {}^6H_{13/2}$ (yellow ⇒ 580 nm)

$^4F_{9/2} \rightarrow {}^6H_{11/2}$ (red ⇒ 670 nm)

The results in Fig. 7 show that the absorption intensity increases with increasing mol% of dopants. It is also well documented that the $^4F_{9/2} \rightarrow {}^6H_{15/2}$ (blue) transition scarcely varies with the environment, whereas the $^4F_{9/2} \rightarrow {}^6H_{13/2}$ (yellow) is the hypersensitive transition, which is strongly influenced by the ligand environment. The relative intensities of these two bands depend strongly on the local symm etry of Dy^{3+} ions. The effect of concentration quenching mech anism on the $^4F_{9/2} \rightarrow {}^6H_{15/2}$ (blue) and $^4F_{9/2} \rightarrow {}^6H_{13/2}$ (yellow) transitions of Dy^{3+} ions in glass samples has been attributed to the exchange interaction among the exited Dy^{3+} ions at higher concentrations [35] (Fig. 7).

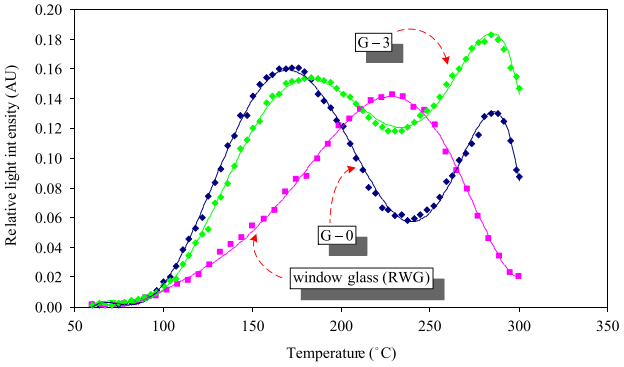

Fig. 5. Glow curve of glass samples irradiated with X-ray photon energy of 100 keV at dose of 14 mGy.

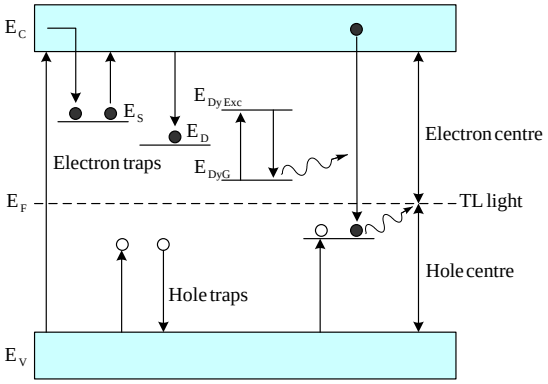

Fig. 6. Brief description of TL mechanism in RWG–Na_2O : Dy^{3+} glasses. Due to the X-ray irradiation electrons and hole become trapped at electron and hole defect energy trapping levels, respectively. E_S represents shallow traps while E_D represents deeper traps of electrons from where the probability of escaping is very less. In this study, E_D may be taken as the energy levels of electron traps surrounded in the vicinity of AlO_4 structural units (as part of the chemical composition of RWG [19]). Due to thermal stimulation of the irradiated samples the electrons at the E_S level gain sufficient energy, escape and recombine with holes giving TL emission. E_{Dy} represents electron trap levels of Dy^{3+} ions.

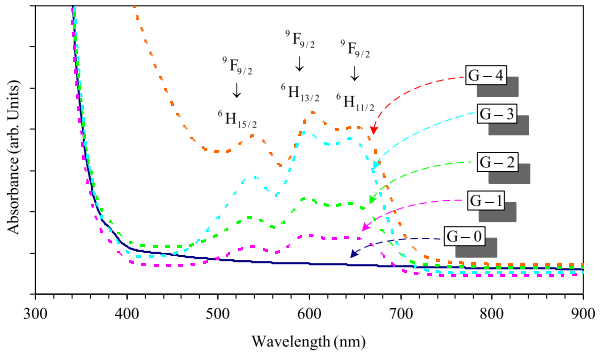

Fig. 7. Optical absorption spectra of glass samples recorded at room temperature.

4. Conclusions

The $(100-x)$RWG$-(x)Na_2O$ glass system with different concentrations of Na_2O was prepared and their integrated TL signals were recorded. The results indicated that the (90)RWG$-$(10)Na_2O glass sample produced the highest TL intensity, thus this glass was selected as base glass (G$-$0). The (90)RWG$-$(10)Na_2O glass system was doped with different concentrations of Dy_2O_3. The physical and thermoluminescent properties were determined. The results of the thermoluminescence testing showed that the G$-$3 glass sample had the highest integrated TL signals and linearity. Therefore, the G$-$3 glass sample was selected to compare variations of trap depth parameters with the G$-$0 un-doped glass sample and RWG. The optical absorption testing of glass samples (G$-$0 to G$-$4) was carried out. Results show that the transitions of Dy^{3+} ions in the glass samples is attributed to the exchange interaction among the exited Dy^{3+} ions at higher concentrations.

Acknowledgments

Financial support of this study has been provided by the Thailand Research Fund (TRF), Office of the Higher Education Commission (OHEC) and Ubon Ratchathani University (UBU) (Grant no. MRG5680114). The results and comments on this article are those of the authors. The TRF, OHEC and UBU are unnecessary always agree. The authors are gratefully Department of Physics, Faculty of Science, Ubon Ratchathani University for facility supports.

References

[1] M.R. Chailanza, J. Castiglioni, L. Fornaro, J. Mater. Sci. 47 (2012) 2339.
[2] W.M. Pontuschka, L.S. Kanashiro, L.C. Courrol, Glass Phys. Chem. 27 (2001) 37.
[3] P. Nageswara Rao, G. Naga Raju, D. Krishna Rao, N. Veeraiah, J. Lumin. 117 (2006) 53.
[4] M. Marrale, A. Longo, A. Bartolotta, M.C. D'Oca, M. Brai, Nucl. Instrum. Methods Phys. Res. B 297 (2013) 58.
[5] G. Venkateswara Rao, P. Yadagiri Reddy, N. Veeraiah, Mater. Lett. 57 (2002) 403.
[6] B.J.R. Swamy, Bhaskar Sanyal, Y. Gandhi, R.M. Kadam, V. Nata Rajan, P. Raghava Rao, N. Veeraiah, J. Non-Cryst. Solids 368 (2013) 40.
[7] Y. Lin, Z. Zhang, Z. Tang, J. Zhang, Z. Zheng, X. Lu, Mater. Chem. Phys. 70 (2001) 156.
[8] M.M. Elkholy, Mater. Chem. Phys. 77 (2002) 321.
[9] S.V.G.V.A. Prasad, M. Srinivasa Reddy, V. Ravi Kumar, N. Veeraiah, J. Lumin. 127 (2007) 637.
[10] K.S.V. Sudhakar, M. Srinivasa Reddy, L. Srinivasa Rao, N. Veeraiah, J. Lumin. 128 (2008) 1791.
[11] B.P. Kore, N.S. Dhoble, K. Park, S.J. Dhoble, J. Lumin. 143 (2013) 337.
[12] L.G. Jacobsohn, A.L. Roy, C.L. McPherson, C.J. Kucera, L.C. Oliveira, E.G. Yukihara, J. Ballato, Opt. Mater. 35 (2013) 2461.
[13] S. Gastélum, E. Cruz-Zaragoza, R. Meléndrez, V. Chernov, M. Barboza-Flores, Nucl. Instrum. Methods Phys. Res. B 248 (2006) 103.
[14] H. Yamamoto, T. Matsuzawa, J. Lumin. 72–74 (1997) 287.
[15] T. Matsuzawa, Y. Aoki, N. Takeuchi, Y. Murayama, J. Electrochem. Soc., 143, 19962670.
[16] J.A. Wani, M.S. Atone, N.S. Dhoble, S.J. Dhoble, J. Lumin. 134 (2013) 640.
[17] A.K. Bakshi, B. Sanyal, V.J. Joshi, M.K. Bhide, V. Natarajan, A. Sharma, Appl. Radiat. Isot. 69 (2011) 254.
[18] L. Hernández, T. Rivera, Y. Jimenez, R. Alvarez, J. Zeferino, A. Vázquez, J. Azorín, Appl. Radiat. Isot. 70 (2012) 1307.
[19] C. Bootjomchai, R. Laopaiboon, Nucl. Instrum. Methods Phys. Res. B 323 (2014) 42.
[20] N.A. Abd El-Malak, Mater. Chem. Phys. 73 (2002) 156.
[21] R.J. Amjad, M.R. Sahar, S.K. Ghoshal, M.R. Dousti, R. Arifin, Opt. Mater. 35 (2013) 1103.
[22] Y.S.M. Alajerami, S. Hashim, W.M.S.W. Hassan, A.T. Ramli, A. Kasim, Physica B 407 (2012) 2398.
[23] Y.S.M. Alajerami, S. Hashim, S.K. Ghoshal, A.T. Ramli, M.A. Saleh, Z. Ibrahim, T. Kadni, D.A. Bradley, Appl. Radiat. Isot. 82 (2013) 12.
[24] J.E. Shelby, Introduction to Glass Science and Technology, Royal Society of Chemistry, Cambridge, 1997.
[25] S.A. Azizan, S. Hashim, N.A. Razak, M.H.A. Mhareb, Y.S.M. Alajerami, N. Tamchek, J. Mol. Struct., 1076, (2014) 20.
[26] T.Y. Lim, H. Wagiran, R. Hussin, S. Hashim, M.A. Saeed, Physica B 451 (2014) 63.
[27] R.S. Gedam, D.D. Ramteke, J. Phys. Chem. Solids 74 (2013) 1399.
[28] B.V. Raghavaiah, C. Laxmikanth, N. Veeraiah, Opt. Commun. 235 (2004) 341.
[29] T. Satyanarayana, I.V. Kityk, K. Ozga, M. Piasecki, P. Bragiel, M.G. Brik V.R. Kumar, A.H. Reshak, N. Veeraiah, J. Alloys Compd. 482 (2009) 283.
[30] P. Kumar, A.K. Shukla, S. Yashonath, Diffus. Fundam. 6 (2007) 1.
[31] S. Hashim, Y.S.M. Alajerami, A.T. Ramli, S.K. Ghoshal, M.A. Saleh, A.B. Abdul Kadir, M.I. Saripan, K. Alzimami, D.A. Bradley, M.H.A. Mhareb, Appl. Radiat. Isot. 91 (2014) 126.
[32] R. Chen, J. Appl. Phys. 40 (1969) 570.
[33] M. Sundara Rao, B. Sanyal, K. Bhargavi, R. Vijay, I.V. Kityk, N. Veeraiah, J. Mol. Struct. 1073 (2014) 174.
[34] R.K. Gartia, L. Rey, Th. Tejkumar Singh, Th. Basanta Singh, Nucl. Instrum. Methods Phys. Res. B 274 (2012) 129.
[35] G.V.L. Reddy, L.R. Moorthy, B.C. Jamalaiah, T. Sasikala, Ceram. Int. 39 (2013) 2675.